Nickel Catalysis and Coordination Chemistry: Synthesis, Reactivity and Ligand Dynamics of Ni SNS Thiolate Complexes

Yahya Albkuri

Thesis submitted to the University of Ottawa

in partial fulfillment of the requirements for the degree of

Doctor of Philosophy, Chemistry

Department of Chemistry and Biomolecular Sciences and

Centre for Catalysis Research and Innovation

University of Ottawa

Abstract

Different metals and metal complexes have been used as catalysts in many industries such as commodity petrochemicals, fine and specialty chemicals, polymers, environmental services, agrochemicals and pharmaceuticals. Although these catalysts allow for increased reaction rates and selectivity, they can also be toxic, expensive and of limited supply (*cf.* Pt group metals). This has led researchers to the intensive study of first row metal catalysts, with nickel standing out as the most widely studied to date. As found for other first row metal catalysts, nickel's easy access to oxidation states 0-3 allows for a number of different one- and two-electron mechanisms and novel transformations. In **Chapter 2** we use a phosphine-free, tridentate N,N,N ligand to generate an active catalyst for the C-N cross-coupling reaction of aryl halides with amines. The catalyst demonstrated excellent turnover numbers (up to 484) for the amination reactions that are proposed to proceed through a Ni(I)-Ni(III) cycle. In **Chapter 3** we investigate the Ni coordination chemistry of a biomimetic SNS thiolate ligand. Protonation of the Ni bis(thiolate) complex, Ni(κ^2-SNS)$_2$, removes one SNS ligand, affording crystals of a thiolate-bridged dimer dication, {[Ni(μ-κ^3-SNS)]$_2$}$^{2+}$ that exhibits unique anionic tridentate ligand dynamics. Dissolving these crystals, even in weakly-coordinating solvents such as dichloromethane, gives a mixture of 'naked' Ni^{2+} and paramagnetic, trinuclear {[Ni(μ-κ^3-SNS)$_2$]$_2$Ni}$^{2+}$. Although this equilibrium lies far to the right (no diamagnetic dication visible in NMR), addition of ancillary ligands proceeds smoothly to provide several mono- and dinuclear Ni thiolate products, [Ni(κ^3-SNS)L]$_n$ – potential bifunctional catalysts for further studies. In **Chapter 4** we demonstrate using chemical and electrochemical techniques that one-electron reduction of Ni(κ^2-SNS)$_2$ triggers quantitative imine C-C bond coupling, forming [Ni(S_2N_2)]$^-$ with a redox-active ligand. Spectroelectrochemical studies indicated reversible oxidation and reduction steps give three stable redox states, ([Ni(S_2N_2)]$^{0/-/2-}$), that were characterized by NMR, EPR and UV-Vis spectroscopy, X-ray diffraction and computational chemistry. While the Ni(0) dianion (and not the Ni(I) anion) reacted reversibly with phenol and carbon dioxide, results from **Chapter 5** showed that reactions with strong electron-acceptor fluoroalkenes proceeded more cleanly with the Ni(I) anion. The latter reactions afforded a mixture of fluoroalkenyl and fluoroalkyl products resulting from C-F bond activation and electron transfer/H atom abstraction, respectively. In **Chapter 6** we discuss our results in the context of the current state of the art and suggest some avenues for future development.

Acknowledgements

First and foremost, I would like to express my deepest thanks to my supervisor, Prof. Tom Baker for giving me the opportunity to work in your research group. I am so grateful to you for your support, encouragement, powerful suggestions, guidance, passion and curiosity of all chemistry throughout the progress of my studies. I can't thank you enough for the valuable lessons I have learned working for you, including working independently, thinking creatively and enjoying chemistry. I will absolutely miss the long chemistry talks on weekends with you.

I would like to thank all Baker group members past and present for making the Baker labs a truly enjoyable place. Special thanks to Uttam and Nick as my best friends and labmates - thank for your great help and advice. I absolutely enjoyed chemistry discussions with both of you and our 'jokes' Nick. Special thanks to Bakr who has been both labmate and close friend. I also thank my summer ICE student Abdul for the great times we spent together in and out the lab and became friends forever. My thanks also go to my Honour's undergraduate student Vivian who put up with me and my requests. To all my other awesome group members, Samira, Saeed, Atousa, Luana, Jessica, Behnaz, Seth, Fernanda, Bakr, Alex Sicard, Alex Daniels, Brandon Fitchett and Matt, thank you all for the great help and time we spent in and out of the lab.

Sincere thanks to my supervisory committee members, Profs. Darrin Richeson and Jaclyn Brusso for your great suggestions and excellent guidance throughout the progress of my independent proposal, seminar and thesis research. Thanks to Dr. Peter Pallister for his help with NMR and EPR techniques and to Dr. Jeff Ovens for all his help with my numerous X-ray structures. Thanks also go to the University of Ottawa and department of chemistry for accepting me to do my studies here. To Profs. Robert Morris (University of Toronto) and Charles MacDonald (Carleton University), thank you so much for your time serving as external examiners for my thesis. Last but not least, I would like to thank all my family and friends for their support through the years of my studies. Special thanks to my Mom for her infinite support - I would not be where I am today without her support and encouragement. I am so thankful to have siblings that they have always been there for me whenever I need support.

Table of Contents

List of Schemes

List of Figures

List of Tables

Abbreviations

Ar	Aryl
a.u.	Atomic units
BM	Bohr magnetons
BTB	1,3-bis(trifluoromethyl)benzene
CH_3CN	Acetonitrile
$CHCl_3$	Chloroform
CNAr/CNxylyl	2,6-dimethylphenyl isocyanide
ca.	*circa*, approximately
cf.	*conferatur*, Compare
CV	Cyclic voltammetry
CTFE	Chlorotrifluoroethylene
DCM	Dichloromethane
DEE	Diethyl ether
DFT	Density functional theory
DMAB	*N*,*N*-Dimethylamine-borane
dmpm	1,2-bis(dimethylphosphino)methane
EPR	Electron paramagnetic resonance
EI-MS	Electron impact mass spectrometry
e^-	Electron
e.g.	Gratia, For example
et al.	*Et alia*, And others
ESI-MS	Electrospray ionization mass spectrometry
Eq./Equiv.	Equivalents
FA	Fluoroalkene
h	Hour(s)
HS	High-spin
HOMO	Highest occupied molecular orbital
HFP	Hexafluoropropene
i.e.	*Id est*, it is
IR	Infrared
IPr	(1,3-bis(2,6-diisopropylphenyl)imidazol-2-ylidene)
i-Pr	Isopropyl
L	Ligand
LS	Low-spin
LUMO	Lowest unoccupied molecular orbital
MCD	Magnetic circular dichroism
Me	Methyl
MHz	Megahertz
MLCT	Metal to ligand charge transfer
NIR	Near infrared
MPB	2-(Methylthio)-phenyl-benzothiazolidine
NMR	Nuclear magnetic resonance
NHC	*N*-heterocyclic carbene
NTf	*N*-(trifluoromethylsulfonyl)

Na/K	Sodium-potassium alloy
ORTEP	Oak Ridge thermal-ellipsoid plot
OTf	Trifluoromethanesulfonate
Ph	Phenyl
PTFE	Polytetrafluoroethylene
R^F	Fluoroalkyl group
RDE	Rotating disk electrode
RB	Round-bottom
RT	Room temperature
TMS	Trimethylsilyl
THF	Tetrahydrofuran
TFE	Tetrafluoroethylene
$TBAPF_6$	Tetrabutylammonium hexafluorophosphate
UV-Vis	Ultraviolet-visible electronic spectroscopy

List of Contributions

Publications resulting from the chapters of this Thesis:

1. Yahya M. Albkuri, Ambar B. RanguMagar, Andrew Brandt, Hunter A. Wayland, Bijay P. Chhetri, Charlette M. Parnell, Peter Szwedo, Anil Parameswaran-Thankam, Anindya Ghosh. C–N Cross-coupling Reactions of Amines with Aryl Halides Using Amide-Based Pincer Nickel(II) Catalyst. *Catal. Lett.* **2020**, *150*, 1669–1678 (Full article).
2. Yahya M. Albkuri, Jeffrey S. Ovens, Jessica L. Martin, R. Tom Baker. Nickel(II)-SNS Thiolate Complexes: Reactivity and Solution Dynamics. *Inorg. Chem.* **2021**(Full article in press).
3. Yahya M. Albkuri, Stephan Steinmann, Jeffrey S. Ovens, Christophe Bucher; R. Tom Baker. Spectroscopic and Electrochemical Characterization and Reactivity of Three Redox States of $Ni(S_2N_2)$ (Full article to be submitted to *Chem. Eur, J.*, **2021**).
4. Yahya M. Albkuri, Jeffrey S. Ovens, R. Tom Baker. Reactions of Reduced $Ni(S_2N_2)$ Complexes with Fluoroalkenes, manuscript in preparation.

Presentations:

1. Yahya M. Albkuri, Jeffrey S. Ovens, Stephan Steinmann, Christophe Bucher, R. Tom Baker. A Nickel for Your Thoughts? Synthesis, Structure and Reactivity of Three $Ni(N_2S_2)$ Redox States - 2021 ACS Spring National Meeting (virtual) (TALK).

2. Yahya M. Albkuri, Jeffrey S. Ovens, R. Tom Baker. Two for One: Reactivity of Nickel SNS Bis(thiolate) and its $Ni(N_2S_2)$ Isomer – 2020 Chemistry and Biochemistry Graduate Research Conference (virtual; organized by Concordia University) (TALK).

3. Yahya M. Albkuri, Jeffrey S. Ovens, R. Tom Baker. Abstract accepted at 2020 Canadian Chemistry Conference and Exhibition, but conference was canceled (TALK).

4. Yahya M. Albkuri - visiting student presentation at ENS-Lyon, France, Feb., 2020.

5. Yahya M. Albkuri, R. Tom Baker. Ni SNS Complexes – 2019 Canadian Chemistry Conference, Quebec City, 2019 (TALK).

6. Yahya M. Albkuri, Jeffrey S. Ovens, R. T. Baker. Bifunctional Ni-SNS Coordination Complexes - 2019 Ottawa-Carleton Chemistry Institute Conference (TALK).

Chapter 1. Introduction

1.1 Introduction Summary and Brief History of Nickel in Catalysis

Nickel was discovered in the 1750s, is present in metallic meteorites, and has been used since ancient times.[1] Nickel and its complexes have been shown to be effective catalysts for a host of important chemical transformations.[2] Nickel metal was first isolated in 1751 in Sweden by Axel Fredrik Cronstedt and its name is derived from the German kupfernickel, meaning either devil's copper or St. Nicholas's copper.[3] The first pure samples were obtained in 1775 by Torbern Bergman. In the 1890s, Mond observed unusual reactivity of nickel and carbon monoxide (CO) at room temperature to give the toxic, low-boiling, green liquid $Ni(CO)_4$.[4] In 1912 Sabatier, Nobel prize winner in chemistry, discovered the first hydrogenation of ethylene using nickel metal.[5] Years later, Wilke and his group at the Max Planck Institute in Germany expanded the organometallic chemistry of nickel complexes by synthesizing $Ni(allyl)_2$, $Ni(C_2H_4)_3$ and $Ni(cod)_2$ and examining catalysis of olefin and diene oligomerization reactions (cod = 1,5-cyclooctadiene).[6] Further work on ethylene oligomerization led to the Shell Higher Olefins Process (SHOP)[7,8] and nickel phosphite catalysts were also employed by Dupont for hydrocyanation of butadiene to adiponitrile, a precursor to Nylon 6,6.[9,10] Following award of the Nobel prize for Pd-catalyzed cross-coupling catalysis in 2005, increasing numbers of nickel catalysts for these reactions were developed[11] and shown to be more mechanistically complex,[12] as detailed in the following sections as an introduction to Chapter 2 of this thesis. Nickel has also been found to play key roles in several metallo-enzymes including superoxide dismutase, CO dehydrogenase, acetyl-CoA synthase / decarbonylase and [NiFe] hydrogenase.[13] Further details are provided below as an introduction to Chapters 3 and 4 which feature some coordination chemistry of biomimetic SNS thiolate and S_2N_2 dithiolate ligands. Finally, after discovering that the $Ni(S_2N_2)$ complex discussed in Chapter 4 exists in three stable redox states, we investigated in Chapter 5 their selective reactivity with prototypical electron-acceptor fluoroalkenes, $CFX=CF_2$ (X = F, Cl, CF_3, OCF_3) for which a brief introduction is also provided here.

1.2 Typical Modes of Action for Nickel Catalysts.

Before going into depth about the applications and reaction mechanisms for nickel complex-catalyzed cross-coupling, we compare the typical reaction steps with those for Pd catalysts (**Figure 1.1**). As a less electronegative metal, oxidative addition is facilitated for zerovalent Ni complexes

and thought to proceed by single-electron transfer through Ni(I) intermediates, in contrast to the three-centered transition state typically invoked for Pd(0) oxidative additions.[14,15] This also allows Ni catalysts to effect cross-coupling with less reactive electrophiles such as phenol derivatives,[16-18] aromatic nitriles[19] and aryl fluorides.[20]

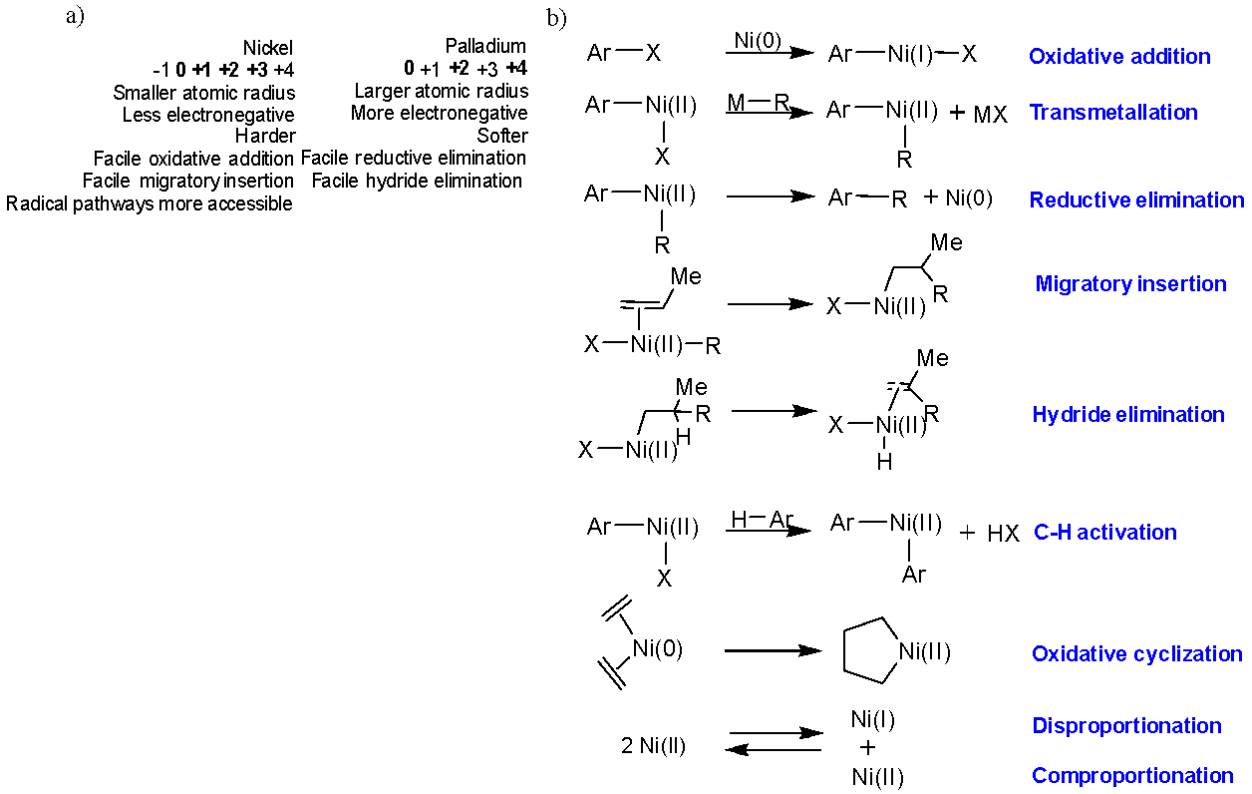

Figure 1.1 (a) Basic properties of Ni and Pd (common oxidation states in bold). (b) Fundamental reactions of Ni complexes in catalytic cycles.[21]

Nickel has a number of oxidation states that can be involved in cross-coupling catalysis whereas Pd typically employs $Pd^{0\text{-}II}$ or $Pd^{II\text{-}IV}$ couples in catalytic cycles. In addition to $Ni^{0\text{-}II}$, easily accessible $Ni^{I\text{-}III}$ couples have been invoked to account for different reactivity.[22] Beta-hydride elimination is also frequently slower with Ni relative to Pd, allowing for a broader scope of alkyl-aryl and alkyl-alkyl couplings.[23] Finally, nickel is roughly 2,000 times less expensive than Pd.

In a recent example, Diao et al. reported that a Ni-catalyzed two-component reductive dicarbofunctionalization of alkenes proceeds via a "sequential reduction" pathway through a radical chain mechanism (**Scheme 1.1**).[24] Reduction of Phen Ni(II) dibromide to Ni(I) by Zn is followed by reaction with bromobenzene to afford NiBrPh(phen) that also gets reduced by Zn to active catalyst NiPh(phen). The latter then reacts with alkyl bromide to form a radical which

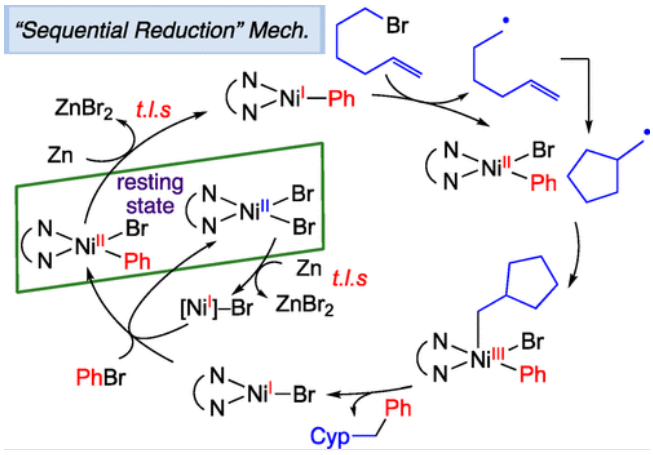

Scheme 1.1. Diao's sequential reduction mechanism for alkene difunctionalization.[24]

cyclizes and subsequently adds to NiBrPh(phen), forming the Ni(III) intermediate prior to reductive elimination. In 2020 Liao and co-workers prepared aryl- and vinyl nitriles from aryl halides and alkynes using Ni(bipy) to catalyze cyanation and hydrocyanation in which the mechanism involved Ni(0)-Ni(II) and Ni(I)-Ni(III) transformations within the same cycle using Zn as reducing agent.[25] Weix et al. reported that the selectivity observed in nickel-catalyzed cross-coupling of aryl halide with alkyl halide electrophiles arises from an unusual catalytic cycle that combines both polar and radical steps to form the new C-C bond (**Scheme 1.2**).[26] These reaction pathways clearly show the versatility of nickel catalysts vs their Pd analogs.

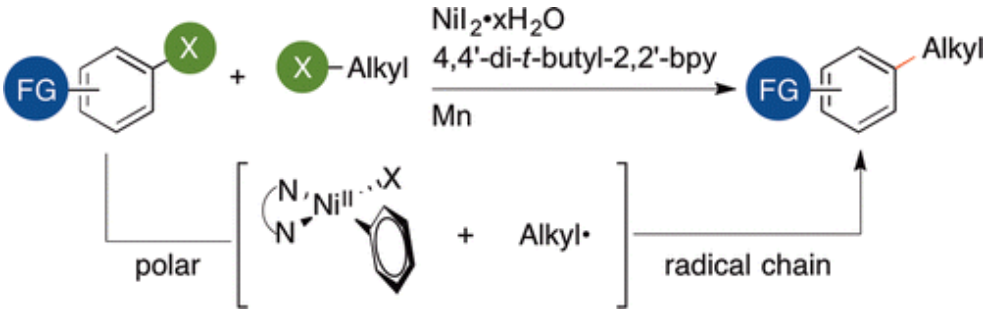

Scheme 1.2. Combined polar-radical mechanism for Ni-catalyzed cross-electrophile coupling.[26]

1.3 Nickel-Catalyzed Cross-coupling Reactions

Since the 1970s, nickel complexes have been the most effective first row transition metal catalysts for cross-coupling reactions. While these reactions were initially developed as a means to synthesize biaryls from aryl halides and aryl metal reagents, the scope of cross-coupling reactions has been extended in recent years to involve many other types of coupling as addressed below.

1.3.1 Cross-coupling of aryl halides

The Suzuki-Miyaura reaction is the most popular cross-coupling reaction due to the stability of the arylboron reagents employed. The advantage of using nickel in these reactions stems from their ready oxidative addition of carbon-heteroatom bonds that ultimately undergo protodeboronation under basic reaction conditions and/or elevated reaction temperature. Hartwig and Ge, used readily activated catalyst **3** to obtained coupled heterocycle products (**Scheme 1.3a**)[27] and Garg and co-workers extended and improved similar reactions of both heteroaryl chlorides and bromides by applying a green solvent (**Scheme 1.3b**).[28]

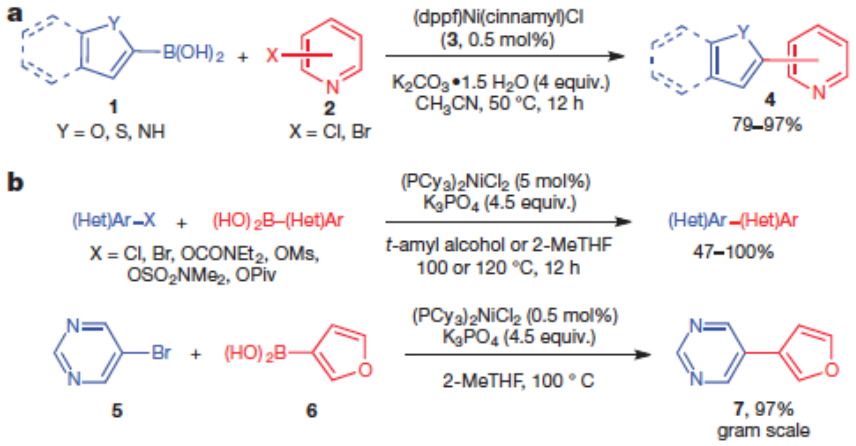

Scheme 1.3 Nickel complex-catalysed Suzuki-Miyaura reactions of heteroaryls.

1.3.2 Cross-coupling of phenol derivatives

Although C-O bond activation by nickel was originally reported in 1979, since then a host of developments have been disclosed.[29,30] In 1989, Kocienski and Dixon developed the first effective Ni(0)-catalysed cross-coupling of vinyl carbamates with organomagnesium reagents[31] and later Snieckus and co-workers developed analogous reactions of aryl carbamates[32] and tertiary aryl sulphonamides[33] with organomagnesium reagents. Dankwardt described the cross-coupling of aryl ethers with arylmagnesium reagents in a Kumada-Corriu-type coupling[34] (**Scheme 1.4a**) followed by Chatani and co-workers who described the first Suzuki-Miyaura cross-coupling of aryl ethers and boronic esters (**Scheme 1.4b**).[35] The Shi and Garg groups reported Suzuki-Miyaura cross-coupling of aryl acetates and aryl pivalates with boronic acids (**Scheme 1.4c**).[36,37]

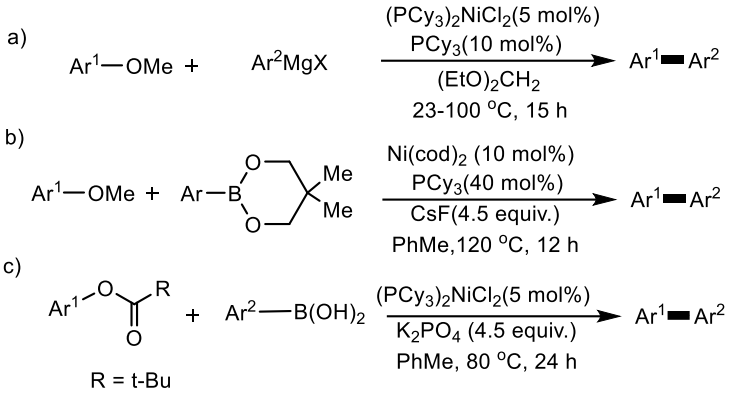

Scheme 1.4 Nickel-catalysed-cross-coupling reactions of aryl ethers and esters.

1.3.3 Cross-coupling of electrophiles with benzylic C-O bonds

A variety of electrophiles with benzylic C-O bonds including ethers, esters, carbonates and carbamates can be activated by low-valent nickel.[38] In 2011 Jarvo and co-workers used the first example of Ni-catalyzed alkyl-alkyl cross-coupling to prepare di- or tri-arylalkanes as drug targets (**Scheme 1.5a**)[39] including anti-cancer agent **16**. The same group demonstrated Suzuki-Miyauara cross-coupling of benzylic esters, carbonates and carbamates with boronic derivatives (**Scheme 1.5b**).[40] Subsequently, Watson and co-workers demonstrated a similar method for synthesizing diarylalkanes and triarylmethanes from benzylic pivalates and boroxines (**Scheme 1.5c**).[41]

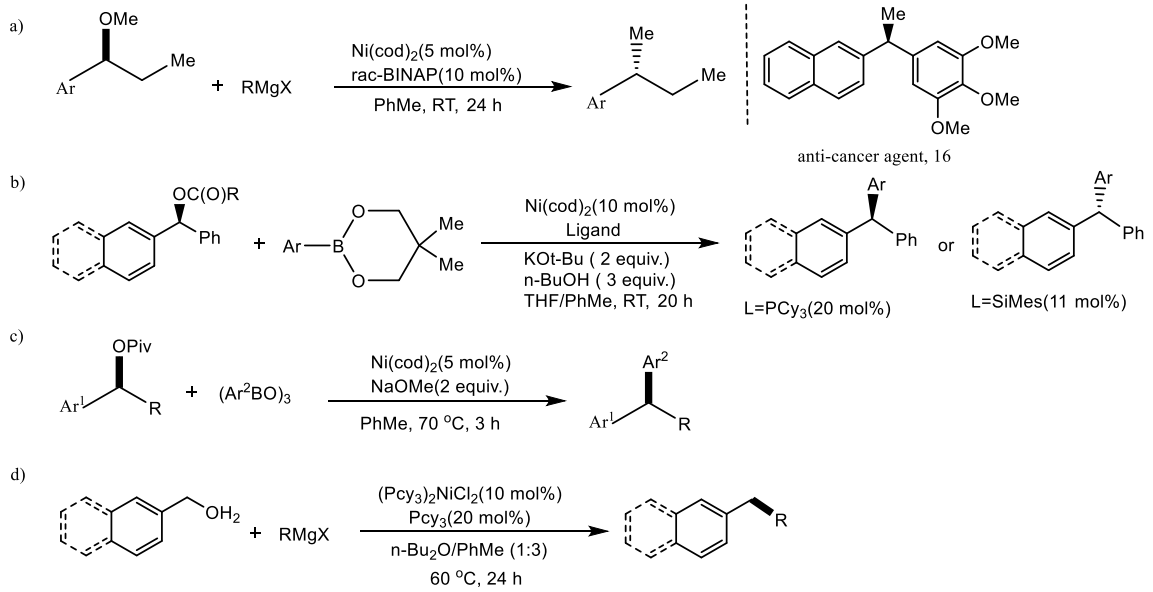

Scheme 1.5 Ni-catalyzed cross-coupling of electrophiles containing benzylic C-O bonds.

1.3.4 Cross-coupling of aziridines

The activation of aziridine C-N bonds by $Ni^{(0)}$ complexes has been known for some years[42] and in 2012 Huang and Doyle demonstrated the successful Negishi coupling of alkyl and arylzinc halides to styrene-derived N-tosyl aziridines to form β-disubstituted amines.[43] (**Scheme 1.6**)

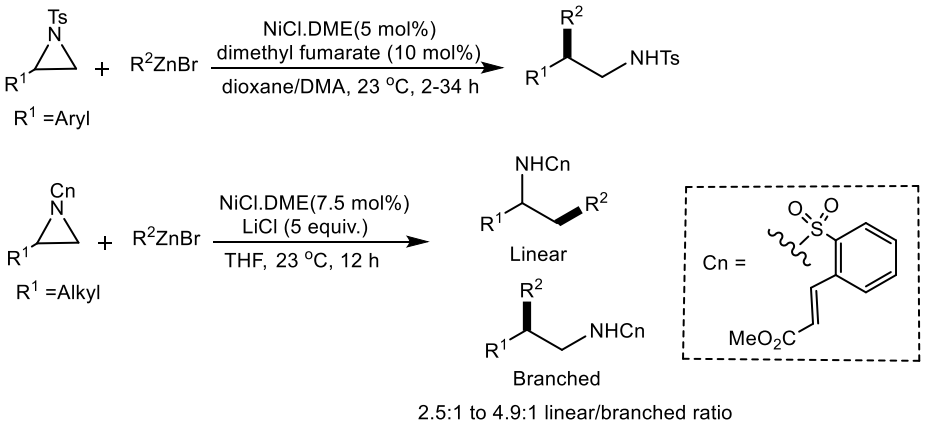

Scheme 1.6 Nickel-catalysed Negishi cross-coupling of aziridines.[43]

1.3.5 C-N cross-coupling

Many heterocyclic molecules, especially those containing nitrogen atoms, are important due to their occurrence in many natural products, and their propensity for interesting biological activity.[44] Formation of aromatic C-N bonds was originally challenging in the medicinal field.[45] due to limitations of the original Ullmann coupling (**Figure 1.2**).[46,47] Since chapter 2 focuses on C-N cross-coupling reaction, background for these reactions follows.

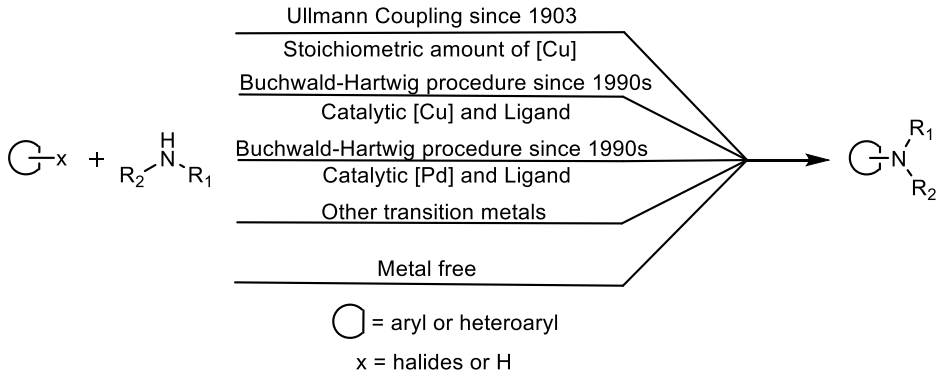

Figure 1.2 C-N bond formation using different metals.[48]

1.3.6 Nickel-catalyzed C-N cross-coupling

Nickel was first used for amination reactions in 1950 when oil company researchers were investigating different metal salts as catalysts for the reaction of methylamine with chlorobenzene.[49] Although Cu^{I} and Cu^{II} chlorides were the most effective catalysts under basic reaction conditions, $NiCl_2$ also worked, albeit at higher temperatures (> 200 °C). Cramer and Coulson then reported a comprehensive study on the effect of changing reaction conditions and catalyst composition for the nickel-catalysed amination reaction[50]. They found that Ni^{0} complexes such as $[Ni(CO)_2(dppe)]$ and $[Ni(CO)_2(PPh_3)_2]$ were almost as effective as $NiBr_2$. Since 1997, Buchwald and other researchers have developed many nickel complexes for cross-coupling amination reactions using a variety of different Ni precursors, ligands and reaction conditions (**Scheme 1.7** and **Figure 1.3**).[51-56]

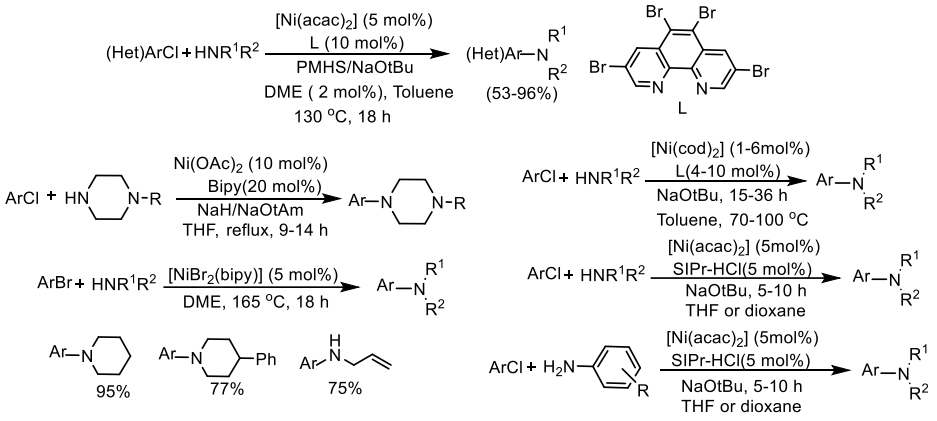

Scheme 1.7 Nickel catalysed amination reactions.[51-55]

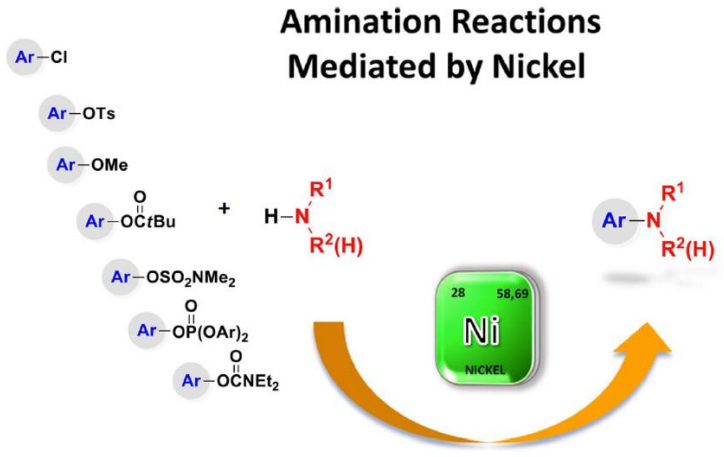

Figure 1.3 Different substrates used for nickel-catalyzed amination.[56]

1.3.7 Nickel-catalyzed amination of phenol-derived electrophiles

In 2008, Gao and Yang described the first example of nickel-catalyzed amination of aryl tosylates, reporting short reaction time using [NiCl(1-naphthyl)(PPh_3)$_2$].[57] Chatani and co-workers later reported the more challenging C-N formation of aryl methyl ethers catalysed by Ni(0).[58] Tobisu, Chatani and coworkers then extended this methodology to the amination of N-heteroaryl methyl ethers[59] and arylcarboxylates.[60] Garg's group reported the amination of aryl sulfamates and carbamates with secondary cyclic and acyclic amines, as well as anilines although sterically hindered examples required higher catalyst loadings.[61,62] In 2011, Huang and Yang reported the use of aryl phosphates as coupling partners (**Scheme 1.8**).[63]

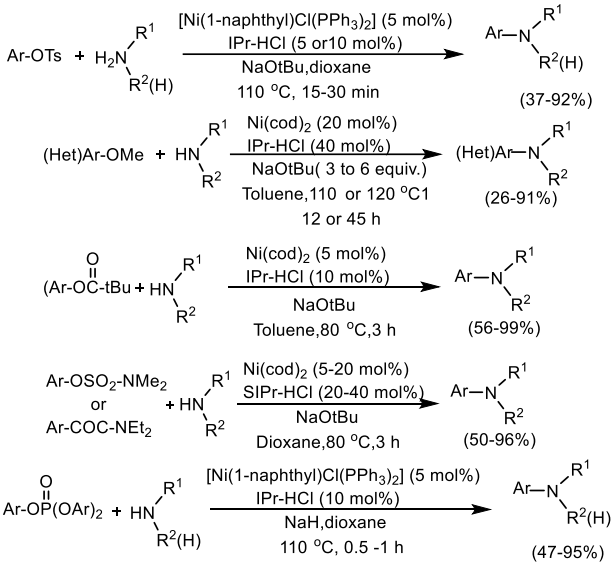

Scheme 1.8 Nickel-catalyzed amination of phenol-derived electrophiles.[61-65]

1.4 Cross-coupling reaction mechanisms

The conventional metal-catalyzed cross-coupling mechanism follows a three-step process (**Figure 1.4**):

1) oxidative addition of the electrophile (R-X) C-X bond to the low-valent metal center, causing a formal oxidation state change of two;
2) transmetalation, in which the nucleophile, MR', often activated by additive Y, is transferred to the metal center;
3) reductive elimination of the coupled product with regeneration of the low-valent metal center.

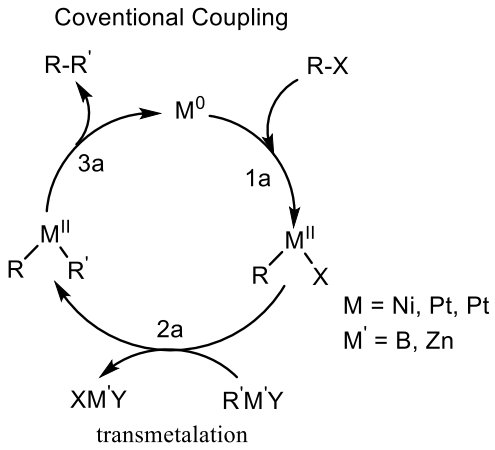

Figure 1.4 General metal-catalyzed cross-coupling reaction mechanism.

1.4.1 Mechanisms of Nickel-catalyzed amination reactions

Mechanistic studies for nickel-catalysed amination have not been investigated to the same level of detail as those for Pd.[66] The easy access to different nickel oxidation states make such studies more challenging and both Ni^0/Ni^{II} and Ni^I/Ni^{III} cycles have been proposed.[67-74]. In 2014, Hartwig and his group reported the first in-depth mechanistic studies of the amination of chloro- and bromoarenes with aliphatic primary amines catalyzed by a Ni^0 complex (**Figure 1.5**).[75] Stewart and co-workers investigated the same mechanism using different techniques including NMR and

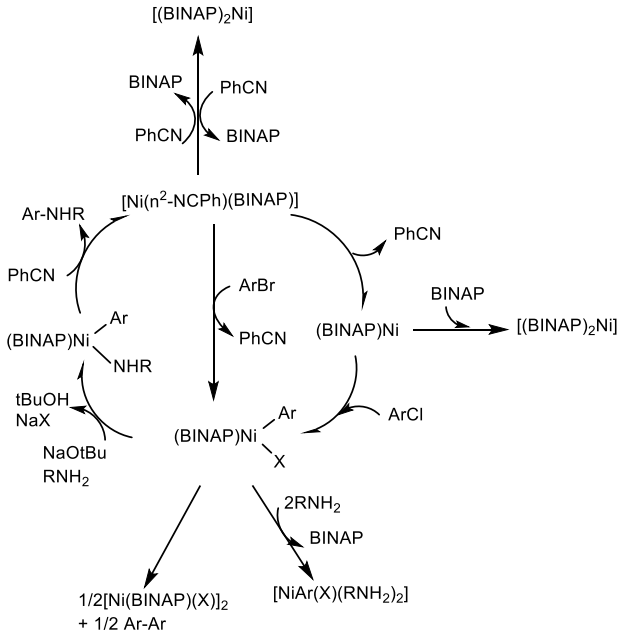

Figure 1.5 Hartwig's proposed mechanism for Ni-catalysed amination of aryl halides with primary amines.[75]

reaction kinetics as well as computational studies.[76] Although they agreed with the Ni^0/Ni^{II} catalytic cycle, there was some conflict with the findings from Hartwig's report, in that the oxidative addition was not the rate-determining step and the reaction rate was dependent on the concentration of aryl chloride (**Figure 1.6**). These are just two examples out of many that prove investigating nickel catalytic mechanisms still remains a challenge.

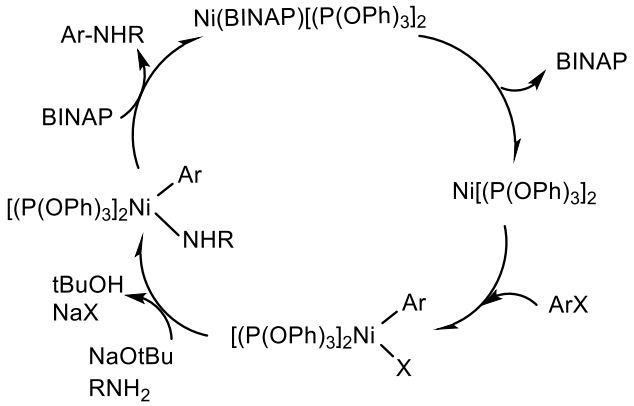

Figure 1.6 Stewart's proposed mechanism for Ni-catalysed amination of aryl halides with primary amines.[76]

As we have seen for other cross-coupling reactions, nickel-catalyzed amination need not be confined to $Ni^{0,2}$ cycles. In 2019 Matsubara and co-workers reported C-N cross-coupling of aryl halides with a variety of amines.[77] They used 2,2'- bipyridyl to stabilize Ni(I) NHC complexes, which efficiently mediated amination of aryl bromides employing a Ni(I)-Ni(III) pathway.

1.5 Biomimetic NS Thiolate Ligands for Metal Coordination Chemistry

1.5.1 Nickel metalloenzymes and their synthetic models

Thiolate and NS thiolate ligands play pivotal roles in a number of metalloenzymes.[78] Hydrogenases, for example, are the most efficient enzymes for reversible conversion of protons and electrons to dihydrogen (Eq. 1). For the [FeFe] hydrogenase, both experimental and theoretical

$$2H^+ + 2e^- \rightleftharpoons H_2 \qquad 1)$$

studies show that the amine motif of the bridging dithiolate (**Figure 1.7**) is essential for hydrogen production,[79] while the [NiFe] hydrogenase typically oxidizes hydrogen to protons.[80] Both Ni- and Fe-bound thiolates are proposed to be involved in the H_2 splitting step (**Scheme 1.9**).[81]

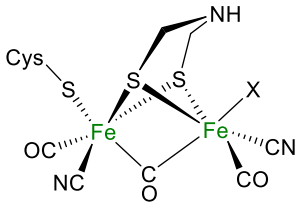

Figure 1.7. Active site of [FeFe] hydrogenase. X marks site of catalytic H_2/proton turnover.[79]

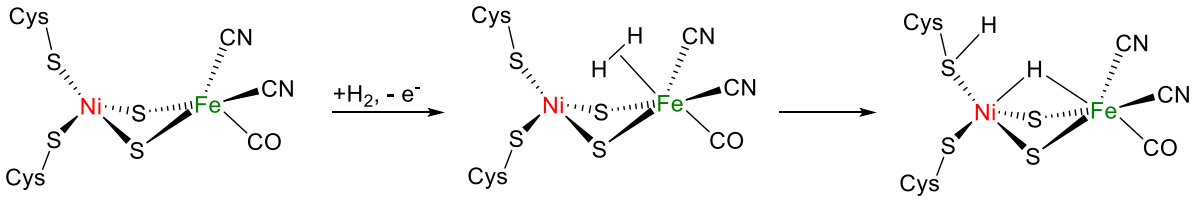

Scheme 1.9 Hydrogen activation by [NiFe] hydrogenase.[81]

Several functional mimics of [NiFe] hydrogenase have been reported[82,83] as well as a series of mononuclear Ni phosphine complexes that employ a pendant, non-bonded amine to assist proton transfer steps.[84]

Superoxide dismutase (SOD) enzymes control reactive oxygen species in cells by converting superoxide and protons to oxygen and hydrogen peroxide (Eq. 2).[85] While metal active

$$2H^+ + 2\,(O_2)^- \longrightarrow H_2O_2 + O_2 \qquad 2)$$

sites in Mn-, Fe- and Cu/Zn-SOD are all bound to N- and O-donors, in Ni-SOD nickel is bound to N- and S-donors.[86] In the oxidized form, the active site includes a low-spin (S = ½) Ni(III) center ligated in an N_3S_2 square pyramidal geometry with an axial imidazole group (**Figure 1.8a**). In the reduced form the imidazole is dissociated and the active site is square planar Ni(II) (**Figure 1.8b**). Using metallopeptide models, Tietze, Buntkowsky and co-workers recently showed that this axial ligand improves catalyst stability to air, but is not required for catalytic activity.[87]

Ni S_2N_2 coordination is also employed by the acetyl co-A synthase enzyme (ACS; **Figure 1.9**) which remarkably involves organometallic intermediates with Ni-C and Co-C bonds.[88,89] This inspired a number of Ni N_2S_2 model studies such as those by Holm and co-workers.[90]

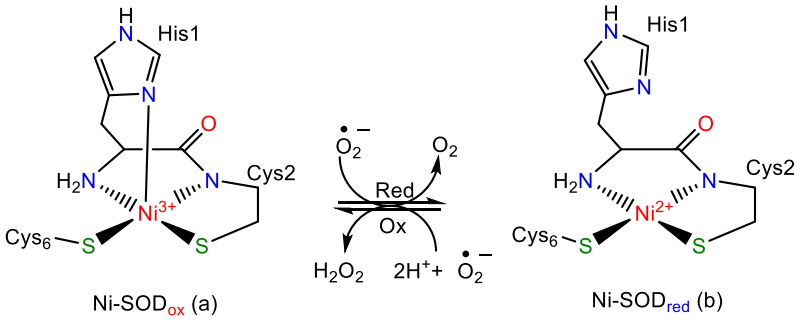

Figure 1.8. Oxidized (a) and reduced (b) forms of Ni-SOD.

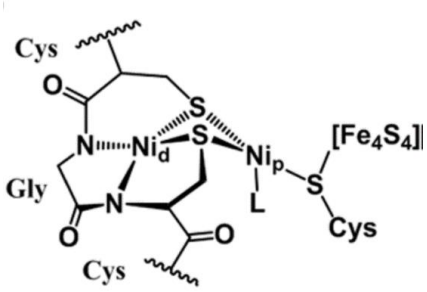

ACS

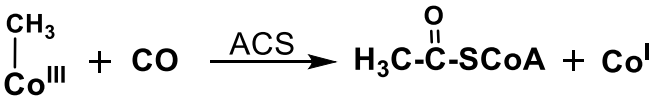

Figure 1.9 Active site of acetyl co-A synthase (ACS) enzyme.[89]

1.5.2 Hemilabile NS ligands

The hemilability of multidentate donor ligands refers to the ease of reversible (de)coordination of at least one of the donors, taking advantage of the different strengths of the metal heteroatom bonds.[91] Metal complexes that take advantage of hemilability have been shown to be more active in many transformations such as hydrogenation, carbonylation, hydroformylation of olefins and epoxides, allylation, olefin metathesis and ring-opening metathesis polymerization.[92] Metal NS complexes can undergo a ring-opening process through the cleavage of the weakest bond (M-N vs. M-S) and can be reversible (**Figure 1.10a**) so that the ligand can provide a vacant metal coordination site during a catalytic cycle.[93] Alternately, hemilability can be effected by external ligand addition which can also be reversible in a catalytic cycle (**Figure 1.10b**). Although hemilability of amine-thiolate NS ligands would involve reversible coordination of the N-donor, most examples consist of reversible thioether coordination. Bassetti et al. reported such an example in which hemilability of a benzyl thioether group helped promote the oxidative addition of methyl

iodide to a cationic Rh(I) complex (**Scheme 1.10**).[94] Reversible dissociation of the thioether generates an equilibrium with the solvent adduct that undergoes addition of MeI much more readily. The authors did not speculate whether hemilability also plays a role in the subsequent methyl migration to the CO ligand.

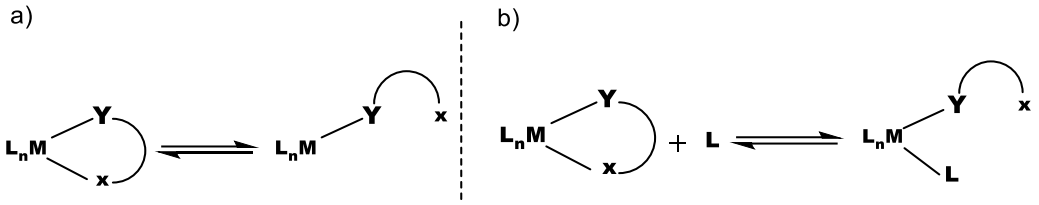

Figure 1.10 Hemilability via ligand dissociation (a) or addition of external ligand (b).[93]

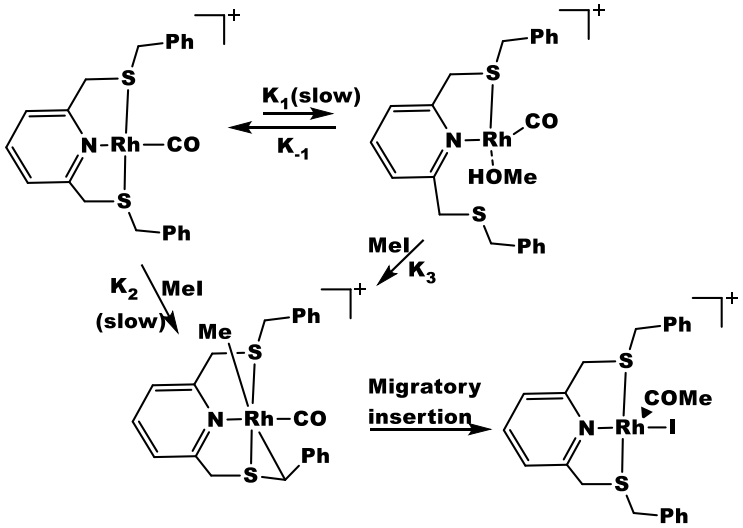

Scheme 1.10 Role of benzyl thioether lability in reaction of Rh(I) with MeI.[94]

In another example reported by Kaim and co-workers hemilability occurs in concert with an oxidation state change of the metal center. Oxidation of the four-coordinate cationic Cu(I) complex gives rise to a five-coordinate Cu(II) complex due to thioether binding (**Scheme 1.11**).[95] Kaim et al. also reported a reversible intramolecular ligand-based oxidation that was accompanied by coordination of the thioether group to the Ir(III) center (**Scheme 1.12**).[96]

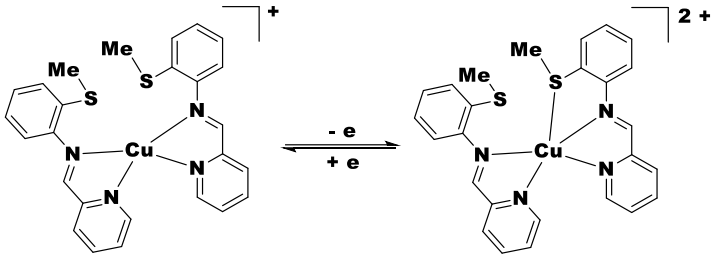

Scheme 1.11 Hemilability occurs through reduction of copper center.[95]

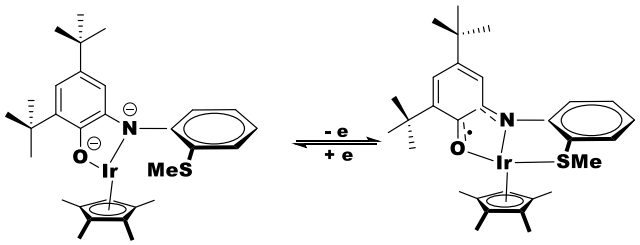

Scheme 1.12 Hemilability of redox-active ligand upon oxidation.[96]

Kinoshita et al. showed that the thioether in their dinucleating tetradentate ligand ($SCNS^R$) can be reversibly replaced with a CO ligand (**Scheme 1.13**).[97] Interestingly, addition of PMe_2Ph results in CO evolution and formation of monomeric, pseudo-octahedral Fe(κ^4-$SCNS^R$)(CO)(PMe_2Ph).

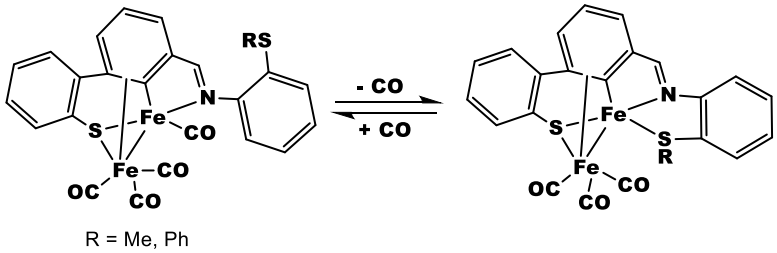

Scheme 1.13 Hemilability of thioether upon carbonyl ligand addition to iron complex.[97]

1.5.3 Conversion of $M(NS)_2$ into $M(S_2N_2)$ complexes

In the 1960s Busch and co-workers conducted extensive studies in nickel macrocyclization reactions of Ni complexes with NS ligands that yielded tetradentate N_2S_2 ligands.[98] They also demonstrated that reactions with electrophiles could occur at the thiolate sulfur. In one example the intermediate thioether species $[Ni^{II}(NS^R)_2]^{2+}$ rearranged to a trinuclear complex with a central

NiS_4 core,[99] later structurally characterized by Dahl and Wei (**Figure 1.11**).[100] A variety of Ni-S_2N_2 metalloligands have been synthesized based on 5- and 6-membered rings (**Figure 1.12**).[101]

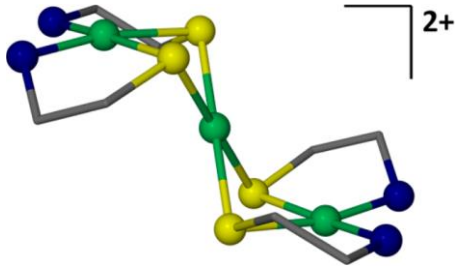

Figure 1.11 Two Ni(S_2N_2) metalloligands bound to a central Ni^{2+}.[100]

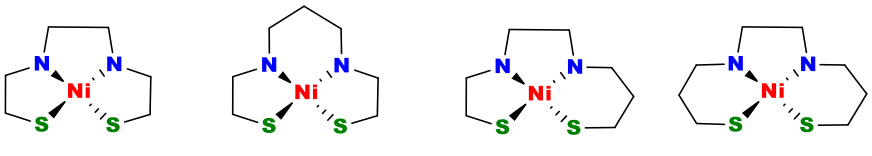

Figure 1.12 Ni S_2N_2 complexes with different ring sizes.[101]

1.5.4 Metrical details in Ni-S_2N_2 complexes

The correlation shown in **Figure 1.13** uses the S-S and N-N distances to show that the S-Ni-S angle varies inversely with the N-Ni-N angle in Ni-S_2N_2 complexes.[102] The distances range over ~0.4 and ~0.6 Å for the S−S versus N−N, respectively. Pinning together the nitrogens opens the S-Ni-S bite angle. More influence on S-Ni-S angles comes from modifying the N to S linker; changing from 2 to 3 carbons increases the N-Ni-N angle and decreases the S-Ni-S bite angle.

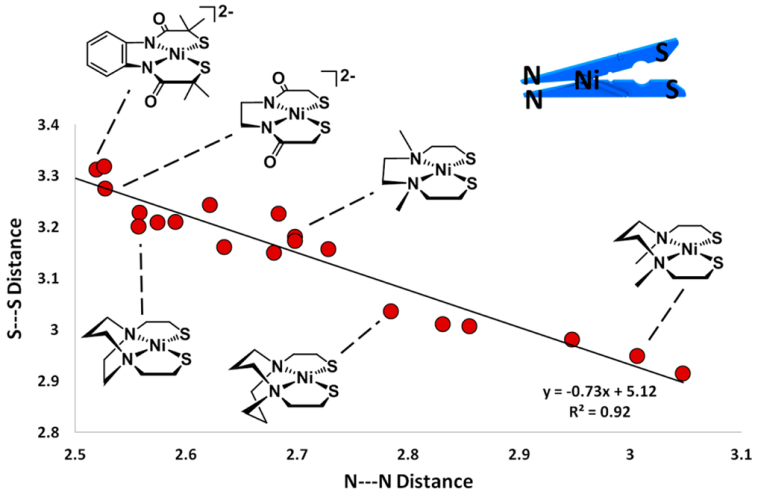

Figure 1.13 Correlation between S-Ni-S and N-Ni-N bite angles portrayed through E⋯⋯E bond distances.[103]

1.5.5 Nickel complexes with redox non-innocent S_2N_2 ligands

In 1997, Kawamoto and Kushi reported the thermal conversion of nickel and cobalt thiolate-imine complexes into the M(S_2N_2) complexes via imine C-C bond formation (**Scheme 1.14**).[103] Moreover, they recognized that two electrons had been transferred to the redox-active S_2N_2 ligand, giving an open shell singlet ground state. The same authors reported a series of Ni-S_2N_2 complexes (**1-3** in **Figure 1.14**) with extended-π-conjugation that allows them to serve as near infrared absorption dyes.[104] Several mono-nuclear Ni-S_2N_2 complexes (**4-9** in **Figure 1.14**) have been reported that have six-membered $NiNC_3S$ rings with phenylene ring linked by N to S.[105-109] In the reactivity aspect of these S_2N_2 ligands, one thio-salen ligand of (**9**) is converted into a thiazole upon connection of a thiolate sulfur with the cyanide on the phenylene ring, leaving only one N/S donor site binding to the nickel center which then needs two salen ligands to form the S_2N_2 donor set.[110]

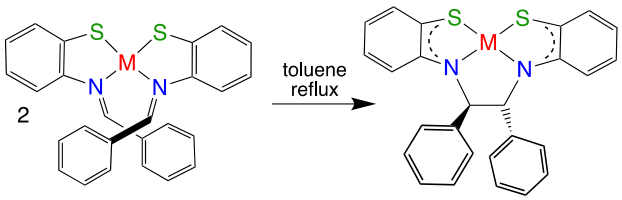

Scheme 1.14 Thermal conversion of M($SN)_2$ to M(S_2N_2) via imine C-C bond formation.

1.5.6 Applications of Ni-S_2N_2 complexes

In 2007, Darensbourg and co-workers showed that the Ni-S_2N_2 complex, N,N′-bis(mercaptoethylene-1,4-diazacyclooctane nickel(II), Ni(bme-daco), can support olefin/CO coupling on palladium, via the [Ni(bme-daco)$Pd^{II}(CH_3)(OEt_2)]^+$ catalyst, (**Scheme 1.15**),[111] in which the Ni metalloligand mimics the diimiine ligand in Brookhart's palladium catalyst developed for the production of polyketoethylene.[112] Moreover, Ogo and co-workers reported that coordination of a Ni-S_2N_2 metalloligand to Ru^{2+} generates a functional model of [NiFe]-hydrogenase (**Scheme 1.16**).[112,113]

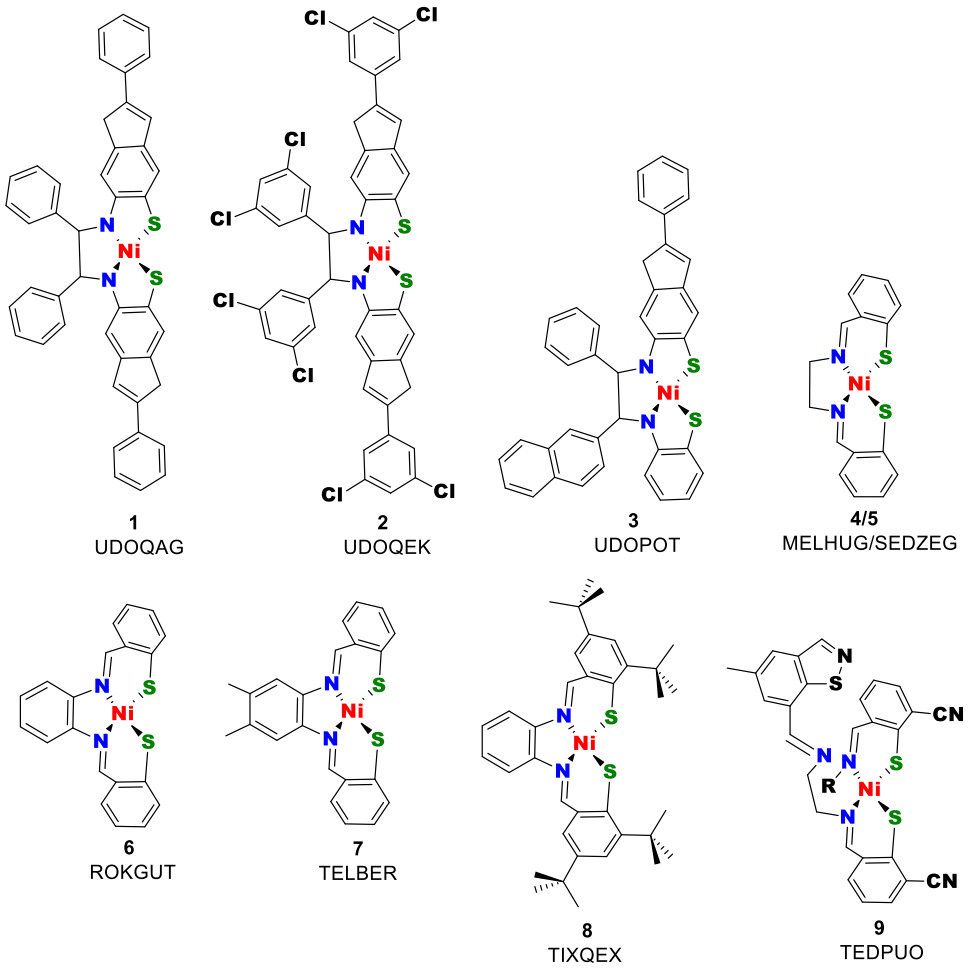

Figure 1.14 Ni-S_2N_2 complexes with mercapto-aniline and thiolate-salen ligands.[101]

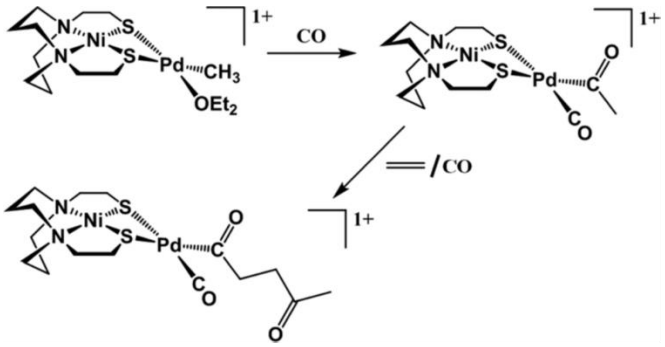

Scheme 1.15 Ni-S_2N_2 complex as metalloligand for Pd-based ethylene-CO copolymerization catalyst.[111]

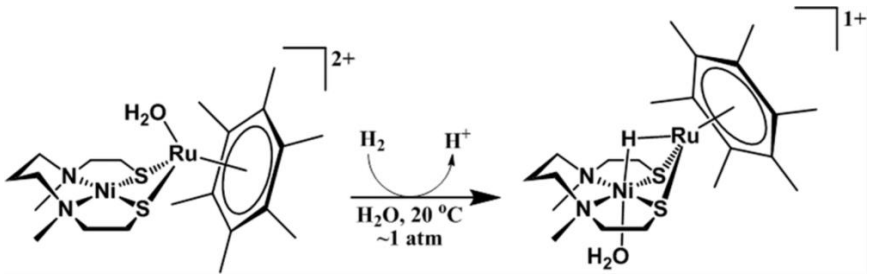

Scheme 1.16 Thiolate-bridged Ni-S_2N_2-Ru complex serves as a functional model for [NiFe] hydrogenase.[113]

1.6 Fluoroalkene Chemistry Mediated by Transition Metal Complexes

1.6.1 Overview

In Chapter 5 of this thesis we investigate the reactivity of reduced Ni(S_2N_2) complexes with easily accessed electron-acceptor fluoroalkenes. In this section we discuss the various ways in which metal complexes have been shown to interact with fluoroalkenes.

Fluoroalkenes are currently seeing an increase in their study and applications due to:

1) The need to replace molecules containing long perfluoroalkylated chains currently employed in a number of industrial and materials applications with smaller ones that could also include hydrogens to reduce their environmental persistence.[115]
2) The pursuit of greener unsaturated hydrofluorocarbons to expand the current 4th generation of refrigerants, propellants and foam-blowing agents.[116]
3) The competitive cost of commercially available fluoroalkenes compared to other chemicals used for installing fluoroalkyl groups on organic molecules for fine chemicals, pharmaceuticals and agrochemicals.[117]

1.6.2 Fluoroalkene Coordination to Metals and Coupling to Form Metallacycles

1.6.2.1 Metal fluoroalkene complexes and metallacyclopropanes

When Parshall and co-workers at DuPont CR&D prepared the first metal complexes of tetrafluoroethylene (TFE), they already recognized that the bonding in Rh complex **A** resembled that for hydrocarbon alkenes such as ethylene [a)] whereas extensive back-bonding in Ir complex **B** led to significant metallacyclopropane character [b)] (**Figure 1.15**).[118,119] Later work by Stone and co-workers expanded the scope of metal centers and fluoroalkenes.[120,121]

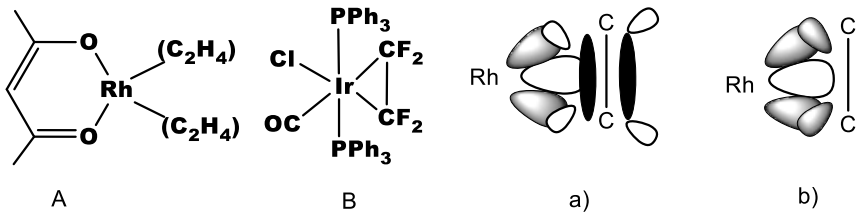

Figure 1.15 a) First metal complexes of TFE. b) Bonding schematic for metal alkene complex vs metallacyclopropane.

1.6.2.2 Metallacyclopentanes and bridged complexes

An early report of $Fe(CO)_3(TFE)_2$ by Nobelist G. Wilkinson[122] was shown in 1961 by Stone[123] to instead be the first example of a fluorometallacycle (**Figure 1.16**). The same group published another d^6 example with Co several years later[124] and then showed that steric bulk of the ancillary ligands dictated the size of Ni d^8 metallacycle formed. (**Scheme 1.17**).[125] In contrast, reaction of TFE with the zerovalent bis(diene) complex $Pt(cod)_2$ afforded the bis-$(C_2F_4)^{2-}$-bridged Pt(II) complex (cod = 1,5-cyclooctadiene; **Figure 1.17a**).[126] A similar reaction with hexafluoropropene (HFP) gave the carbene-bridged diplatinum product resulting from a fluoride shift (**Figure 1.15b**).[127]

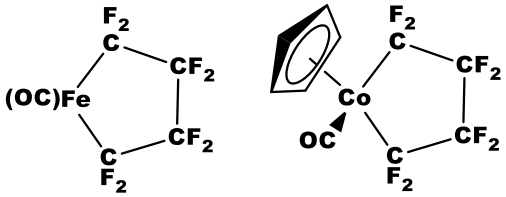

Figure 1.16. First perfluorometallacyclopentane complexes.[123,124]

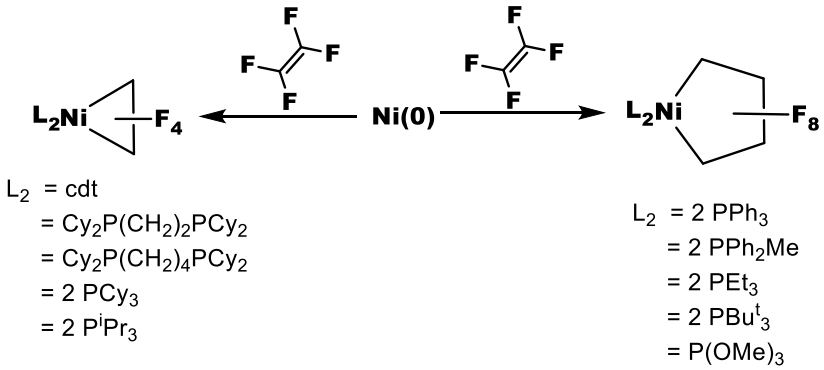

Scheme 1.17: Ligand effects in nickel perfluorometallacycle formation.[125]

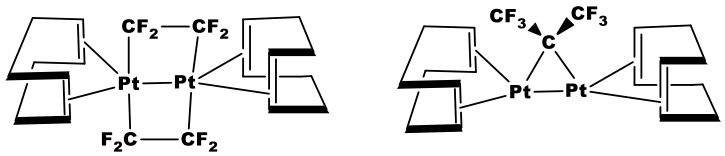

Figure 1.17. Fluorocarbon bridged complexes from TFE and HFP reactions with $Pt(cod)_2$.[124,125]

1.6.2.3 Metallacyclobutanes from metal fluorocarbenes

Baker et al. showed that nucleophilic d^8 cobalt fluorocarbenes[128] such as $CpCo{=}CF_2(PMePh_2)$ react with TFE to form stable fluorometallacyclobutanes[129] via an unusual radical pathway.[130] In the presence of Me_3SiOTf fluoride abstraction gives the *trans*-alkenyl complex whereas reversible fluoride abstraction using a catalytic amount (3-6 mol%) of $HNTf_2$ gave the metallacyclopropane via isomerization/ring contraction (**Scheme 1.18**). Synthesis of d^{10} nickel fluorocarbenes[131] then led to the first example of metal fluorocarbene metathesis (**Scheme 1.19**), shown to be an independent pathway to that which gives the metallacyclobutane.[132]

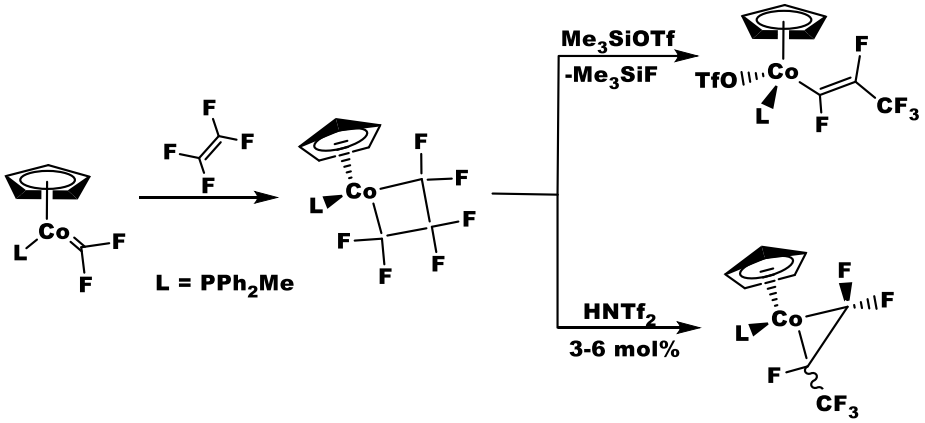

Scheme 1.18 Formation and C-F bond activation of perfluorocobaltacyclobutane complex.[129]

1.6.3 Fluoroalkene C-F Bond Activation by Metal Complexes

Although C-F bonds are typically stronger than C-H bonds,[133] the polarity of the former allows for its activation via fluoride ion abstraction as described for metallacyclobutanes above. Although a comprehensive review of C-F bond activation is beyond the scope of this introduction, several examples will be discussed so the reader can understand the potential impact of the work reported in Chapter 5.

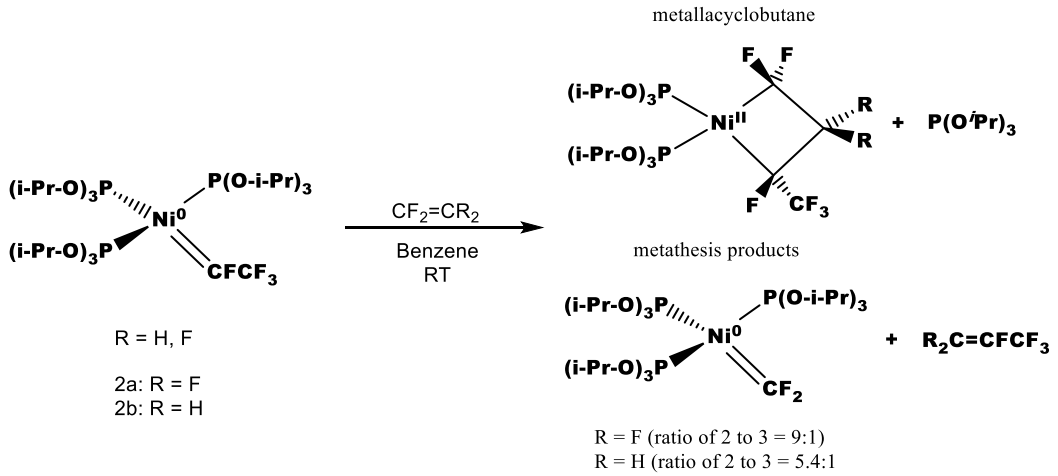

Scheme 1.19 Stoichiometric metathesis of nickel fluorocarbene and TFE.[132]

1.6.3.1 C(sp^3)-F bond activation (stoichiometric)

A number of studies have demonstrated the Lewis-acid promoted fluoride abstraction from fluorometallacycles such as the Pt examples in **Scheme 1.20**.[134] Burch and co-workers showed that treatment of a perfluoronickelacyclopentane with BF_3 induced phosphine migration to Cα (**Scheme 1.21**).[135] In 2013, Baker's group demonstrated a similar reaction with a [P,S]-ligated nickel complex.[136] Treatment of the resulting phosphonium zwitterion with the xylyl-isonitrile ligand induced cleavage of the Cβ-F bond affording a ring-opened product. In contrast, hydrolysis afforded a single isomer of the TFE dihydrodefluoro-dimerization product (**Scheme 1.22**).

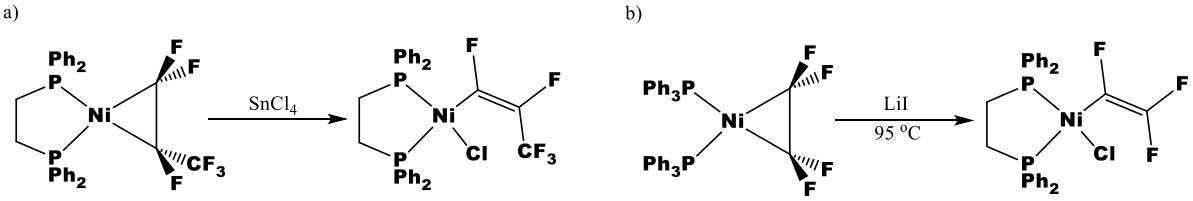

Scheme 1.20 Lewis acid-induced C-F bond activation in Pt perfluorometallacyclopropanes.[134]

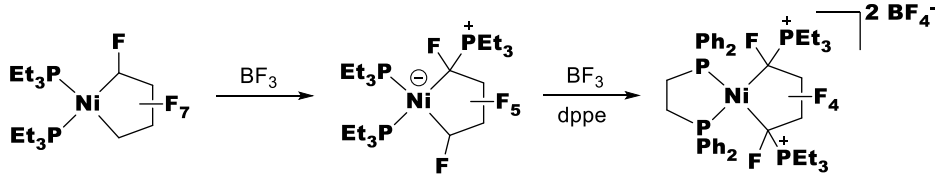

Scheme 1.21 Cα-F abstraction in Ni perfluorometallacycle.[135]

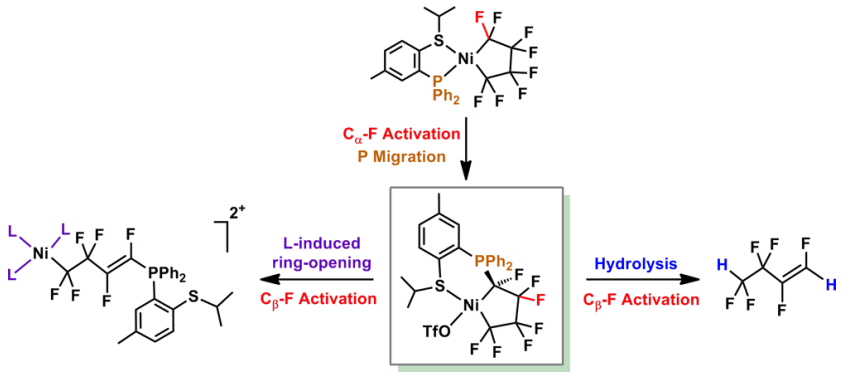

Scheme 1.22 Metallacycle Cα-F bond activation and resulting reactivity.[136]

1.6.3.2 C(sp^3)-F bond activation (catalytic)

Ogoshi's group reported the first example of C(sp^3)-F activation in trifluorotoluene which oxidatively adds to the nickel(0)-NHC (N-heterocyclic carbene) complex to afford *trans*-difluorobenzyl Ni(II) fluoride. Using silanes to convert Ni-F to Ni-H allowed for catalytic hydrodefluorination proceeding via a *syn*-S_N2' type mechanism (**Scheme 1.23**).[137]

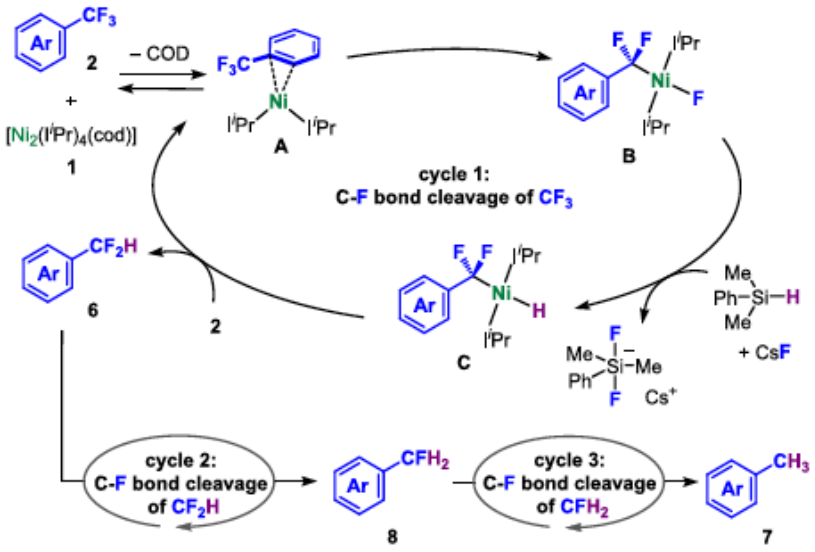

Scheme 1.23 C(sp^3)-F bond activation of fluoroarenes catalyzed by Ni-NHC.[137]

1.6.3.3 C(sp^2)-F bond activation (stoichiometric)

In 1997, Perutz's group reported the selective C-F bond activation of fluorinated heteroaromatics in which reactions of R-tetrafluoropyridine (R= H, F) with a nickel (0) complex successfully gave the desired product.[138] (**Scheme 1.24**). In 2002, Braun's group reported the Ni-mediated chemoselective C-X bond cleavage in which the bulkier phosphine ligand led to exclusive C-F

bond cleavage (**Scheme 1.25**).[139] The same group showed that $RhH(PEt_3)_3$ effected vinylic C-F bond activation of hexafluoropropene (HFP) in the presence of base (**Scheme 1.26**).[140] Presumably the extensive back-bonding from Rh to HFP allows for the Rh-H to be removed as a proton.

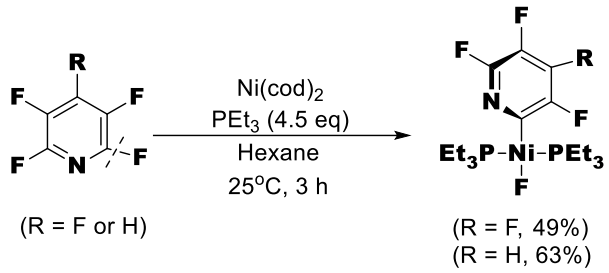

Scheme 1.24 C-F activation by nickel phosphine complex.[138]

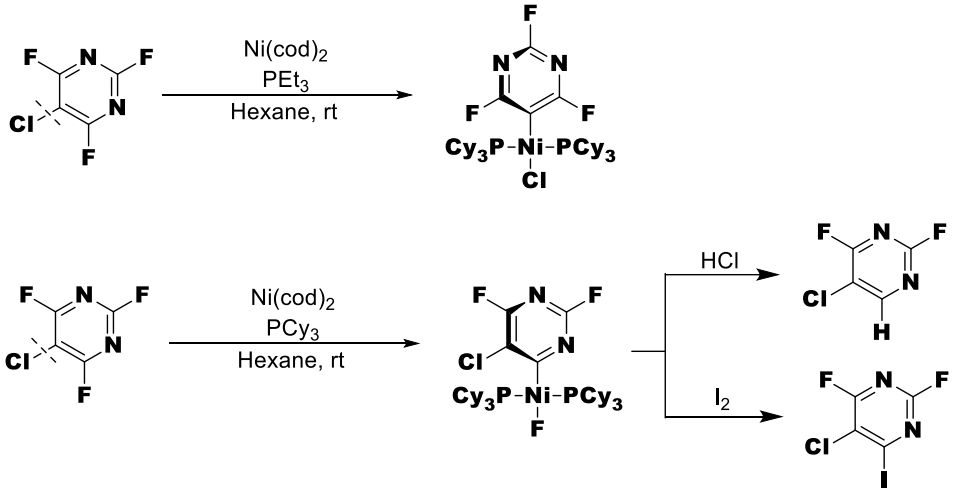

Scheme 1.25 Phosphine-dependent chemoselective C-X activation by nickel complex.[139]

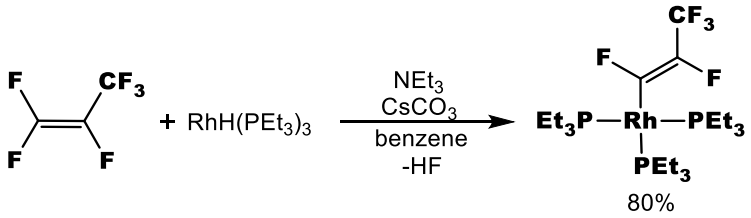

Scheme 1.26 Fluoroalkene C-F bond activation by rhodium hydride complex.[140]

The traditional pathway of nucleophilic substitution in organic synthesis goes through substitution at carbon that has halide anion as a good leaving group. Another possibility is nucleophilic attack at halogen (S_N^2Hal) with carbanion leaving group, first reported by Witting and Schollkopf[141] and Sunthankar and Gilman[142] for organolithiums in organic reactions known as halogenophilic reactions.[143] It was demonstrated that for reactions of halopentafluorobenzenes,

bromotrifluoroethylene[144-150] and other substrates, coupling of the carbanion and metal carbonyl halide intermediates is found to be a second reaction step giving the nucleophilic substitution product (**Scheme 1.27a**). Moreover, many other cases of nucleophilic vinylic or aromatic substitution with metal carbonyl anions undergo the traditional carbophilic addition–elimination (Ad_NE) pathway[147-150] (**Scheme 1.27b**).

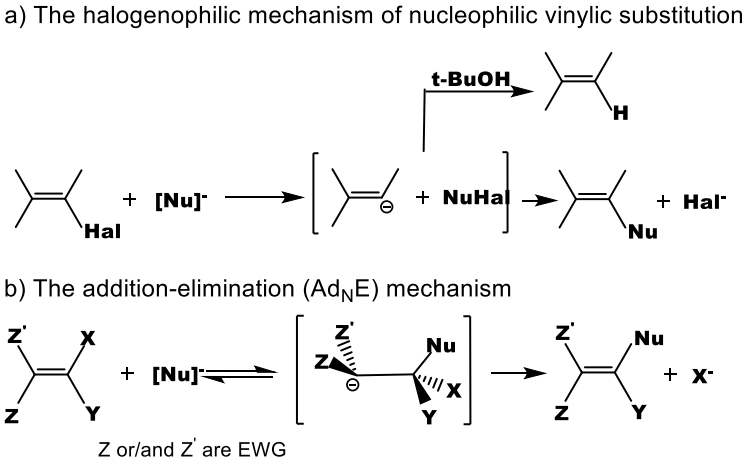

Scheme 1.27 Two different nucleophilic substitution mechanisms.

Transition metal carbonyl anions, carbonylmetallates, contain a large family of metal-centered anions that are relatively stable and easily accessible due to strong charge delocalization on the carbonyl ligands (**Scheme 1.28**). Thus, the counter cation M^* in complexes such as $M^*[M(CO)_nL]$ can coordinate to the carbonyl oxygen atom, as reported by Beletskaya et al. for lanthanide salts that can form i) ion pair with semi-bridging CO group (**Figure 1.18a**); ii) complete insertion of CO (**Figure 1.18b**) or iii) direct covalent Ln-M bond.[151] (**Figure 1.18c**). Hanna et al.[152] investigated supernucleophiles, such as $[CpFe(CO)_2]^-$ and even more powerful nucleophiles such as $[Re(CO)_5]^-$ demonstrating the viability of single electron transfer (SET) as an alternative to the usual S_N2 mechanism.

1.6.3.4. Nucleophilic vinylic substitution

The first report of carbonylmetallate reactions with polyfluorinated alkenyl halides by Beletskaya et al. in 2003 showed the nucleophilic vinylic substitution proceeded through the halogenophilic mechanism. They reported that reaction of $(CF_3)_3CCF=CFX$ (X=Cl, Br) and $CF_2=CFBr$ with $Na[Re(CO)_5]$ formed halo(acyl)rhenates, $Na[R_f CF=CFC(O)Re(CO)_4X]$, derived from alkenyl anion attack on the coordinated CO ligand (**Scheme 1.29**).[153] Using the same

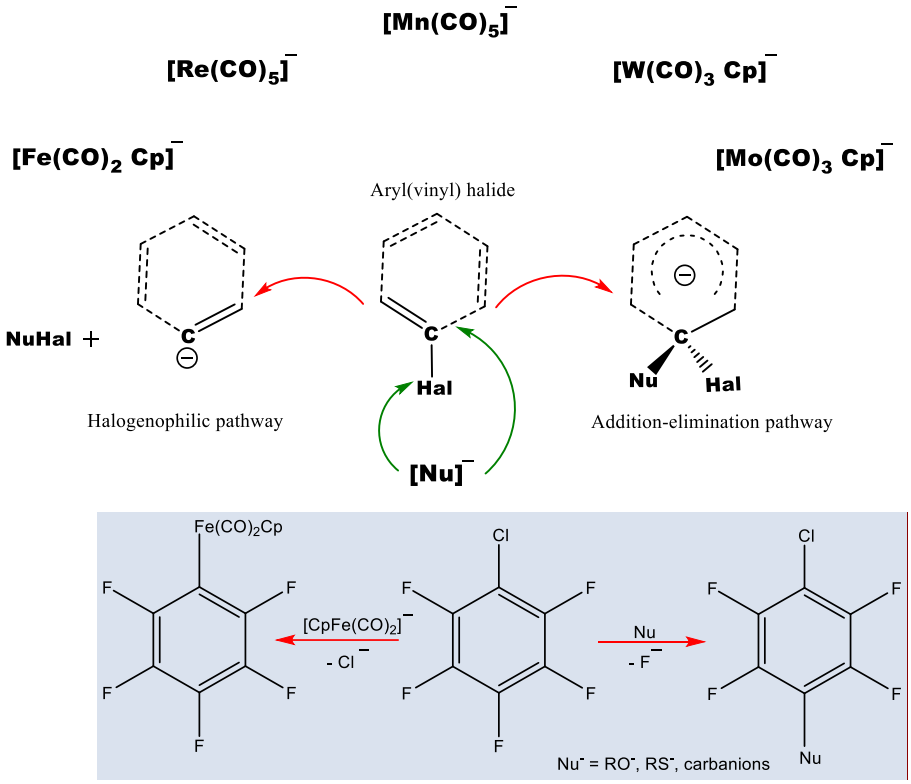

Scheme 1.28 C-X bond activation by halogenophilic (SET) or addition-elimination (Ad_NE) pathway.

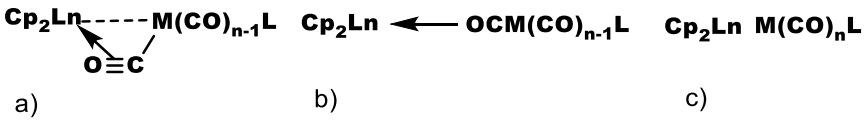

Figure 1.18 Bonding in lanthanide carbonylmetallate salts.[151]

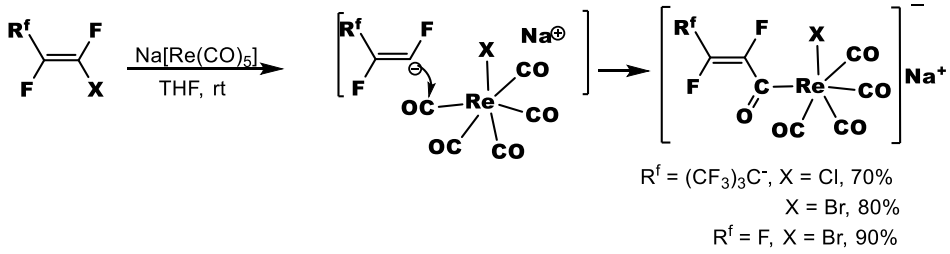

Scheme 1.29 Reaction of $Na[Re(CO)_5]$ with polyfluorinated alkenes.[153]

substrates with $K[CpFe(CO)_2]$ gave a more complicated product slate resulting from competing halogenophilic and Ad_NE pathways. (**Scheme 1.30**).[154] The ready dimerization of the $CpFe(CO)_2$ radical allows for some fluoride elimination from the fluoroalkenyl carbanion, thus generating the

reactive fluoroalkyne that gives rise to alkynyl iron product $CpFe(C{=}CPh)(CO)_2$ or $[CpFe(CO)_2]_2(\mu\text{-}C_2)$ from $CF_2{=}CFCl$. As expected, no acetylene-derived products were formed in presence of a proton source.

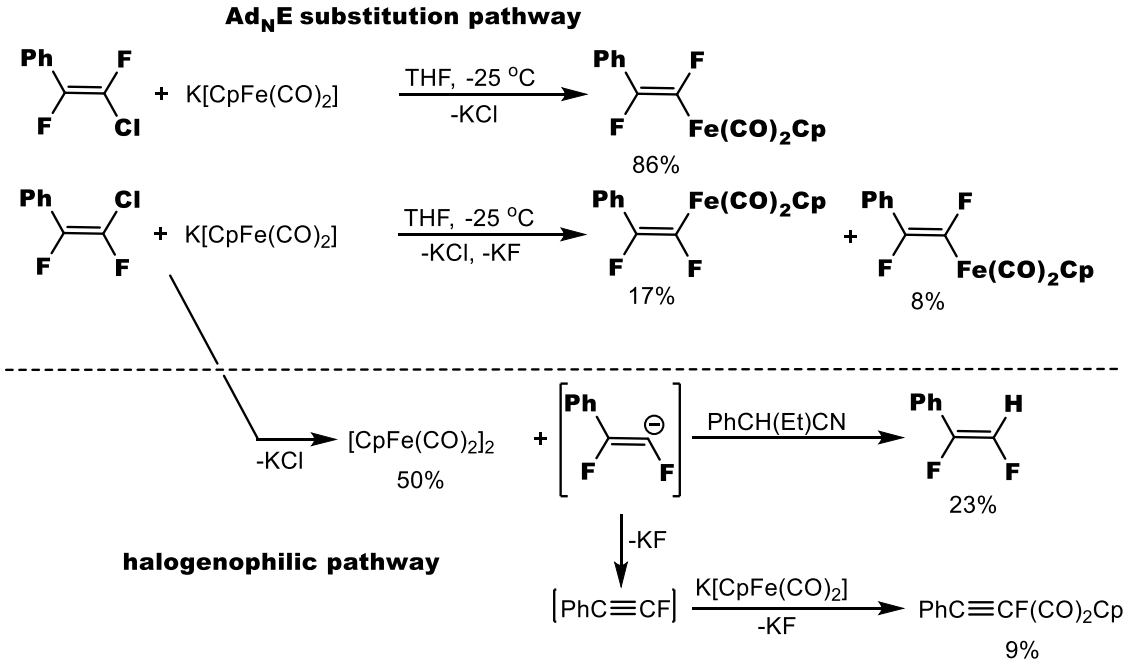

Scheme 1.30 Reactions of 2-chloro-1,2-difluorostyrene isomers with $K[CpFe(CO)_2]$.[154]

1.6.3.5 C(sp^2)-F bond activation (catalytic)

The catalytic hydrodefluorination of hexafluoropropene was reported first by Holland et al. They demonstrated that a catalytic amount of Fe(II) fluoride in the presence of triethylsilane yielded a mixture of 1,1,3,3,3-pentafluoropropene(E/Z) and 1,2,3,3,3-pentafluoropropene (**Scheme 1.31**).[155] NMR data and stoichiometric reactions showed that an iron(II) hydride was the active hydrodefluorination catalyst. In 2020, Tomson's group reported the Kumada cross-coupling of

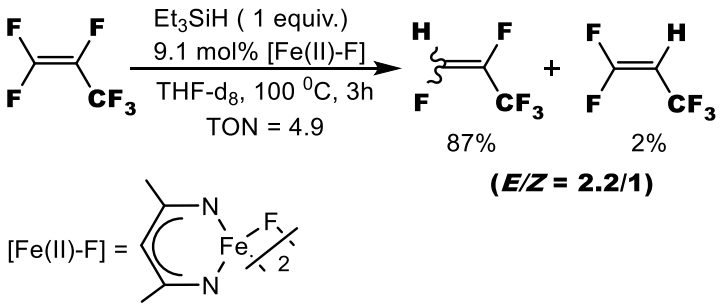

Scheme 1.31 Hydrodefluorination of hexafluoropropene catalyzed by iron complex.[155]

aryl Grignard reagents with fluoroarenes proposed to proceed through a palladium–magnesium bimetallic intermediate (**Scheme 1.32**).[156]

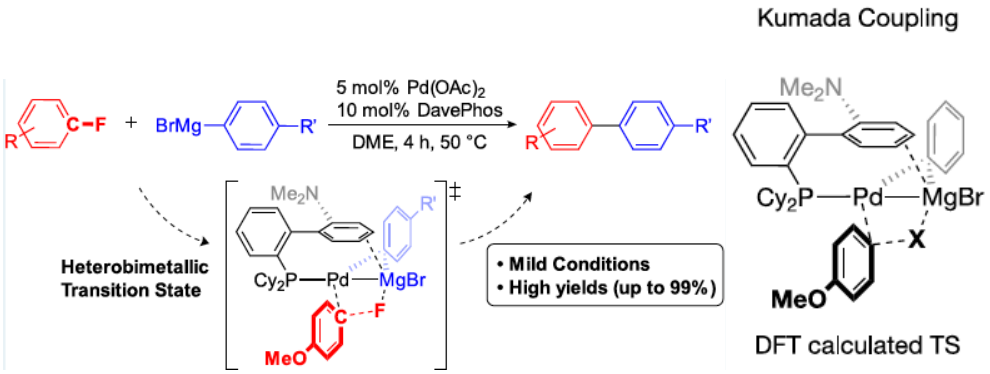

Scheme 1.32 Bimetallic Pd-Mg intermediate in catalyzed Kumada cross-coupling of fluoroarenes.[156]

1.7 Scope of Thesis Work

The work detailed in this thesis is the result of two different research experiences. First with Prof. Anindya Ghosh at the University of Arkansas at Little Rock (USA) (Chapter 2) and then with Prof. R. Tom Baker at the University of Ottawa (Chapters 3-5). In **Chapter 2** we applied an anionic nickel complex with a tridentate N,N,N ligand as a precatalyst for C-N cross coupling amination of aryl chlorides. The focus of the work was on catalyst lifetime so all reactions were conducted for 3 h using just 0.2 mol% catalyst. Our substrate scope included both primary and secondary alkyl- and arylamines with both electron-rich and electron-poor aryl chlorides. Kinetic studies and examples from prior publications pointed to a Ni(I)-Ni(III) catalytic cycle.

In the Baker group a previous PhD student investigated the iron coordination chemistry of an easily prepared, biomimetic SNS thiolate-imine-thioether ligand. In **Chapter 3** we explored the analogous chemistry with nickel that includes isolation of the first bis(thiolate) complex (**3-1**) with this ligand. Protonation of this complex gives a crystalline dicationic thiolate-bridged dimer (**3-3**) that is converted into a paramagnetic trinuclear complex upon dissolution in all solvents tested. The hemi lability of the thioether donor proved to be the source of the observed ligand dynamics. Nonetheless, addition of ancillary ligands to **3-3** gave a variety of mono- and dinuclear cations containing strong σ-donor ligands such as PMe_3 and π-acceptors such as $P(OMe)_3$ and CNxylyl. Using a strong donor *N*-heterocyclic carbene ligand, we demonstrated an alternate S-C bond cleavage pathway to the one known, allowing access to the neutral, mononuclear dithiolate complex.

Another feature of the SNS ligand is its ability to convert to a redox-active S_2N_2 ligand via imine C-C bond formation. In **Chapter 4** our electrochemical studies of **3-1** led to an improved synthetic route to the Ni(N_2S_2) complex (**3-2**). We identified three stable redox states and showed that doubly reduced $[Ni(N_2S_2)]^{2-}$ reacts reversibly with both phenol and carbon dioxide, although we did not investigate its use as an electrocatalyst for CO_2 reduction. In **Chapter 5** we discovered that singly reduced $[Ni(N_2S_2)]^{-}$ reacts cleanly with four different electron-acceptor fluoroalkenes, leading to a neutral Ni(II) fluoroalkenyl complex derived from C(sp^2)-F bond activation and/or an anionic Ni(II) fluoroalkyl complex resulting from electron transfer and H atom abstraction.

In **Chapter 6** we assess our results in light of the current state of the art and comment on future prospects for our work.

1.8 References

(1) Baldwin, W. H. The story of Nickel. I. How "Old Nick's" Gnomes Were Outwitted. *J. Chem. Ed*. **1931**, *9*, 1749-1761. doi:10.1021/ed008p1749.

(2) Jolly, P. W.; Wilke, G. *The Organic Chemistry of Nickel*: *Vol. 1 Organonickel Complexes* Elsevier, **1974**. https://doi.org/10.1016/B978-0-12-388401-5.X5001-5.

(3) Nickel - Element information, properties and uses | Periodic Table https://www.rsc.org/periodic-table/element/28/nickel.

(4) Mond, L.; Langer, C.; Quincke, F. The Action of Cabon Monoxide on Nickel. *J. Chem. Soc.* **1890**, *62*, 749.

(5) Che, M. Nobel Prize in Chemistry 1912 to Sabatier: Organic Chemistry or Catalysis? *Catal. Today* **2013**, *218-219*, 162-171.

(6) Wilke, G. Contributions to Organo-Nickel Chemistry. *Angew. Chem. Int. Ed. Engl.* **1988**, *27* (1), 185–206. https://doi.org/10.1002/anie.198801851.

(7) Keim, W. Oligomerization of Ethylene to α-Olefins: Discovery and Development of the Shell Higher Olefin Process (SHOP). *Angew. Chem. Int. Ed.* **2013**, *52* (48), 12492–12496. https://doi.org/10.1002/anie.201305308.

(8) Lutz, E. F. Shell Higher Olefins Process. *J. Chem. Ed.* **1986,** *63* (3), 202-203. https://doi.org/10.1021/ed063p202

(9) Tolman, C. A.; McKinney, R. J.; Seidel, W. C.; Druliner, J. D.; Stevens, W. R. Homogeneous Nickel-Catalyzed Olefin Hydrocyanation. *Adv. Catal.* **1985**, *33* (C), 1–46. https://doi.org/10.1016/S0360-0564(08)60257-6.

(10) Liu, K.; Zhang, S.; Han, M. Mechanistic Investigation on Hydrocyanation of Butadiene: A DFT Study. *Catalysts* **2020**, *10* (8), 818. https://doi.org/10.3390/catal10080818.

(11) Ogoshi, S., Ed. *Nickel Catalysis in Organic Synthesis*,Wiley, **2020**. https://doi.org/10.1002/9783527813827.

(12) Hu, X. Nickel-Catalyzed Cross Coupling of Non-Activated Alkyl Halides: A Mechanistic

Perspective. *Chem. Sci*. **2011**, *10*, 1867–1886. https://doi.org/10.1039/c1sc00368b.
(13) Boer, J. L.; Mulrooney, S. B.; Hausinger, R. P. *Arch. Biochem. Biophys.* **2014**, *544*, 142-152.
(14) Tsou, T. T.; Kochi, J. K. Mechanism of Oxidative Addition. Reaction of Nickel(0) Complexes with Aromatic Halides. *J. Am. Chem. Soc.* **1979**, *101* (21), 6319–6332. https://doi.org/10.1021/ja00515a028.
(15) Lanni, E. L.; McNeil, A. J. Mechanistic Studies on Ni(dppe)Cl_2-Catalyzed Chain-Growth Polymerizations: Evidence for Rate-Determining Reductive Elimination. *J. Am. Chem. Soc.* **2009**, *131* (45), 16573–16579. https://doi.org/10.1021/ja904197q.
(16) Li, B. J.; Yu, D. G.; Sun, C. L.; Shi, Z. J. Activation of "Inert" Alkenyl/Aryl C-O Bond and Its Application in Cross-Coupling Reactions. *Chem. Eur. J.* **2011**, *17* (6), 1728–1759. https://doi.org/10.1002/chem.201002273.
(17) Rosen, B. M.; Quasdorf, K. W.; Wilson, D. A.; Zhang, N.; Resmerita, A. M.; Garg, N. K.; Percec, V. Nickel-Catalyzed Cross-Couplings Involving Carbon-Oxygen Bonds. *Chem. Rev.* **2011**, *111* (3), 1346–1416. https://doi.org/10.1021/cr100259t.
(18) Mesganaw, T.; Garg, N. K. Ni- and Fe-Catalyzed Cross-Coupling Reactions of Phenol Derivatives. *Org. Proc. Res. Dev.* **2013**, *17* (1), 29–39. https://doi.org/10.1021/op300236f.
(19) Garcia, J. J.; Brunkan, N. M.; Jones, W. D. Cleavage of Carbon-Carbon Bonds in Aromatic Nitriles Using Nickel(0). *J. Am. Chem. Soc.* **2002**, *124* (32), 9547-9555. https://doi.org/10.1021/ja0204933.
(20) Tobisu, M.; Xu, T.; Shimasaki, T.; Chatani, N. Nickel-Catalyzed Suzuki-Miyaura Reaction of Aryl Fluorides. *J. Am. Chem. Soc.* **2011**, *133*, 19505–19511. https://doi.org/10.1021/ja207759e.
(21) Tasker, S. Z.; Standley, E. A.; Jamison, T. F. Recent Advances in Homogeneous Nickel Catalysis. *Nature* **2014**, *509*, 299–309. https://doi.org/10.1038/nature13274.
(22) Cornella, J.; Gómez-Bengoa, E.; Martin, R. Combined Experimental and Theoretical Study on the Reductive Cleavage of Inert C−O Bonds with Silanes: Ruling out a Classical Ni(0)/Ni(II) Catalytic Couple and Evidence for Ni(I) Intermediates. *J. Am. Chem. Soc.* **2013**, *135*,1997-2009. https://doi.org/10.1021/ja311940s.
(23) Lin, B.-L.; Liu, L.; Fu, Y.; Luo, S.-W.; Chen, Q.; Guo, Q.-X. Comparing Nickel-and Palladium-Catalyzed Heck Reactions. *Organometallics* **2004**, *23* (9), 2114-2123. https://doi.org/10.1021/om034067h.
(24) Lin, Q.; Diao, T. Mechanism of Ni-Catalyzed Reductive 1,2-Dicarbofunctionalization of Alkenes. *J. Am. Chem. Soc*. **2019**, *141*, 17937−1794.
(25) Chen, H.; Sun, S. H.; Liu, Y. A.; Liao, X. B. Nickel-Catalyzed Cyanation of Aryl Halides.
(26) Biswas, S.; Weix, D. J. Mechanism and Selectivity in Nickel-Catalyzed Cross-Electrophile Coupling of Aryl Halides with Alkyl Halides. *J. Am. Chem. Soc*. **2013**, *135*, 16192-16197. 10.1021/ja407589e.

(27) Ge, S.; Hartwig, J. F. Highly Reactive, Single-component Nickel Catalyst Precursor for Suzuki-Miyaura Cross-Coupling of Heteroaryl Boronic Acids with Heteroaryl Halides. *Angew. Chem. Int. Ed.***2012,** *51*, 12837-12841. https://doi.org/10.1002/anie.201207428.

(28) Ramgren, S. D.; Hie, L.; Ye, Y.; Garg, N. K. Nickel-Catalyzed Suzuki-Miyaura Couplings in Green Solvents. *Org. Lett.* **2013**, *15*, 3950-3953. https://doi.org/10.1021/ol401727y.

(29) Tobisu, M.; Chatani N. A. Cross-Couplings Using Aryl Ethers via C-O Bond Activation Enabled by Nickel Catalysts *Acc. Chem. Res.* **2015**, *48*, 1717-1726.

(30) Ho, G.-M.; Sommer, H.; Marek, I. Highly *E* -Selective, Stereoconvergent Nickel-Catalyzed Suzuki–Miyaura Cross-Coupling of Alkenyl Ethers. *Org. Lett.* **2019**, *21* (8), 2913–2917. https://doi.org/10.1021/acs.orglett.9b00946.

(31) Kocienski, P.; Dixon, N. Stereoselective Synthesis of Homoallylic Alcohols by Migratory Insertion Reactions of Higher-Order Cyanocuprates and Nickel-Catalysed Coupling Reactions Involving Enol Carbamates. *Synlett* **1989**, *1*, 52-54. DOI:10.1055/s-1989-34703

(32) Sengupta, S.; Leite, M.; Raslan, D. S.; Quesnelle, C.; Snieckus, V. Nickel(0)-Catalyzed Cross Coupling of Aryl O-Carbamates and Aryl Triflates with Grignard Reagents. Directed Ortho Metalation-Aligned Synthetic Methods for Polysubstituted Aromatics via a 1,2-Dipole Equivalent. *J. Org. Chem.* **1992**, *57* (15), 4066–4068. https://doi.org/10.1021/jo00041a004.

(33) Milburn, R. R.; Snieckus, V. The Tertiary Sulfonamide as a Latent Directed-Metalation Group: Ni^0-Catalyzed Reductive Cleavage and Cross-Coupling Reactions of Aryl Sulfonamides with Grignard Reagents. *Angew. Chem. Int. Ed.* **2004**, *43* (7), 888–891. https://doi.org/10.1002/anie.200352633.

(34) Dankwardt, J. W. Nickel-Catalyzed Cross-Coupling of Aryl Grignard Reagents with Aromatic Alkyl Ethers: An Efficient Synthesis of Unsymmetrical Biaryls. *Angew. Chem. Int. Ed.* **2004**, *43* (18), 2428–2432. https://doi.org/10.1002/anie.200453765.

(35) Tobisu, M.; Shimasaki, T.; Chatani, N. Nickel-Catalyzed Cross-Coupling of Aryl Methyl Ethers with Aryl Boronic Esters. *Angew. Chem. Int. Ed.* **2008**, *47* (26), 4866–4869. https://doi.org/10.1002/anie.200801447.

(36) Guan, B. T.; Wang, Y.; Li, B. J.; Yu, D. G.; Shi, Z. J. Biaryl Construction via Ni-Catalyzed C-O Activation of Phenolic Carboxylates. *J. Am. Chem. Soc.* **2008**, *130* (44), 14468–14470. https://doi.org/10.1021/ja8056503.

(37) Quasdorf, K. W.; Tian, X.; Garg, N. K. Cross-Coupling Reactions of Aryl Pivalates with Boronic Acids. *J. Am. Chem. Soc.* **2008**, *130* (44), 14422–14423. https://doi.org/10.1021/ja806244b.

(38) Guan, B.-T.; Xiang, S.-K.; Wang, B.-Q.; Sun, Z.-P.; Wang, Y.; Zhao, K.-Q.; Shi, Z.-J. Direct Benzylic Alkylation via Ni-Catalyzed Selective Benzylic sp^3 C−O Activation. *J. Am. Chem. Soc.* **2008**, *130* (11), 3268–3269. https://doi.org/10.1021/ja710944J.

(39) Taylor, B. L. H.; Swift, E. C.; Waetzig, J. D.; Jarvo, E. R. Stereospecific Nickel-Catalyzed Cross-Coupling Reactions of Alkyl Ethers: Enantioselective Synthesis of

Diarylethanes. *J. Am. Chem. Soc.* **2011**, *133* (3), 389–391. https://doi.org/10.1021/ja108547u.

(40) Greene, M. A.; Yonova, I. M.; Williams, F. J.; Jarvo, E. R. Traceless Directing Group for Stereospecific Nickel-Catalyzed Alkyl−Alkyl Cross-Coupling Reactions. *Org. Lett.* **2012**, *14* (16), 4293–4296. https://doi.org/10.1021/ol300891k.

(41) Zhou, Q.; Srinivas, H. D.; Dasgupta, S.; Watson, M. P. Nickel-Catalyzed Cross-Couplings of Benzylic Pivalates with Arylboroxines: Stereospecific Formation of Diarylalkanes and Triarylmethanes. *J. Am. Chem. Soc.* **2013**, *135* (9), 3307–3310. https://doi.org/10.1021/ja312087x.

(42) Lin, B. L.; Clough, C. R.; Hillhouse, G. L. Interactions of Aziridines with Nickel Complexes: Oxidative-Addition and Reductive-Elimination Reactions that Break and Make C−N Bonds. *J. Am. Chem. Soc.* **2002**, *124* (12), 2890-2891. https://doi.org/10.1021/JA017652N.

(43) Huang, C.-Y. (Dennis); Doyle, A. G. Nickel-Catalyzed Negishi Alkylations of Styrenyl Aziridines. *J. Am. Chem. Soc.* **2012**, *134* (23), 9541–9544. https://doi.org/10.1021/ja3013825.

(44) Cho, S. H.; Kim, J. Y.; Kwak, J.; Chang, S. Recent Advances in the Transition Metal-Catalyzed Twofold Oxidative C-H Bond Activation Strategy for C-C and C-N Bond Formation. *Chem. Soc. Rev* **2011**, *5*, 5068–5083. https://doi.org/10.1039/c1cs15082k.

(45) Hili, R.; Yudin, A. K. Making Carbon-Nitrogen Bonds in Biological and Chemical Synthesis. *Nat. Chem. Biol.* **2006**, *2* (6), 284–287. https://doi.org/10.1038/nchembio0606-284.

(46) Goldberg, I. Ueber Phenylirungen Bei Gegenwart von Kupfer Als Katalysator. *Berichte der Dtsch. Chem. Gesellschaft* **1906**, *39* (2), 1691–1692. https://doi.org/10.1002/cber.19060390298.

(47) Ullmann, F. Ueber Eine Neue Bildungsweise von Diphenylaminderivaten. *Berichte der Dtsch. Chem. Gesellschaft* **1903**, *36* (2), 2382–2384. https://doi.org/10.1002/cber.190303602174.

(48) Bariwal, J.; Van der Eycken, E. C–N Bond Forming Cross-Coupling Reactions - An Overview. *Chem. Soc. Rev.* **2013**, *44*, 9283-9303. https://doi.org/10.1039/C3CS60228A.

(49) Hughes, E. C.; Veatch, F.; Elersich, V. *N*-Methylaniline from Chlorobenzene and Methylamine. *Ind. Eng. Chem.* 1**950**, *42* (5) 787-790.

(50) Cramer, R.; Coulson, D. R. Nickel-Catalyzed Displacement Reactions of Aryl Halides. *J. Org. Chem.* **1975**, *40* (16), 2267-2273.

(51) Manolikakes, G.; Gavryushin, A.; Knochel, P. An Efficient Silane-Promoted Nickel-Catalyzed Amination of Aryl and Heteroaryl Chlorides. *J. Org. Chem.* **2008**, *73* (4), 1429-1434. https://doi.org/10.1021/JO7022558. https://doi.org/10.1021/JO702219F.

(52) Matsubara, K.; Ueno, K.; Koga, Y.; Hara, K. Nickel−NHC-Catalyzed α-Arylation of Acyclic Ketones and Amination of Haloarenes and Unexpected Preferential N-Arylation of 4-Aminopropiophenone. *J. Org. Chem.* **2007**, *72* (14), 5069-5076.

https://doi.org/10.1021/JO070313D.
(53) Desmarets, C.; Schneider, R.; Fort, Y.; Walcarius, A. 1,3,5-Tris(4-Aminophenyl)Benzene Derivatives: Design, Synthesis via Nickel-Catalysed Aromatic Amination and Electrochemical Properties. *J. Chem. Soc. Perkin Trans. 2* **2002**, *11*, 1844–1849. https://doi.org/10.1039/b206689k.
(54) Omar-Amrani, R.; Thomas, A.; Brenner, E.; Schneider, R.; Fort, Y. Efficient Nickel-Mediated Intramolecular Amination of Aryl Chlorides. *Org. Lett.* **2003**, *5* (13), 2311-2314. https://doi.org/10.1021/OL034659W.
(55) Wolfe, J. P.; Buchwald, S. L. Nickel-Catalyzed Amination of Aryl Chlorides. *J. Am. Chem Soc.* **1997**, *119* (26), 6054-6058. https://doi.org/10.1021/JA964391M.
(56) Marín, M.; Rama, R. J.; Nicasio, M. C. Ni-Catalyzed Amination Reactions: An Overview. *Chem. Rec.* **2016**, 1819–1832. https://doi.org/10.1002/tcr.201500305.
(57) Gao, C.-Y.; Yang, L. M. Nickel-Catalyzed Amination of Aryl Tosylates. *J. Org. Chem.* **2008**, *73* (4), 1624-1627. https://doi.org/10.1021/JO7022558.
(58) Tobisu, M.; Shimasaki, T.; Chatani, N. Ni^0-Catalyzed Direct Amination of Anisoles Involving the Cleavage of Carbon–Oxygen Bonds. *Chem. Lett.* **2009**, *38* (7), 710–711. https://doi.org/10.1246/cl.2009.710.
(59) Tobisu, M.; Yasutome, A.; Yamakawa, K.; Shimasaki, T.; Chatani, N. Ni(0)/NHC-Catalyzed Amination of *N*-Heteroaryl Methyl Ethers through the Cleavage of Carbon–Oxygen Bonds. *Tetrahedron* **2012**, *68* (26), 5157–5161. https://doi.org/10.1016/J.TET.2012.04.005.
(60) Shimasaki, T.; Tobisu, M.; Chatani, N. Nickel-Catalyzed Amination of Aryl Pivalates by the Cleavage of Aryl C-O Bonds. *Angew. Chem.* **2010**, *49* (16), 2929–2932. https://doi.org/10.1002/anie.200907287.
(61) Mesganaw, T.; Silberstein, A. L.; Ramgren, S. D.; Nathel, N. F. F.; Hong, X.; Liu, P.; Garg, N. K. Nickel-Catalyzed Amination of Aryl Carbamates and Sequential Site-Selective Cross-Couplings. *Chem. Sci.* **2011**, *2* (9), 1766. https://doi.org/10.1039/c1sc00230a.
(62) Ramgren, S. D.; Silberstein, A. L.; Yang, Y.; Garg, N. K. Nickel-Catalyzed Amination of Aryl Sulfamates. *Angew. Chem. Int. Ed.* **2011**, *50* (9), 2171–2173. https://doi.org/10.1002/anie.201007325.
(63) Huang, J.-H.; Yang, L.-M. Nickel-Catalyzed Amination of Aryl Phosphates through Cleaving Aryl C–O Bonds. *Org. Lett.* **2011**, *13* (14), 3750–3753. https://doi.org/10.1021/ol201437g.
(64) Tobisu, M.; Shimasaki.; T.; Chatani, N. Ni^0-catalyzed Direct Amination of Anisoles Involving the Cleavage of Carbon–Oxygen Bonds. *Chem. Lett.* **2009**, *38*, 710. https://doi.org/10.1246/cl.2009.710
(65) Ackermann, L.; Sandmann, R.; Song, W. Palladium- and Nickel-Catalyzed Aminations of Aryl Imidazolylsulfonates and Sulfamates. *Org. Lett.* **2011**, *13*, 1784. https://doi.org/10.1021/ol200267b

(66) Tobisu, M.; Takahira, T.; Chatani, N. Nickel-Catalyzed Cross-Coupling of Anisoles with Alkyl Grignard Reagents via C–O Bond Cleavage. *Org. Lett.* **2015**, *17* (17), 4352–4355. https://doi.org/10.1021/acs.orglett.5b02200.

(67) Yue, H.; Guo, L.; Liu, X.; Rueping, M. Nickel-Catalyzed Synthesis of Primary Aryl and Heteroaryl Amines via C−O Bond Cleavage. *Org. Lett.* **2017**, 19, 1788-1791.

(68) Shekhar, S.; Ryberg, P.; Hartwig, J. F., Mathew, J. S., Blackmond, D. G., Strieter, E. R.; Buchwald, S. L. Reevaluation of the Mechanism of the Amination of Aryl Halides Catalyzed by BINAP-Ligated Palladium Complexes. *J. Am. Chem. Soc.* **2006**, 128, 3584-3591.

(69) Gao, C.-Y.; Cao, X.; Yang, L.-M. Nickel-Catalyzed Cross-Coupling of Diarylamines with Haloarenes. *Org. Biomol. Chem.* **2009**, *7* (19), 3922. https://doi.org/10.1039/b911286c.

(70) Nagao, S.; Matsumoto, T.; Koga, Y.; Matsubara, K. Monovalent Nickel Complex Bearing a Bulky *N*-Heterocyclic Carbene Catalyzes Buchwald-Hartwig Amination of Aryl Halides under Mild Conditions. *Chem. Lett.* **2011,** *40*, 1036-1038.

(71) Kampmann, S. S.; Sobolev, A. N.; Koutsantonis, G. A.; Stewart, S. G. Stable Nickel(0) Phosphites as Catalysts for C-N Cross-Coupling Reactions. *Adv. Synth. Catal.***2014**, *356*, 1967–1973.

(72) Li, X.-L.; Wu, W.; Fan, X.-H.; Yang, L.-M. Nickel-catalyzed Triarylamine Synthesis: Synthetic and Mechanistic Aspects. *Org. Biomol. Chem.* **2014**, *12*, 1232.

(73) Matsubara, K.; Ueno, K.; Shibata, Y. Synthesis and Structures of Nickel Halide Complexes Bearing Mono- and Bis-coordinated N-Heterocyclic Carbene Ligands, Catalyzing Grignard Cross-Coupling Reactions. *Organometallics* **2006**, *5*, 3422-3427. https://doi.org/10.1021/OM0602658.

(74) Desmarets, C.; Schneider, R.; Fort, Y. Nickel(0)/Dihydroimidazol-2-ylidene Complex Catalyzed Coupling of Aryl Chlorides and Amines. *J. Org. Chem.* **2002**, *67*, 3029-3036.

(75) Ge, S.; Green, R. A.; Hartwig, J. F. Controlling First-Row Catalysts: Amination of Aryl and Heteroaryl Chlorides and Bromides with Primary Aliphatic Amines Catalyzed by a BINAP-Ligated Single-Component Ni(0) Complex. *J. Am. Chem. Soc.* **2014**, *136*, 1617-1627.

(76) Kampmann, S. S.; Skelton, B. W.; Wild, D. A.; Koutsantonis, G. A.; Stewart, S. G. An Air-Stable Nickel(0) Phosphite Precatalyst for Primary Alkylamine C-N Cross-Coupling Reactions. *Eur. J. Org. Chem.* **2015**, 5995–6004.

(77) Inatomi, T.; Fukahori, Y.; Yamada, Y.; Ishikawa, R.; Kanegawa, S.; Koga, Y.; Matsubara, K. Ni(I)-Ni(III) Cycle in Buchwald-Hartwig Amination of Aryl Bromide Mediated by NHC-ligated Ni(I) Complexes. C*atal. Sci. Technol.* **2019**, 9, 1784-1793.

(78) Ragsdale, S. W. Metals and Their Scaffolds to Promote Difficult Enzymatic Reactions. *Chem. Rev.* **2006**, *106*, 3317-3337.

(79) Wittkamp, F.; Senger, M.; Stripp, S. T.; Apfel, U.-P. [FeFe]-Hydrogenases: Recent Developments and Future Perspectives. *Chem. Commun.* **2018**, *47*, 5934-5942.

(80) a) Shafaat, H. S.; Rudiger, O.; Ogata, H.; Lubitz, W. [NiFe]-Hydrogenases: A Common Active Site for Hydrogen Metabolism under Diverse Conditions. *Biochim. Biophys. Acta - Bioenergetics* **2013**, *1827*, 986-1002. b) Ogata, H.; Lubitz, W.; Higuchi, Y. Structure and Function of [NiFe]-Hydrogenases. *J. Biochem.* **2016**, *160*, 251-258.

(81) P. E. M. Siegbahn, S. L. Chen and R. Z. Liao. Theoretical Studies of Nickel-Dependent Enzymes. *Inorganics* **2019**, *7*, 95.

(82) Barton, B. E.; Whaley, C. M.; Rauchfuss, T. B.; Gray, D. L. Nickel-Iron Dithiolato Hydrides Relevant to the [NiFe]-Hydrogenase Active Site. *J. Am. Chem. Soc.* **2009**, *131*, 6942-6943.

(83) Weber, K.; Krämer, T.; Shafaat, H. S.; Weyhermüller, T.; Bill, E.; van Gastel, M.; Neese, F.; Lubitz, W. A Functional [NiFe]-Hydrogenase Model Compound that Undergoes Biologically Relevant Reversible Thiolate Protonation. *J. Am. Chem. Soc.* **2012**, *134*, 20745-20755.

(84) DuBois, D. L.; Bullock, R. M. Molecular Electrocatalysts for the Oxidation of Hydrogen and the Production of Hydrogen: The Role of Pendant Amines as Proton Relays. *Eur. J. Inorg. Chem.* **2011**, 1017-1027.

(85) Sheng, Y.; Abreu, I. A.; Cabelli, D. E.; Maroney, M. J.; Miller, A.-F.; Teixeira, M.; Valentine, J. S. Superoxide Dismutases and Superoxide Reductases. *Chem. Rev.* **2014**, *114*, 3854-3918.

(86) Shearer, J. Insight into the Mechanism of Nickel-Containing Superoxide Dismutases Derived from Peptide-Based Mimics. *Acc. Chem. Res.* **2014**, *47*, 2332-2341.

(87) Tietze, D.; Sartorius, J.; Seth, B. K.; Herr, K.; Heimer, P.; Imhof, D.; Mollenhauer, D.; Buntkowsky, G. New Insights into the Mechanisms of Nickel Superoxide Degradation from Studies of Model Peptides. *Nat. Sci. Rep.* **2017**, *7*, 17194.

(88) Can, M.; Armstrong, F. A.; Ragsdale, S. W. Structure, Function, and Mechanism of the Nickel Metalloenzymes, CO Dehydrogenase and Acetyl-CoA Synthase. *Chem. Rev.* **2014**, *114*, 4149-4174.

(89) Seravelli, J.; Gu, W.; Tam, A.; Strauss. E.; Begley, T. P.; Cramer, S. P. Functional Copper at the Acetyl-CoA Synthase Active Site. *Proc. Natl. Acad. Sci.* **2003**, *100* (7), 3689-3694.

(90) Rao, P. V.; Bhaduri, S.; Jiang, J.; Holm, R. H. Sulfur Bridging Interactions of Cis-planar Ni^{II}-S_2N_2 Coordination Units with Nickel(II), Copper(I,II), Zinc(II), and Mercury(II): A Library of Bridging Modes, Including $Ni^{II}(\mu^2\text{-}SR)_2M^{I,II}$ Rhombs. *Inorg. Chem.* **2004**, *43*, 5833–5849.

(91) Blacquiere, J. M. Structurally-Responsive Ligands for High Performance Catalysts. *ACS Catal.* **2021**, *11* (9), 5416-5437.

(92) a) Braunstein, P. & Naud, F. Hemilability of Hybrid Ligands and the Coordination Chemistry of Oxazoline-based Systems. *Angew. Chem. Int. Ed.* **2001**, *40*, 680–699. b) Slone, C. S.; Weinberger, D. A.; Mirkin, C. A. *Prog. Inorg. Chem.* **1999**, *48*, 233-350.

(93) Bassetti, M. Kinetic Evaluation of Ligand Hemilability in Transition Metal Complexes. *Eur. J. Inorg. Chem.* **2006,** 4473–4482.

(94) Bassetti, M., Capone, A. & Salamone, M. Kinetic Evidence of an Arm-Off Mechanism in Complexes of Hemilabile Hybrid Ligands. Oxidative Addition of Methyl Iodide to the Rhodium(I) Complex [Rh(2,6-bis(benzylthiomethyl)pyridine)(CO)]PF_6 via Competitive Pathways. *Organometallics* **2004**, *23*, 247–252.

(95) Schnödt, J.; Manzur, J.; García, A.-M.; Hartenbach, I.; Su, C.-Y.; Fiedler, J.; Kaim, W. Coordination of a Hemilabile N,N,S Donor Ligand in the Redox System $[CuL_2]^{+/2+}$, L = 2-Pyridyl-*N*-(2′-alkylthio-phenyl)methyleneimine. *Eur. J. Inorg. Chem.* **2011**, 1436-1441.

(96) Hübner, R.; Weber, S.; Strobel, S.; Sarkar, B.; Zalis, S.; Kaim, W. Reversible Intramolecular Single-electron Oxidative Addition Involving a Hemilabile Noninnocent Ligand. *Organometallics* **2011**, *30*, 1414–1418.

(97) a) Hirotsu, M.; Santo, K.; Tanaka, Y.; Kinoshita, I. Iron Carbonyl Complexes of N,C,S-Pincer Ligands with a Pendant Thioether Arm: Synthesis, Structures and Reactivity. *Polyhedron* **2018**, *143*, 201–208 . b) Santo, K.; Hirotsu. M.; Kinoshita. I. Formation, reactivity and redox properties of carbon- and sulfur-bridged diiron complexes derived from dibenzothienyl Schiff bases: effect of N,N- and N,P-chelating moieties. *Dalton Trans.* **2015**, *44*, 4155. https://doi.org/10.1039/C4DT03422H.

(98) Thompson, M. C.; Busch, D. H. Reactions of Coordinated Ligands. IX. Utilization of the Template Hypothesis to Synthesize Macrocyclic Ligands *in Situ. J. Am. Chem. Soc.* **1964,** *86*, 3651.

(99) Jicha, D. C.; Busch, D. H. Complexes Derived from Strong Field Ligands. XIV. Heterotrimetallic Trinuclear Complexes of β-Mercatoethylamine. *Inorg. Chem.* **1962**, *1*, 878-883.

(100) Wei, C. W.; Dahl, L. F. Structural Characterization of Crystalline Tetrakis (2-aminoethanethiol) trinickel (II) chloride. **1970**, *9*, 1878–1887.

(101) Denny, J. A.; Darensbourg, M. Y. Metallodithiolates as Ligands in Coordination, Bioinorganic, and Organometallic Chemistry. *Chem. Rev.* **2015**, *115*, 5248–5273.

(102) Stibrany, R. T.; Fox, S.; Bharadwaj, P. K.; Schugar, H. J.; Potenza, J. A. Structural and Spectroscopic Features of Mono-and Binuclear Nickel(II) Complexes with Tetradentate $N(amine)_2$ $S(thiolate)_2$ Ligation. *Inorg. Chem.* **2005**, *44*, 8234-8242.

(103) Kawamoto, T.; Kuma, H.; Kushi, Valence Isomerization. Synthesis and Characterization of Cobalt and Nickel Complexes with Non-Innocent N_2S_2 Ligand. *Bull. Chem. Soc. Jpn.* **1997**, *70*, 1599-16046.

(104) Kawamoto, T.; Takeda, K.; Nishiwaki, M.; Aridomi, T.; Konno, T. Square-Planar $N_2S_2Ni^{II}$ Complexes with an Extended π-Conjugated System. *Inorg. Chem.* **2007**, *46*, 4239-4237.

(105) Fierro, C. M.; Murphy, B. P.; Smith, P. D.; Coles, S. J.; Hursthouse, M. B. The Formation and Isolation of Benzisothiazole Rings from the Reactions of Oxime-thiophenolate Ligands. *Inorg. Chim. Acta* **2006**, *359*, 2321–2327. https://doi.org/10.1016/J.ICA.2005.11.047.

(106) Henderson, R. K.; Bouwman, E.; Reedijk, J; Powell, A. K. [N,N'-Bis(2-thiobenzylidene)-

1,2-dimethyl-4,5-phenylenediaminato]nickel(II), Ni(tsaldimph). *Acta Crystallogr. Sect. C Cryst. Struct. Commun.* **1996,** *52*, 2696–2698.

(107) Stenson, P. A.; Board, A.; Marin-Becerra, A.; Blake, A. J.; Davies, E. S.; Wilson, C.; McMaster, J.; Schröder, M. Molecular and Electronic Structures of One-Electron Oxidized Ni^{II}–(Dithiosalicylidenediamine) Complexes: Ni^{III}–Thiolate versus Ni^{II}–Thiyl Radical States. *Chem. Eur. J.* **2008**, *14*, 2564–2576.

(108) Smeets, W. J. J.; Spek, A. L.; Henderson, R. K.; Bouwman, E.; Reedijk, J. [*N*,*N*'-Bis(2-thiobenzylidene)-1,2-phenylenediaminato]nickel(II). *Acta Crystallogr. Sect. C Cryst. Struct. Commun.* **1997,** *53*, 1564–1566.

(109) Yamamura, T.; Tadokoro, M.; Tanaka, K.; Kuroda, R. Syntheses and Structures of Ni S_2N_2 Compounds. [*N*,*N* ′-Bis(*o*-mercaptobenzyliden)ethylenediaminato]nickel(II), Ni(tsalen), and [*N*,*N* ′-Bis(*o*-mercaptobenzyl)ethylenediaminato]nickel(II), Ni(ebmba). *Bull. Chem. Soc. Jpn.* **1993**, *66*, 1984–1990.

(110) Goswami, N.; Eichhorn, D. M. Incorporation of Thiolate Donation using 2,2′-Dithiodibenzaldehyde: Synthesis of Ni, Fe, and Cu Complexes. Crystal Structures of [M(tsalen)] (tsalen=N,N′-ethylenebis(thiosalicylidene)imine); M=Cu, Ni) showing a tetrahedral distortion of Cu(tsalen). *Inorg. Chim. Acta* **2000**, *303*, 271–276.

(111) Rampersad, M. V.; Zuidema, E.; Ernsting, J. M.; Van Leeuwen, P. W. N. M.; Darensbourg, M. Y. CO and Ethylene Migratory Insertion Reactions and Copolymerization Involving Palladium Complexes of a NiN_2S_2 Metallodithiolate Ligand. *Organometallics* **2007**, *26*, 783–792.

(112) Ittel, S. D.; Johnson, L. K.; Brookhart, M. Late-metal Catalysts for Ethylene Homo- and Copolymerization. *Chem. Rev.* **2000**, *100*, 1169–1203.

(113) Ogo, S.; Kabe, R.; Uehara, K.; Kure, B.; Nishimura, T.; Menon, S. C.; Harada, R.; Fukuzumi, S.; Higuchi, Y.; Ohhara, T.; Tamada, T.; Kuroki, R. A Dinuclear Ni(μ-H)Ru Complex Derived from H_2. *Science* **2007**, *316*, 585–588.

(114) Ogo, S.; Ichikawa, K.; Kishima, T.; Matsumoto, T.; Nakai, H.; Kusaka, K.; Ohhara, T. A Functional [NiFe]Hydrogenase Mimic that Catalyzes Electron and Hydride Transfer from H_2. *Science* **2013**, *339*, 682–684.

(115) Ritter, S. K. The Shrinking Case For Fluorochemicals. *Chem. Eng. News* **2015**, *93*(28), 27. https://doi.org/10.1021/cen-09328-scitech1

(116) Bell, I. H.; Domanski, P. A.; McLinden, M. O.; Linteris, G. T. The Hunt for Nonflammable Refrigerant Blends to Replace R-134a. *Int. J. Refrig.* **2019**, *104*, 484–495. https://doi.org/10.1016/j.ijrefrig.2019.05.035.

(117) Lantaño, B.; Torviso, M. R.; Bonesi, S. M.; Barata-Vallejo, S.; Postigo, A. Advances in Metal-Assisted Non-Electrophilic Fluoroalkylation Reactions of Organic Compounds. *Coord. Chem. Rev.* **2015**, *285*, 76–108. https://doi.org/10.1016/j.ccr.2014.11.004.

(118) Parshall, G. W.; Jones, F. N. Fluoroolefin Complexes of Transition Metals. *J. Am. Chem. Soc.* **1965**, *87* (23), 5356–5361. https://doi.org/10.1021/ja00951a017.

(119) Cramer, R.; Parshall, G. W. Tetrafluoroethylene Complexes of Transition Metals. *J. Am. Chem. Soc.* **1965**, *87* (6), 1392–1393. https://doi.org/10.1021/ja01084a048.
(120) Treichel P.; F. G. A. Stone. Fluorocarbon Derivatives of Metals. *Adv. Organomet. Chem.* **1964**, *1*, 143–220. https://doi.org/10.1016/S0065-3055(08)60067-2.
(121) Stone, F. G. A. *Leaving No Stone Unturned: Pathways in Organometallic Chemistry*. Wiley VCH, **1993**. https://doi.org/10.1002/anie.199421191.
(122) a) Watterson, K. F.; Wilkinson, G. *Chem. Ind.* 1960, 1358. b) Hoehn, H. H.; Pratt, L.; Watterson, K. F.; Wilkinson, G. Transition-Metal Fluorocarbon Complexes. 1. Derivatives of Perfluoro-olefins. *J. Chem. Soc.* **1961**, 2738-2745. https://doi.org/10.1039/JR9610002738.
(123) Manuel, T. A.; Stafford, S. L.; Stone, F. G. A. Chemistry of the Metal Carbonyls. VII. Perfluoroalkyl Iron Compounds. *J. Am. Chem. Soc.* **1961,** *83* (1), 249–250. https://doi.org/10.1021/ja01462a052.
(124) Coyle, T. D.; King, R. B.; Pitcher, E.; Stafford, S. L.; Teichel, P.; Stone, F. G. A. A Novel Heterocyclic Cobalt Compound. *J. Inorg. Nucl. Chem*. **1961**, 172–173. https://doi.org/10.1016/0022-1902(61)80481-8.
(125) a) Browning, J.; Cundy, C. S.; Green, M.; Stone, F. G. A. Hexafluoroacetone and Hexafluorothioacetone Nickel Complexes. *J. Chem. Soc. A* **1969**, 20–23. `https://doi.org/10.1039/J19690000020. b) Cundy, C. S.; Green, M.; Stone, F. G. A. Reactions of Low-valent Metal Complexes with Fluorocarbons. Part XII. Fluoro-olefin Reactions of Zerovalent Nickel Complexes *J. Chem. Soc. (A)*, **1970**, 1647-1653.
(126) Maples, P. K.; Green, M.; Stone, F. G. A. *J. Chem. Soc., Dalton Trans.* **1973**, 2069.
(127) Hacker, M. J.; Littlecott, G. W.; Kemmitt, R. D. W. Reactions of fluoro-olefins, chloro-olefins and related molecules with carbonatobis(triphenylarsine)platinum(II) in ethanol *J. Organomet. Chem.* **1973**, *47*, 189.
(128) Harrison, D. J.; Gorelsky, S. I.; Lee, G. M.; Korobkov, I.; Baker, R. T. Cobalt Fluorocarbene Complexes. *Organometallics* **2013**, *32* (1), 12–15. https://doi.org/10.1021/om3010959.
(129) Harrison, D. J.; Lee, G. M.; Leclerc, M. C.; Korobkov, I.; Baker, R. T. Cobalt Fluorocarbenes: Cycloaddition Reactions with Tetrafluoroethylene and Reactivity of the Perfluorometallacyclic Products. *J. Am. Chem. Soc.* **2013**, *135* (49), 18296–18299. https://doi.org/10.1021/ja411503c.
(130) Fuller, J. T.; Harrison, D. J.; Leclerc, M. C.; Baker, R. T.; Ess, D. H.; Hughes, R. P. A New Stepwise Mechanism for Formation of a Metallacyclobutane via a Singlet Diradical Intermediate. *Organometallics* **2015**, *34*, 5210-5213.
(131) Harrison, D. J.; Daniels, A. L.; Korobkov, I.; Baker, R. T. d^{10} Nickel Difluorocarbenes and their Cycloaddition Reactions with Tetrafluoroethylene. *Organometallics,* **2015**, *34*, 5683-5686.
(132) Harrison, D. J.; Daniels, A. L.; Guan, J.; Gabidullin, B. M.; Hall, M. B.; Baker, R. T. Nickel Fluorocarbene Metathesis with Fluoroalkenes. *Angew. Chem. Int. Ed.* **2018**, *57*

(20), 5772–5776. https://doi.org/10.1002/anie.201802090.

(133) a) Kiplinger, J. L.; Richmond, T. G.; Osterberg, C. E. Activation of Carbon-Fluorine Bonds by Metal Complexes. *Chem. Rev.* **1994,** *94*, 373-431. b) Amii, H.; Uneyama, K. C-F Bond Activation in Organic Synthesis. *Chem. Rev.* **2009**, *109* (5), 2119–2183. https://doi.org/10.1021/cr800388c.

(134) Hacker, M.; Littlecott, G.; Kemmitt, R. Reactions of Fluoro-olefins, Chloro-olefins and Related Molecules with Carbonato Bis(triphenylarsine)platinum(II) in Ethanol *J. Organomet. Chem.* **1973**, *47*, 189–193. https://doi.org/10.1016/S0022-328X(00)92854-7.

(135) Burch, R. R.; Calabrese, J. C.; Ittel, S. D. Fluoroorganometallic Chemistry: Carbon-Fluorine Bond Activation in Perfluorometallacyclopentane Complexes. *Organometallics* **1988**, *7* (7), 1642–1648. https://doi.org/10.1021/om00097a030.

(136) Giffin, K. A.; Harrison, D. J.; Korobkov, I.; Tom Baker, R. Activation of C−F and Ni−C Bonds of [P,S]-Ligated Nickel Perfluorometallacycles. *Organometallics* **2013**, *32*, 3. https://doi.org/10.1021/om400933k.

(137) Iwamoto, H.; Imiya, H.; Ohashi, M.; Ogoshi, S. Cleavage of C(sp^3)-F Bonds in Trifluoromethylarenes Using a Bis(NHC)Nickel(0) Complex. *J. Am. Chem. Soc.* **2020**, *142* (45), 19360–19367. https://doi.org/10.1021/jacs.0c09639.

(138) Cronin, L.; Higgitt, C. L.; Karch, R; Perutz, R. N. Rapid Intermolecular Carbon-Fluorine Bond Activation of Pentafluoropyridine at Nickel(0): Comparative Reactivity of Fluorinated Arene and Fluorinated Pyridine Derivatives. *Organometallics* **1997**, *16*, 4920-4928.

(139) Sladek, M. I.; Braun, T.; Neumann, B.; Stammler, H.-G. Aromatic C–F Activation at Ni in the Presence of a Carbon–Chlorine Bond: The Nickel Mediated Synthesis of New Pyrimidines. *J. Chem. Soc., Dalt. Trans.* **2002**, *3*, 297. https://doi.org/10.1039/b110128e.

(140) a) Braun, T.; Noveski, D.; Neumann, B.; Stammler, H.-G. Conversion of Hexafluoropropene into 1,1,1-Trifluoropropane by Rhodium-Mediated C-F Activation. *Angew. Chem. Int. Ed.* **2002**, *41* (15), 2745–2748. https://doi.org/10.1002/1521. b) Noveski, D.; Braun, T.; Schulte, M.; Neumann, B.; Stammler, H.-G. C-F Activation and Hydrodefluorination of Fluorinated Alkenes at Rhodium. *Dalton Trans.* **2003**, 21, 4075-4083. https://doi.org/10.1039/B306635E.

(141) Wittig, G.; Schöllkopf, U. Zum Chemismus Der Halogen-Lithium-Austauschreaktion. *Tetrahedron* **1958**, *3* (1), 91–93. https://doi.org/10.1016/S0040-4020(01)82616-8.

(142) Gilman, H.; Gaj, B. J. Preparation and Stability of Some Organolithium Compounds in Tetrahydrofuran. *J. Am. Chem. Soc.* **1950**, *22*, 1165–1168.

(143) Zefirov, N. S.; Makhon'kov, D. I. X-Philic Reactions. *Chem. Rev.* **1982**, *82*, 615-624.

(144) Sazonov, P. K.; Artamkina, G. A.; Khrustalev, V. N.; Antipin, M. Y.; Beletskaya, I. P. Nucleophilic Vinylic Substitution with Transition Metal Carbonyl Anions - A Rare Case of a Halophilic Reaction Mechanism. Formation of Halo(Acyl)Rhenate Complexes and X-ray Structure of Cis-[CF_2=CF(CO)Re(CO)$_4$Br]Na. *J. Organomet. Chem.* **2003**, *681* (1–2), 59–69. https://doi.org/10.1016/S0022-328X(03)00531.

(145) Ivushkin, V. A.; Sazonov, P. K.; Artamkina, G. A.; Beletskaya, I. P. Halophilic Reactions of Pentafluorohalobenzenes with Transition-Metal Carbonyl Anions. *J. Organomet. Chem.* **2000**, *597* (1–2), 77–86. https://doi.org/10.1016/S0022-328X(99)00598.

(146) Artamkina, G. A.; Sazonov, P. K.; Ivushkin, V. A.; Beletskaya, I. P. The Reaction of the $[CpFe(CO)_2]^-$ Anion with Pentafluorochlorobenzene: Nucleophilic Aromatic Substitution by Halogen - Metal Exchange. *Chem. Eur. J.* **1998**, *4* (7), 1169–1178. https://doi.org/10.1002/(SICI)1521.

(147) Sazonov, P. K.; Artamkina, G. A.; Beletskaya, I. P. Nucleophilicity of Metal Carbonyl Anions in Vinylic Substitution Reactions. *J. Phys. Org. Chem.* **2008**, *21* (3), 198–206. https://doi.org/10.1002/poc.1279.

(148) Sazonov, P. K.; Artamkina, G. A.; Beletskaya, I. P. Halogenophilic and Classical Ad_NE Mechanisms in Nucleophilic Vinylic Substitution Reactions Involving the Anions of Transition Metal Carbonyls. *Theor. Exp. Chem.* **2011**, *46* (6), 350–358. https://doi.org/10.1007/s11237-011-9165-2.

(149) Sazonov, P. K.; Ivushkin, V. A.; Artamkina, G. A.; Beletskaya, I. P. Metal Carbonyl Anions as Model Metal-Centered Nucleophiles in Aromatic Andvinylic Substitution Reactions. *Arkivoc* **2003**, *2003* (10), 323–334. https://doi.org/10.3998/ark.5550190.0004.a30.

(150) Sazonov, P. K., Artamkina, G. A. & Beletskaya, I. P. Anions of Transition Metal Carbonyls in Nucleophilic Vinyl Substituiton. VII. *Russ. J. Org. Chem.* **2001**, 37, 480-495.

(151) Beletskaya, I. P. *et al.* Bimetallic Lanthanide Complexes with Lanthanide-Transition Metal Bonds. Molecular Structure of $(C_4H_8O)(C_5H_5)_2LuRu(CO)_2(C_5H_5)$. The Use of ^{139}La NMR Spectroscopy. *J. Am. Chem. Soc.* **1993**, *115*, 3156–3166.

(152) Baer, H. H.; Hanna, H. R. Chain Elongation by Use of an Iron Carbonyl Reagent: A Facile Synthesis of 6-Deoxyheptosiduronic acids. *Carbohydr. Res.* **1982**, *102*, 169-183.

(153) Sazonov, P. K.; Oprunenko, Y. F.; Beletskaya, I. P. Predicting the Direction of Nucleophilic Attack in Vinyl Halides: Halogenophilic versus Carbophilic Reactivity of Metal Carbonyl Anions. *J. Phys. Org. Chem.* **2013**, *26* (2), 151–161. https://doi.org/10.1002/poc.2995.

(154) Sazonov, P. K.; Beletskaya, I. P. Carbonylmetallates - A Special Family of Nucleophiles in Aromatic and Vinylic Substitution Reactions. *Chem. Eur. J.* **2016**, *22* (11), 3644–3653. https://doi.org/10.1002/chem.201504423.

(155) Sazonov, P. K.; Artamkina, G. A.; Lyssenko, K. A.; Beletskaya, I. P. A New Mechanism of Nucleophilic Vinylic Substitution and Unexpected Products in the Reaction of Chlorotrifluoroethylene with $[Re(CO)_5]Na$ and $[CpFe(CO)_2]K$. *J. Organomet. Chem.* **2006**, *691*, 2346–2357.

(156) Wu, C.; McCollom, S. P.; Zheng, Z.; Zhang, J.; Sha, S. C.; Li, M.; Walsh, P. J.; Tomson, N. C. Aryl Fluoride Activation through Palladium-Magnesium Bimetallic Cooperation: A Mechanistic and Computational Study. *ACS Catal.* **2020**, *10* (14), 7934–7944.

Chapter 2. C–N Cross-coupling Reactions of Amines with Aryl Halides Using Amide-Based Pincer Nickel(II) Catalyst.

2.1 Published contribution

Y. M. Albkuri, A. B. RanguMagar, A. Brandt, H. A. Wayland, B. P. Chhetri, C. M. Parnell, P. Szwedo, A. Parameswaran-Thankam and A. Ghosh, *Catal. Lett.*, **2020**, *150*, 1669–1678.

Albkuri and Ghosh wrote the manuscript with Wayland's assistance. Albkuri performed most of the experiments, Parnell obtained the ESI-MS data for intermediate complexes. The rest of the co-authors were involved in cleaning up the manuscript and fixing the figures.

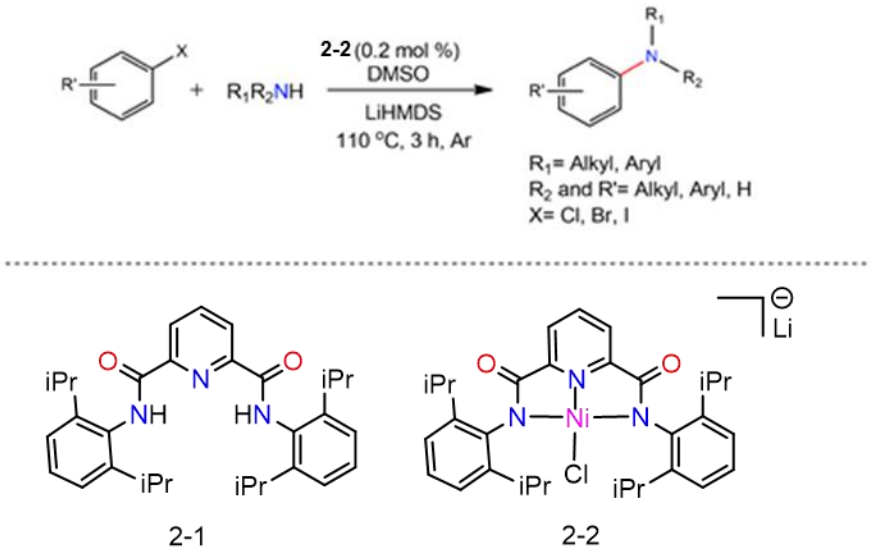

Abstract

An approach to C–N cross-coupling reactions of aryl halides with amines in the presence of an amide-based pincer nickel(II) catalyst (**2**) is described. For 3 h reactions at 110 °C with 0.2 mol% catalyst, aryl bromides gave higher turnover numbers (TON) than the corresponding chlorides or iodides. Both primary and secondary amines could be used with the former giving higher TON. However, sterically hindered amines showed lower TON. In elucidating the mechanism of this nickel complex-catalyzed C–N cross coupling reaction it was found that the rate of reaction was unchanged in the presence of radical quenchers and a plausible Ni(I)–Ni(III) pathway is proposed.

2.2 Introduction

Using transition metal complexes for amination of aryl halides to form arylamines has become a prevailing methodology[1]. In this context, heterocyclic compounds containing nitrogen atoms are of significant importance due to their abundance in natural products and their roles in biological and bio-inspired reactions[2]. Carbon–nitrogen (C–N) bond-containing aromatic and aliphatic compounds have also found multiple applications as polymers, dyes, and agrochemicals[3,4]. However, one of the primary avenues for exploration of C–N bond-containing molecules is their value in medicinal chemistry[5]. Some prevalent pharmaceutical compounds containing C–N bonds are shown in (**Figure 2.1)**. Due to these and many more potential applications, it is highly desirable to develop improved methodologies for facile and economical generation of C–N bonds.

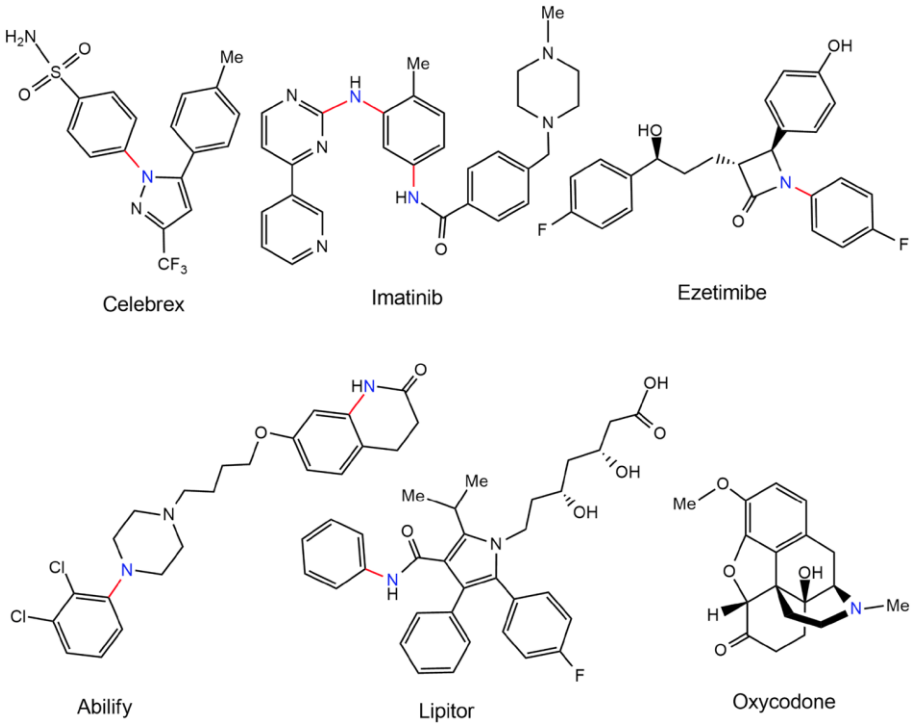

Figure 2.1 Significant pharmaceutical compounds of different classes containing C–N bonds.

Development of versatile catalyzed processes for arylamine synthesis took chemists over a century to achieve success. In 1903, Ullmann and Goldberg showed that copper salts enabled reactions of activated aryl halides with amine nucleophiles[6,7]. However, these reactions used stoichiometric copper and typically harsh reaction conditions. In the 1990s, Buchwald[8,9] and Hartwig[10,11] worked independently to successfully develop palladium catalyzed N-arylation using phosphine ligands. Since that time the Buchwald–Hartwig amination has brought great advances in C–N cross-

coupling reactions[12,13]. In attempts to reduce catalyst loading and reaction times, design of new catalysts for efficient C–N coupling reactions continues as a vigorous research area[14]. In a recent example, aryl chlorides, bromides and iodides could be efficiently coupled using 1 mol% CuBr with a simple 8-oxyquinoline N-oxide ligand[15].

With a view to performing C–N coupling catalysis on larger scales, recent interest has focused on advancing nickel catalysis[16-18] beyond the original reports[19-21]. In contrast to Pd and Cu catalysts, nickel catalyzed C–N bond-forming reactions often proceed through paramagnetic Ni(I)/(III) intermediates via redox processes[22-24] although systems have been developed recently to favor Ni(0)/(II)[17,25]. Therefore, developing new nickel-based catalysts with geometrical constraints enforced by pincer ligands may allow for improved catalysts. We have previously used a diamidopyridine-ligated nickel complex for cross-coupling reactions of multiple C–Cl bonds[26] and activation of sp^3 and sp^2 C–H bonds in alkylation and arylation[27]. In this study, we show that the nickel complex effects the selective cross-coupling amination of unactivated aryl halides with various aliphatic and aromatic amines with low catalyst loading and short reaction times.

2.3 Experimental Section

2.3.1 Materials and instrumentation

All reactions were carried out under an inert (Ar) atmosphere using oven-dried glassware. All solvents and chemicals such as anhydrous dimethylsulfoxide (DMSO), amines, anhydrous aryl halides, KO^{t}Bu, and all chemicals for ligand synthesis were obtained from Sigma-Aldrich, USA, Acros Organics, USA, and Alfa Aesar, USA and were used as received without any further purification unless otherwise stated. All amines were purified by passing through activated alumina prior to use. Gas chromatography-mass spectrometry (GC–MS) spectra were collected using a Shimadzu QP2010 GC–MS, where parameters were maintained at 275 °C interface, 3 injections at 24 and 50 min. Characterization of the ligand and metal catalyst were performed by electrospray ionization mass spectrometry (ESI–MS). The fourier transform infrared spectrometer (FT/IR), and nuclear magnetic resonance (NMR) instruments used were as reported previously[26,27].

2.3.2 Synthesis of N,N'-bis(2,6-di-isopropylphenyl)-2,6-pyridinedicarboxamide (1)

The ligand was synthesized according to a previous synthetic route with slight modifications[26,27]. In a 100 mL round bottom flask with a stir bar, 2,6-pyridinedicarboxylic acid (5 g, 0.03 mol) and 15 mL 1,2-dimethoxyethane were added followed by addition of thionyl chloride (5 mL, 0.07 mol).

The reaction mixture was refluxed for 3 h. After completion, the excess solvent and thionyl chloride were removed under reduced pressure to obtain a white product, followed by crystallization from concentrated hexane to obtain 2,6-pyridinedicarbonyl dichloride. The acid chloride was then treated with 2,6-diisopropylaniline and triethylamine of anhydrous

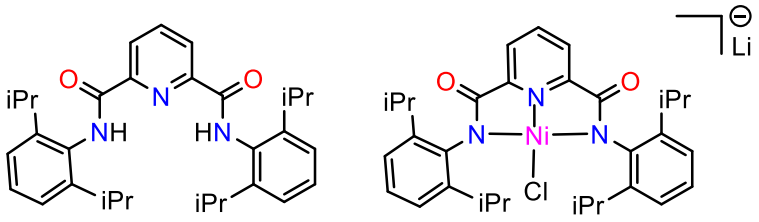

2-1 2-2

Figure 2.2 Structures of ligand **1** and pincer nickel(II) catalyst **2**.

tetrahydrofuran (THF) cooled to 0 °C and stirred for 3 h. On warming the reaction was further stirred at room temperature for another 9 h. The reaction mixture was then filtered and THF was removed under reduced pressure to obtain the crude ligand (**2-1**) (**Figure 2.2**). See Figure A2.1 and A2.2 for ^{1}H NMRs.

2.3.3 Synthesis of Pincer Nickel(II) Complex (2)

Our previous work has described the synthesis of pincer-nickel(II) complex (**2-2**) (**Figure 2.2)**[26,27]. In short, a 100 mL Schlenk flask fitted with a magnetic stir bar was charged with **2-1**. The flask was sealed with a septum and stirred for 5 minutes while purging with N_2. Dry THF was added using a gas tight syringe, and n-butyllithium was added to the ice bath-cooled (0 °C) reaction mixture to deprotonate the ligand, followed by addition of anhydrous nickel(II) chloride to yield the deep red nickel(II) complex **2-2** (Figure 2.2). The catalyst was characterized using ^{1}H-NMR, ESI–MS, FT/IR, and ultraviolet–visible (UV–Vis) spectroscopy as described in the previous reports[26,27].

2.3.4 General Amination Procedure of Aryl Halides Using Different Amines

A representative amination method using chlorobenzene, pentylamine, and KO^{t}Bu in DMSO is described here. All other amination reactions including different aryl halides, primary (1°) and secondary (2°) amines, solvents and bases were performed using a similar method. A 4 mL reaction vial containing a magnetic stir bar was charged with 1.4 mL of anhydrous DMSO. The reaction vial, after being sealed with a septum and parafilm, was purged with Ar for 10 min. Chlorobenzene [0.4 mL, 3.9 mmol, 2.25 equivalent (eq.)], pentylamine (0.21 mL, 1.8 mmol, 1.0 eq.), anhydrous

powdered KO^{t}Bu (70 mg, 0.63 mmol, 0.3 eq.), and 2 (2 mg, 0.2 mol%) were added sequentially. The reaction mixture was stirred for 5 min while continually purging with Ar. The vial was then sealed with a Teflon screw cap. The reaction mixture was stirred for 3 h at 110 °C in a preheated oil bath, then allowed to cool to room temperature and filtered by passing through Celite to remove the base and the catalyst. 30 µL of the solution was then dissolved in 1 mL absolute ethanol, and 10 µL of decane was added as an internal standard. Turn over number (TON) was determined using GC–MS.

2.4. Results and Discussion

2.4.1 Optimization of reaction solvent and base

To best facilitate the amination, reactions conditions were optimized by changing solvents and bases (**Table 2.1**). Many solvents gave low TON (Entries 1–3) most likely due to the low solubility of the catalyst and/or base. The low boiling point of the solvents may also have played a role in the product conversion. Solvents with high polarity and boiling point, such as dimethylacetamide (DMA), produced moderate results (TON 69) (Entry 6), whereas none of the desired product was obtained using dimethylformamide (DMF) (Entry 1), presumably due to thermal decomposition. DMSO proved to be the most effective solvent, yielding a TON of 243 (Entry 7). Therefore, DMSO was used to further optimize the C–N coupling reaction conditions.

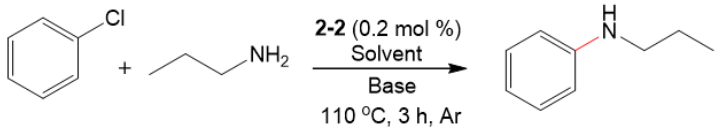

3a **4a** **5aa**

Entry	Solvent	Base	TON
1	DMF	KO^{t}Bu	NR
2	MTBE	KO^{t}Bu	3 ± 1
3	Dioxane	KO^{t}Bu	25 ± 2
4	THF	KO^{t}Bu	36 ± 7
5	Toluene	KO^{t}Bu	68 ± 14
6	DMA	KO^{t}Bu	69 ± 5
7	DMSO	KO^{t}Bu	243 ± 29
8	DMSO	Cs_2CO_3	NR
9	DMSO	K_2CO_3	NR
10	DMSO	DMAP	NR
11	DMSO	DBU	NR
12	DMSO	KOH	20

Table 2.1 Amination of chlorobenzene using various solvents and bases.

One of the requirements for many cross-coupling reactions, and particularly for aminations, is the use of a base[28,29]. None of cesium carbonate (Cs_2CO_3), potassium carbonate (K_2CO_3), 4-dimethylaminopyridine (DMAP) or DBU (1,8-diazabicyclo[5.4.0]undec-7-ene) yielded any product (Entries 8–11), while relatively stronger bases such as KOH gave high yields (Entry 12). Results showed that KO^{t}Bu was most effective (Entry 7) presumably due to its better reducing power and was thus used for all subsequent reactions.

2.4.2 Optimizing reaction temperature and aryl halide comparison

In reactions run at temperatures ranging from 70 to 120 °C, increasing the temperature resulted in higher yields and TONs (**Figure 2.3**). The TON of the reaction increased slightly from 70 to 100 °C with values of 169, 174, 181 and 195, respectively. Similar trends were observed at 110 and 120 °C, with values of 212 and 219, respectively, with maximum TON observed at 120 °C.

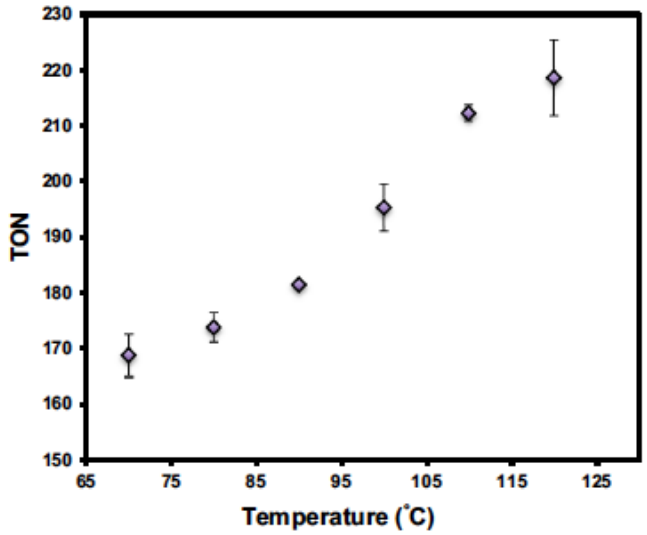

Figure 2.3 Effect of temperature (70 to 120 °C) on the amination reaction using **2-2** and KO^{t}Bu in DMSO. Yields represent an average of two runs after 3 h.

After identifying the optimal amination conditions using **2-2**, we investigated the amination of chloro-, bromo and iodobenzene with morpholine in DMSO with KO^{t}Bu. In order to focus on low catalyst loadings and short reaction times, all reactions were heated at 110 °C for 3 h under argon (**Table 2.2**). Bromobenzene yielded the desired product with highest TON of 484 (Entry 3) compared to chlorobenzene (361, Entry 2) and iodobenzene (317, Entry 1). Note that 484 turnovers amount to 97% conversion of the bromobenzene limiting reagent with a selectivity of 95% due to

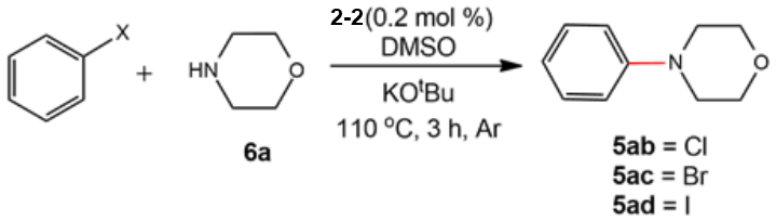

Entry	X	TON
1	I	316.9±3.8
2	Cl	361.3±0.07
3	Br	484.1±1.1

Table 2.2 Evaluation of various electrophiles.

a small amount of biphenyl formation. Nonetheless, aryl chlorides were chosen as the major focus of this work as they are less expensive and more widely available than their bromo and iodo analogs.

2.4.3 Chlorobenzene amination scope with aliphatic/aromatic amines.

A series of 1° amines were tested for cross-coupling reactions using chlorobenzene under the same conditions as previously stated (**Scheme 2.1**). Good TONs were obtained for most 1° amines tested. Among the series of linear aliphatic amines (**7a**–**h**), there was no clear-cut trend for the smaller compounds (**7a**–**c**). However, as the amine chain length increased, a rise in TON (from 173 to 365) was observed (**7d**–**h**). All linear aliphatic amines were found to react with chlorobenzene to produce the desired products (143–365 TON). Octyl- and decyl-amines yielded high TONs of 331 and 365, respectively (**7f, h**). The steric bulk of the amines was found to negatively influence the outcome of the desired products, as *t*-butylamine produced low TON of 55 (**7i**). Similarly, other sterically bulky amines also showed dimished activities (**7j**, **k**). Two of the amine products (**7l**, **m**) were isolated from the reaction mixture for the purpose of ^{1}H and ^{13}C NMR analysis and these characterizations are included in the figure A3.

Reactions of chlorobenzene with alkyl and aromatic 2° amines with varying degrees of steric bulk and nucleophilicity were also investigated (**Scheme 2.2**). Alkyl amines with relatively less steric hindrance furnished the desired products with TONs in the range of 156–215 (**8a**–**d**, **f**), while more hindered amines showed lower activity, as in the case of diisopropylamine (**8e**).

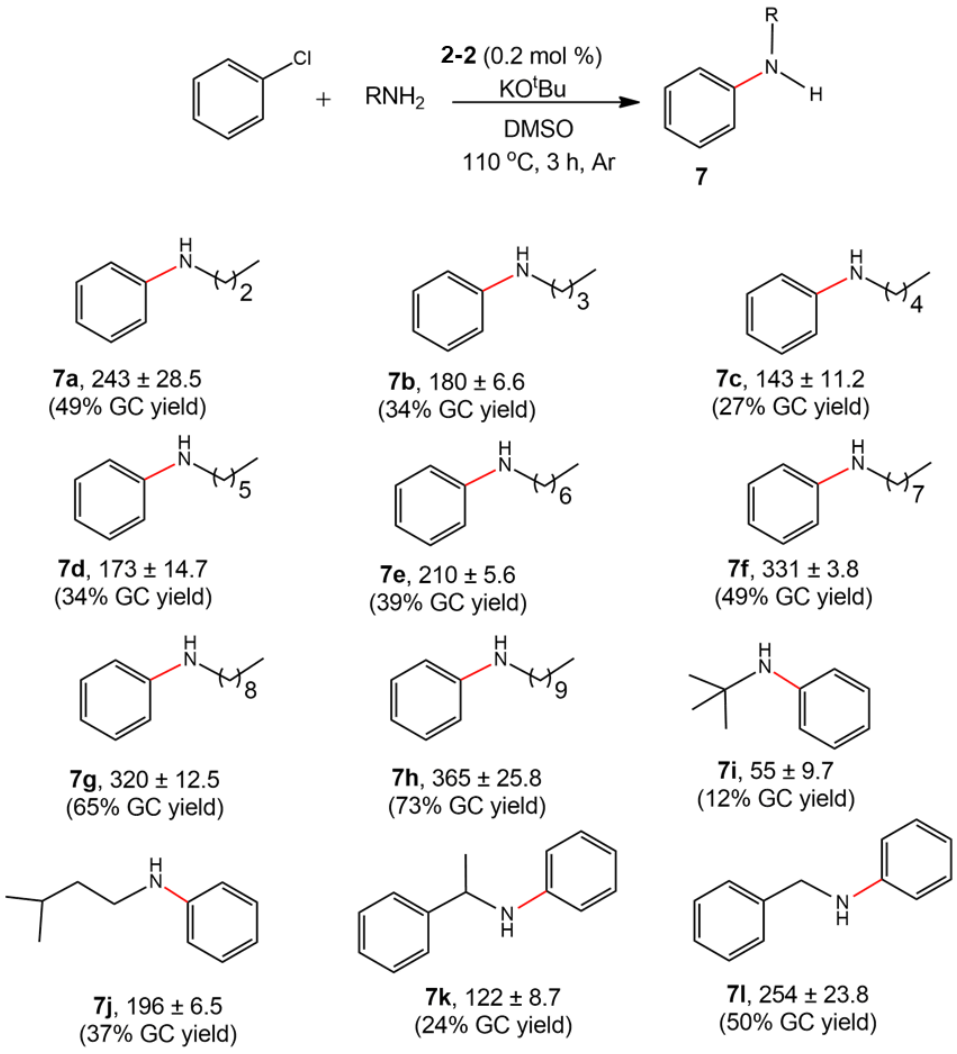

Scheme 2.1 Pincer nickel catalyzed amination of chlorobenzene with 1° amines. Yields represents an average of two runs. TON was measured in GC by using decane as an internal standard.

2.4.4 Scope of substituted aryl jalide amination with aniline

Establishing optimal conditions for nickel-catalyzed amination of substituted aryl bromides has proved challenging, generally requiring complicated catalyst systems and often giving low yields.[28,29] Indeed, using complex **2-2** with varying ratios of KO^{t}Bu gave insignificant conversions. However, using 1 eq. of LiHMDS as a base, the desired coupling products were obtained from aniline and several substituted aryl bromides in poor to fair yields (3–30% **9a**–**c**, (**Scheme 2.3**).

Applying a similar protocol (but using 2 eq. of LiHMDS) to the amination of several substituted aryl chlorides catalyzed by **2-2** gave fair to moderate yields of the coupled products (7, 21% **10a**, **b**).

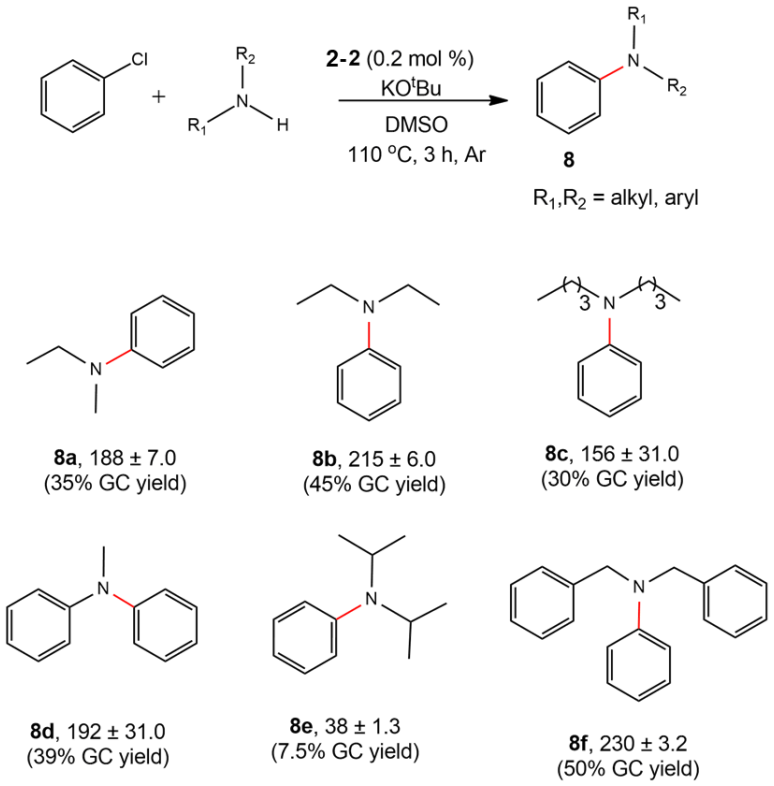

Scheme 2.2 Pincer nickel catalyzed amination of chlorobenzene with 2° amines. Yields represent an average of two runs. TON was measured in GC by using decane as an internal standard.

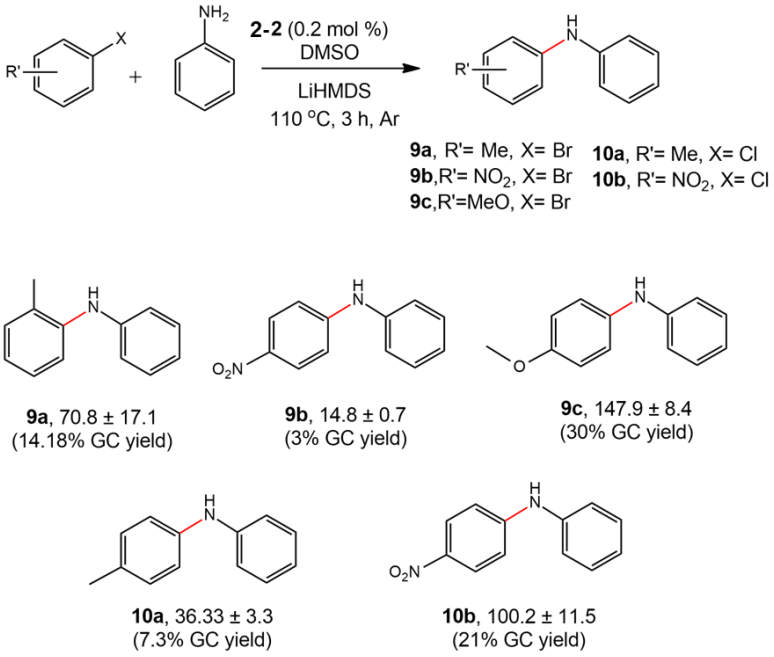

Scheme 2.3 Pincer nickel-catalyzed amination of substituted aryl bromides and chlorides with 1° amine. Yields represents an average of two runs. TON was measured in GC by using decane as an internal standard. **10a** and **10b**, LiHMDS (0.66 mL, 2 equiv. to substrate).

2.4.5 Kinetic study of chlorobenzene amination using aniline and catalyst 2-2

Initial rates of chlorobenzene amination using aniline and KOtBu in DMSO at 110 °C were measured with respect to catalyst, aryl chloride, amine and base. Plots of concentrations of diphenylamine versus time at various concentrations of amine, catalyst, base, and aryl chloride along with their reaction schemes are shown in our publication's Supporting Information.[32] The first observation of note was that no reaction was observed for the first 20–30 min depending on the ratio of base to catalyst precursor, suggesting that the active catalyst is slow to form, even at 110 °C. Plots of the initial amination rate versus time at various concentrations of amine, catalyst, base, and aryl chloride are shown in figure A2.4. The results are consistent with a first order rate dependence on the concentrations of catalyst and aryl chloride and zero order for the base and amine. Similar observations have been reported previously with other Ni catalysts.[17] At high concentrations of aryl chloride using **2-2**, however, the rate is suppressed, likely due to catalyst deactivation.

2.5 Proposed Reaction Pathway of Pincer Nickel Complex-Catalyzed Amination of Aryl Halides with Amines.

As mentioned in the literature for different Ni- and Pd complexes, reactions usually occur via oxidative addition of aryl halides followed by reductive elimination from a metal-amido intermediate[16]. While catalysts have been designed to accomplish these steps exclusively through Ni(0–II) intermediates[17], many Ni(II) pre-catalysts are proposed instead to involve paramagnetic Ni(I–III) intermediates in which the base serves as the initial reductant[30,31]. We propose a similar scheme using anionic catalyst **2-2**.

In our reaction system, loss of chloride from **2-2** is likely required before the complex can be reduced to the Ni(I) anion, where either amines or KO^{t}Bu can reduce the metal by single electron transfer process[30,31], likely present as the amine complex **A** (**Figure 2.4**). Following aryl halide oxidative addition, halide elimination would again be required to recoordinate the amine in intermediate **B**. Deprotonation of the coordinated amine will also be favored from the neutral Ni(III) intermediate **B** and subsequent reductive elimination of the product and recoordination of the amine regenerates the active Ni(I) catalyst **A**. The slow reduction of **2-2** to **A** presumably gives rise to the long induction period whereas rate-limiting oxidative addition of the aryl halide is consistent with the first order rate dependence on both catalyst and aryl halide. The reaction was also performed in the presence of a radical quencher, namely 2,2,6,6-tetramethyl-1-piperidinyloxy

(TEMPO) to assess its effect on the rate. The rate of reaction was found to be unaffected in the presence of TEMPO. Therefore, it can be inferred that organic radicals are not involved in the catalyst cycle.

2.6 Conclusion

Nickel pincer-based catalyst **2-2** was used for the first time in C–N cross coupling amination of aryl halides with amines. The catalyst is stable and relatively easy to handle under atmospheric conditions and after an induction period, low catalyst loading (0.2 mol%) and short reaction times afford significant product yields for both 1° and 2° amines with a variety of substituted aryl halides. Various amines and aryl halides were examined, and the catalyst demonstrated moderate to high TONs (up to 400). Kinetic studies revealed that the reaction

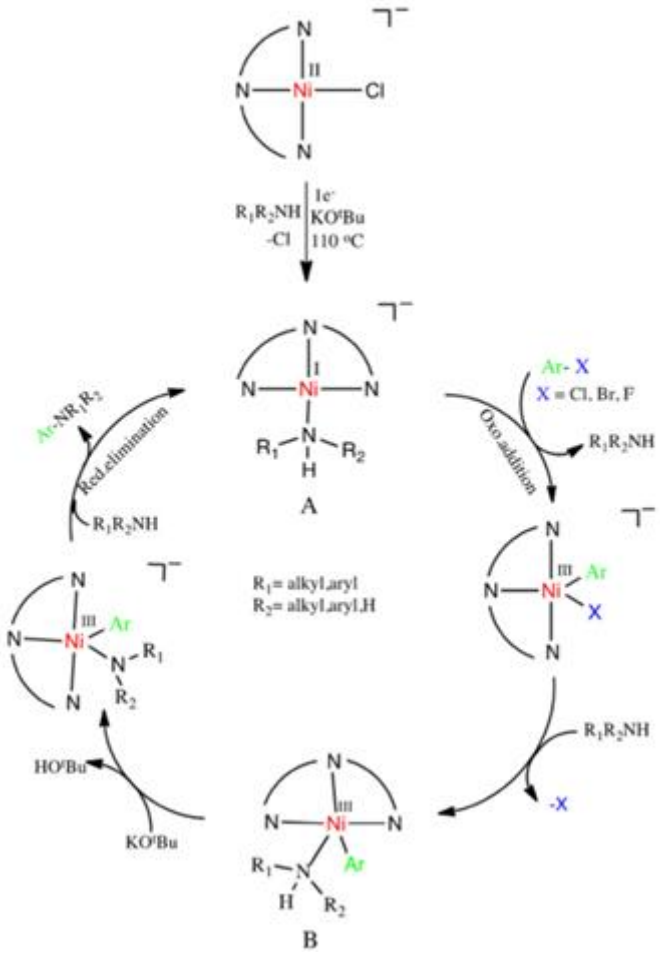

Figure 2.4 Proposed mechanism for the nickel catalyzed amination of aryl halides with amines using catalyst **2-2.**

proceeds with first-order kinetics with respect to catalyst and aryl halide concentrations while amine and base concentrations did not affect the overall reaction rate. The proposed reaction pathway involves the oxidative addition of aryl halides to the anionic Ni(I) catalyst **A** and loss of halide to give a neutral Ni(III) amine intermediate **B.** Deprotonation of the coordinated amine in **B** is followed by reductive elimination of the N-arylamine product. The reaction does not proceed through organic radical intermediates as revealed by radical quencher studies. In future studies, generation, isolation and reactivity of the reduced version of **2-2** will likely be informative.

2.7 References

(1) Ricci, A. *Modern Amination Methods*. Wiley: Weinheim, **2000**.

(2) Garella, D.; Borretto, E.; Di Stilo, A.; Matina, K.; Cravotto, G.; Cintas, P. Microwave-assisted Synthesis of N-Heterocycles in Medicinal Chemistry. *Med.Chem.Comm*. **2013**, *4*(10), 1323–1343.

(3) Xu, S.; Kim, E. H.; Wei, A.; Negishi, E. Pd-and Ni-Catalyzed Cross-Coupling Reactions in the Synthesis of Organic Electronic Materials. *Sci .Technol. Adv. Mater*. **2014**, *15*(4), 044201.

(4) Hili, R.; Yudin, A. K. Making Carbon-nitrogen Bonds in Biological and Chemical Synthesis. *Nat. Chem. Biol*. **2006**, *2*(6), 284.

(5) Taylor, R. D.; MacCoss, M.; Lawson, A. D. G. Rings in Drugs: Miniperspective. *J. Med. Chem*. **2014** *57*(14), 5845–5859.

(6) Ullmann, F. Ueber. eine neue bildungsweise von diphenylaminderivaten. *Ber. Dtsch. Chem. Ges*. **1903**, *36*(2), 2382–2384.

(7) Goldberg, I. Ueber. phenylirungen bei gegenwart von kupferals katalysator. *Ber. Dtsch. Chem. Ges. 1906, 39*(2),1691–1692.

(8) Wolfe, J. P.; Wagaw, S.; Marcoux, J.-F.; Buchwald, S. L. Rational Development of Practical Catalysts for Aromatic Carbon−Nitrogen Bond Formation. *Acc. Chem. Res*, **1998**, *31*(12), 805–818.

(9) Yang, B. H.; Buchwald, S. L. Palladium-catalyzed Amination of Aryl Halides and Sulfonates. *J. Organomet. Chem*. **1999**, *576*(1–2), 125–146.

(10) Hartwig, J. F. in: Negishi, E. I. (Ed.) *Handbook of Organopalladium Chemistry for Organic Synthesis*. Wiley: Hoboken, **2002**.

(11 Hartwig, J. F. Transition Metal-Catalyzed Synthesis of Arylamines and Aryl Ethers from Aryl Halides and Triflates: Scope and Mechanism. *Angew. Chem. Int. Ed*. **1998**, *37*(15), 2046–2067.

(12) Heravi, M. M.; Kheilkordi, Z.; Zadsirjan, V.; Heydari, M.; Malmir, M. Buchwald–Hartwig Reaction: An Overview. *J. Organomet. Chem*. **2018**, *861*,17–104.

(13) Forero-Cortés, P. A.; Haydl, A. M. The 25th Anniversary of the Buchwald–Hartwig Amination: Development, Applications, and Outlook. *Org. Proc. Res. Dev*. **2019**, *23*(8), 1478–1483.

(14) Balcells, D.; Nova, A. Designing Pd and Ni Catalysts for Cross-coupling Reactions by Minimizing Off-cycle Species. *ACS. Catal*. **2018**, *8*(4), 3499–3515.

(15) Yang, K.; Qiu, Y.; Li, Z.; Wang, Z.; Jiang, S. Ligands for Copper-catalyzed C−N Bond Forming Reactions with 1 Mol% CuBr as Catalyst. *J. Org .Chem*. **2011**, *76*(9), 3151–3159.

(16) Desmarets, C.; Schneider, R.; Fort, Y. Nickel (0)/d=Dihydroimidazol-2-ylidene Complex Catalyzed Coupling of Aryl Chlorides and Amines. *J. Org. Chem*. **2002**, *67*(9), 3029–3036.

(17) Ge, S.; Green, R. A.; Hartwig, J. F. Controlling First-row Catalysts: Amination of Aryl and Heteroaryl Chlorides and Bromides with Primary Aliphatic Amines Catalyzed by a BINAP-ligated Single-component Ni (0) Complex. *J. Am. Chem. Soc*. **2014**, *136*(4), 1617–1627.

(18) Park, N. H.; Teverovskiy, G.; Buchwald, S. L. Development of an Air-stable Nickel Precatalyst for the Amination of Aryl Chlorides, Sulfamates, Mesylates, and Triflates. *Org. Lett*. **2014**, *16*(1), 220–223.

(19) Hidai, M.; Kashiwagi, T.; Ikeuchi, T.; Uchida, Y. Oxidative Additions to Nickel (0): Preparation and Properties of a New Series of Arylnickel(II) Complexes. *J. Organomet.Chem*. **1971**, *30*(2), 279–282.

(20 Wolfe, J. P., Buchwald, S. L. Nickel-catalyzed Amination of Aryl Chlorides. *J. Am. Chem. Soc*. **1997** *119*(26), 6054–6058.

(21) Brenner, E.; Fort Y. New Efficient Nickel(0) Catalysed Amination of Aryl Chlorides. *Tetrahedron. Lett*. **1998**, *39*(30), 5359–5362.

(22) Tasker, S. Z.; Standley, E. A.; Jamison, T. F. Recent Advances in Homogeneous Nickel Catalysis. *Nature* **2014**, *509*(7500), 299.

(23) Li, C.; Kawamata, Y.; Nakamura, H.; Vantourout, J. C.; Liu, Z.; Hou, Q.; Bao, D.; Starr, J. T.; Chen, J.; Yan, M.; Baran, P. S. Electrochemically Enabled, Nickel-catalyzed Amination. *Angew. Chem. Int. Ed*. **2017**, *56*(42), 13088–13093.

(24) Kawamata, Y.; Vantourout, J. C.; Hickey, D. P.; Bai, P.; Chen, L.; Hou, Q.; Qiao, W.; Barman, K.; Edwards, M. A.; Garrido-Castro, A. F.; deGruyter, J. N.; Nakamura, H.; Knouse, K.; Qin, C.; Clay, K. J.; Bao, D.; Li, C.; Starr, J. T.; Garcis-Irizarry, C.; Sach, N.; White, H. S.; Neurock, M.; Minteer, S. D.; Baran, P. S. Electrochemically Driven, Ni-catalyzed Aryl Amination: Scope, Mechanism and Applications. *J. Am. Chem. Soc*. **2019**, *141*(15), 6392–6402.

(25) Rull, S. G.; Funes-Ardoiz, I.; Maya, C.; Maseras, F.; Fructos, M. R.; Belderrain, T. R. Nicasio, M. C. Elucidating the Mechanism of Aryl Aminations Mediated by NHC-supported Nickel Complexes: Evidence for a Nonradical Ni(0)/Ni(II) Pathway. *ACS Catal*. **2018**, *8*(5), 3733–3742.

(26) Gartia, Y., Biswas, A.; Stadler, M.; Nasini, U. B.; Ghosh, A. Cross-coupling Reactions of Multiple C-Cl Bonds of Polychlorinated Solvents with Grignard Reagent using a Pincer Nickel Complex. *J. Mol. Catal. A* **2012**, *363–364*, 322–327.

(27) Gartia, Y.; Ramidi, P.; Jones, D. E.; Pulla, S.; Ghosh, A. Nickel Complex-catalyzed Efficient Activation of sp^3 and sp^2 C–H Bonds for Alkylation and Arylation of Oxygen-containing Heterocyclic Molecules. *Catal. Lett*. **2014**, *144*(3), 507–515.

(28) Lavoie, C. M.; MacQueen, P. M.; Rotta-Loria, N. L.; Sawatzky, R. S.; Borzenko, A.; Chisholm, A. J.; Hargreaves, B. K. V.; McDonald, R.; Ferguson, M. J.; Stradiotto, M. Challenging Nickel-catalysed Amine Arylations Enabled by Tailored Ancillary Ligand Design. *Nat. Commun*. **2016**, *7*, 1–11073.

(29) Tassone, J. P.; England, E. V.; MacQueen, P. M.; Ferguson, M. J.; Stradiotto, M. PhPAd-Dal-Phos: Ligand-enabled, Nickel-catalyzed Cross-coupling of (hetero) Aryl Electrophiles with Bulky Primary Alkylamines. *Angew. Chem. Int. Ed*. **2019**, *58*(8), 2485–2489.

(30) Zheng, B., Tang, F., Luo, J.; Schultz, J. W.; Rath, N. P. Mirica, L. M. Organometallic Nickel(III) Complexes Relevant to Cross-coupling and Carbon–heteroatom Bond Formation Reactions. *J. Am. Chem. Soc*. **2014**, *136*(17), 6499–6504.

(31) Barham, J. P.; Coulthard, G., Emery, K. J.; Doni, E.; Cumine, F.; Nocera, G.; John, M. P.; Berlouis, L. E. A.; McGuire, T.; Tuttle, T.; Murphy, J. A. KOtBu: A Privileged Reagent for Electron Transfer Reactions? *J. Am. Chem. Soc*. **2016**, *138*(23), 7402–7410.

(32) Albkuri, Y. M.; RanguMagar, A. B.; Brandt, A.; Wayland, H. A.; Chhetri, B. P.; Parnell, C. M.; Szwedo, P.; Parameswaran-Thankam, A.; Ghosh, A. C–N Cross-coupling Reactions of Amines with Aryl Halides Using Amide-Based Pincer Nickel(II) Catalyst. *Catal. Lett.* **2020**, *150*, 1669–1678.

Chapter 3. Nickel (II)-SNS Thiolate Complexes: Reactivity and Solution Dynamics

3.1 Published Contribution

Yahya M. Albkuri, Jeffrey S. Ovens, Jessica Martin and R. Tom Baker, *Inorg. Chem.* **2021**, accepted. DOI: 10.1021/acs.inorgchem.1c00446.

Albkuri performed all the experiments, Martin collected and analyzed the ESI-MS data for some complexes and Ovens was responsible for X-ray diffraction data collection and structure refinement. Albkuri and Prof. Baker wrote the manuscript.

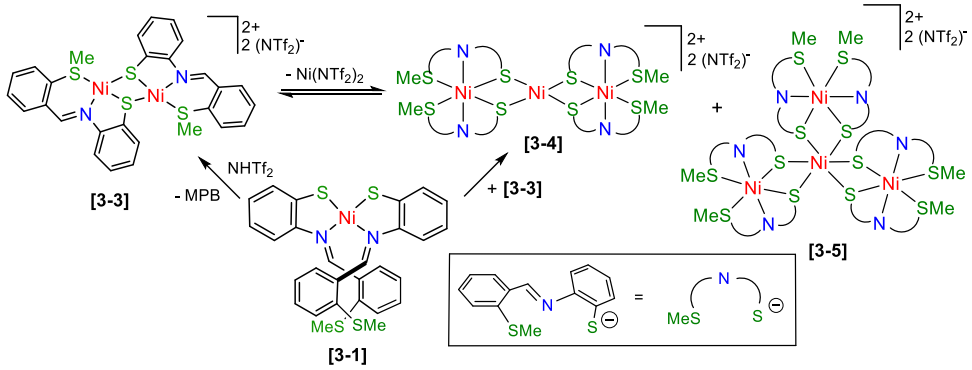

Abstract

Nickel coordination chemistry with a biomimetic thiolate-imine-thioether SNS^{Me} ligand is accompanied by diverse reactivity and anionic tridentate ligand dynamics. Reaction of $Ni(acac)_2$ with two equiv of 2-(methylthio)-phenyl-benzothiazolidine (MPB) affords the bis(arylimino-phenylene-thiolate) complex $Ni(\kappa^2\text{-}SNS^{Me})_2$ (**3-1**; acac = acetylacetonate). Thermolysis of **3-1** in refluxing toluene is accompanied by imine C-C bond formation, yielding $[Ni(N_2S_2)]$ (**3-2**) with a redox-active ligand. Protonation of **3-1** with $NHTf_2$ at low temperature released one equiv of MPB, yielding crystals of the dimeric dication $\{[Ni(\mu\text{-}\kappa^3\text{-}SNS^{Me})]_2\}(NTf_2)_2$ (**3-3**; Tf = SO_2CF_3) in high yield. In contrast, the same reaction at room temperature gave also paramagnetic complexes $\{Ni[\mu\text{-}Ni(\kappa^3\text{-}SNS^{Me})_2]_2\}(NTf_2)_2$ (**4-3**) and $\{Ni[\mu\text{-}Ni(\kappa^3\text{-}SNS^{Me})_2]_3\}(NTf_2)_2$ (**3-5**) that feature coordination of two or three pseudo-octahedral, paramagnetic $Ni(\kappa^3\text{-}SNS^{Me})_2$ units to a central Ni(II) dication via thiolate bridges. Remarkably, dissolution of **3-3** in a variety of solvents, including weakly-coordinating CH_2Cl_2, rapidly generates a mixture of **3-4** and $Ni(NTf)_2$. This transformation is apparently fully reversible as reactions of **3-3** with Lewis bases L gave high yields of dimers $\{[Ni(\mu\text{-}\kappa^3\text{-}SNS^{Me})L]_2\}(NTf_2)_2$ for L = CNXylyl (**3-6a**) and $\{[Ni(\mu\text{-}\kappa^3\text{-}SNS^{Me})]_2(\mu\text{-dmpm})\}(NTf_2)_2$ (**3-6b**; dmpm = bis(dimethylphosphino)methane) or monomers $[Ni(\kappa^3\text{-}SNS^{Me})L](NTf_2)$ for L =

PMe_3 (**3-7a**), $P(OMe)_3$ (**3-7b**). Addition of 2 equiv of the strong donor *N*-heterocyclic carbene ligand, IPr, to **3-3,** however, led to methylium cation abstraction from the coordinated thioether, affording neutral dithiolate complex, Ni(κ^3-SNS)(IPr) (**3-8**). Reaction products were characterized by NMR, IR and UV-vis spectroscopy and mass spectrometry and complexes **3-(1-5)**, **3-6a**,**b**, **3-7a** and **3-8** by single-crystal X-ray diffraction.

3.2 Introduction

Transition metal complexes bearing 'pincer' ligands tend to exhibit improved thermal stability, reactivity and catalytic activity /selectivity when compared to their monodentate analogs.[1-5] Inspired by a plethora of multiple N,S coordination geometries in metallo-enzymes[6-9] and their synthetic models,[10,11] we have been preparing new first row metal SNS complexes (**Figure 3.1**)[12-16] in order to assess and compare the roles of 'hard' amido and 'soft' thiolate donors as cooperative ligands in catalysis.[17]

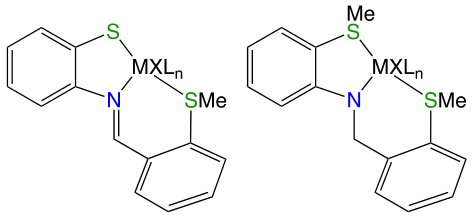

Figure 3.1 First row metal SNS thiolate and amido complexes.

The thiolate SNS proligand, 2-(methylthio)-phenyl-benzothiazolidine (MPB; **Scheme 3.1**), is readily prepared in a single step from the appropriate aldehyde and aniline precursors. The S-Bu^t analog prepared by Bouwman et al.[18] showed a solution equilibrium between the 'open' S-H and cyclic N-H tautomers.[19] With iron we isolated cationic SNS^{Me} thiolate complexes in which two neutral Fe^{II} bis(thiolate) units are coordinated to a central Fe^{2+} ion (**Scheme 3.1A**).[12] In contrast, using a neutral Fe precursor bearing an 'internal' base yielded not the targeted bis(thiolate) complex, but an Fe(N_2S_3) product due to facile imine C-C bond formation (**Scheme 3.1B**). The latter contains a redox-active ligand and proved to be an efficient and selective catalyst for hydroboration of aldehydes.[14] In contrast, copper complexes with an *N*-heterocyclic carbene ancillary ligand showed κ^2-SNS^{Me} binding with the thiolate complex also serving as an efficient (0.5 mol%, RT) outer-sphere carbonyl hydroboration catalyst (**Scheme 3.1C**).[16]

In another finding relevant to this work, we showed that electron-rich ancillary ligands led to selective C_{aryl}-S bond cleavage with subsequent formation of a coordinated dianionic CNS pincer ligand (**Scheme 3.2**).[15,20]

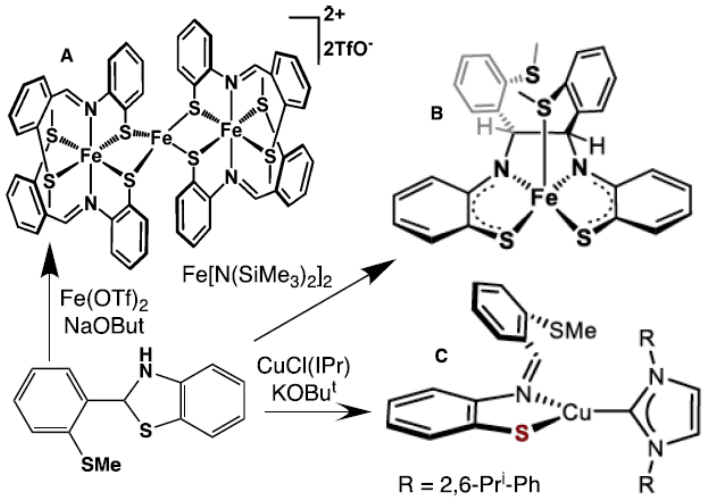

Scheme 3.1. Synthesis of first row M-SNS thiolate complexes.

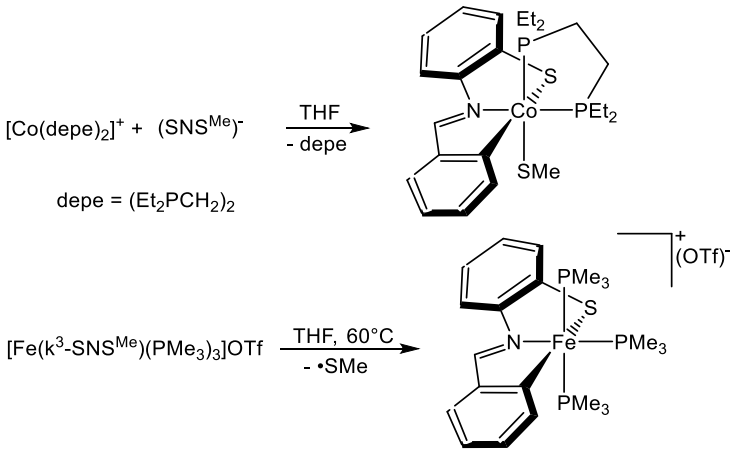

Scheme 3.2 Selective C_{aryl}-S bond cleavage.

For nickel, there are three relevant previous reports. Bouwman et al. prepared Ni(κ^2-SNS$^{t\text{-}Bu}$)$_2$ from Ni acetate and showed that heating in toluene effected selective C-S$_{Bu}{}^t$ bond cleavage, affording dithiolate-bridged [Ni(μ-κ^3-SNS)]$_2$ presumably by release of isobutene and protonated ligand (**Scheme 3.3A**).[18] Using phenylimino-phenylene-thiolate NS ligand, first reported with nickel by Kochin et al.,[21] Kawamoto and coworkers described the facile thermal conversion of Ni(κ^2-NS)$_2$ to Ni(N_2S_2) via imine C-C bond formation[22] as discussed above (**Scheme 3.3B**).[14] In later work

they extended the aryl ring π-conjugation to prepare near-infrared absorbing dyes.[23] In this work we detail the nickel coordination chemistry with the SNS^{Me} ligand, including solid state molecular structures, reactivity studies and ligand dynamics.

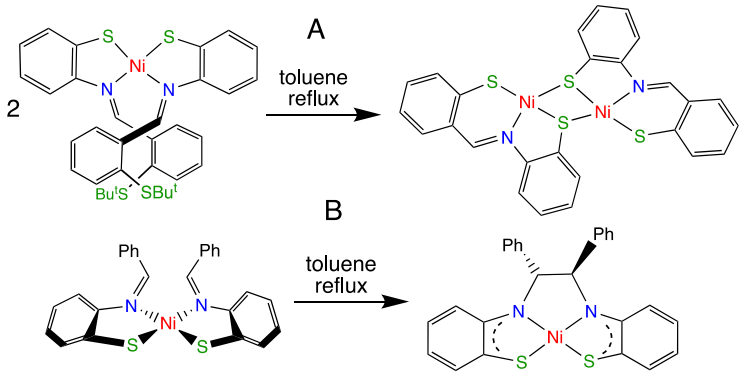

Scheme 3.3 Ni(II) SNS thiolate complexes.

3.3 Results

3.3.1 Synthesis and structure of neutral Ni(II) bisthiolate complex

*Synthesis of Ni bis(thiolate) Complex (**3-1**):* Treatment of Ni(acac)$_2$ with 2 equiv of the MPB proligand afforded Ni(κ^2-SNS^{Me})$_2$ (**3-1**) as an air-stable red solid (**Scheme 3.4**; acac = acetylacetonate).

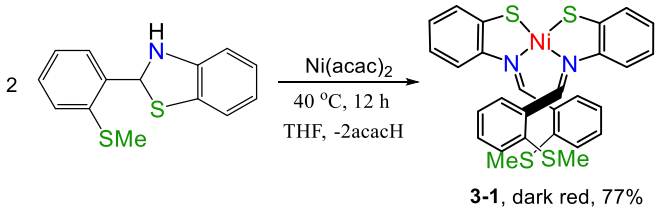

Scheme 3.4 Synthesis of Ni bis(thiolate) complex **1**.

The molecular structure of **3-1** determined by single crystal X-ray diffraction shows a distorted square planar (12.2(1)° twist between the two N-Ni-S planes vs. 18.6(3)° in the S-Bu^t analog)[18] geometry about Ni with *cis*-thiolate and imine donors (**Figure 3.2**). The N-Ni-S bite angles average 86.6° with the bulkier N centers giving rise to a N-Ni-N angle of 100.0°. The arylimino groups are located on the same side of the NiN$_2$S$_2$ unit with a face-to-face interaction between the aryl rings as seen in the Ni(SN)$_2$ complex.[21,22] The Ni-S and Ni-N bond distances are within normal ranges for four-coordinate imino-thiolate complexes.[25,26]

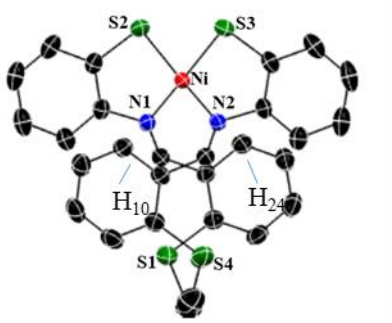

Figure 3.2 Molecular structure of **3-1**. H atoms are omitted for clarity. Selected bond lengths (Å) and angles (deg) can be found in **Table 3.1.**

Bond Lengths (Å)		Bond Angles (deg)	
Ni−S(1)	2.174 (7)	S(1)-Ni-S(3)	87.96(3)
Ni−S(3)	2.170(7)	S(1)-Ni-N(1)	86.52(6)
Ni-N(1)	1.944(2)	S(1)-Ni-N(2)	169.38(6)
Ni-N(2)	1.939(2)	S(3)-Ni-N(1)	170.14(6)
		S(3)-Ni-N(2)	86.59(6)
		N(1)-Ni-N(2)	100.1(8)

Table 3.1 Selected bond lengths (Å) and angles (deg) for **3-1**.

The ^{1}H NMR spectrum of **3-1** is consistent with effective C_2 symmetry, giving rise to a single imine C-H resonance at δ 8.4 and just 8 different aryl H resonances, including one doublet at low field (δ 10.4, $^{2}J_{HH}$ = 7 Hz) (Figure A3.1). A similar resonance at δ 10.95 for the S-Bu^{t} analog[18] was suggested to be due to interaction with the Ni dz^2 orbital, as observed in the solid-state structure (avg. Ni-H = 2.55 Å vs 2.58 Å for Ni-H(10,24) and 2.42 Å in the Ni(SN)$_2$ complex).[22]

3.3.2 Synthesis and comparison of neutral Ni(II)(S_2N_2) thiolate complex

*Thermolysis of **3-1**:* For the previously reported Ni(SN)$_2$ complex, conversion to the Ni(N_2S_2) product (**Scheme 3.3 B**) was achieved after 1 d in DCM at room temperature or 10 min at toluene reflux in yields of 30 and 56%, respectively.[22] In contrast, **3-1** is stable under ambient conditions and conversion to the analogous Ni(N_2S_2) complex **3-2** required 12 h at toluene reflux to obtain just a 20% yield (**Scheme 3.5**). The molecular structure of **3-2** is similar to that determined by Kawamoto et al.[22] (Figure A3.2). The ^{1}H NMR spectrum of **3-2** includes a singlet at δ 7.1 ppm due to the backbone hydrogens. The ground state electronic structure of **3-2** (S = 0) is in contrast

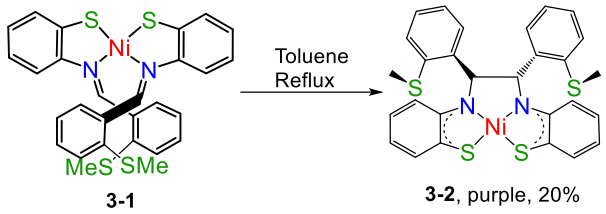

Scheme 3.5 Synthesis of Ni(N_2S_2) complex **3-2**.

to that of the isoelectronic $[Co(N_2S_2)]^-$ anion which has a doublet ground state, suggesting that the two ligand-based electrons in the redox-active ligand constitute a singlet diradical (i.e. α and β spins) in **3-2**. A full analysis of the electronic structure of **3-2** and its two reduced spin states will appear in chapter 4.

3.3.3 Synthesis of di- (3-3), tri- (3-4) and tera- (3-5) nuclear nickel thiolate complexes

*Protonolysis of **1**:* In previous work, we showed that protonation of the Fe SNS bis(amido) complex occurs at nitrogen, facilitating $S^{Me}N^{H}S^{Me}$ ligand loss and providing access to cationic $[Fe(S^{Me}NS^{Me})L_n]^+$ complexes with ancillary ligands L.[13] Protonation of **3-1** with one equiv of bis(trifluoromethane)-sulfonimide, $NHTf_2$ at -35°C in a toluene-DCM solvent mixture occurs at sulfur with subsequent release of the MPB proligand and precipitation of dinuclear thiolate-bridged complex $\{[Ni(\mu\text{-}\kappa^3\text{-}SNS^{Me})]_2\}(NTf_2)_2$ (**3-3**; Tf = SO_2CF_3; **(Scheme 3.6)**(Figure A3.5 & A3.6). In contrast, protonation of **3-1** at room temperature also afforded two crystalline

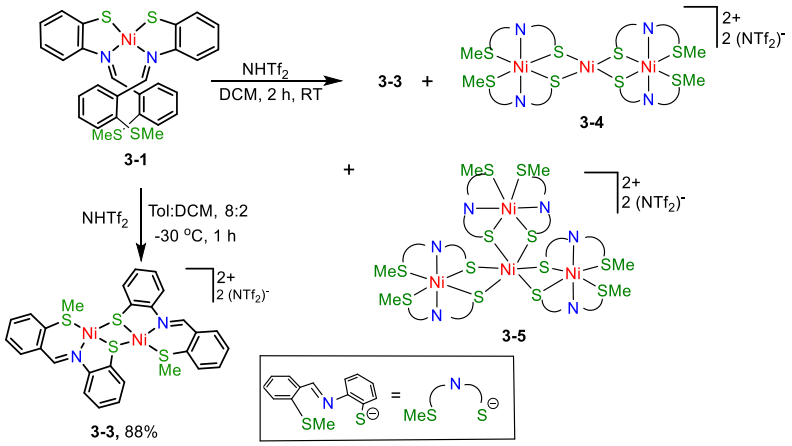

Scheme 3.6 Protonation of **3-1** to give dinuclear thiolate-bridged complex **3-3** or a mixture of **3-4** and **3-5**

paramagnetic products shown by X-ray diffraction to be tri- and -tetranuclear $\{Ni[\mu Ni(\kappa^3SNS^{Me})_2]_2\}(NTf_2)_2$ (**3-4**) and $\{Ni[\mu\text{-}Ni(\kappa^3\text{-}SNS^{Me})_2]_3\}(NTf_2)_2$ (**3-5**). Alternatively, the

triflate salts **3-4'** and **3-5'** can be generated by treating $Ni(OTf)_2$ with 2 equiv and excess (ca. 5 equiv) of **3-1**, respectively (Figure A3.12).

The molecular structure of dication **3-3** (**Figure 3.3**) consists of two distorted square planar Ni centers (N,S bite angles of 5- and 6-membered rings = 80 and 96.5 °) linked by a bent dithiolate bridge (angle between best $NiNS_3$ square planes is 103°), resulting in a fairly short Ni-Ni distance [2.792(5) Å]. The κ^3-SNS^{Me} ligand is meridionally coordinated (S-Ni-S = 172.4(3) °). As in Bouwman's neutral dithiolate complex,[18] the Ni-$S_{thiolate}$ bond distances *trans* to the imine N (avg 2.200(6) Å) are longer than those *trans* to thioether (avg 2.178(8) Å).

The molecular structures of **3-4** and **3-5** feature central NiS_4 and NiS_6 units coordinated by two and three Ni bis(thiolate) metalloligands (**Figs 3.4** and **3.5**).[26] The progressive flattening of the NiS_2Ni bridges is accompanied by longer central Ni-S bonds going from **3-3** (avg 2.18 Å) to **3-4**

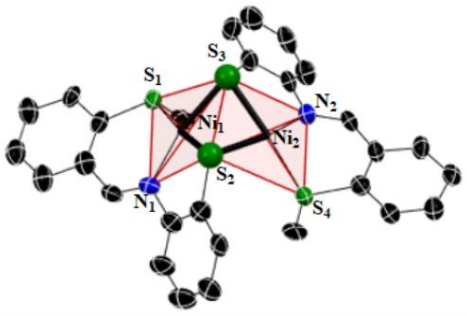

Figure 3.3 Molecular structure of **3-3** showing bent bridge. NTf_2 counter-ion and H atoms are omitted for clarity. Selected bond lengths (Å) and angles (deg) can be found in **Table 3.2**.

Bond Lengths (Å)		Bond Angles (deg)	
Ni(1)·····Ni(2)	2.792(5)	S(2)-Ni(2)-S(3)	80.0(2)
Ni(1)−S(1)	2.178(8)	S(2)-Ni(2)-S(4)	94.2(2)
Ni(1)-S(2)	2.171(8)	S(2)-Ni(2)-N(2)	167.7(5)
Ni(1)-S(3)	2.204(6)	S(3)-Ni(2)-S(4)	172.4(3)
Ni(1)-N(1)	1.90(1)	S(3)-Ni(2)-N(2)	89.8(5)
Ni(2)-S(2)	2.196(6)	S(4)-Ni(2)-N(2)	96.5(5).
Ni(2)-S(3)	2.165(7)		
Ni(2)-S(4)	2.163(6)		
Ni(2)-N(2)	1.94(2)		

Table 3.2 Selected bond lengths (Å) and angles (deg) for **3-3**.

(avg 2.23 Å) and **3-5** (avg 2.45 Å). Moreover, the imines *trans* to thiolate in **3-3** lead to shorter Ni-N bond distances (avg 1.92(2) Å) as compared to those with *trans* imine donors in **3-4** (avg 2.057(3) Å) and **3-5** (avg 2.126(8) Å).

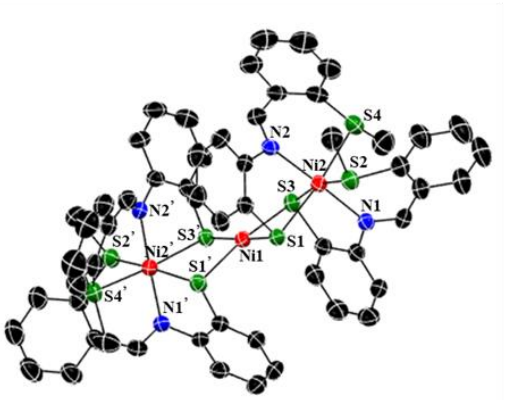

Figure 3.4. Molecular structure of **3-4**. NTf_2 counter-ion and H atoms are omitted for clarity. Selected bond lengths (Å) and angles (deg) can be found in **Table 3.3**.

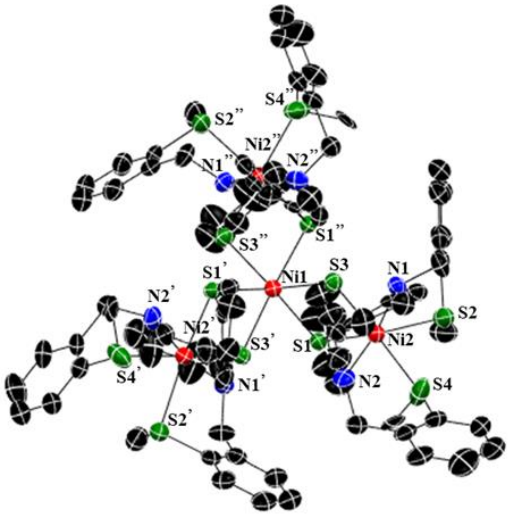

Figure 3.5. Molecular structure of **3-5**. NTf_2 counter-ion and H atoms are omitted for clarity. Selected bond lengths (Å) can be found in **Table 3.4**.

Bond Lengths (Å)		Bond Angles (deg)	
Ni(1)·····Ni(2)	3.313(1)	S(1)-Ni(2)-S(2)	166.90(4)
Ni(1)-S(1)	2.246(1)	S(1)-Ni(2)-S(3)	82.82(4)
Ni(1)-S(3)	2.226(1)	S(1)-Ni(2)-S(4)	94.78(4)
Ni(2)-S(1)	2.357(1)	S(1)-Ni(2)-N(2)	93.76(9)
Ni(2)-S(2)	2.431(1)	S(1)-Ni(2)-N(1)	86.17(9)
Ni(2)-S(3)	2.369 (1)	N(1)-Ni(2)-N(2)	177.7(1)
Ni(2)-S(4)	2.420 (1)		
Ni(2)-N(1)	2.062(3)		
Ni(2)-N(2)	2.052(3)		

Table 3.3 Selected bond lengths (Å) and angles (deg) for **3-4**.

The diamagnetic nature of **3-3** was confirmed by its solid state $^{13}C\{^1H\}$ NMR spectrum (Figure A3.5). In contrast, dissolution of **3-3** in a number of solvents, including weakly

Bond Lengths (Å)	
Ni(1)·····Ni(2)	3.475
Ni(1)-S(1)	2.459(2)
Ni(1)-S(3)	2.438(2)
Ni(2)-S(1)	2.390(2)
Ni(2)-S(2)	2.511(2)
Ni(2)-S(3)	2.359(3)
Ni(2)-S(4)	2.434(4)
Ni(2)-N(1)	2.144(8)
Ni(2)-N(2)	2.108(8)

Table 3.4 Selected bond lengths (Å) for **3-5**.

coordinating CH_2Cl_2, gave broad resonances in the ^{1}H NMR spectrum that were identical to those due to **3-4** (**Figure 3.6**). Although several of the resonances sharpened and shifted on cooling to (-30 °C), no evidence for diamagnetic **3-3** was provided. Moreover, melting a heterogeneous mixture of solid **3-3** and frozen acetone-d_6 in the NMR probe at -75°C gave only **3-4** after just a few minutes of data collection (Fig. A3.14).

3.3.4 Solution dynamics of (3), (4) and (5) complexes

Conversion of **3-3** to **3-4** upon dissolution involves an increase of the ligand:Ni ratio from 1:1 to 4:3, suggesting some formation of $Ni(NTf)_2$ (**Scheme 3.7**). Attempts to further elucidate this dynamic process using UV-Vis spectroscopy met with limited success (Fig. A3.10). An alternate stoichiometric route to trinuclear **3-4** involving reaction of **3-3** with **3-1** also gave a small amount of **3-5** which has a ligand:Ni ratio of 6:4 (Fig.A3.13). The latter could also be obtained by reaction of **3-3** with one equiv of the $(SNS^{Me})^-$ anion (Fig. A3.15).

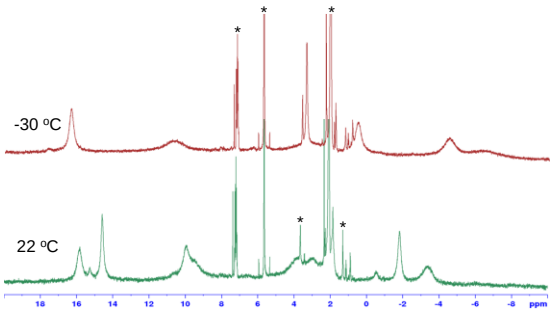

Figure 3.6 300 MHz ^{1}H NMR spectra of **3-4** obtained by dissolution of **3-3** in acetone-d_6. * toluene, DCM and THF solvents.

The equilibrium between the dications of **3-4** and **3-5** was confirmed by reactions of $[Ni(NCMe)_4](OTf)_2$ with **3-1** (Fig. A3.12). Finally, reaction of $[Ni(NCMe)_4](OTf)_2$ with one equiv of $Na(SNS^{Me})$ gives product **3-4** directly (Fig. A3.15) as with the iron reaction shown in **Scheme 1**. Unlike Fe, however, addition of a second equivalent of ligand cleanly affords bis(thiolate) complex **3-1**.

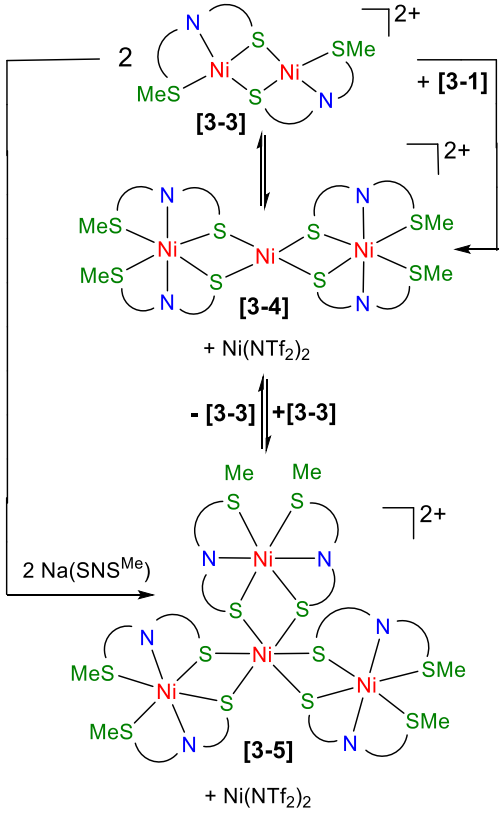

Scheme 3.7 Ligand dynamics of complexes **3-3, 3-4** and **3-5**.

3.3.5 Reactivity of 3-3 with co-ligand Ar-NC

In spite of the observed rapid conversion of **3-3** to **3-4** in solution, addition of donor ligands L to dicationic Ni dimer **3-3** afforded several classes of well-defined products depending on the nature of L. Treatment of **3-3** with two equiv of 2,6-dimethylphenyl isonitrile gave dinuclear$\{[Ni(\mu\text{-}\kappa^3\text{-}SNS^{Me})L]_2\}(NTf_2)$ (**3-6a)** in 62% yield (**Scheme 3.8**). The molecular structure of **3-6a** consists of square bipyramidal nickel centers with a planar bis(thiolate) bridge and isonitrile ligands *trans* to imine nitrogens on opposite sides of the NiS_2Ni bridge (**Figure 3.7**).

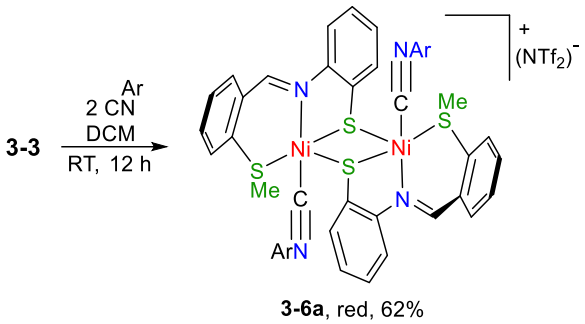

Scheme 3.8. Synthesis of dinuclear, thiolate-bridged Ni isonitrile complex **3-6a.**

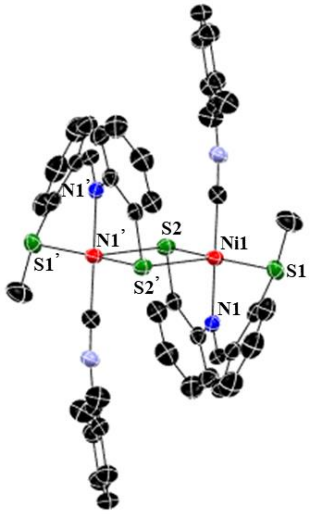

Figure 3.7 Molecular structure of **3-6a.** NTf_2 counter-ion and H atoms are omitted for clarity. Selected bond lengths (Å) and angles (deg) can be found in **Table 3.5**

Bond Lengths (Å)		Bond Angles (deg)	
Ni(1)−S(1)	2.1925(8)	S(1)-Ni(1)-S(2)	166.41(3)
Ni(1)-S(2)	2.1883(8)	S(1)-Ni(1)-S(2')	98.97(2)
Ni(1)-S(2')	2.1904(8)	S(1)-Ni(1)-N(1)	88.61(6)
Ni(1)-N(1)	1.924(2)	S(2)-Ni(1)-N(1)	88.92
Ni(1)-C(15)	1.823(2)	S(2)-Ni(1)-S(2')	94.42(2)
		N(1)-Ni(1)-S(2')	90.71(6)
		Ni(1)-S(2)-Ni(1)	85.58(2)

Table 3.5 Selected bond lengths (Å) and angles (deg) for **3-6a**.

3.3.6 Reactivity of 3-3 with co-ligand dmpm

Addition of chelating bis(phosphine) dmpm to **3-3** gave dinuclear complex {[Ni(μ-κ^3-SNS^{Me})]$_2$(μ-dmpm)}$(NTf_2)_2$ (**3-6b**; dmpm = **bis**(dimethylphosphino)methane; **Scheme 3.9**) in 84 % yield. The

molecular structure of **3-6b** also consists of a planar NiS_2Ni bridge with P trans to imine N that are now on the same side of the bridge (**Figure 3.8**).

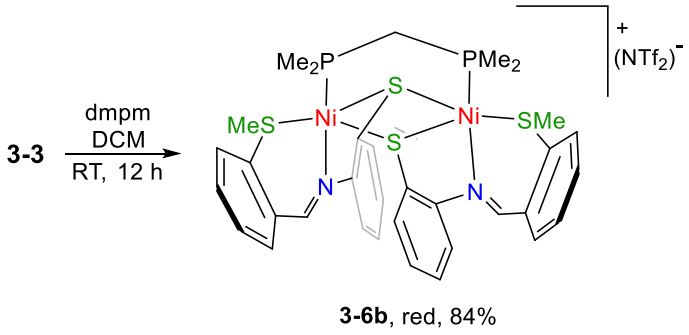

Scheme 3.9. Synthesis of dmpm-bridged dinuclear Ni thiolate complex **3-6b.**

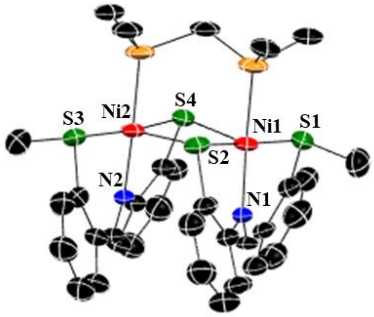

Figure 3.8 Molecular structure of **3-6b**. NTf_2 counter-ion and H atoms are omitted for clarity. Selected bond lengths (Å) and angles (deg) can be found in **Table 3.6.**

Bond Lengths (Å)		Bond Angles (deg)	
Ni(1)−Ni(2)	3.158(2)	S(3)-Ni(2)-S(4)	171.50(9)
Ni(1)-S(1)	2.191(2)	S(3)-Ni(2)-P(2)	91.40(9)
Ni(1)-S(2)	2.179(2)	S(3)-Ni(2)-N(2)	93.4(2)
Ni(1)-S(4)	2.850(3)	S(4)-Ni(2)-P(2)	85.89(9)
Ni(1)-P(1)	2.190(2)	S(4)-Ni(2)-N(2)	88.2(2)
Ni(1)-N(1)	1.954(6)	P(2)-Ni(2)-N(2)	170.6(2)
Ni(2)−S(2)	2.846(3)	Ni(1)-S(1)-Ni(2)	76.62(7)
Ni(2)-S(3)	2.192(2)		
Ni(2)-S(4)	2.176(2)		
Ni(2)-P(2)	2.191(2)		
Ni(2)-N(2)	1.952(6)		

Table 3.6 Selected bond lengths (Å) and angles (deg) for **3-6b**.

3.3.7 Reactivity of 3-3 with co-ligands PMe_3 and $P(OMe)_3$

Addition of monodentate ligands to **3-3** afforded mononuclear cationic thiolate complexes [Ni(κ^3-SNS^{Me})L](NTf_2) with L = PMe_3 (**3-7a**; 80%), $P(OMe)_3$ (**3-7b**; 73%) (**Scheme 3.10**). The molecular structure of **3-7a** consists of a distorted square planar geometry about nickel with S-Ni-N bite angles of 88.7(1) and 93.1(1)° for the 5- and 6-membered rings and a short Ni-$S_{thiolate}$ distance of 2.154(2)Å. (**Figure 3.9**).

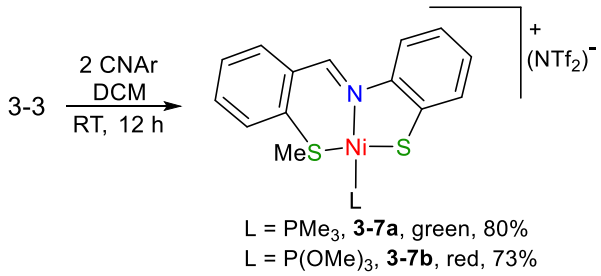

Scheme 3.10. Synthesis of mononuclear Ni thiolate cations.

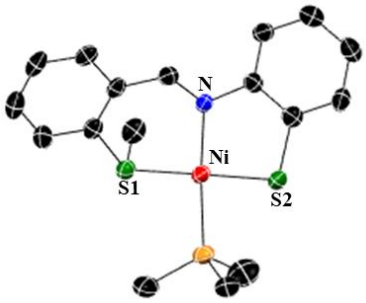

Figure 3.9. Molecular structure of the cation of (**3-7a**). NTf_2 counter-ion and H atoms are omitted for clarity. Selected bond lengths (Å) and angles (deg) can be found in **Table 3.7**

Bond Lengths (Å)		Bond Angles (deg)	
Ni-S(1)	2.182(1)	S(1)-Ni-S(2)	173.33(5)
Ni-S(2)	2.154(2)	S(1)-Ni-P	92.59(5)
Ni-P	2.188(1)	S(1)-Ni-N	93.06(9)
Ni-N	1.954(3)	S(2)-Ni-P	85.91(5)
		S(2)-Ni-N	88.7(1)
		P-Ni-N	173.9(1)

Table 3.7 Selected bond lengths (Å) and angles (deg) for **3-7a**.

3.3.8 Reactivity of 3-3 with NHC co-ligand IPr

In contrast to the P-donor ligands, addition of the NHC ligand IPr (1,3-bis(2,6-diisopropylphenyl)imidazol-2-ylidene) to complex **3-3** afforded a mixture of products. Using 2 equiv of IPr per Ni, however gave a clean reaction that resulted in selective S-C_{Me} cleavage, forming neutral complex [Ni(κ^3-SNS)(IPr)] (**3-8**) in good yield along with [*N*-Me-IPr]NTf_2 (**Scheme 3.11**).

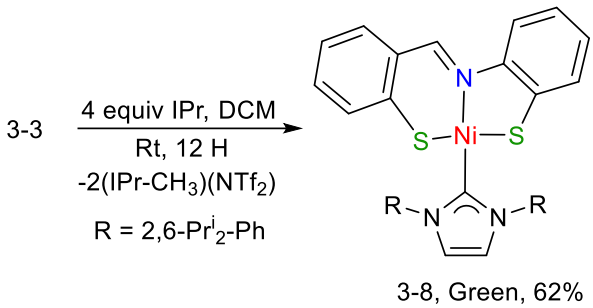

Scheme 3.11 Synthesis of neutral NHC Ni bis(thiolate) complex **3-8**.

The molecular structure of **3-8** exhibits a similar distorted square planar geometry to that of **3-7a** with similar Ni-$S_{thiolate}$ bond distances and a somewhat shorter Ni-N distance (1.915(6) vs 1.954(3)Å; **Figure 3.10**).

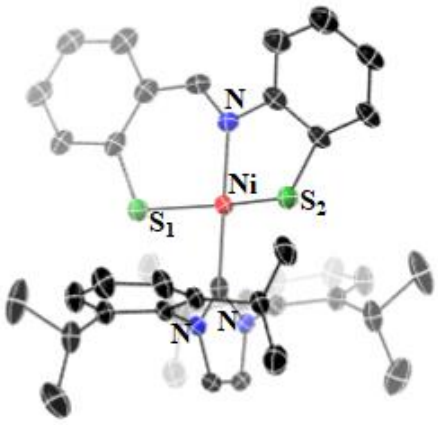

Figure 3.10. Molecular structure of (**3-8**). H atoms are omitted for clarity. Selected bond lengths (Å) and angles (deg) can be found in **Table 3.8**.

Bond Lengths (Å)		Bond Angles (deg)	
Ni-S(1)	2.164(4)	S(1)-Ni-S(2)	173.7(2)
Ni-S(2)	2.153(4)	S(1)-Ni-N	88.9(2)
Ni-C	1.910(4)	S(1)-Ni-C	90.7
Ni-N	1.915(6)	S(2)-Ni-N	97.1(2)
		S(2)-Ni-C	83.3(2)
		N-Ni-C	179.6(3)

Table 3.8 Selected bond lengths (Å) and angles (deg) for **3-8**.

3.4 Discussion

Comparing the rich coordination chemistry of d^8 Ni SNS thiolate complexes to that of the d^6 Fe analogs reveals a number of stark differences. The pseudo-octahedral Fe bis(thiolate) moiety has only been accessed as components of the trinuclear dication as attempts to prepare it directly yielded instead the Fe(N_2S_3) complex exclusively (**Scheme 3.1**).[12,28] In contrast, the Ni bis(thiolate) complex is stable as a distorted square planar complex with uncoordinated SMe donors. Upon protonation, however, loss of one MPB proligand affords crystals of the thiolate-bridged dinuclear dication **3-3** with κ^3-SNS^{Me} meridional coordination – a similar structure to Bouwman's neutral Ni dithiolate dimer (**Scheme 3.3**).[18] Remarkably, dissolution of crystals of ..**3-3** even in weakly-coordinating solvents such as DCM drives its conversion to an analogous trinuclear complex in which now two paramagnetic, pseudo-octahedral Ni bis(thiolate) moieties coordinate to a square planar Ni^{2+} cation. Indeed, the minimal steric requirements of the Ni bis(thiolate) unit even permit formation of the tetranuclear dication that includes an octahedral central NiS_6 unit. These ligand dynamics require formation of a 'naked' anion-stabilized Ni center as demonstrated by reactions of $[Ni(NCMe)_4](OTf)_2$ with neutral Ni bis(thiolate) complex **3-1** to generate multinuclear complexes **3-4'** and **3-5'**. Moreover, reaction of $[Ni(NCMe)_4](OTf)_2$ with one equivalent of Na(SNS^{Me}) affords **3-4** directly, just as observed for the Fe system.[12] Intermolecular dynamics of multidentate, anionic ligands have been little studied, especially for their potential role in homogeneous catalysis.

The reactivity of these Ni SNS thiolate complexes can be compared to those introduced previously. Inclusion of the SMe group prevented thermal C-S bond cleavage to the dithiolate ligand as seen for Bouwman's SBu^t analog.[18] It is surprising that inclusion of the *ortho*-SMe group has such a stabilizing effect on the Ni bis(thiolate) complex (relative to $Ni(SN)_2$ that slowly

converts to Ni(N_2S_2) via imine C-C bond formation even at 25°C).[21] While these isomerizations are also accompanied by side-reactions that limit reaction yields (56% from $Ni(SN)_2$ and just 25% from **3-1**), work in the next chapter shows that this coupling can be effected quantitatively upon 1e- reduction of **3-1**.

Although we were unable to detect any diamagnetic **3-3** in solution, the fact that it can be recrystallized from concentrated DCM suggests that its conversion to **3-4** is reversible. Nonetheless, ancillary ligand additions may proceed directly from **3-4** as observed previously with Fe which also gave both mono- and dinuclear thiolate complexes.[12] With the most electron-rich NHC ligand, however, demethylation of the coordinated thioether affords neutral dithiolate complex **3-8**, returning us once again to Bouwman's results,[18] albeit presumably proceeding by a different C-S bond cleavage mechanism.[29] Note that this selective C-S_{Me} bond cleavage contrasts with the C-S_{aryl} bond cleavage depicted for electron-rich Fe[15] and Co precursors[20] in **Scheme 3.2**.

3.5 Conclusion

The work reported herein reveals further the versatility of the simple thiolate-imine-thioether tridentate SNS pincer ligand. Protonation of the κ^2-bis(thiolate) Ni complex **3-1** affords the dimeric κ^3-thiolate bridged dication **3-3** that exhibits a similar structure as Bouwman's neutral dithiolate dimer. Addition of a variety of ligands to **3-3**, greatly expands the ancillary ligand coordination chemistry of these SNS ligand complexes which differ from their pseudooctahedral Fe analogues.[12] Using a strong donor *N*-heterocyclic carbene ligand, we demonstrated an alternate S-C bond cleavage pathway to the one known, allowing access to additional complexes containing Bouwman's dianionic dithiolate pincer ligand. Most remarkably, we showed that **3-3** undergoes facile anionic tridentate ligand dynamics in which coordination of the hemilabile thioether donor constructs multimetallic, thiolate-bridged arrays containing paramagnetic, pseudooctahedral Ni(II) centers. Although there are a number of studies of bidentate anionic ligand dynamics such as carboxylates,[30] such studies with tridentate X-ligands are rare.[31]

With a variety of neutral and cationic Ni SNS thiolate complexes in hand with ancillary ligands ranging from strong donors to powerful π-acceptors, we are currently in the process of investigating their potential as homogeneous catalysts for reductive transformations.

3.6 Experimental Section

3.6.1 General Considerations All experiments were carried out under nitrogen, using a Schlenk line or an MBraun glovebox unless otherwise stated. All solvents were deoxygenated by purging with nitrogen. Toluene, hexanes, diethyl ether, and THF were dried on columns of activated alumina using a J. C. Meyer (formerly Glass Contour) solvent purification system. Anhydrous benzene (Aldrich), C_6D_6 and acetone-d_6 were dried with activated alumina (ca. 10 wt %) overnight, followed by filtration. Dichloromethane (DCM) and $CDCl_3$ were refluxed over calcium hydride under nitrogen, collected by distillation, dried further by passing through activated alumina (ca.10 wt%), and stored over activated 4 Å molecular sieves (heated at 250 ºC for 3 d under vacuum). Ligand precursor 2-(methylthio)-benzaldehyde[24] and the $SN^{H}S^{Me}$ (MPB) proligand[12] were prepared according to literature procedures. Other chemicals were used as obtained commercially: 2-(methylthio)-aniline (Alfa Aesar, 98%), $Ni(acac)_2$ (Oakwood chemical, 95%), 2,6-dimethylphenyl isonitrile (CNxylyl, Aldrich, 96%), bis(dimethylphosphino)methane (dmpm, Strem, 98%), trimethylphosphite [$P(OMe)_3$, Strem, 97%], trimethylphosphine [PMe_3, Strem, 98%], trifluoromethane sulfonimide ($NHTf_2$, Aldrich >95%) and 1,3-bis(2,6-diisopropylphenyl)imidazolium chloride (IPr•HCl, Aldrich, 97%). ^{1}H, ^{19}F, and ^{31}P NMR spectra were recorded on a 300 MHz Bruker Avance or Avance II instrument at room temperature (21−25 °C) and $^{13}C\{^{1}H\}$ NMR and MAS NMR spectra were recorded on a 500 MHz Bruker Avance instrument. ^{13}C and ^{1}H NMR spectra were referenced respectively to solvent carbons and residual protons (C_6D_6, δ 7.15; $CDCl_3$, δ 7.26) with respect to tetramethylsilane at δ 0.00. ^{19}F and ^{31}P NMR chemical shifts were referenced to external $CFCl_3$ and H_3PO_4 at 0 ppm. UV−vis spectra were recorded on an Agilent Cary 7000 universal measurement spectrophoto-meter. IR data were collected on a Thermo Scientific Nicolet 6700 FT-IR spectrometer. Mass spectra were recorded on an AB Sciex Q1MS mass spectrometer with electrospray ionization (ESI-MS) in positive mode (ion spray voltage: 5000.0 V, TEM: 400 °C, declustering potential: 11.00 V and focusing potential: 300.0 V) with samples prepared to *ca.* 0.05 mg/mL in acetonitrile or dichloro-methane. For electron impact (EI), solid samples were prepared by drying products under vacuum, and spectra obtained using a Kratos Concept S1 instrument (Hres 7000−10000). X-ray diffraction data were collected on a Bruker Smart or Kappa diffractometer equipped with an ApexII CCD detector and a sealed-tube Mo K source (λ = 0.71073 Å). Elemental analyses were performed by University of

Guelph Elemental Analysis service (all charged products gave poor results likely due to incomplete combustion of the $(NTf_2)^-$ anion).

3.6.2 X-ray Crystallographic Details. Crystallographic data collection and processing were performed via the X-Ray Core Facility at the University of Ottawa. Crystals were mounted on MiTeGen sample holders using Parabar oil. Data were collected on a Bruker Smart (**3-1, 3-4, 3-6a,b, 3-7a** and **3-8**) or Kappa (**3-2, 3-3** and **3-5**) diffractometer equipped with an ApexII CCD detector and a sealed-tube Mo K source (λ = 0.71073 A). During collection, crystals were cooled to approx. 200 K. Sample cooling was effected via a refrigerated, dry compressed air stream. Raw data collection and processing were performed with the Apex3 software package from Bruker.[31] Initial unit cell parameters were determined from 36 data frames from select ω scans. Semi-empirical absorption corrections based on equivalent reflections were applied.[32] Systematic absences in the diffraction data-set and unit-cell parameters were consistent with the assigned space group. Compound **3** crystallized as a non-merohedral twin. The twin law was discovered using CELL_NOW,[33] and accounted for in the absorption correction via twinabs.[34] The twin law was also accounted for and twin fractions refined during final refinements. The initial structural solutions for all structures were determined using ShelxT direct methods,[35] and refined with full-matrix least-squares procedures based on F^2 using ShelXle.[36] Carbon and nitrogen-based hydrogen atoms were placed geometrically and refined using a riding model, all other hydrogen atoms were placed via the difference map and refined with restraints. Structures of complexes **4** and **5** contained solvent molecules which could not be rationalized by the XRD data. The electron density was thus accounted for using Squeeze.[37]

3.6.3 Synthesis of $Ni^{II}(\kappa^2\text{-}SNS^{Me})_2$ (3-1). A 50 mL round-bottom Schlenk flask was charged with $Ni(acac)_2$ (149 mg, 0.58 mmol) in 10 mL of THF and a solution of the MPB proligand (300 mg, 1.16 mmol) in 20 mL of THF was added dropwise. The color changed rapidly from green to red-brown. After stirring for 12 h at 60 °C, the solvent was removed under vacuum. The resulting red solid was then washed with hexane (3 X 5 mL), benzene (3 X 5 mL) and dried in vacuum yielding 255 mg (77 %). Crystals of (**3-1**) suitable for X-ray crystallography were obtained from a concentrated DCM solution at −35 °C. ^{1}H NMR (300 MHz, $CDCl_3$) δ 10.70 (d, 7, 1H, Ar-*H*), 8.87 (br s, imine C-*H*), 7.40 (d, 7, 1H, Ar-*H*), 7.32 (tr, 7.5, 1H, Ar-*H*), 7.24 (d, 1H, Ar-*H*), 6.98 (tr, 7, 1H, Ar-*H*), 6.75 (tr, 7, 1H, Ar-*H*), 6.67 (tr, 7, 1H, Ar-*H*), 6.31 (d, 8,1H, Ar-*H*), 2.66 (s, 3H, S−CH_3) (Fig. A3.1). $^{13}C\{^1H\}$ NMR (125.8 MHz, $CDCl_3$) δ 165.0, 150.8, 145.0 (C=N), 139.8 (br), 133.6,

131.8, 131.3, 129.0 (br), 127.6 (br), 126.1, 121.5, 117.4, 17.2 (S-CH_3) (Fig. A3.2). Anal. Calcd for $C_{28}H_{24}N_2NiS_4$: C, 58.44; H, 4.20; N, 4.87. Found: C, 58.33; H, 4.45; N, 5.10.

3.6.4 Synthesis of Ni(N_2S_2) (3-2). A solution of 100 mg, 0.17 mmol) **3-1** in 15 mL of toluene was heated at reflux overnight under N_2 with no noticeable color change. The solvent was removed under vacuum and the resulting residue dissolved in ca. 5 mL of dichloro-methane and filtered. The filtrate was then purified by chromatography on silica gel eluting with DCM to provide 25 mg of violet solid **(3-2)** (25% yield). Single crystals were obtained from concentrated DCM by layering with hexane at -35 ºC. ^{1}H NMR (500 MHz, C_6D_6) δ 7.56 (ov mult, 4H, Ar-*H*), 7.46 (dd, 8, 1, 2H, Ar-*H*), 7.10 (s, 2H, backbone C-*H*), 7.04 (d, 8, 2H, Ar-*H*), 6.76 (tr d, 7.5, 1, 2H, Ar-*H*), 6.62 (ov mult, 4H, Ar-*H*), 6.36 (tr d, 7.5, 1, 2H, Ar-*H*), 2.12 (s, 6H, S−CH_3) (Fig. A3.3).^{13}C{^{1}H} NMR (126 MHz, C_6D_6) δ 162.7 (Ar−C=N), 161.1 (Ar−C=N), 142.9 (Ar−C), 137.5 (Ar−C), 131.9 (Ar−C), 126.7 (Ar−C), 126.1 (Ar−C), 123.1 (Ar−C), 120.6 (Ar−C), 79.2 (backbone C), 17.4 (S-CH_3) (Fig. A3.4).Anal. Calcd for $C_{28}H_{24}N_2NiS_4$: C, 58.44; H, 4.20; N, 4.87. Found: C, 58.16; H, 5.11; N, 4.79.

3.6.5 Synthesis of {[Ni(μ-κ^3-SNS^{Me})$_2$}(NTf$_2$)$_2$ (3-3). A 20 mL scintillation vial was charged with **3-1** (100 mg, 0.17 mmol) in 2 mL of DCM cooled to -35 ºC. To this cooled solution, was added dropwise 49 mg (0.17 mmol) of bis(trifluoromethane)sulfonimide, $NHTf_2$, in 8 mL of toluene. The resulting bright brown solution was stirred for 2 h at room temperature with precipitation of red solid **3** that was filtered, washed with toluene (3 X 10 mL) and dried in vacuum to give 97 mg (88 %). Crystals of **3-3** suitable for X-ray crystallography were obtained from a concentrated DCM solution at −35 °C. Selected ^{1}H NMR resonances (actually due to **3-4**; 300 MHz, acetone-d_6) δ 15.8 (br s, 4H), 14.5 (br s, 4H), 9.9 (ov br s, 8H), 3.8 (br m, 4H), 1.9 (br s), -1.8 (br s, 4H), -3.3 (br s, 4H) (Fig. A3.5). ^{13}C{^{1}H} MAS NMR (126 MHz, Fig. S6) δ 166.9 (ov s), 157.5 (ov s), 142.0 (ov s), 140.2 (ov s), 136.1 (ov s), 134.4 (ov s), 133.0 (ov s), 132.1 (ov s), 130.3 (ov s), 124.8 (s), 123.6 (ov s), 121.1 (ov s), 26.4 (ov s, S-*C*H_3) (Fig. A3.6). MS: [M$^+$-2Me] 601.9 Calcd 601.910 (Fig. S8) and [Ni(SNS^{Me})]$^+$ 315.736 Calcd 315.977 (Fig. A3.8).

3.6.6 Isolation of {Ni[μ-Ni(κ^3-SNS^{Me})$_2$]$_2$}(OTf)$_2$ (3-4') and {Ni[μ-Ni(κ^3-SNS^{Me})$_2$]$_3$}(OTf)$_2$ (3-5'). A A 20 mL vial was charged with **3-1** (100 mg, 0.17 mmol) in 15 mL of DCM and to this solution was added a solution of [Ni(MeCN)$_4$](OTf)$_2$ (0.5 equiv for **3-4'** and 0.2 equiv for **3-5'**) in 5 mL of DCM. No significant color change was observed. The resulting brown solution was stirred for 2 h at room temperature and the solvent was removed under vacuum. The remaining red solid

was washed with benzene (3 X 10 mL) and hexane (2 X 10 mL) and dried to obtain 75 mg (72%) and 52 mg (80 %) yield of complex **3-4'** and **3-5'**, respectively. Selected ^{1}H NMR resonances for **3-4'** (300 MHz, acetone-d_6) δ 15.84 (br, s), 14.55 (br,s), 10.07 (br, s), 7.55 (br, s), 6.76 (br, s), 6.43 (s), -0.83 (br, s), -1.89 (br, s), -3.47 (br, s), -4.34 (br, s) (Figure A3.12). ^{19}F NMR (282 MHz, acetone-d_6) -78.5 ppm (br, s, OTf) (Fig. A3.12).Selected ^{1}H NMR resonances for **3-5'** (300 MHz, acetone-d_6) δ 15.8 (br s), 7.53 (br s), 6.75 (br s), 6.4 (br s), -0.79 (br, s), -4.32 (br s).

3.6.7 Reaction of complex (3-3) with (3-1). To an NMR tube charged with a purple solution of (**3-1**) (10 mg, 0.017 mmol) in 0.5 mL of acetone-d_6 was added (**3-3**) (10 mg, 0.016 mmol, 1.0 equiv). The NMR tube was shaken continuously for 10 min affording a dark red solution that was characterized by ^{1}H NMR spectroscopy (Fig. A3.13).

3.6.8 Reaction of complex (3-3) with Na(SNS^{Me}). A 10 mL scintillation vial was charged with 11.0 mg of $S^{Me}N^{H}S$ ligand (0.04 mmol) in 10 mL of THF. To this solution was added 4 mg NaO^{t}Bu (0.04 mmol) in 3 mL of THF. The resulting yellow/brown solution was stirred for 30 min and solvent was removed under vacuum. The residue was dissolved in 0.4 mL of acetone-d_6 and added to an NMR tube containing 24 mg of **3-3** (0.04 mmol) in 0.4 mL of acetone-d_6 yielding a red solution. Continuous shaking of the NMR tube for 10 min gave a red solution that was characterized by ^{1}H NMR spectroscopy (Fig. A3.15).

3.6.9 Synthesis of {[Ni(μ-κ^3-SNS^{Me})(CNxylyl)]$_2$}(NTf$_2$)$_2$ (3-6a). A 20 mL scintillation vial was charged with **3-3** (100 mg, 0.16 mmol) in 10 mL of DCM and 41 mg (0.32 mmol) of 2,6-dimethylphenylisonitrile in 3 mL of DCM was added dropwise using a micro-syringe. The red solution was stirred for 12 h after which the solvent was removed and the remaining red solid washed with hexane (3 X 10 mL) and cold diethyl ether (4 X 15 mL). Drying under vacuum gave 92 mg (62%). Crystals suitable for X-ray diffraction were obtained by layering hexane on a concentrated dichloromethane solution at room temperature. ^{1}H NMR (300 MHz, acetone-d_6) δ 8.21 (br s, 2H), 7.51 (br s, 2H), 7.36 (br s, 2H), 7.13 (ov br s, 4H), 6.91 (br s, 2H), 6.65 (ov s, tr, 4H), 6.52 (d, 7, 6H, CNAr-*H*), 6.31 (br s, 2H), 2.54 (s, 6H, S-CH_3), 1.72 (s, 6H, CNAr-CH_3), 1.27 (s, 6H, CNAr-CH_3) (Fig. A3.16). ^{19}F NMR (282 MHz, acetone-d_6) δ −78.6 (br, s, NTf_2). ESI-MS [Ni(SNS^{Me})(CNAr)]$^+$ 447.0491 Calcd 447.0500 (Fig. A3.17).

3.6.10 Synthesis of {[Ni(μ-κ^3-SNS^{Me})]$_2$(μ-dmpm)}(NTf$_2$)$_2$ (3-6b). A 20 mL scintillation vial was charged with **3-3** (20 mg, 0.03 mmol) in 20 mL of DCM and bis(dimethylphosphino)methane (4 mg, 0.03 mmol) was added dropwise using a micro-syringe. The resulting red solution was stirred

for 12 h, the solvent was removed under reduced pressure and the remaining red solid was washed with hexanes (3 X 10 mL) and cold diethyl ether (4 X 15 mL) and dried under vacuum to yield 20 mg (84%). Crystals suitable for X-ray diffraction were grown from concentrated DCM layering with pentane solution at -35 °C. ^{1}H NMR (300 MHz, $CDCl_3$) δ 8.62 (br s, 2H), 7.72 (ov mult, 4H), 7.55 (br, 2H), 7.44 (br, 4H), 7.03 (ov mult, 4H), 6.75 (d, 7.5, Ar-*H*), 4.44 (br, s), 3.12 (br, s), 2.50 (br, m), 1.96 (br, d), 1.72 (br, m) (Fig. A3.18). ^{31}P{^{1}H} NMR (121 MHz, $CDCl_3$) -45.5 ppm (s) (Fig. A3.19). ^{19}F NMR (282 MHz, acetone-d_6) -78.6 ppm (br, s, NTf_2). ESI-MS $[M\text{-}Me]^+$ 752.9844 Calcd 752.9865 (Fig. A3.20).

3.6.11 Synthesis of [Ni(κ^3-SNS^{Me})(PMe$_3$)](NTf$_2$), (3-7a). A 20 mL scintillation vial was charged with **3-3** (80 mg, 0.13 mmol) in 15 mL of DCM. To this solution, trimethylphosphine (19 mg, 0.25 mmol) was added dropwise using a micro-syringe. The resulting red solution was stirred for 2 h after which the solvent was removed and the red solid product was washed with cold diethyl ether (3 X 2 mL) and hexanes (3 X 3 mL). Drying in vacuum afforded 45 mg (80%). Crystals suitable for X-ray diffraction were grown from a concentrated DCM solution at –35 °C. ^{1}H NMR (300 MHz, $CDCl_3$) δ 8.49 (s, 1H, C-*H*), 7.98 (d, 7.5, 1H, Ar-*H*), 7.92 (d, 8, 1H, Ar-*H*), 7.78 (t, 7.5, 1H, Ar-*H*), 7.68 (t, 7.5, 1H, Ar-*H*), 7.41 (d, 8, 1H, Ar-*H*), 7.33 (d, 8, 1H, Ar-*H*), 7.18 (t, 7.5, 1H, Ar-*H*), 7.02 (t, 7.5, 1H, Ar-*H*), 2.84 (s, 3H, S-CH_3), 1.54 (d, 11.5, 9H, P-CH_3) (Fig. A3.21). ^{31}P{^{1}H} NMR (121 MHz, $CDCl_3$) -8.6 ppm (s) (Fig. A3.22). ^{19}F NMR (282 MHz, $CDCl_3$) -78.6 ppm (br s, NTf_2). ESI-MS M+ 392.0166 Calcd 392.0207 (Fig. A3.23).

3.6.12 Synthesis of [Ni(κ^3-SNS^{Me})(P(OMe)$_3$)](NTf$_2$), (3-7b). A 20 mL scintillation vial was charged with **3-3** (70 mg, 0.11 mmol) in 15 mL of DCM. Trimethylphosphite (27 mg, 0.22 mmol) was added dropwise to the solution using a micro-syringe. After stirring for 2 h the solvent was removed and the red solid washed with cold diethyl ether (3 X 2 mL) and hexanes (3 X 3 mL). Drying the solid gave 40 mg (73%). ^{1}H NMR (300 MHz, $CDCl_3$) δ 8.64 (s, 1H, C-*H*), 8.00 (d, 7, 1H, Ar-*H*), 7.90 (d, 7, 1H, Ar-*H*), 7.76 (tr, 7, 1H, Ar-*H*), 7.70 (tr, 7, 1H, Ar-*H*), 7.55 (d, 7, 1H, Ar-*H*) 7.33 (d, 7, 1H, Ar-*H*), 7.17 (tr, 7, 1H, Ar-*H*), 7.04 (tr, 7, 1H, Ar-*H*), 3.92 (d, 11.5, 9H, P-OCH_3), 2.83 (s, 3H, S-CH_3) (Fig. A3.25). ^{31}P{^{1}H} NMR (121 MHz, $CDCl_3$) 106.7 ppm (s) (Fig. A3.26). ^{19}F NMR (282 MHz, $CDCl_3$) −78.6 ppm (br, s, NTf_2). ESI-MS M^+ 440.0023 Calcd 440.0054 (Fig. S27) (Fig. A3.27).

3.6.13 Synthesis of Ni(κ^3-SNS)(IPr), (3-8). A 20 mL scintillation vial was charged with **3-3** (100 mg, 0.16 mmol) in 15 mL of DCM. To this solution, 1-(2,6-diisopropylphenyl)-imidazol-2-ylidene

(245 mg, 0.64 mmol) in 5 mL DCM was added dropwise. The resulting red solution was stirred for 12 h at room temperature after which the solvent was removed. The residue was extracted with toluene, filtered through Celite and the solvent removed. After washing with cold diethyl ether (3 X 2 mL) and hexanes (3 X 3 mL), drying in vacuum afforded 87 mg (81%). Crystals suitable for X-ray diffraction were grown from a concentrated DCM solution at room temperature. ^{1}H NMR (300 MHz, C_6D_6) δ 7.97 (d, 8, 1H), 7.86 (s, 1H, imine C-H), 7.71 (d, 8, 1H), 7.11 (ov mult, 4H), 6.96 (ov mult, 3H), 6.79 (d, 8, 1H), 6.70 (d, 7.5, 1H), 6.66 (s, 2H, IPr backbone C-*H*), 6.56, 2H, IPr), 3.62, 3.45 (sept, IPr ^{i}Pr C-*H*, 2H), 1.66, 1.57, 1.10, 1,08 (d, 6.5, 6H, IPr ^{i}Pr CH_3) (Fig. A3.28). EI-MS [M-1]+ 603.33.

3.7 References

(1) Morales-Morales, D.; Jensen, C. M. *The Chemistry of Pincer Compounds*, Elsevier, Amsterdam, 2007.

(2) van Koten, G.; Milstein, D. *Organometallic Pincer Chemistry*, Springer-Verlag: Berlin-Heidelberg, 2013.

(3) Peris, E.; Crabtree, R. H. Key Factors in Pincer Ligand Design. *Chem. Soc. Rev.* **2018**, *47*, 1959-1968.

(4) Lawrence, M. A. W.; Green, K-A.; Nelson, P. N.; Lorraine, S. C. Review: Pincer Ligands – Tunable, Versatile and Applicable. *Polyhedron* **2018**, *143*, 11-27.

(5) Maser, L.; Vondung, L.; Langer, R. The ABC in Pincer Chemistry – From Amine- to Borylene- and Carbon-based Pincer Ligands. *Polyhedron* **2018**, *143*, 28-42.

(6) Ragsdale, S. W. Metals and Their Scaffolds to Promote Difficult Enzymatic Reactions. *Chem. Rev.* **2006**, *106*, 3317-3337.

(7) Can, M.; Armstrong, F. A.; Ragsdale, S. W. Structure, Function, and Mechanism of the Nickel Metalloenzymes, CO Dehydrogenase and Acetyl-CoA Synthase. *Chem. Rev.* **2014**, *114*, 4149-4174.

(8) Boer, J. L.; Mulrooney, S. B.; Hausinger, R. P. Nickel-Dependent Metalloenzymes, *Arch. Biochem. Biophys.* **2014**, *544*, 142-152.

(9) Siegbahn, P. E. M.; Chen, S.-L.; Liao, R. Z. Theoretical Studies of Nickel-Dependent Enzymes. *Inorganics* **2019**, *7*, 95 (29 pp).

(10) van der Vlugt, J. I.; Meyer, F. Synthetic Models for the Active Sites of Nickel-Containing Enzymes in *Nickel and Its Surprising Impact in Nature, Vol. 2*, Sigel, A.; Sigel, H.; Sigel, R. K. O., eds. John Wiley and Sons: Hoboken, 2007, Chap. 5, pp. 189-239.

(11) McQuilken, A. C.; Jiang, Y.; Siegler, M. A.; Goldberg, D. P. Addition of Dioxygen to an N_4S(thiolate) Iron(II) Cysteine Dioxygenase Model Gives a Structurally Characterized Sulfinato−Iron(II) Complex. *J. Am. Chem. Soc.* **2012**, *134*, 8758-8761.

(12) Das, U. K.; Daifuku, S. L.; Gorelsky, S. I.; Korobkov, I.; Neidig, M. L.; Le Roy, J. J.; Murugesu, M.; Baker, R. T. Mononuclear, Dinuclear, and Trinuclear Iron Complexes Featuring a New Monoanionic SNS Thiolate Ligand. *Inorg. Chem.* **2016**, *55*, 987–997.

(13) Das, U. K.; Daifuku, S. L.; Ianuzzi, T. E.; Gorelsky, S. I.; Korobkov, I.; Gabidullin, B. M.; Neidig, M. L.; Baker, R. T. Fe(II) Complexes of a Hemilabile SNS Amido Ligand. *Inorg. Chem.* **2017**, *56*, 987–997.

(14) Das, U. K.; Higman, C. S.; Korobkov, I.; Gabidullin, B. M.; Hein, J. E.; Baker, R. T. Efficient and Selective Iron Complex-Catalyzed Hydroboration of Aldehydes. *ACS Catal.* **2018**, *8*, 1076-1081.

(15) Elsby, M. R.; Ghostine, K.; Das, U. K.; Korobkov, I.; Gabidullin, B. M.; Baker, R. T. Fe-SNS and -CNS Complexes: C_{aryl}-S Bond Cleavage and Amine-Borane Dehydrogenation Catalysis. *Organometallics* **2019**, *38*, 3844-3851.

(16) Elsby, M. R.; Baker, R. T. Cu(I)-SNS Complexes for Outer-sphere Hydroboration and Hydrosilylation of Carbonyls. *Chem. Commun.* **2019**, *55*, 13574-13577.

(17) Elsby, M. R.; Baker, R. T. Strategies and Mechanisms of Metal-ligand Cooperativity in First-row Transition metal Complex Catalysts. *Chem. Soc. Rev.* **2020**, *49*, 8933-8987.

(18) Bouwman, E.; Henderson, R. K.; Powell, A. K.; Reedijk, J.; Smeets, W. J. J.; Spek, A. L.; Veldman, N.; Wocadlo, S. Anion Dependent Deprotection of a Thioether Group in Schiff Base NS_2 Ligands Results in New Mononuclear and Dinuclear Thiolato Nickel Complexes. *J. Chem. Soc., Dalton Trans.* **1998**, 3495–3499.

(19) Goetz, F. J. Heterocyclic Tautomerisms. III. An Investigation of the 2-Arylbenzo-thiazoline-2-(benzylideneamino)thiophenol Tautomerism. Part 3. *J. Heterocyclic Chem.* **1968**, *5*, 509-512.

(20) Fitchett, B. Oxidation State Roulette: Synthesis and Reactivity of Cobalt Complexes Containing SNS Ligands. University of Ottawa MSc thesis, 2018.

(21) a) Kochin, S. G.; Garnovskii, A. D.; Kogan, V. A.; Osipov, O. A.; Sushko, T. G. *Russ. J. Inorg. Chem.* **1969**, *14*, 748. b) D'yachenko, O. A.; Atovmyan, L. O.; Aldoshin, S. M.; Kogan, V. A.; Kochin, S. G. Osipov, O. A. Study of the X-ray Crystal Struture of bis(benzylidene-2'-mercaptoanilinato)nickel. *Bull. Acad. Sci. USSR. Div. Chem. Sci.* **1975**, *4*, 2019.

(22) a) Kawamoto, T.; Kushi, Y. *Chem. Lett.* **1992**, 893. b) Kawamoto, T.; Kuma, H.; Kushi, Y. Valence Isomerization. Synthesis and Characterization of Cobalt and Nickel Complexes with Non-Innocent N_2S_2 Ligand. *Bull. Chem. Soc. Jpn.* **1997**, *70*, 1599-16046.

(23) Kawamoto, T.; Takeda, K.; Nishiwaki, M.; Aridomi, T.; Konno, T. Square-Planar $N_2S_2Ni^{II}$ Complexes with an Extended π-Conjugated System. *Inorg. Chem.* **2007**, *46*, 4239–4247.

(24) Bieszczad, B.; Barbasiewicz, M. The Key Role of the Nonchelating Conformation of the Benzylidene Ligand on the Formation and Initiation of Hoveyda-Grubbs Metathesis Catalysis. *Chem. Eur. J.* **2015**, *21*, 10322-10325.

(25) Henderson, R. K.; Bouwman, E.; Reedijk, J.; Powell, A. K. [*N*,*N*'-Bis(2-thio-benzylidene)-1,2-dimethyl-4,5-phenylene-diaminato]nickel(II), Ni(tsaldimph). *Acta Cryst.* **1996**, *C52*, 2696-2698.
(26) Smeets, W. J. J.; Spek, A. L.; Bouwman, E.; Reedijk, J. [*N*,*N*'-Bis(2-thiobenzylidene)-1,2-phenylenediaminato]nickel(II). *Acta Cryst.* **1997**, *C53*, 1564-1566.
(27) Denny, J. A.; Darensbourg, M. Y. Metallodithiolates as Ligands in Coordination, Bioinorganic, and Organometallic Chemistry. *Chem. Rev.* **2015**, *115*, 5248-5273.
(28) The only exception is the carbonyl complex, Fe(κ^3-SNS^{Me})(κ^2-SNS^{Me})(CO) formed reversibly from CO and the Fe(N_2S_3) complex (ref. 14).
(29) S_N2 demethylation of S-Me groups from sulfonium ions is commonly catalyzed by S-adenosylmethionine-dependent methyl transferase enzymes: cf. Woodard, R. W.; Tsai, M. D.; Floss, H. G.; Crooks, P. A.; Coward, J. K. Stereochemical Course of the Transmethylation Catalyzed by Catechol O-Methyl Transferase. *J. Biol. Chem.* **1980**, *255*, 9124-9127.
(30) a) Ryde, U. Carboxylate Binding Modes in Zinc Proteins: A Theoretical Study. *Biophys. J.* **1999**, *77*, 2777-2787. b) Lu, X. L.; Ng, S. Y.; Vittal, J. J.; Tan, G. K.; Goh, L. Y.; Hor, T. S. A. Structural Dynamics and Ligand Mobility in Carboxylate and Dithiocarbamate Complexes of Ru(II) Containing 1,1'-bis(diphenylphosphino)ferrocene (dppf). *J. Organomet. Chem.* **2003**, *688*, 100-111.
(31) Santoro, A.; Holub, J.; Fik-Jaskółka, M. A.; Vantomme, G.; Lehn, J.-M. Dynamic Helicates Self-Assembly from Homo- and Heterotopic Dynamic Covalent Ligand Strands. *Chem. Eur. J.* **2020**, *26*, 15664-15671.
(32) APEX Softward Suite v 2010 Bruker AXS Inc. Madison Wisconsin USA, 2010.
(33) Blessing, R. H. An Empirical Correction for Absorption Anisotropy. *Acta Crystallogr.* 1995, *A51*, 33–38.
(34) Sheldrick, G. M. (2008). CELL_NOW. Georg-August-Universität, Göttingen, Germany.
(35) Sheldrick, G. M. (2012). TWINABS 2012/1. Bruker, Madison, Wisconsin, USA.
(36) Sheldrick, G. M. A Short History of SHELX *Acta Crystallogr.* **2008**, *A64*, 112–122.
(37) Hübschle, C. B.; Sheldrick, G. M.; Dittrich, B. *ShelXle*: a Qt graphical user interface for *SHELXL*. *J. Appl. Crystallogr.* 2011, *44*, 1281–1284.

Chapter 4. Spectroscopic and Electrochemical Characterization and Reactivity of Three Redox States of Ni(S_2N_2).

4.1 Contribution for publication

Yahya M. Albkuri, Jeffrey S. Ovens, Stephan Steinmann,* Christophe Bucher* and R. Tom Baker,* to be submitted to *Chem. Eur. J.*, August, 2021.

Albkuri performed chemical and some electrochemical experiments with Bucher. Steinmann performed computational chemistry and Ovens collected X-ray diffraction data and solved the structure. Bucher, Steinmann, Baker and Albkuri all wrote the manuscript.

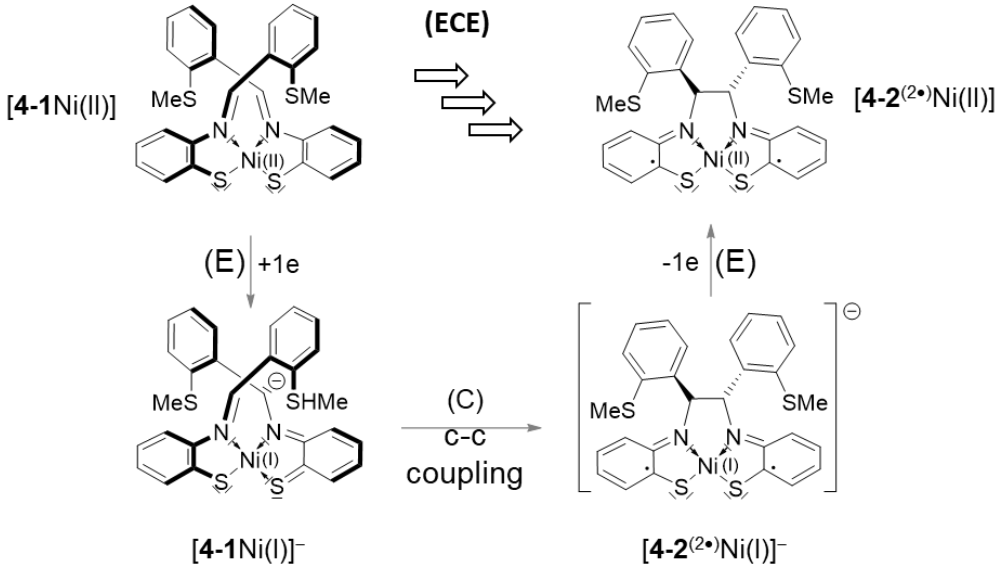

Abstract

Metal thiolate-imine complexes, $M(SN)_2$ are known to undergo imine C-C bond formation to $M(S_2N_2)$ complexes (M = Fe, Co, Ni) containing a redox-active ligand. Although these transformations with nickel are accompanied by side-products, we demonstrate here that one-electron reduction of a related Ni bis(thiolate) complex affords the corresponding paramagnetic $[Ni(S_2N_2)]^-$ anion **(2)**$^-$ exclusively. Moreover, spectroelectrochemical studies indicate that a second 1e- reduction affords the diamagnetic dianion. In this work, we characterize and investigate the electronic structures of the three $Ni(S_2N_2)$ redox states of **2** by DFT and compare their reactivity with phenol and carbon dioxide.

4.2 Introduction

First–row transition metal complexes are increasingly playing a broader role in both homo- and heterogeneous catalysis as their unique one-electron transformations continue to be more efficiently harnessed.[1] For molecular catalysts, novel transformations have been effected with the assistance of functional ligands.[2] In a recent example, the Chirik group showed that an Fe complex containing the redox-active bis(imino)pyridine ligand catalyzes both the [2+2] cycloaddition-oligomerization of 1,3-butadiene to (1,n'-divinyl)oligocyclobutane and its deoligomerization, demonstrating the first closed-loop recycling of a hydrocarbon polymer.[3]

In 1992, Kawamoto and Kushi demonstrated the thermal conversion of a Ni bis(thiolate) complex, $M(SN)_2$ to its $M(S_2N_2)$ isomer via imine C-C bond formation (**Scheme 4.1**).[4] They recognized that the resulting S_2N_2 ligand was redox non-innocent and likely a dianionic ligand with two electrons in the ligand framework. Subsequent work by Wieghardt and co-workers on Fe, Co and Zn complexes applied a combination of spectroscopic, crystallographic and theoretical techniques to more accurately assess the oxidation state of both the metal and the ligand (**Scheme 4.2**).[5-14] For the Co case they showed that intimate sharing of the electrons by the nearly isoenergetic metal and ligand orbitals prevented a clear assignment of the Co oxidation state.[13]

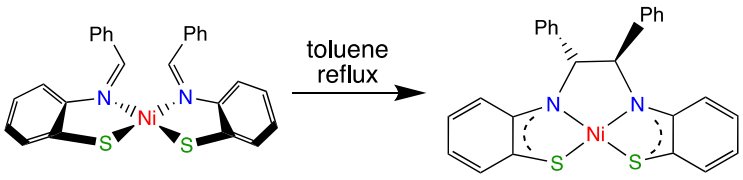

Scheme 4.1 Thermal conversion of $Ni(NS)_2$ to $Ni(S_2N_2)$ complex.

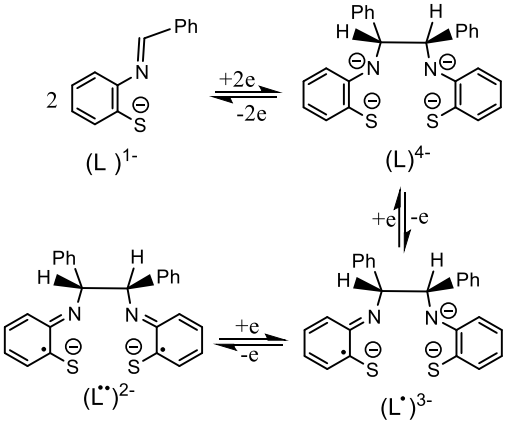

Scheme 4.2 Three ligand redox states derived from imine C-C bond coupling of $(NS)^-$ ligand.

Square planar metal complexes with redox-active ligands have been employed extensively as catalysts for multielectron transformations such as the hydrogen evolution reaction (HER) or oxygen evolution reaction (OER) in order to obtain powerful solar-driven or electrochemically–driven systems for hydrogen generatiion from water.[15-19] In a recent example by Sakai and co-workers,[20] two-electron reduction of a Ni bipy dithiolene complex occurs into both Ni d and bipy π* orbitals, rising the basicity of the Ni d orbital and promoting the proton-coupled electron transfer needed to generate H_2 from protons (**Scheme 4.3**).

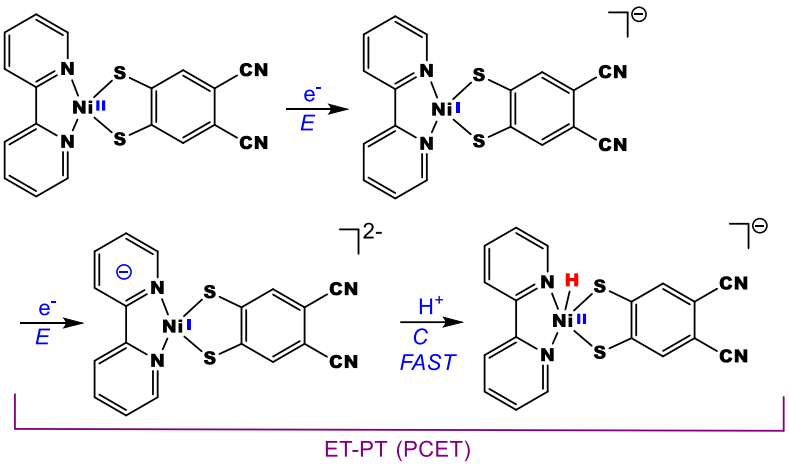

Scheme 4.3. Proposed pathway for HER catalysis using Ni(II)(bipy)(dcbdt), in which E or ET is the electron transfer process, and C or PT is the protonation step.[28]

In this chapter we employ spectroelectrochemistry, NMR and EPR spectroscopy and computational chemistry to access and characterize three stable Ni(S_2N_2) redox states and investigate their electronic structures and reactivity with phenol and carbon dioxide.

4.3 Results and Discussion

4.3.1 Electrochemistry of 4-1.

The electrochemical properties of Ni(κ^2-SNS^{Me})$_2$ (**4-1**; same as **3-1** from Chapter 3) were investigated in THF in the presence of tetra-*n*-butylammonium hexafluorophosphate (0.1 M). Initial studies revealed that the electrochemical response depends on scan rate as shown in **Figure 4.1**. The curve recorded at a low scan rate (10 mV•s^{-1}) displays two consecutive irreversible reduction waves below −1 V while that recorded at 100 mV•s^{-1} exhibits only one broad electron reduction wave at E_{pc} = −1.125 V (Figure **4-1B**). Another key feature of the CV curve shown is

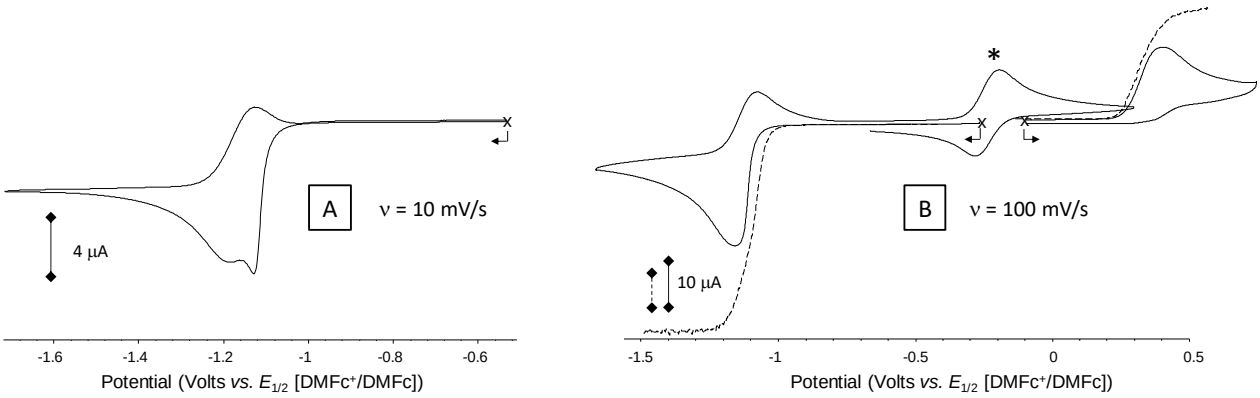

Figure 4.1 CV (full lines) and RDE (dashed lines) curves recorded for **4-1** in THF (1 mM, $TBAPF_6$ 0.1 M) at glassy carbon working electrodes at A) 10 mV•s^{-1} and B) 100 mV•s^{-1} (Ø = 3 mm, 500 rd•min^{-1} for RDE, E vs dimethylferrocene^{+}/ ^{0}.

the fully reversible oxidation wave at *ca* $E_{1/2}$ = –0.27 V, which is only observed when scanning back from –1.5 V to the initial open circuit potential. On first examination, these drastic effects could be attributed to the limited stability of the oxidized and reduced species on the time scale of the CV experiment and to the existence of coupled chemical reactions yielding redox-active products. More specifically, these features are consistent with an ECE mechanism including a chemical step (C) coupled to the initial one-electron reduction (E) of **4-1** at E_{pc} = –1.125 V yielding a new species that can be both reduced right after **4-1** and oxidized at $E_{1/2}$ = –0.27 mV. These data are consistent with an electron-triggered dimerization of **4-1** to $[Ni(S_2N_2)]^-$ (**4-2**$^-$) proceeding through the unstable intermediate, $[Ni(\kappa^2\text{-}SNS^{Me})_2]^-$ (**4-1**$^-$) (**Scheme 4.4**).

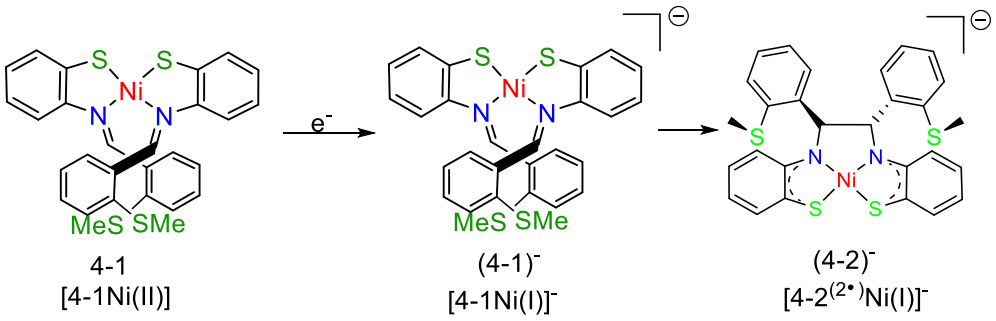

Scheme 4.4 Electron-triggered dimerization of **4-1** to (**4-2**)$^-$ via unstable (**4-1**)$^-$.

Further support for this conclusion came from additional investigations involving exhaustive electrochemical reduction of **4-1** monitored by electrochemical methods coupled to time-resolved *in situ* UV-visible absorption measurements. The potentiostatic coulometry experiment was carried out at a platinum plate working electrode with potential held constant at E_{app} = -1.6 V. The UV-visible spectra recorded throughout the electrolysis are shown in **Figure 4.2**. In the first stage of the electrolysis, up to a charge corresponding to addition of one electron/mole, reduction led to the progressive disappearance of the broad MLCT band at λ_{max} = 460 nm at the expense of two bands growing in at λ_{max} = 696 and 903, along with a clean isosbestic point at 581 nm, reaching maximum intensities after addition of 1e- per molecule of **4-1** (**Figure 4.2A**).

Electrochemical measurements conducted in stationary and transient regimes furthermore showed that the well-defined intermediate compound [(**4-2**)$^{-}$] formed in solution at this stage of the electrolysis undergoes two Nernstian electron transfers between 0 and -1.5 V: a one electron oxidation at $E_{1/2}$ = –0.27 V to **4-2** as well as a one-electron reduction at $E_{1/2}$ = –1.17 V to (**4-2**)$^{2-}$ (thin solid line in **Figures 4.3A** and **B**).

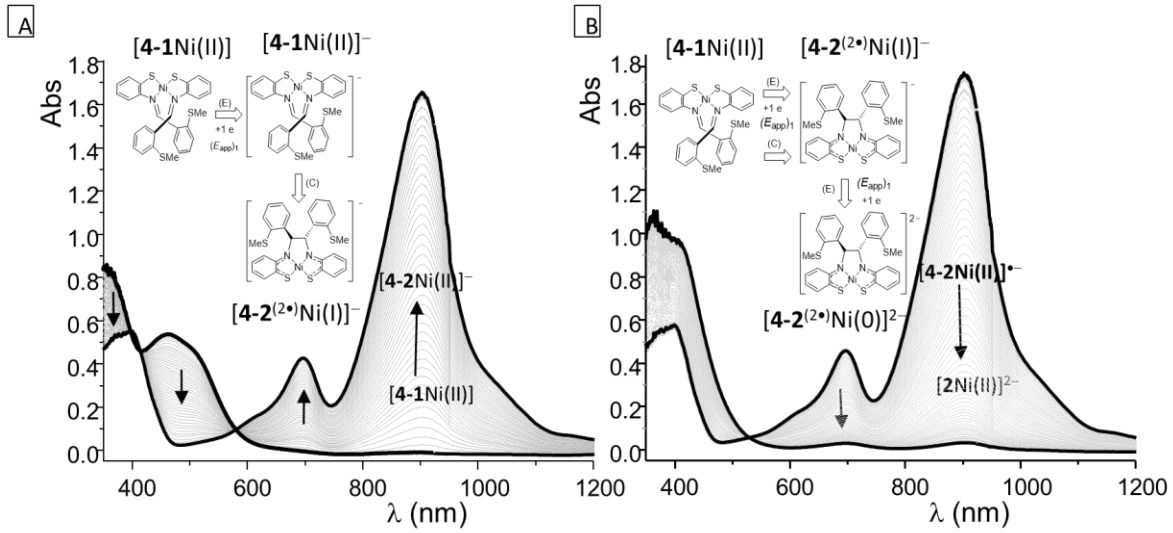

Figure 4.2 Superimposition of UV/Vis spectra recorded during the exhaustive reduction of **4-1** at E_{app} = -1.6 V after addition of A) 1 electron *per* mole and B) 2 electrons *per* mole. (THF + 0.1 M $TBAPF_6$, 1 mM, 10 mL, *l* = 1 mm, t ≈ 30 min, Pt).

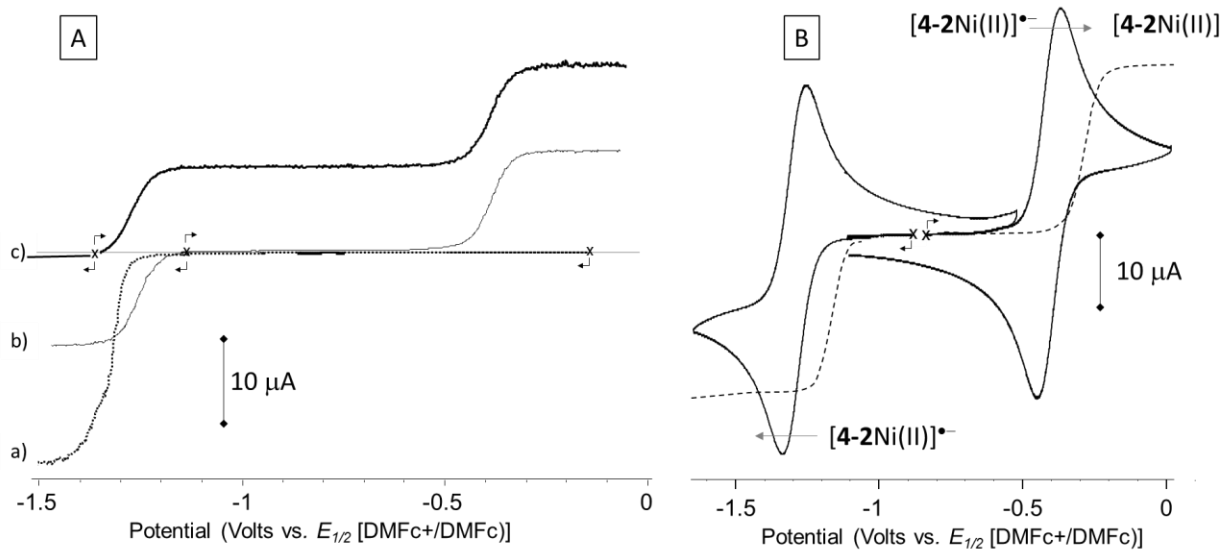

Figure 4.3 [A] RDE curves recorded before a) and after b) one- and c) two-electron reduction of **4-1** at E_{ap} = −1.4 V (Pt, 1 mM in THF+$TBAPF_6$); **[B]** CV and RDE curves recorded at a glassy carbon working electrode (Ø = 3 mm, 10 mV•s^{-1}, 500 rd•min^{-1}) after 1e- reduction of **4-1** at E_{ap} = −1.4 V (Pt, 1 mM in THF+$TBAPF_6$). CV and RDE curves recorded at glassy carbon working electrode, Ø = 3 mm at 100 mV•s^{-1} (CV) or at 10 mV•s^{-1} / 500 rd•min^{-1} (RDE); E vs $DMFc^{+}/^{0}$).

*4.3.2 Electrochemistry of **4-2**.*

While the reversible reductions of **4-2** shown in **Figure 4.4** are attributed to Ni-based reductions from Ni(II) to Ni(I) and Ni(0), on the anodic side, the shape and relative position of the CV curves are consistent with two successive one-electron oxidation processes centered on both mercapto-aniline moieties (**Scheme 4.5a**). Under this assumption, the shift in potential observed between both waves can be attributed to through-bond or through-space "communication" processes occurring between both mercapto-anilines, the oxidation of the first one making the oxidation of the second harder. This attribution relies on i) the number of electrons involved in these waves (2x1e) ii) DFT data indicating that the organic subunits of the complex are more likely to be oxidized than the metal center.

The reduced species $(\mathbf{4\text{-}2})^{-/2-}$ were further characterized by spectroelectrochemistry measurements, upon collecting time-resolved UV-vis spectra during the successive reduction of **4-2**. As can be seen in **Figure 4.5**, accumulation of $(\mathbf{4\text{-}2})^{-}$ in solution during the electrolysis at E_{app} = -0.8 V led to the progressive disappearance of the broad signal centered at 834 nm at the expense of less intense ones at λ_{max} =697 and 902 nm. Observation of a clean isosbestic point at 875 nm also confirms that no secondary reactions occur over the considered time range. Further reduction

of the sample at E_{app} = -1.4 V led to the disappearance of the signals attributed to (**4-2**)$^{-}$ at the expense of new bands developing at much higher energy) (λ<500 nm) attributed to (**4-2**)$^{2-}$.

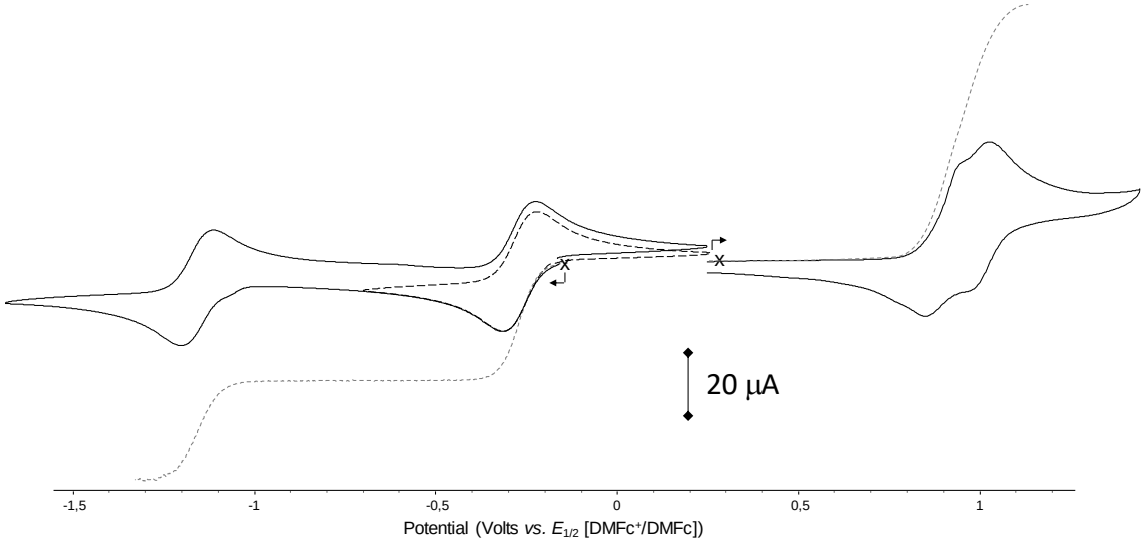

Figure 4.4 CV measurement of reduction and oxidation of neutral **4-2**. CV and RDE curves recorded in THF (1 mM, $TBAPF_6$ 0.1 M) at glassy carbon working electrode at v = 0.1 V s^{-1} (CV) or 10 mV•s^{-1} (RDE, 500 rd•min^{-1}) (Ø = 3 mm, E vs $DMFc^+$/DMFc).

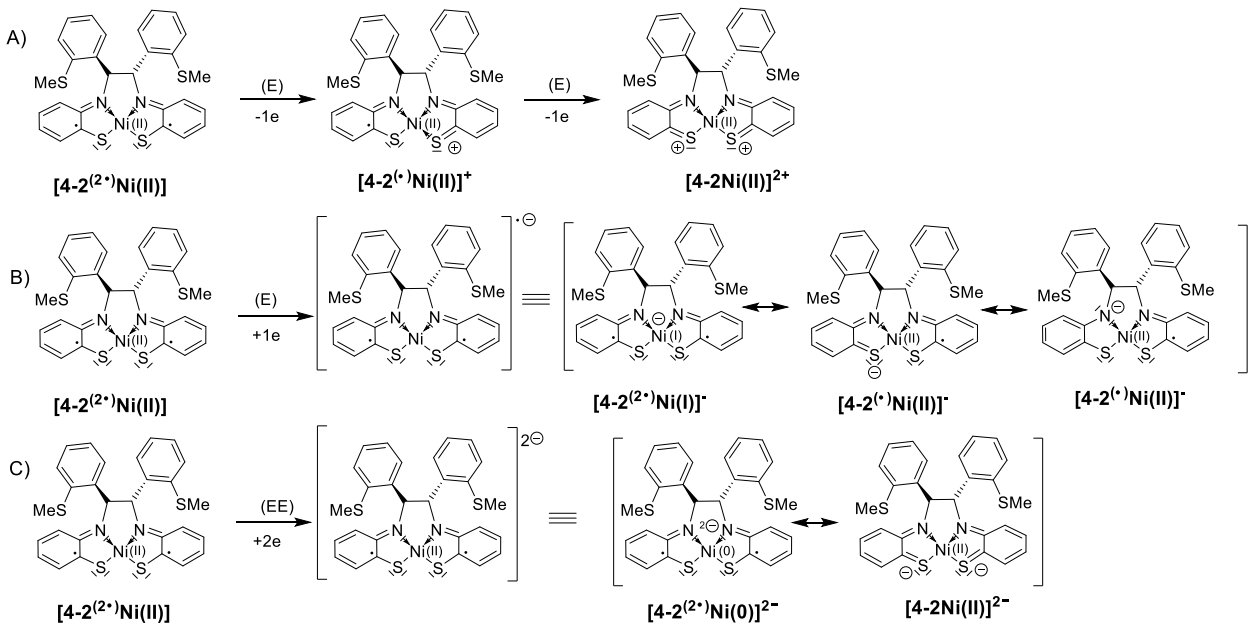

Scheme 4.5 Oxidation and reduction of **4-2**.

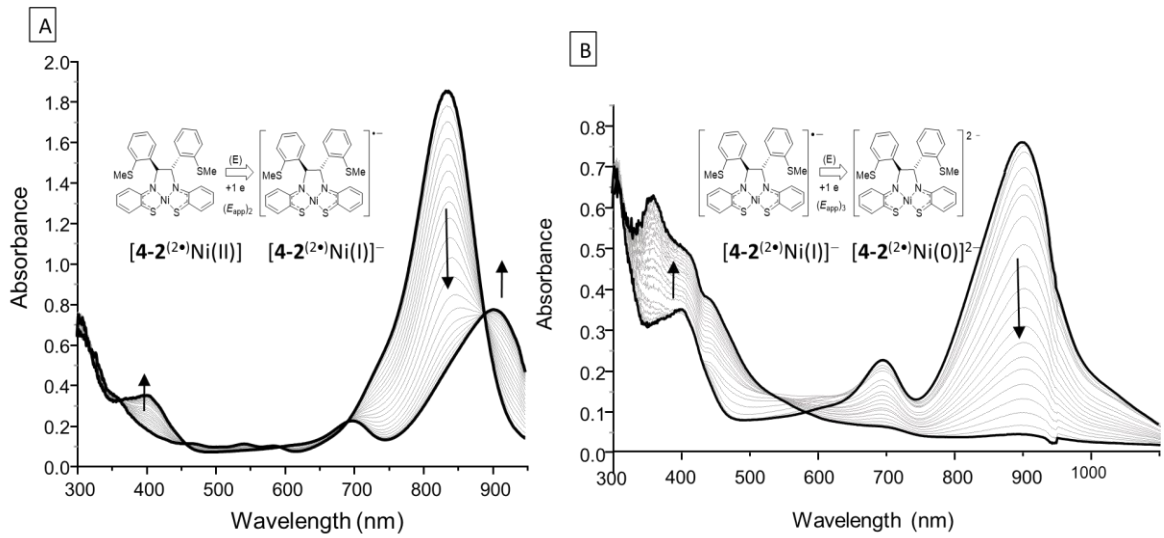

Figure 4.5 Superimposition of UV/Vis spectra recorded during the exhaustive reduction of **4-2** at A) $(E_{app})_1$ = -0.7 V (1 electron *per* mole) and B) $(E_{app})_1$ = -1.4 V (1 electron *per* mole). (THF + 0.1 M TBAPF6, 1 mM, 10 mL, *l* = 1 mm, t ≈ 30 min, Pt).

*4.3.3 Step-by-step ESR studies of reduced **4-2.***

Formation of Ni(I) and Ni(0) was further demonstrated by ESR measurements carried out at each stage of the electrolysis. The spectrum collected after addition of one electron per mole is shown as a full/bolded black line in (**Figure 4.6A**). Based on simulation analyses and on experimental literature data reported for relevant Ni(I) compounds,[16-19] we assign the intense signals observed at g_x = 1.995 g_y = 2.022 and g_z = 2.118 to **(4-2)**$^-$ with an *S* = 1/2 spin state. This attribution was further supported by simulation studies showing that the multiplicity of the of g_x signal results from hyperfine coupling with two equivalent nitrogen atoms (a_N = 8.8 G, full black line in (**Figure 4.6B**). ESR measurements carried out on the two-electron reduced complex gave a silent spectrum featuring only a residual signal attributed to traces of the Ni(I) intermediate (dashed line in Figure 4.6A). This absence of signal is in agreement with formation of diamagnetic **(4-2)**$^{2-}$.

4.3.4 Electrochemical reactivity studies of reduced Ni(S_2N_2) complexes.

Noting that both d^9 **(4-2)**$^-$ and d^{10} complex **(4-2)**$^{2-}$ cannot achieve their preferred pseudo-tetrahedral geometry when coordinated to the tetradentate $(S_2N_2)^{2-}$ ligand, we were interested in investigating their reactivity with the weak acid phenol and challenging reactant carbon dioxide. As shown in **Figure 4.7**, performing the CV experiment on **4-2** in THF in the presence of phenol has little effect on the first reduction wave. In contrast, the second quasireversible reduction takes place about 80

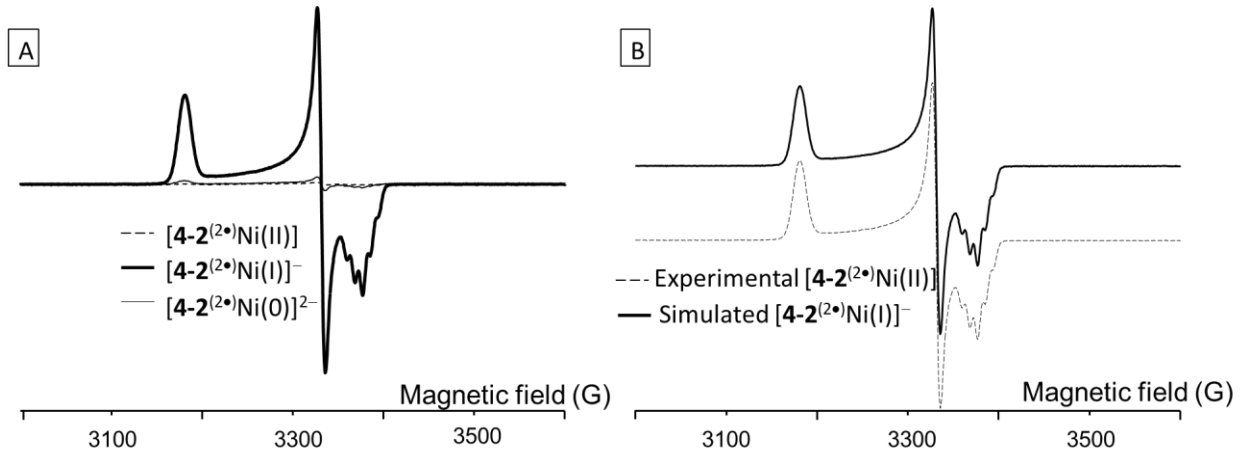

Figure 4.6 A) experimental X-band EPR spectra (110 K, microwave power = 6 mW; modulation amplitude = 2 G) recorded before (dashed line) and after exhaustive electrochemical reduction of **4-2** in THF (0.1 M $TBAPF_6$) at E_{app} = –0.8 V (bolded black line) and at E_{app} = –1.4 V (thin black line) B) experimental and simulated EPR spectra of **(4-2)$^{2-}$**.

mV before that of **(4-2)$^{-}$** indicating formation of a new product that is easily reversed upon reoxidation to **(4-2)$^{-}$**. In **Figure 4.8** we see that a second irreversible reduction occurs under a CO_2 atmosphere at a slightly *increased* voltage, relative to that of **(4-2)$^{-}$**. Again reoxidation shows reversibility of the reaction of **(4-2)$^{2-}$** with CO_2. These promising reactivity findings will be expanded on in chapter 5 towards fluoroalkenes.

4.3.5 Synthesis and molecular structure of Ni(S_2N_2) complexes.

Building on the above electrochemical results, we treated a purple solution of complex **4-1** in THF with one equiv of sodium benzophenone to afford green crystals of **(4-2)$^{-}$** as the $[Na(THF)_6]^+$ salt in high yield (**Figure 4.9**). On comparing the molecular structures of **4-2** and **(4-2)$^{-}$** we see in **Table 4.1** that the bond alternation in the mercapto-aniline ring is consistent with the $(L^{\bullet\bullet})^{2-}$ formulation in Figure 4.1 (*cf.* avg N-C1 = 1.356 *vs* 1.475 Å for the N-C7 single bond). This similarity between the two structures is consistent with a metal-based reduction from Ni(II) to Ni(I).

In Chapter 3 we showed that heating **4-1** in refluxing toluene gave **4-2** in low yield as formation of by-products necessitated a chromatographic separation to obtain pure product. Similar results were obtained by Kawamoto and Kushi using the $Ni(SN)_2$ complex shown in Figure 4.1 (56% yield).[4b] As one-electron reduction of **4-1** affords **(4-2)$^{-}$** as the only product, subsequent chemical oxidation should afford neutral **4-2** in high yield. Indeed, treatment of **(4-2)$^{-}$** with $[Fe(C_5H_5)_2](BF_4)$ in THF gave **4-2** in 80% yield after simple work-up.

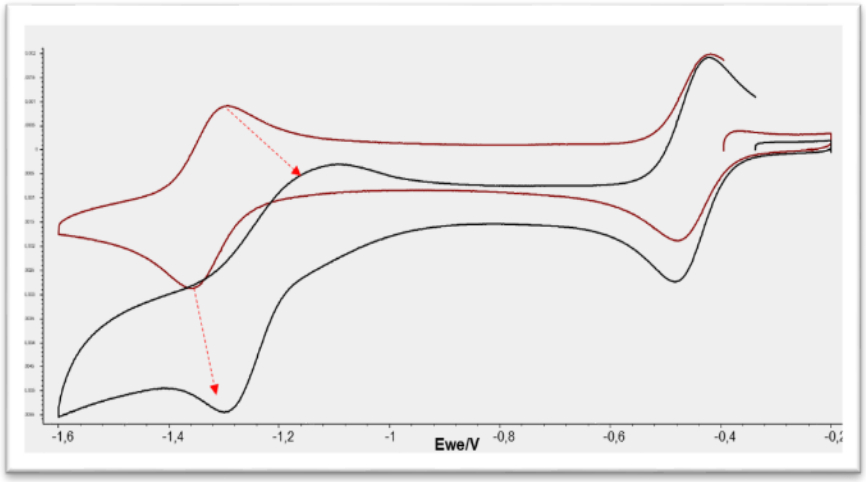

Figure 4.7 Cyclic voltammogram (100 mV•s^{-1}) of **4-2** + phenol in THF / $TBAPF_6$ on cathodic side.

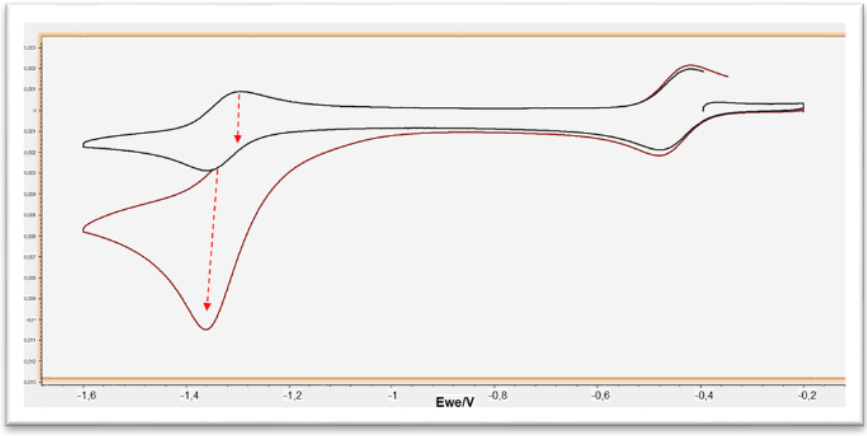

Figure 4.8 Cyclic voltammogram (100 mV•s^{-1}) of **4-2** in THF / $TBAPF_6$ on cathodic side under a CO_2 atmosphere.

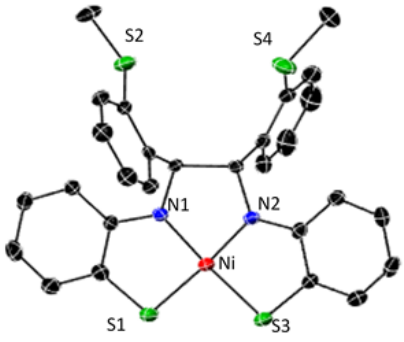

Figure 4.9 Molecular Structure of (**4-2**)[$Na(THF)_6$] with 40% thermal ellipsoids. H atoms are omitted for clarity.

Table 4.1 Bond distance metrics for **4-2** and **(4-2)**$^{-}$

$Ni(S_2N_2)$	$[Ni(S_2N_2)]^{-}$
N-C1 = 1.352(4), 1.359(3)	N-C1 = 1.362(7), 1.352(7)
N-C7 = 1.479(4), 1.471(3)	N-C7 = 1.464(5), 1.481(6)
S-C6 = 1.723(4), 1.723(3)	S-C6 = 1.755(6), 1.747(5)
C1-C2 = 1.417(5), 1.415(4)	C1-C2 = 1.388(8), 1.415(7)
C2-C3 = 1.368(5), 1.362(4)	C2-C3 = 1.41(1), 1.370(8)
C3-C4 = 1.390(6), 1.407(5)	C3-C4 = 1.39(1), 1.365(8)
C4-C5 = 1.364(6), 1.362(5)	C4-C5 = 1.364(6), 1.362(5)
C5-C6 = 1.407(5), 1.398(4)	C5-C6 = 1.396(8), 1.390(7)
C1-C6 = 1.423(5), 1.419(4)	C1-C6 = 1.415(7), 1.405(7)
C7-C7' = 1.551(4)	C7-C7' = 1.556(7)
Ni-N = 1.811(2), 1.815(2)	Ni-N = 1.829(4), 1.835(4)
Ni-S = 2.1310(9), 2.1311(9)	Ni-S = 2.154(2)), 2.147(2)

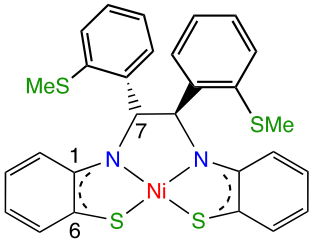

The clean generation of yellow solutions of diamagnetic **(4-2)**$^{2-}$ was best effected using Na/K alloy in THF. The ^{1}H NMR spectrum (Fig. A4.2) showed significant shifting of the ligand resonance to high field vs. those for neutral **(4-2)**.

*4.3.6 DFT calculations of Ni(SNS)$_2$ (**4-1**) and Ni(S$_2$N$_2$) redox states [**(4-2)**$^{0/1-/2-}$].*

Density functional theory computations have been performed to shed more light on the electronic structures, reactivity and spectroscopic properties of (**4-1**) and **(4-2)**$^{0/1-/2-}$. By analogy to the complexes described by Wieghardt et al.,[14] the ground state of **4-2** is an open-shell singlet, while **4-1** is a closed shell complex. The optimized geometries are very similar to the crystal structures (**Figure 4.10**). The geometry of transient **(4-1)**$^{-}$ shows more conformational flexibility with a near tetrahedral conformer being only 1.7 kcal/mol higher in energy than the near square-planar one. The oxidation of **(4-1)**$^{-}$ leads to a doublet ground state at a potential of 0.9 V vs SHE. The oxidation is centered on the organic ligand, as clearly visible in the density-difference with respect to the neutral complex shown in **Figure 4.11A**. A second oxidation process is predicted to occur at ~+1.6 V vs SHE, involving the oxidation of a "free" thiolate. This latter finding is not in agreement with

the experimental data displayed in **Figure 4.4**, showing two successive and very close one-electron oxidations in the accessible potential range.

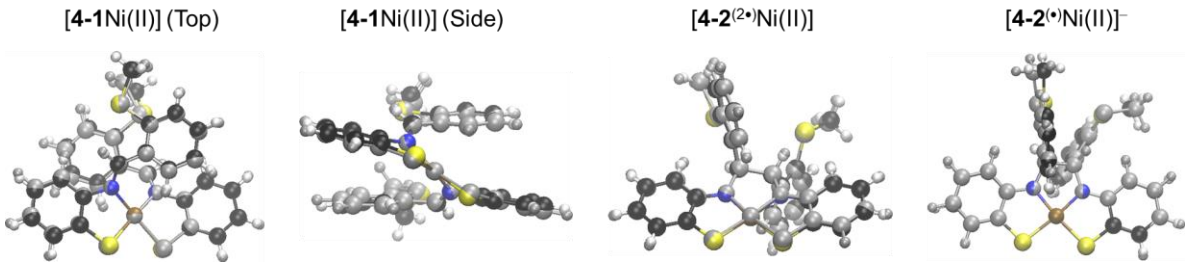

Figure 4.10 Overlay between X-ray (color) and DFT (grey) geometries.

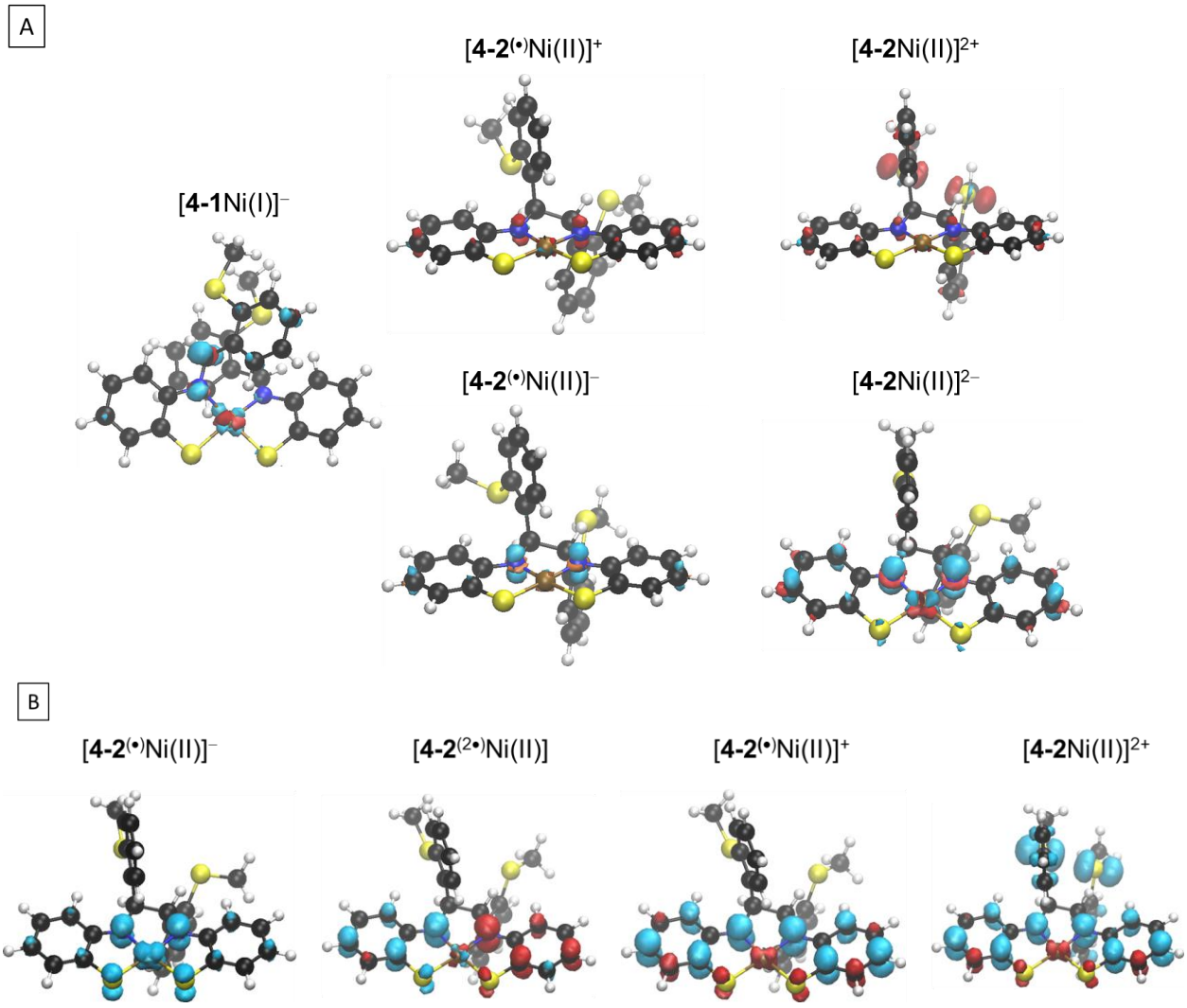

Figure 4.11 A: Isodensity surfaces (0.005 a.u.) of the charge difference of various complexes with respect to the neutral complex. Charge accumulation and depletion are depicted in blue and orange, respectively. B: Spin-density iso-surfaces (0.005 a.u.); blue α-electron excess, red: β-electron excess.

The first reduction of **4-2** occurs at -0.4 V vs SHE, generating a doublet ground-state. The charge is mostly accumulating on the nitrogen atoms (

Figure 4.11B), with the spin-density being dominant on Ni, in agreement with the ESR measurements. A second reduction (at -1.7 V vs SHE) generates a closed-shell dianion, where the additional charge is located on Ni, N and, to a minor extent, on the mercapto-aniline ligand. The reduction of **4-1** also leads to a doublet, but the additional charge is mostly located on the C=N double bond of the imine moiety, with the largest contribution on the carbon atom.

*4.3.7 DFT calculations of intramolecular C-C bond formation from **4-1** and **(4-1)**$^-$*

We also studied the electron-triggered coupling reaction with DFT methods. The transition state for the C-C bond formation has been identified for both the neutral and radical anion states (**Figure 4.12**). The geometry of this TS is very similar in both cases, except that the forming C-C

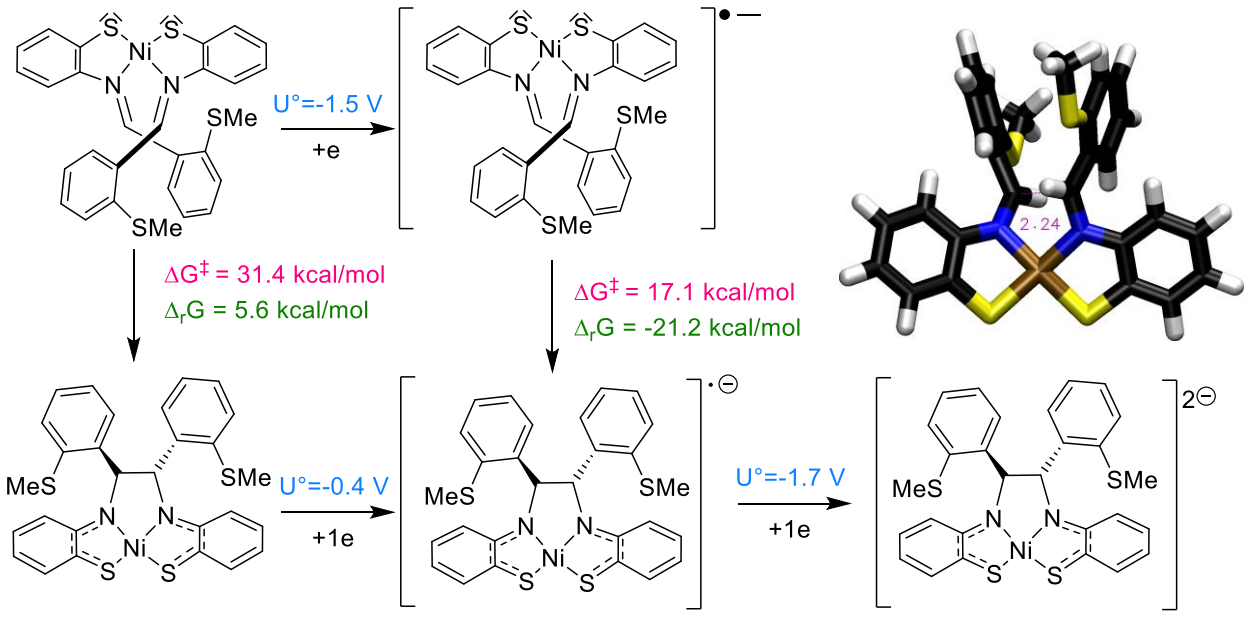

Figure 4.12 Left: Summary of theoretical results at the PBE0/def2-TZVP, SMD(THF) level of theory. U°: vs SHE; the value for ferrocene/ferrocenium is, at the same level of theory, equal to 0.8 V. Right: Transition state for the C-C bond formation in the radical anion state. In the neutral state, the geometry is very similar, except that the forming C-C bond is reduced to 2.05 Å.

bond is 2.24 Å in the radical anion, while it is shortened to 2.05 Å in the neutral complex. The activation energy of 17.1 kcal/mol in the radical anion is compatible with the reactivity discussed in the experimental part, especially since **(4-2)**$^-$ is 21.2 kcal/mol more stable than **(4-1)**$^-$, revealing

a significant thermodynamic driving force. This contrasts with the situation for neutral **4-1** in which not only is the barrier (31.4 kcal/mol) excessively high at room temperature, but also the reaction energy shows a complete reversal: **4-1** is 5.6 kcal/mol more stable than **4-2**.

*4.3.8 TD-DFT studies of three redox states of **4-2**.*

Time-dependent density functional theory (TDDFT) was applied to investigate the spectroscopic properties of **4-2**, **(4-2)**$^{-}$ and **(4-2)**$^{2-}$. The computed spectra are summarized in (**Figure 4.13**). A qualitative agreement with experiment is obtained: The most intense transition in the visible region is located at 615 and 763 nm for the neutral and radical anion, respectively, while the dianion has no transitions in this region. The nature of these transitions has been characterized via the corresponding natural transition orbitals, shown in (**Figure 4.13**). They reveal a mixed metal/ligand character, i.e., the electron is delocalized both in the ground and excited state across the square planar complex. The strong involvement of the metal center in this transition rationalizes the absence of the corresponding transition for **(4-2)**$^{2-}$ for which the Ni d-orbitals are filled and thus no longer available.

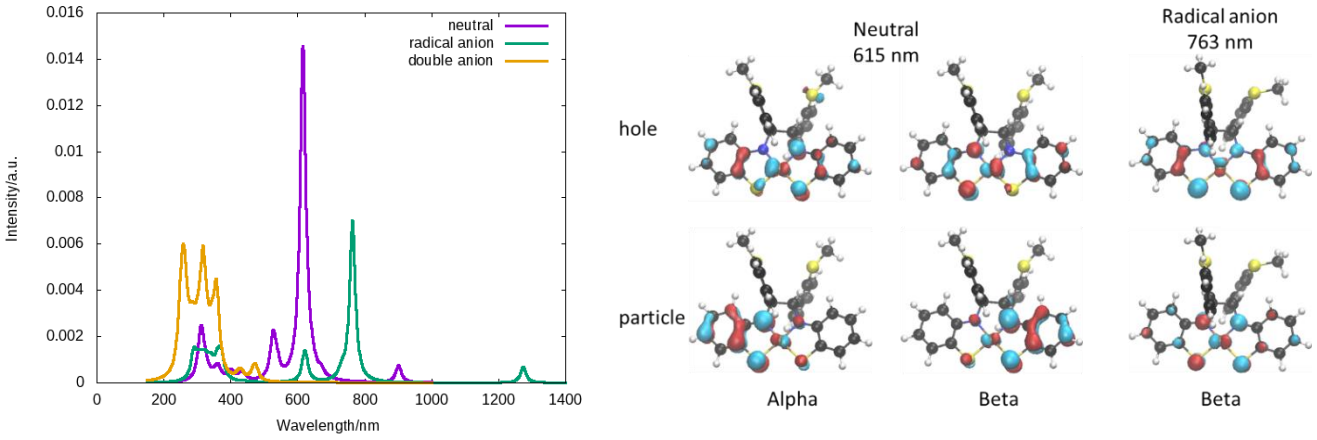

Figure 4.13 Left: UV-Vis spectrum for ***4-2***, **(4-2)**$^{-}$ *and* **(4-2)**$^{2-}$ at the TD-PBE0/def2-TZVP level of theory. Right: Iso-surfaces (0.05 a.u.) for the dominant natural transition orbitals for the hole (top row) and particle (bottom row) for the most intense transition. For **(4-2)**$^{-}$ only the beta electrons participate significantly in the corresponding transition.

4.4 Conclusion

Employing a combination of CV, rotating disk electrode and controlled potentiometry, we showed that reduction of Ni bis(thiolate) complex **4-1** led to reductive coupling of the imines, forming exclusively paramagnetic Ni(I) complex **(4-2)**$^{-}$ that contains the redox-active $(S_2N_2)^{2-}$ ligand.

Moreover, this can be reduced by a second e^- to form diamagnetic **(4-2)$^{2-}$**. Furthermore, **(4-2)$^-$** undergoes reversible oxidation and reduction, providing three different redox states. Although the valence electrons are delocalized between the metal and ligand orbitals in both ground and excited states, the reductions are largely metal-based, suggesting a novel square planar Ni(0) complex for **(4-2)$^{2-}$**. The latter reacts readily with both the weak acid phenol and carbon dioxide, indicating a potential role in multielectron electrocatalysis.

4.5 Experimental Section

4.5.1 General Considerations

Synthetic chemistry was carried out under nitrogen, using an MBraun glovebox. THF and hexanes were dried on columns of activated alumina using a J. C. Meyer (formerly Glass Contour) solvent purification system. NMR solvent C_6D_6 was dried with activated alumina (ca. 10 wt %) overnight, followed by filtration. Sodium, potassium and benzophenone were obtained from Aldrich, ferrocenium-tetrafluoroborate from Strem, and complex **4-1** was prepared as described in Chapter 3. ^{1}H NMR spectra were recorded on a 300 MHz Bruker Avance II instrument at room temperature (21−25 °C) and referenced to residual protons (C_6D_6, δ 7.15) with respect to tetramethylsilane at δ 0.00.

Electrochemistry: Electrochemical studies were performed in a glovebox (Jacomex) (O_2 < 1 ppm, H_2O < 1 ppm) with a home-designed 3- electrode cell. Cyclic voltammetry (CV) curves were recorded using a SP300 Biologic potentiostat. All studies were conducted in a standard one-compartment, three-electrode electrochemical cell using an automatic ohmic drop compensation procedure. Vitreous carbon (Ø = 3 mm) working electrodes (ALS instruments) were systematically polished with 2 mm diamond paste (PRESI SA) before recording. The non-aqueous reference electrode (ALS Instruments) was made of a silver wire dipped in a $AgNO_3$ solution (10^{-2} M + TBAP 10^{-1}M in CH_3CN). The counter electrode was a platinum wire and ferrocene or dimethylferrocene served as internal reference. THF (anhydrous, ≥99.9%, inhibitor-free) was purchased from Aldrich and further purified on activated alumina before use. Tetrabutylammonium hexafluorophosphate ($TBAPF_6$) was synthesized from tetra-n-butylammonium hydroxide and HPF_6, recrystallized several times from $EtOH/H_2O$ and then dried under vacuum at 60°C for 24 h before use. Spectroelectrochemical (SEC) measurements were carried out in a “thin layer” (0.5 mm) SEC quart cell (ALS Co) connected to a Biologic ESP-300

potentiostat equipped with a 1 A/48 V booster and a linear scan generator. Absorption measurements were carried out in remote mode with the SEC cell coupled to an MCS 500 UV-NIR Zeiss spectrophotometer through optical fibers. All measurements were carried out at room temperature in THF (anhydrous, 99.9% Acroseal) using $TBAPF_6$ as the electrolyte (0.2 M). The Ag+/Ag reference electrode was made of a silver wire immersed in a solution containing a known concentration of Ag+ ($AgNO_3$ (10^{-2} M) + tetrabutylammonium perchlorate (0.1 M) in THF). The counter electrode was a large surface platinum grid isolated from the main solution through a home-made electrolytic bridge.

Computational details: All computations have been performed with Orca 4.2.1. The adopted density functional was PBE0-D3 applied in conjunction with the def2-TZVP basis set. The RIJCOSX option was activated to accelerate the computations. The numerical grid quality was increased with respect to the default and set to Grid6 and GridX6. The SMD implicit solvent model was used with parameters corresponding to THF.

X-ray Crystallographic Details: Crystallographic data collection and processing were performed via the X-ray Core Facility at the University of Ottawa. Crystals were mounted on MiTeGen sample holders using Parabar oil. Data were collected on a Bruker Smart diffractometer equipped with an ApexII CCD detector and a sealed-tube Mo K source (λ = 0.71073 A). During collection, crystal was cooled to approx. 200 K. Sample cooling was effected via a refrigerated, dry compressed air stream. Raw data collection and processing were performed with the Apex3 software package from Bruker.[20] Initial unit cell parameters were determined from 36 data frames from select ω scans. Semi-empirical absorption corrections based on equivalent reflections were applied.[21] Systematic absences in the diffraction data-set and unit-cell parameters were consistent with the assigned space group. Carbon and nitrogen-based hydrogen atoms were placed geometrically and refined using a riding model, all other hydrogen atoms were placed via the difference map and refined with restraints. Data collection and structure refinement details are provided in Table A5.1.

4.5.2 Synthesis of three Ni(S_2N_2) redox states

Synthesis of [4-2][Na(THF)$_6$]. A 20 mL scintillation vial was charged with 100 mg of **4-1** (0.17 mmol) in 15 mL of THF. To this solution was added dropwise 37 mg of sodium benzophenone (0.17 mmol, 1 equiv) in 5 mL of THF. The resulting yellow/brown solution was stirred for 16 h at room temperature and the solvent was removed under reduced pressure. The resulting green solid

was washed with hexanes (3 X 10 mL) and dried under vacuum to yield 97 mg (93%). Crystals suitable for X-ray diffraction were grown from concentrated THF layering with hexanes at -35 °C**.** ^{1}H NMR (300 MHz, C_6D_6, Fig. A4.1) δ 12.13 (ov mult, 4H, Ar-*H*), 7.46 (dd, 2H, Ar-*H*), 8.34 (br, 2H, backbone C-*H*), 7.42 (d, 2H, Ar-*H*), 7.03 (tr d, 2H, Ar-*H*), 6.89 (s, 4H, Ar-*H*), 6.66 (ov mult, 2H, Ar-*H*), 3.15 (s, 6H, S−CH_3).

Generation of [4-2](M^I)$_2$ (M^I = Na$^+$, K$^+$). A 40 mL scintillation vial was charged with **4-1** (300 mg, 0.52 mmol) in 25 mL of THF. To this solution, was added dropwise 64 mg (1.04 mmol, 2 equiv) of sodium-potassium alloy, NaK. The resulting bright brown solution was stirred for 16 h at room temperature after which the yellow solution was filtered, solvent was removed and the remaining yellow solid dried in vacuum to give 328 mg (85 %). ^{1}H NMR (300 MHz, CD_3CN, Fig. A4.2) δ 9.83 (d, 1H, Ar-*H*), 7.38 (s, 2H, backbone C-*H*), 7.25 (mult, 1H, Ar-*H*), 7.22-7.06 (ov mult, Ar-*H*), 6.46 (dd, Ar-*H*), 6.14 (tr, Ar-*H*), 5.61 (dd, br, 2H), 4.45 (br, 2H, backbone C-*H*), 2.50 (s, 6H, S−CH_3).

High-yield synthesis of [Ni(S$_2$N$_2$)] (4-2). A 20 mL scintillation vial was charged with [**4-2][Na(THF)$_6$]** (70 mg, 0.12 mmol) in 10 mL of THF. Ferrocenium-tetrafluoroborate $[Fe(C_5H_5)_2]BF_4$ (32 mg, 0.12 mmol) was added dropwise to the solution using a micro-syringe. After stirring for 16 h the solution was filtered and solvent was removed. The resulting violet solid was washed with cold THF (2 X 1 mL) and hexanes (2 X 1 mL) and dried to yield 54 mg (80%).

4.5.3 Reactions of phenol and CO_2 with Ni(S$_2$N$_2$)$^{-/2-}$ anions

In the glovebox a solution of $TBAPF_6$ (970 mg, 2.5 mmol, 0.1 M) in THF was placed in a home-designed 3-electrode cell. After CV blank measurements were run, a solution (6 mg, 0.01 mmol, 1μM) of **4-2** in THF was added and characterized by a reductive scan. This step was then repeated in the presence of phenol (0.9 mg, 0.01 mmol) (**Figure 4.7**). In another experiment with the **4-2 +** $TBAPF_6$ solution in THF, the E-cell was taken to a pre-set up Schlenk line connected to two dry THF bubblers to ensure a dry source of CO_2. A cannula transfer line was inserted into the 3-electrode cell and after a 1 min CO_2 purge the CV measurement was taken (**Figure 4.8**).

4.6 References

(1) Gebbink, R. J. M. K., Moret, M.-E., Eds. *Non-Noble Metal Catalysis: Molecular Approaches and Reactions*, Wiley, 2019.

(2) Fritz, M.; Schneider, S. The Renaissance of Base Metal Catalysis Enabled by Functional Ligands in *The Periodic Table II*, Mingos, D. M. P., Ed. Springer, pp 1-36, 2019.

(3) Beromi, M. M.; Kennedy, C. R.; Younker, J. M.; Carpenter, A.E.; Mattler, S. J.; Throckmorton, J. A.; Chirik, P. J. Iron Catalyzed Synthesis and Chemical Recycling of Telechelic, 1,3-Enchained Oligocyclobutanes. *Chem Rxiv*, 2021.

(4) a) Kawamoto, T.; Kushi, Y. Carbon-Carbon Bond Formation in Helical Nickel(II) Complex, *cis*-Bis[2-*N*-(phenylmethylideneamine)benzenethiolato]nickel(II). *Chem. Lett.* **1992**, 893. b) Kawamoto, T.; Kuma, H.; Kushi, Y. Valence Isomerization. Synthesis and Characterization of Cobalt and Nickel Complexes with Non-Innocent N_2S_2 Ligand. *Bull. Chem. Soc. Jpn.* **1997**, *70*, 1599-16046.

(5) Ghosh, P.; Begum, A.; Herebian, D.; Bothe, E.; Hildenbrand, K.; Weyhermüller, T.; Wieghardt, K. Coordinated *o*-Dithio- and *o*-Iminothiobenzosemiquinonate(1-) π Radicals in $[M^{II}(bpy)(L\cdot)](PF_6)$ Complexes. *Angew. Chem. Int. Ed.* **2003**, *42*, 563-567.

(6) Ghosh, P.; Begum, A.; Bill, E.; Weyermüller, T.; Wieghardt, K. Molecular and Electronic Structures of Iron(II)/(III) Complexes Containing N,S-coordinated, Closed-shell *o*-Aminothiophenolato(1-) and *o*-Iminothiophenolato(2-) Ligands. *Inorg. Chem.* **2003**, *42*, 3208-3215.

(7) Ghosh, P.; Bill, E.; Weyhermüller, T.; Wieghardt, K. Molecular and electronic structures of iron complexes containing N,S-coordinated, open-shell o-iminothionebenzosemi-quinonate(1-) π radicals. *J. Am. Chem. Soc.* **2003**, *125*, 3967-3979.

(8) Ray, K.; Petrenko, T.; Wieghardt, K.; Neese, F. Joint Spectroscopic and Theoretical Investigations of Transition Metal Complexes Involving Non-innocent Ligands. *Dalton Trans.* **2007**, 1552-1566.

(9) Roy, N.; Sproules, S.; Bill, E.; Weyhermüller, T.; Wieghardt, K. Molecular and Electronic Structure of the Square Planar Bis(o-amidobenzenethiolato)iron(III) Anion and its Bis(o-quinoxalinedithiolato) Iron(III) Analogue. *Inorg. Chem.* **2008**, *47*, 10911-10920.

(10) Roy, N.; Sproules, S.; Weyhermüller, T.; Wieghardt, K. Trivalent Iron and Ruthenium Complexes with a Redox Non-innocent (2-Mercaptophenylimino)-methyl-4,6-di-tert-butylphenolate(2-) Ligand. *Inorg. Chem.* **2009**, *48*, 3783-3791.

(11) Roy, N.; Sproules, S.; Bothe, E.; Weyhermüller, T.; Wieghardt, K. Polynuclear Complexes Containing the Redox Non-innocent Schiff Base Ligand 2-[(E)-2-Mercaptophenylimino]methyl-4,6-di-tert-butylphenolate(2-). *Eur. J. Inorg. Chem.* **2009**, 2655-2663.

(12) Sproules, S.; Wieghardt, K. *o*-Dithiolene and *o*-Aminothiolate Chemistry of Iron: Synthesis, Structure and Reactivity. *Coord. Chem. Rev.* **2010**, *254*, 1358-1382.

(13) Sproules, S.; Kapre, R. R.; Roy, N.; Weyhermüller, T.; Wieghardt, K. The Molecular and Electronic Structures of Monomeric Cobalt Complexes Containing Redox Non-innocent *o*-Aminobenzenethiolate Ligands. *Inorg. Chim. Acta* **2010**, *363*, 2702-2714.

(14) Presow, S. R.; Ghosh, M.; Bill, E.; Weyhermüller, T.; Wieghardt, K. Molecular and Electronic Structures of New Iron Complexes Containing N,S-Coordinated *o*- Imino-thionebenzosemiquinonate(1-) π Radical Ligands: An Experimental and Density Functional Theoretical Study. *Inorg. Chim. Acta* **2010**, *347*, 226-239.

(15) Brudvig, G. W.; Reek, J. N. H.; Sakai, K.; Spiccia, L.; Sun, L. Catalytic Systems for Water Splitting. *ChemPlusChem*. **2016**, 1017–1019. https://doi.org/10.1002/cplu.201600436.

(16) Esswein, A. J.; Nocera, D. G. Hydrogen Production by Molecular Photocatalysis. *Chem. Rev*. **2007**, *107*, 4022–4047. https://doi.org/10.1021/cr050193e.

(17) Hisatomi, T.; Kubota, J.; Domen, K. Recent Advances in Semiconductors for Photo-catalytic and Photoelectrochemical Water Splitting. *Chem. Soc. Rev*. **2014**, 7520–7535. https://doi.org/10.1039/c3cs60378d.

(18) Swierk, J. R.; Mallouk, T. E. Design and Development of Photoanodes for Water-Splitting Dye-Sensitized Photoelectrochemical Cells. *Chem. Soc. Rev.* **2013**, *42* (6), 2357–2387. https://doi.org/10.1039/c2cs35246j.

(19) Wang, Y.; Chen, K. S.; Mishler, J.; Cho, S. C.; Adroher, X. C. A Review of Polymer Electrolyte Membrane Fuel Cells: Technology, Applications, and Needs on Fundamental Research. *Appl. Energy* **2011**, *88*, 981–1007. https://doi.org/10.1016/j.apenergy.2010.09.030.

(20) Koshiba, K.; Yamauchi, K.; Sakai, K. Ligand-Based PCET Reduction in a Heteroleptic Ni(Bpy)(Dithiolene) Electrocatalyst Giving Rise to Higher Metal Basicity Required for Hydrogen Evolution. *ChemElectroChem.* **2019**, *6* (8), 2273–2281. https://doi.org/10.1002/celc.201900400.

(21) Schultz, J. W.; Fuchigami, K.; Zheng, B.; Rath, N. P.; Mirica, L. M. Isolated Organo-metallic Nickel(III) and Nickel(IV) Complexes Relevant to Carbon−Carbon Bond Formation Reactions. *J. Am. Chem. Soc* **2016**, *138*, 12928-12934.

(22) Davidson, A.; Tempere, J. F.; Che, M.; Roulet, H.; Dufour, G. Spectroscopic Studies of Nickel(II) and Nickel(III) Species Generated upon Thermal Treatments of Nickel/Ceria-Supported Materials. *J. Phys. Chem.* **1996**, *100* (12), 4919–4929.

(23) Fuchigami, K.; Watson, M. B.; Tran, G. N.; Rath, N. P.; Mirica, L. M. Synthesis and Reactivity of (N_2P_2)Ni Complexes Stabilized by a Diphosphonite Pyridinophane Ligand. *Organometallics* **2021**, ASAP. doi.org/10.1021/acs.organomet.1c00003.

(24) Chmielewski, P.; Grzeszczuk, M.; Latos-grazynski, L.; Lisowski, J. Studies of the Reduction of the Nickel(II) Complex of 5,10,15,20-Tetraphenyl-21-Thiaporphyrin To Form Corresponding Nickel(I) Complexes. *Inorg. Chem.* **1989**, *28* (18), 3546–3552. https://doi.org/10.1021/ic00317a030.

(25) Wagner, C. L.; Herrera, G.; Lin, Q.; Hu, C. T.; Diao, T. Redox Activity of Pyridine-Oxazoline Ligands in the Stabilization of Low-Valent Organonickel Radical Complexes. *J. Am. Chem. Soc.* **2021**, *143* (14), 5295–5300.
(26) APEX Software Suite v 2010 Bruker AXS Inc. Madison Wisconsin USA, **2010**.
(27) Blessing, R. H. An Empirical Correction for Absorption Anisotropy. *Acta Crystallogr.* 1995, *A51*, 33–38.

Chapter 5. Reactions of Fluoroalkenes with d^9 Nickel-SNS Thiolate Complexes

5.1 Contribution for publication

Yahya M. Albkuri, Jeffrey S. Ovens and R. Tom Baker, communication in preparation.

Albkuri did all the experiments and Ovens did the X-ray diffraction data collection and structure refinement. Albkuri and Prof. Baker are writing the manuscript.

Abstract

Fluoroalkenes (FAs) are strong electron-acceptors that are also prone to reductive C-F bond activation. Reduction of bis(thiolate) complex, $Ni(SNS)_2$ using 1 or 2 equiv of Na/K alloy generates the $Ni(S_2N_2)$ mono- and dianion, respectively, which have been evaluated for their reactions with $CFX=CF_2$, where X = F, Cl, OCF_3 and CF_3. While reactions of the dianion with these FAs give a number of products, the monoanion reacts cleanly to afford a mixture of neutral *cis*- and *trans*-$Ni(S_2N_2)(CF=CFX)$ and anionic $[Ni(S_2N_2)(CF_2\text{-}CFXH)]^-$. The reactions are proposed to proceed via initial electron transfer, followed by hydrogen atom abstraction or fluoride elimination. High dilution was required to cleanly obtain the alkenyl product from hexafluoropropene.

5.2 Introduction

Catalytic routes to organofluorine compounds offer an attractive target considering the environmental downside associated with current synthetic methods. Installation of fluoride (-F)[1], trifluoromethyl ($-CF_3$)[2], difluoromethyl ($-CHF_2$)[3], and difluoromethylene ($-CF_2-$)[3] to organic substrates typically proceed through M-F or $M\text{-}R^F$ intermediates using electrophilic or nucleophilic fluorine or fluoroalkyl sources that have been studied extensively. With the advent of photoredox catalysis, efficient metal-mediated transfer of fluoroalkyl radicals has also been achieved.[4] However, stoichiometric studies of $M\text{-}R^F$ complexes obtained by single-electron transfer (SET) from the metal center are less common, especially for metal alkenyl complexes. Beletskaya and co-workers employed metal carbonyl anions ($[M(CO)_nL]^-$ to investigate halogenophilic versus carbophilic reactivity of aryl- and alkenyl halides.[5] They proposed a pathway involving initial attack at halogen with subsequent coupling of carbanion and $HalM(CO)_nL$ intermediates.[6] While reaction of $K[CpFe(CO)_2]$ with polyfluorinated alkenyl halides gave some substituted products,

$CpFe(CO)_2(CF{=}CFR^F)]$, $Na[Re(CO)_5]$ afforded the acyl product with selective C-Cl and C-Br activation versus C-F (**Scheme 5.1**). In 2001, the same authors examined less reactive alkenyl chlorides, RCF=CFCl (R= Ph, F), with the same metal carbonyl anions and showed that no substituted products were derived from direct attack of the carbonylmetallate at the vinylic carbon atom.[7]

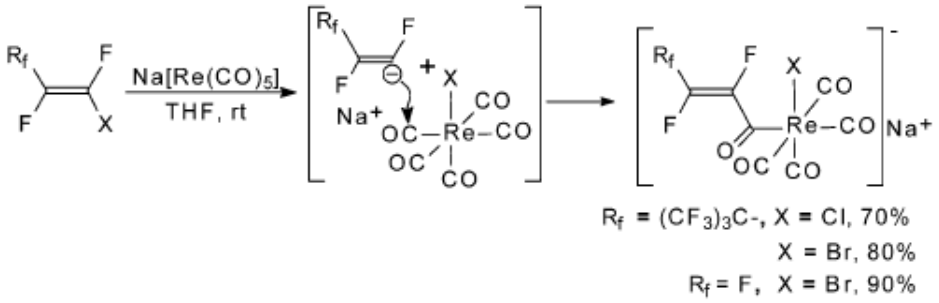

Scheme 5.1 Reactivity of fluoroalkenes with $Na[Re(CO)_5]$.[5]

In this chapter, we demonstrate that reduced $Ni(S_2N_2)$ complexes react readily with fluoroalkenes affording both neutral Ni-fluoroalkenyl and anionic Ni-fluoroalkyl products. Moreover, with chlorotrifluoroethylene d^9 $[Ni(S_2N_2)]^-$ exhibits high selectivity for C-F versus C-Cl bond activation.

5.3 Results and Discussion

5.3.1 Synthesis of reduced $Ni(S_2N_2)$ complexes

In the previous Chapter we demonstrated the accessibility and stability of the $Ni(S_2N_2)$ mono- and dianions generated electrochemically. Chemical reduction was achieved conveniently using sodium benzophenone or Na/K alloy, affording complexes **Ni-3** through **Ni-6** (**Scheme 5.2**).

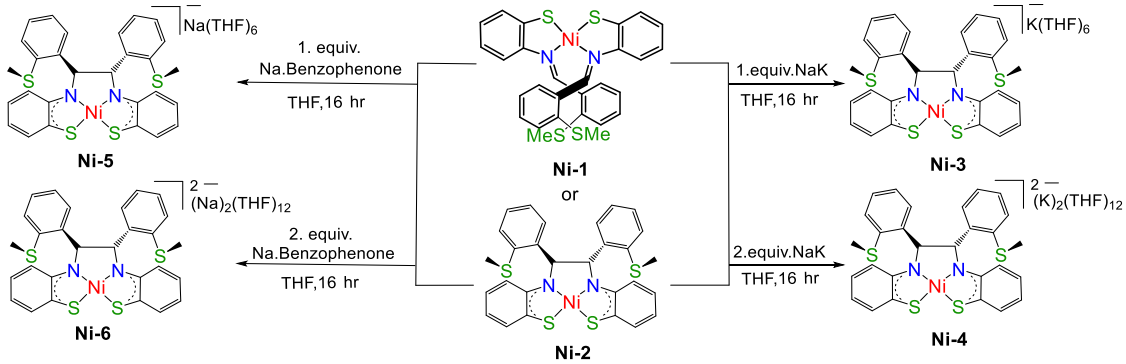

Scheme 5.2 Chemical reduction of $Ni(SNS)_2$ or $Ni(S_2N_2)$.

The ^{1}H NMR spectra showed that the dianion in **Ni-4** and **Ni-6** is diamagnetic; the EPR spectrum of the monoanion was displayed and discussed in Chapter 4.

5.3.1 Reactions of reduced Ni(S_2N_2) complexes with chlorotrifluoroethylene (CTFE)

Neither **Ni-1** nor neutral **Ni-2** showed any reactivity with CTFE, whereas dianionic **Ni-4** and **Ni-6** both gave a mixture of products (yellow to green colour change) even when the addition was performed at -78 °C (**Figure 5.1**). In contrast, monoanionic **Ni-3** and **Ni-5** both gave clean reactions with CTFE even at RT accompanied by a colour change from green to green-blue after 16 h (**Scheme 5.3**). The ^{19}F NMR spectrum indicated formation of three products: *cis*- and *trans*-Ni(S_2N_2)(CF=CFCl) *(***Ni-7)** and **[**Ni(S_2N_2)(CF_2CFClH)]M^I (**Ni-8**), where $M^I = Na^+, K^+$, in a 5:4:12 ratio (**Figure 5.2**). The alkenyl products are distinguished by their $^{3}J_{FF}$ coupling constants which are 15 Hz for *cis*-**Ni-7** and 140.5 Hz for *trans*-**Ni-7**. The diastereotopic $C_\alpha F_2$ resonances for **Ni-8** include a large $^{2}J_{FF}$ coupling constant (219 Hz) and small $^{3}J_{FH}$ of 8 and 4 Hz, whereas the $C_\beta F$ resonance has $^{2}J_{FH}$ of 38 Hz confirming attack of the Ni-based nucleophile at the CF_2 group of CTFE followed by H atom abstraction from solvent. The expected doublet of doublet of doublets resonance of the terminal C-*H* was observed at δ 5.90 in the ^{1}H NMR spectrum (Fig. A5.1). On consideration of these reaction products we surmise that formation of **Ni-7** is accompanied by loss of M^I-F whereas formation of **Ni-8** involves hydrogen atom abstraction from the solvent. The 3:4 ratio of C-F bond activation to hydrogen atom abstraction was not significantly affected by switching to acetonitrile solvent (Cα-H bond dissociation energy = 91 vs. 92 kcal/ mol for THF), but no reaction at all was observed in toluene (benzylic C-H BDE = 88 kcal/mol),[8] suggesting that solvent polarity may also play a key role.

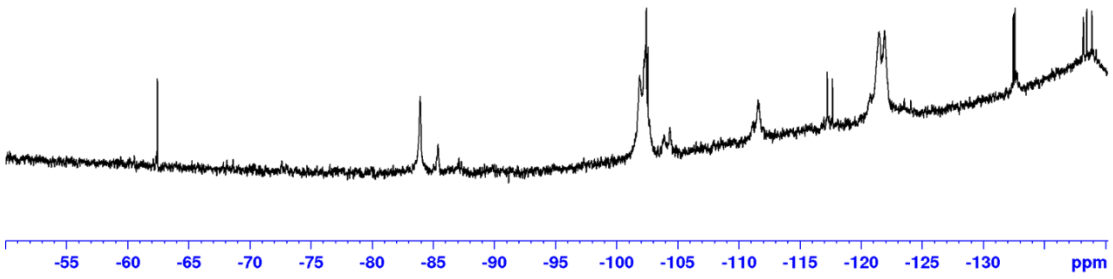

Figure 5.1 ^{19}F NMR (282 MHz, C_6D_6) spectrum of reaction products from **Ni-4** (Ni^0, d^{10}) + CTFE in THF.

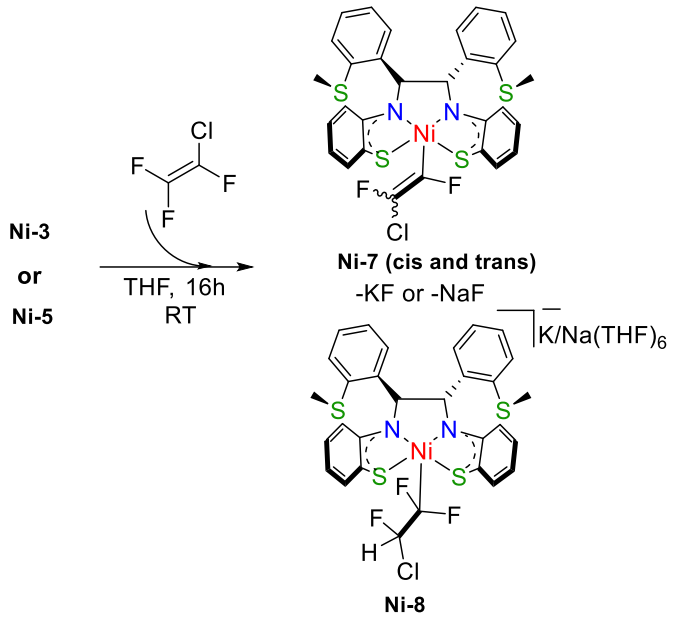

Scheme 5.3 Reaction of **Ni-3** or **Ni-5** (Ni^{I}, d^{9}) with CTFE.

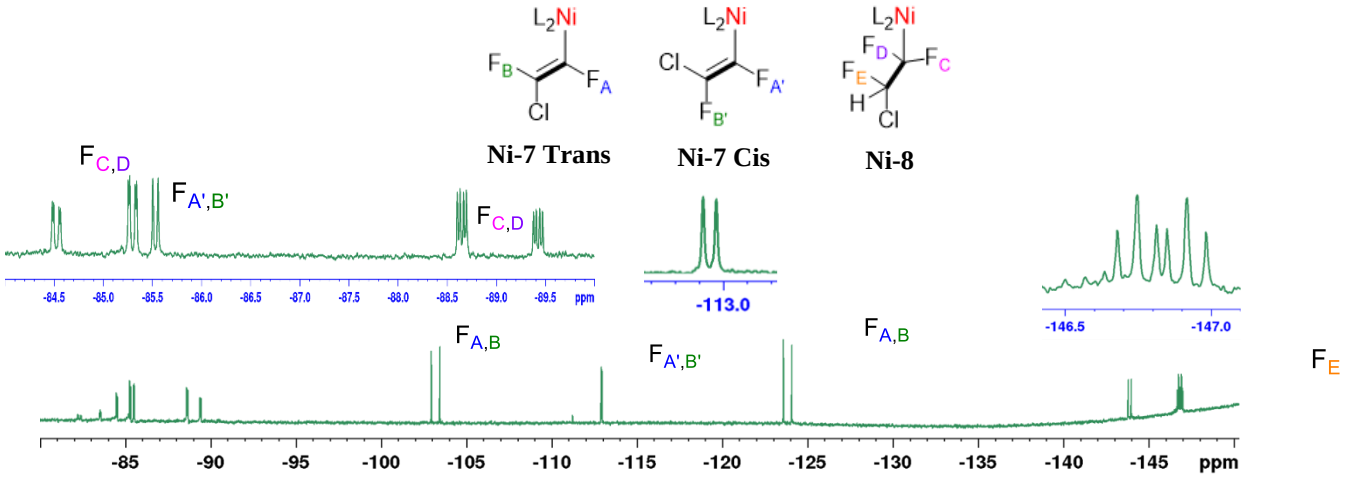

Figure 5.2 ^{19}F NMR (282 MHz, C_6D_6) spectrum of *cis*- and *trans*-**Ni-7** and **Ni-8**.

in these reactions. Moreover, in forming **Ni-7**, we might have expected activation of the weaker C-Cl (vs. C-F) bond but similar observations have been attributed to better carbanion stabilization by Cl vs. F.[9]

5.3.2 Reactions of reduced Ni(S_2N_2) complexes with perfluoro(methyl vinyl ether) (PMVE)

Substitution of the Cl in CTFE with the OCF_3 group in PMVE did not significantly affect the reaction course with the reduced Ni(S_2N_2) complexes. As above, dianion **Ni-4** gave a mixture of products and a broad ^{19}F NMR spectrum (**Figure 5.3**) whereas **Ni-3** showed a cleaner reaction to *cis*- and *trans*-{Ni(S_2N_2)[CF=CF(OCF_3)]} (**Ni-9**) and **{**Ni(S_2N_2)[$CF_2CHF(OCF_3)$]}M^{I} (**Ni-10**) in

a 12:10:5 ratio (**Scheme 5.4**). The alkenyl complexes were again distinguished by their $^{3}J_{FF}$ coupling constants (26 Hz for *cis*-**Ni-9** and 129.5 Hz for *trans*-**Ni-9**) but only one F of the former was coupled to the OCF_3 group ($^{4}J_{FF}$ = 4.5 Hz), in contrast to the latter in which both alkenyl F resonances were doublet of doublets ($^{4}J_{FF}$ and $^{5}J_{FF}$ = 4.5 Hz) (**Figure 5.4**). The diastereotopic $C_{\alpha}F_2$ resonances for **Ni-10** included a large $^{2}J_{FF}$ coupling constant (226 Hz) and small $^{3}J_{FH}$ of 12.5 and 13 Hz, whereas the $C_{\beta}F$ resonance (also coupled to OCF_3) has $^{2}J_{FH}$ of 54.5 Hz, again confirming attack of Ni at the CF_2 group of PMVE followed by H atom abstraction from solvent. Although there were several unidentified co-products (one major), the ^{19}F NMR spectra provided no evidence for a Ni[$CF(OCF_3)CF_2H$] group. In an effort to control the selectivity, the reaction was

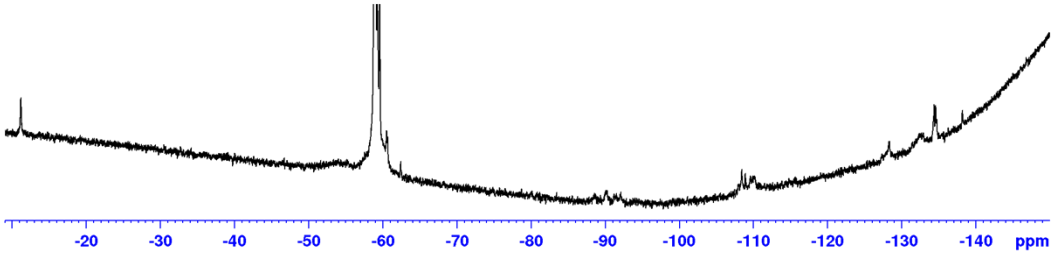

Figure 5.3 ^{19}F NMR (300 MHz, C_6D_6) spectrum of **Ni-4** with PMVE.

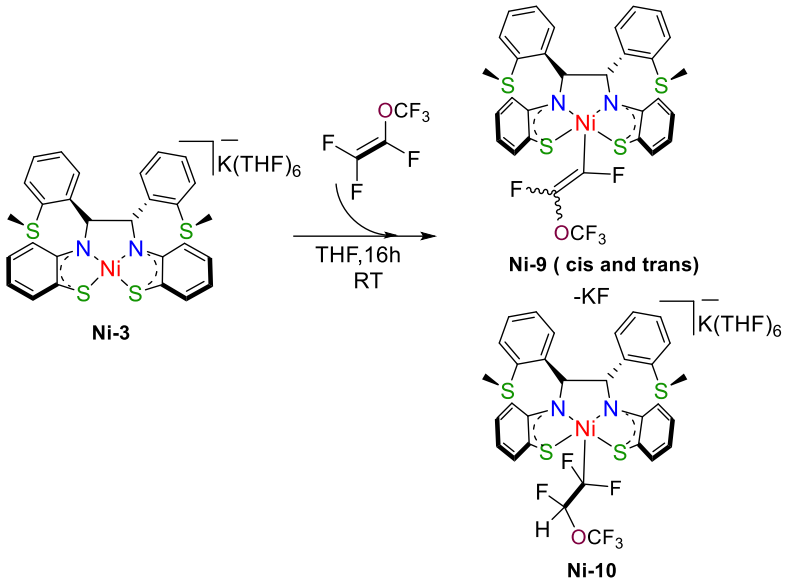

Scheme 5.4 Reaction of **Ni-3** with PMVE.

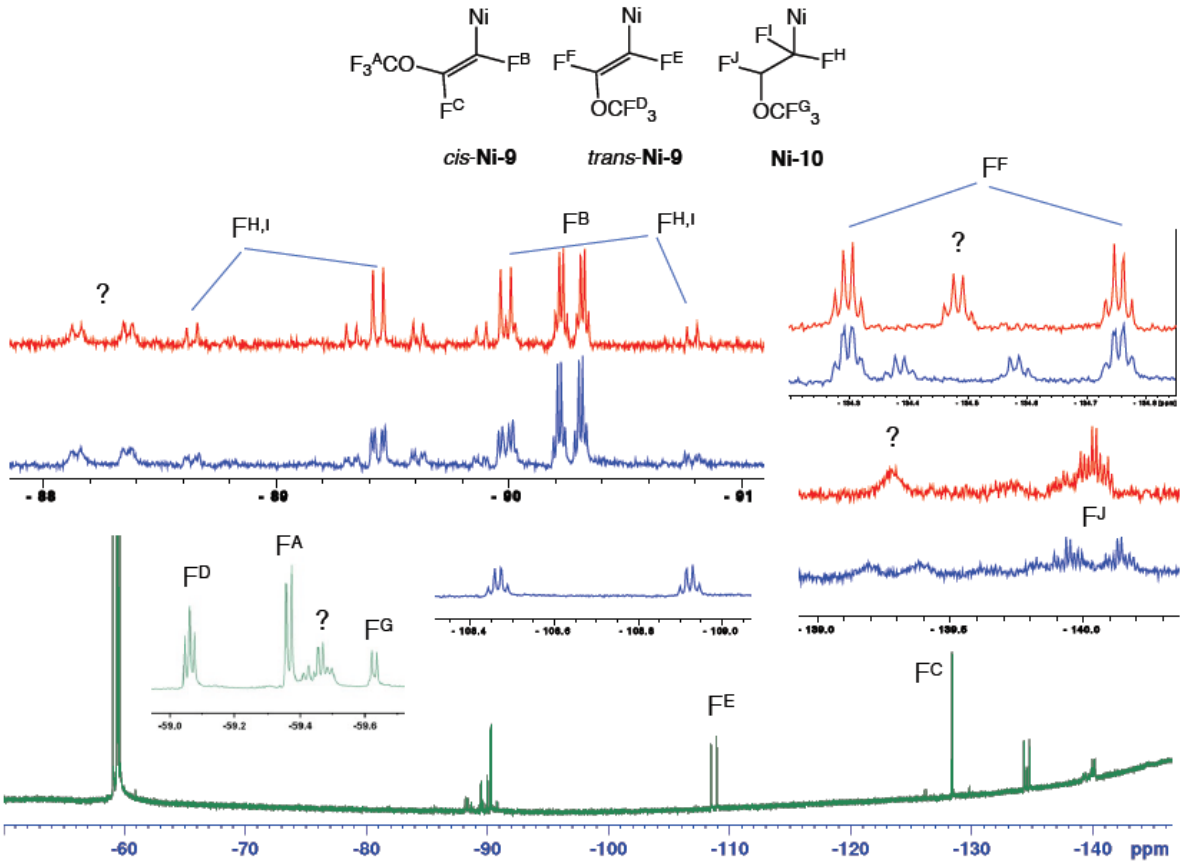

Figure 5.4 ^{19}F NMR (282 MHz, C_6D_6) spectrum of **Ni-3** reaction with PMVE (red is proton-decoupled).

performed at – 78 ^{o}C but the relative selectivity for C-F bond activation and H atom abstraction (> 4:1) was unchanged. Longer reaction times also had no effect on product selectivity.

5.3.3 Reactions of reduced Ni(S_2N_2) complexes with tetrafluoroethylene (TFE) and hexafluoropropene (HFP)

As with the other fluoroalkenes, TFE reactions with dianion **Ni-4** afforded green solutions that gave broad ^{19}F NMR spectra of a mixture of unidentified products (Fig. A5.3). Attempts to improve the reaction by changing solvent, temperature and stoichiometry were unsuccessful. However, **Ni-3** and TFE afforded both perfluorovinyl (**Ni-11**) and tetrafluoroethyl (**Ni-12**) products in a 3:10 ratio (**Scheme 5.5**).

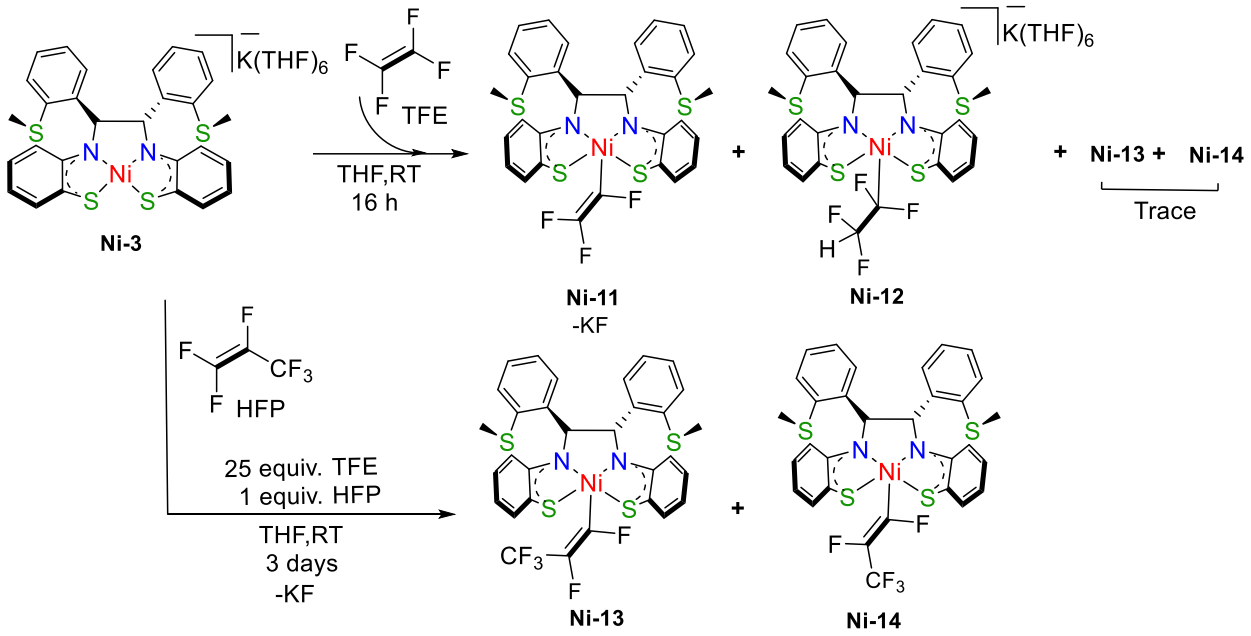

Scheme 5.5 Reactions of TFE and HFP impurity with **Ni-3**.

The ^{19}F NMR spectrum of this reaction mixture (**Figure 5.5)** showed two additional alkenyl products (*cis- and trans*-Ni(S_2N_2)[CF=CF(CF_3)] in a 1:2.5 ratio) (**Ni-13)** apparently derived from hexafluoropropene (HFP) which is a 3% impurity in the TFE gas. The perfluorovinyl group in **Ni-11** is distinguished by the large *trans*- $^3J_{FF}$ coupling constant (124.5 Hz) and the tetrafluoroethyl group in **Ni-12** by the 3.5 and 54 Hz J_{FH} coupling constants for the $C_\alpha F_2$ and $C_\beta F_2H$ groups, respectively. Both fluorines in *trans*-**Ni-13** ($^3J_{FF}$ = 146 Hz) are coupled to the CF_3 group (J_{FF} = 21 and 12 Hz) as they are in *cis*-**Ni-13** ($^3J_{FF}$ = 6 Hz; J_{FF} to CF_3= 11 and 10 Hz). The large amount of **Ni-13** shown in Figure 5.5 reflects the much higher reactivity of HFP relative to TFE. Indeed, using 25 equiv. of TFE gave **Ni-13** almost exclusively (Fig. A5.4). In contrast, direct reactions of **Ni-3** with HFP gave no colour change and broad ^{19}F NMR spectra (Fig. A5.6) indicating a mixture of products, due again to the high reactivity of the latter. Similar behavior was observed using **Ni-4** (Fig A5.7).

5.3.4 Reactions of reduced Ni(S_2N_2) complexes with 1,1-difluoroethylene (VDF) and 3,3,3-trifluoropropene (TFP)

In a last attempt to obtain clean products from dianion Ni-4, we investigated less reactive CH_2=CF_2 (VDF) and CH_2=CF(CF_3) (TFP). Although both gases effected a colour change from yellow to green, no diamagnetic products were observed by ^{19}F NMR.

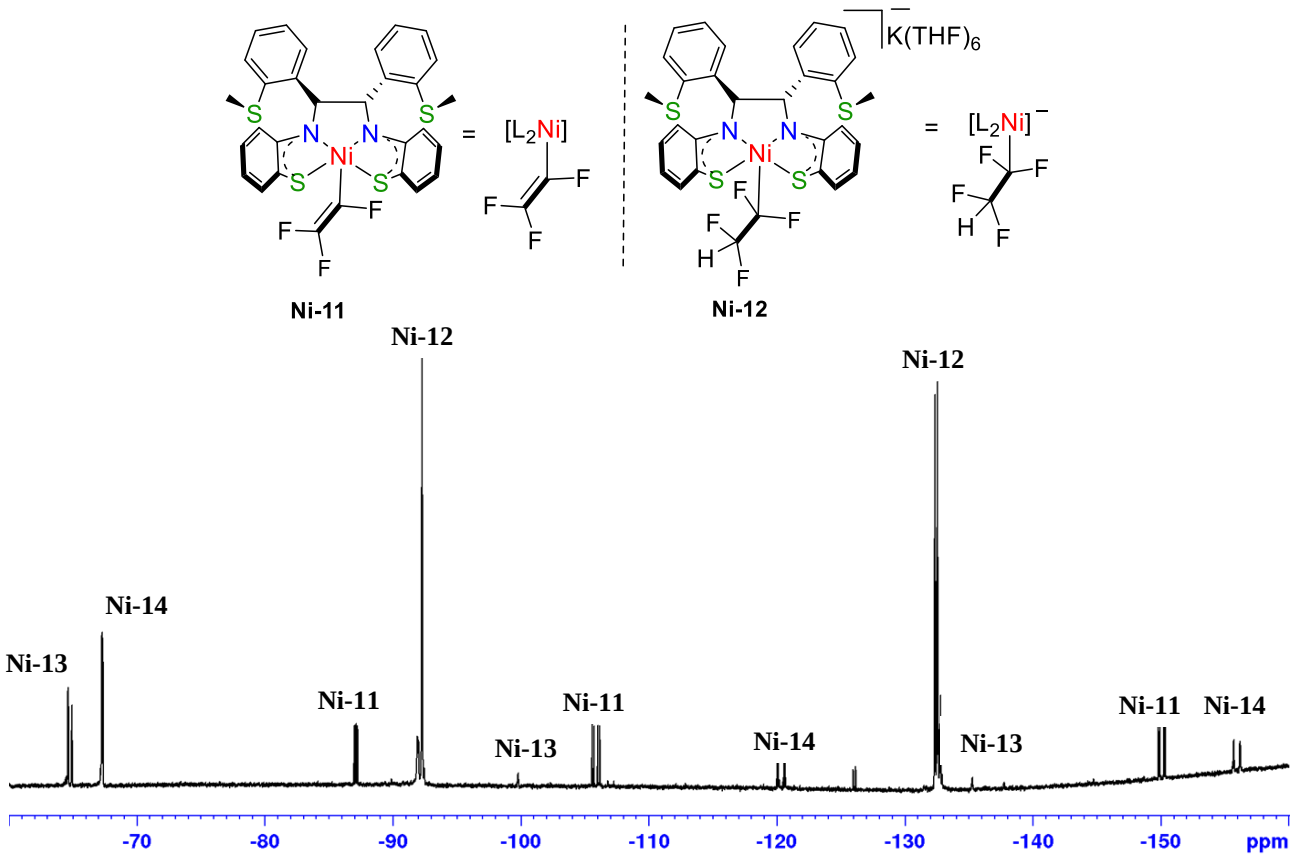

Figure 5.5 ^{19}F NMR spectrum (282 MHz, C_6D_6) of **Ni-3** + TFE:HFP (97:3).

5.4 Conclusion

This work has expanded our knowledge about C-F activation of fluoroalkenes. Starting from simple Ni-bisthiolate and reduced by one electron has shown great reactivity that can be seen by Ni(I)-SNS complex to give different type of fluorinated nickel-SNS complexes. While treatment of **Ni-3** with CTFE led to different products, one of them favor HAA, but the other one favor the usual vinyl product, the **Ni-3** reacted with PMVE differently and favor the HAA pathway to make two isomers. Variable temperature had no effect on the selectivity. Moreover, using a poor source of proton also did not improve the selectivity. Finally and interestingly, **Ni-3** has shown great and different reactivity towards TFE, changing the TFE ratio with **Ni-3** showed different products, ^{19}F NMR confirmed that there are two intermediates form in suti- and that led to the unusual **Ni-11** and **Ni-12**.

5.5 Experimental Section

5.5.1 General Considerations. All experiments were carried out under nitrogen, using a Schlenk line or an MBraun glovebox unless otherwise stated. All solvents were deoxygenated by purging with nitrogen. Toluene, hexanes, diethyl ether, and THF were dried on columns of activated alumina using a J. C. Meyer (formerly Glass Contour) solvent purification system. Anhydrous benzene (Aldrich), C_6D_6 and acetone-d_6 were dried with activated alumina (ca. 10 wt %) overnight, followed by filtration. Dichloromethane (DCM) and $CDCl_3$ were refluxed over calcium hydride under nitrogen, collected by distillation, dried further by passing through activated alumina (ca.10 wt%), and stored over activated 4 Å molecular sieves (heated at 250 ^oC for 3 d under vacuum). Glassware was oven-dried at 150^oC overnight. Ligand precursor 2-(methylthio)-benzaldehyde[7] and the SN^HS^{Me} (MTB) ligand[8] were prepared according to literature procedures and reduced Ni(S_2N_2) complexes were generated as described in Chapter 4 Experimental section. Other chemicals were used as obtained commercially: Sodium cubes (contains mineral oil, Aldrich, 99.9%), Potassium cubes (contains mineral oil, Alfa Aesar, 99.5%), NaK reagent was made K:Na 4:1 ratio. Tetrafluoroethylene was made by pyrolysis of polytetrafluoroethylene (Scientific Polymer Products, powdered) under vacuum, using a slightly modified literature procedure (10−20 mTorr, 650 °C, 30 g scale, product stabilized with (R)- (+)-limonene (Aldrich, 97%), giving TFE of ca. 97% purity).[9,10] ^1H and ^{19}F NMR spectra were recorded on a 300 MHz Bruker Avance or Avance II instrument at room temperature (21−25 °C). ^{19}F and ^1H NMR spectra were referenced respectively to solvent carbons and residual protons (C_6D_6, δ 7.15; $CDCl_3$, δ 7.26) with respect to tetramethylsilane at δ 0.00. Mass spectra were recorded on an AB Sciex Q1MS mass spectrometer with electrospray ionization (ESI-MS) in positive mode (ion spray voltage: 5000.0 V, TEM: 400 °C, declustering potential: 11.00 V and focusing potential: 300.0 V) with samples prepared to *ca.* 0.05 mg/mL in acetonitrile or dichloromethane. X-ray diffraction data were collected on a Bruker Smart or Kappa diffractometer equipped with an ApexII CCD detector and a sealed-tube Mo K source (λ = 0.71073 Å). Elemental analyses were performed by University of Guelph Elemental Analysis service.

5.5.2 Reaction of CTFE with (Ni-4) and (Ni-6). A 50 mL one-neck vacuum flask fitted with rubber septum was charged with **Ni-4** (40 mg, 0.061 mmol) in 15 mL of THF solution. CTFE (1.5 mL, 0.061 mmol, 1 equiv.) was added to the solution using a syringe at room temperature. The yellow color solution was immediately turned green. The reaction mixture was stirred for 16 h at

room temperature after which the solvent was removed under vacuum and the remaining green/blue solid was dissolved in cold hexane (2 mL) and THF (1mL) and kept at -35 ^{o}C for 3 hrs, solution was filtered and remove the solvent under vacuum to give a mixture of products as a green/blue solid.

Same experimental procedure was followed using **Ni-6**

5.5.3 Synthesis of *cis*- and *trans*-Ni(S_2N_2)(CF=CFCl) (Ni-7) and [Ni(S_2N_2)(CF_2CFClH)]M^I (Ni-8) (M^I = Na^+, K^+). A 50 mL one-neck vacuum flask fitted with rubber septum was charged with **Ni-3** (40 mg, 0.065 mmol) in 15 mL of THF. CTFE (1.6 mL, 0.065 mmol, 1 equiv.) was added to the solution using a syringe at room temperature. The resulting green solution was stirred for 16 h at room temperature after which the solvent was removed under vacuum and the remaining blue-green solid was dissolved in cold hexane (2 mL) and THF (1 mL) and kept at -35 ^{o}C for 3 hrs. The solution was then filtered and the solvent removed under vacuum to give a mixture of *cis*- and *trans*-**Ni-7** and **Ni-8** as a purple solid. ^{1}H NMR for **Ni-7** and **Ni-8** (300 MHz, C_6D_6) 8.89 (br, Ar-H), 8.25-8.33 (dd, Ar-H), 7.57 (m, Ar-H), 7.42 (s, Ar-H), 7.05-6.99 (m, Ar-H), 6.78 (m, Ar-H), 2.25 (s, S-CH_3) (Fig. A5.1). ^{19}F{^{1}H} NMR (282 MHz, C_6D_6): *cis*-**Ni-7:** -85.5, -112.9 ppm (d, $^{3}J_{FF}$ = 15 Hz); *trans*-**Ni-7:** -103.2, -123.8 ppm (d, $^{3}J_{FF}$ = 140.5 Hz); **Ni-8**: -84.9 (ddd, $^{2}J_{FF}$ = 219, $^{3}J_{FF}$ = 20, $^{3}J_{FH}$ = 4 Hz, 1F, C*F*$_2$), -89.0 (ddd, $^{2}J_{FF}$ = 219, $^{3}J_{FF}$ = 18, $^{3}J_{FH}$ = 8 Hz, 1F, C*F*$_2$), -146.8 ppm (ddd, $^{3}J_{FF}$ = 20, 18, $^{3}J_{FH}$ = 38 Hz, 1F, CH*F*Cl).

Same experimental procedure was followed to synthesize **Ni-7** and **Ni-8** using **Ni-5**.

5.5.4 Reaction of PMVE with (Ni-4).

(20 mg, 0.031 mmol) of **Ni-4** dissolved in 0.5 mL of THF was transferred to an NMR tube equipped with a septum. To the solution, a 1.0 equiv portion of PMVE (0.75 ml, 0.031 mmol) was added, giving an immediate colour changed from yellow to green. The NMR was shaken vigorously for 10 min, the solvent was removed in vacuo and the residue re-dissolved in C_6D_6.

5.5.5 Synthesis of *cis*- and *trans*-{Ni(S_2N_2)[CF=CF(OCF_3)]} (Ni-9) and {Ni(S_2N_2)[$CF_2CHF(OCF_3)$]}M^I (Ni-10) (M^I = Na^+, K^+). A 50 mL one-neck vacuum flask fitted with a rubber septum was charged with **Ni-3** (40 mg, 0.065 mmol) in 15 mL of THF. PMVE (1.6 mL, 0.065 mmol, 1 equiv.) was added to the solution using a syringe at room temperature. The resulting green solution turned into blue in 10 min and was stirred for 16 h after which the solvent was removed under vacuum and the remaining solid was dissolved in cold hexane (2 mL) and THF

(1mL) and kept at -35 ºC for 3 h. The solution was then filtered and the solvent under vacuum to give a mixture of **Ni-9** and **Ni-10** as a purple solid. $^{19}F\{^{1}H\}$ NMR (282 MHz, C_6D_6) *cis*-**Ni-9:** -59.4 (d, $^{5}J_{FF}$ = 4.5 Hz, OC*F*$_3$), -90.3 (dq, $^{3}J_{FF}$ = 26, $^{5}J_{FF}$ = 4.5 Hz), -128.4 ppm (d, 26). *trans*-**Ni-9:** -59.0 (tr, $^{5}J_{FF}$ = 4.5 Hz, OC*F*$_3$), -108.7 (dq, $^{3}J_{FF}$ = 129.5, $^{5}J_{FF}$ = 4.5 Hz), -134.5 ppm (dq, 129.5, $^{4}J_{FF}$ = 4.5 Hz). **Ni-10:** -59.6 (d, $^{4}J_{FF}$ = 4.5 Hz, OC*F*$_3$), -89.0 (ddd, $^{2}J_{FF}$ = 226, $^{3}J_{FF}$ = 13, $^{3}J_{FH}$ = 4 Hz, 1F, C*F*$_2$), -90.0 (ddd, ,226, $^{3}J_{FF}$ = 12.5, $^{3}J_{FH}$ = 8 Hz, 1F, C*F*$_2$), -140.0 ppm (ddd, $^{3}J_{FF}$ = 13, 12.5, $^{3}J_{FH}$ = 54.5 Hz, 1F, CH*F*Cl). Additional resonances: -59.5 (d, 4.5), -88.3 (dd, 62.5, 10), -134.5 (dq, $^{2}J_{FH}$ = 55, J_{FF} = 4.5 Hz), -139.3 (br d mult, $^{2}J_{FH}$ = 54 Hz).

5.5.6 Synthesis of Ni(S$_2$N$_2$)(CF=CF$_2$)] (Ni-11) and [Ni(S$_2$N$_2$)(CF$_2$CF$_2$H)]M^{I} (Ni-12) (M^{I} = Na^{+}, K^{+}). A 50 mL one-neck vacuum flask fitted with a rubber septum was charged with **Ni-3** (40 mg, 0.065 mmol) in 15 mL of THF. TFE (1.6 mL, 0.065 mmol, 1 equiv.) was added to the solution using a syringe at room temperature. The resulting green solution was stirred for 16 h at room temperature after which the solvent was removed under vacuum and the remaining purple solid was dissolved in cold hexane (2 mL) and THF (1 mL) and kept at -35 ºC for 3 hrs. The solution was filtered and the solvent removed under vacuum to give a mixture of **Ni-11** and **Ni-12** as a purple solid. ^{1}H NMR for **Ni-11** and **Ni-12** (300 MHz, C_6D_6) 8.87 (s, Ar-H), 8.26 (m, Ar-H), 7.57 (d, Ar-H), 7.40-7.14 (ov mult, Ar-H), 7.03 (s, Ar-H), 7.0-6.8 (ov mult, Ar-H), 6.83-6.64 (ov mult, Ar-H), 5.52 (t, 1H, -CF_2-CF_2H), 5.34 (t, 1H, -CF_2-CF_2H), 5.17 (t, 1H, -CF_2-CF_2H), 3.16 (br), 2.26 (s, S-CH_3) (Figure A5.2). $^{19}F\{^{1}H\}$ NMR (282 MHz, C_6D_6): **Ni-11:** -87.1 (dd, J_{FF} = 44, 33 Hz), -105.9 (dd; $^{2}J_{FF}$ = 124, J_{FF} = 44 Hz), -150.1 (dd, 124, 33 Hz). **Ni-12**: -92.3 (trd, $^{2}J_{FF}$ = 10, $^{3}J_{FH}$ = 3.5 Hz), Cα*F*$_2$), -132.5 ppm (dtr, $^{2}J_{FH}$ = 54 Hz, $^{2}J_{FF}$ = 10 Hz).

5.5.7 Synthesis of *cis*- and *trans*-[Ni(S$_2$N$_2$)(CF=CFCF$_3$)] *(*Ni-13). A 50 mL one-neck vacuum flask fitted with rubber septum was charged with **Ni-3** (40 mg, 0.065 mmol) in 15 mL of THF. TFE (38.8 mL, 1.625 mmol, 25 equiv.) HFP (1.3 mL, 0.065 mmol, 1 equiv.) was added to the solution using a syringe at room temperature. The resulting green solution was stirred for 3 days at room temperature after which the solvent was removed under vacuum and the remaining purple solid was dissolved in cold hexane (2 mL) and THF (1mL) and kept at -35 ºC for 3 h. The solution was filtered and the solvent removed under vacuum to give a mixture of *cis*- and *trans*-**Ni-13** as a purplish solid. ^{1}H NMR (300 MHz, C_6D_6) 8.25 (ov mult, Ar-H), 7.48 (d, Ar-H), 7.42 (s, Ar-H), 6.92-6.80 (m, Ar-H), 6.77-6.63 (ov mult, Ar-H), 6.62-6.33 (ov mult, Ar-H), 2.25 (s, S-CH_3) (Figure A5.8). $^{19}F\{^{1}H\}$ NMR (282MHz, C_6D_6): *cis*-**Ni-13**: -64.9 (dd, J_{FF} = 11, 10 Hz), -99.8 (qd,

J_{FF} = 10, 6 Hz), -135.4 ppm (qd, J_{FF} = 11, 6 Hz). *trans*-**Ni-13:** -67.3 (dd, J_{FF} = 21, 12 Hz), -120.4 (dq, J_{FF} = 146, 21 Hz), -156.0 ppm (dq, J_{FF} = 146, 12 Hz).

5.5.8 Reaction of HFP with (Ni-3) and (Ni-4).

Two NMR tubes was prepared with rubber septa: the first tube was charged with **Ni-3** (20 mg, 0.033 mmol). A 1.0 equiv portion of HFP (0.8 ml, 0.033 mmol) was added to the NMR tube and it was shaken vigorously for 10 min and kept inside the glovebox for 16 hrs; no color change was observed. The solvent was removed and the residue re-dissolved in C_6D_6. The second NMR tube was charged with **Ni-4** (20 mg, 0.031 mmol). A 1.0 equiv portion of HFP (0.75 ml, 0.031 mmol) was added to the NMR tube and it was shaken vigorously for 10 min; the colour changed immediately from yellow to green. After 16 hrs, the solvent was removed and the residue dissolved in C_6D_6.

5.5.9 Reaction of 1,1-difluoroethylene, 3,3,3-trifluoropropene with (Ni-4) and (Ni-6).

Two NMR tubes were prepared and each filled with **Ni-4** (20 mg, 0.031 mmol) dissolved in ca. 1 mL THF. A 1.0 equiv portion of the fluoroalkene (0.75 ml, 0.031 mmol) was then added to the NMR tube giving an immediate colour change from yellow to dark green. After 16 h, THF solvent was removed from each NMR tube and the residue dissolved in C_6D_6.

5.6 References

(1) Hoover, A. J.; Lazari. M.; Ren, H.; Narayanam, M. K.; Murphy, J. M.; Van Dam, R. M.; Hooker, J. M.; Ritter, T. A. Transmetalation Reaction Enables the Synthesis of [^{18}F]5-Fluorouracil from [^{18}F] Fluoride for Human PET Imaging. *Organometallics* **2016**, *35* (7), 1008-1014. https://doi.org/10.1021/acs.organomet.6b00059.

(2) Tomashhenko, O. A.; Grushin, V. V. Aromatic Trifluoromethylation with Metal Complexes. *Chem. Rev.* **2011**, *111*, 4475-4521 https://doi.org/10.1021/cr1004293.

(3) Chen, B.; Vicic, D. A. Transition metal catalyzed Difluoromethylation, Difluoromethylenation, and Polydifluoromethylenation Reactions. *Organometallic Fluorine Chemistry*, Springer, *Top. Organomet. Chem.* **2015**, *52*, 113-141. https://doi.org/10.1007/3418_2014_87.

(4) Line, C. Y.; Power, P. P. Complexes of Ni(I): A "Rare" Oxidation State of Growing Importance. *Chem. Soc. Rev.* **2017**, *46*, 5347-5399. https://doi.org/10.1039/c7cs00216e.

(5) Sazonov, P. K.; Beletskaya, I. P. Carbonylmetallates - A Special Family of Nucleophiles in Aromatic and Vinylic Substitution Reactions. *Chem. Eur. J.* **2016**, *22*, 3644–3653. https://doi.org/10.1002/chem.201504423.

(6) Sazonov, P. K.; Artamkina, G. A.; Beletskaya, I. P. Anions of Transition Metals Carbonyls in Nucleophilic Vinyl Substitution: VII. *Russ. J. Org. Chem.* **2001**, *37*(4) 480-495.

(7) Goebbert, D. J.; Velarde, L.; Khuseynov, D.; Sanov, A. C-H Bond Dissociation Energy of Malononitrile. *J. Phys. Chem. Lett.* **2010**, *1*, 792–795. https://doi.org/10.1021/jz900379t.

Chapter 6. Conclusions and Future Outlook

The work presented in this thesis adds to our understanding of phosphine-free nickel catalysts for cross-coupling catalysis, nickel coordination chemistry and dynamics of thiolate-imine-thioether SNS ligands, and electronic structure and reactivity of a nickel S_2N_2 complex in three redox states. In this Chapter we consider these advancements in the context of the current state of the art and suggest some ideas for future development.

In **Chapter 2** our work builds on earlier catalysis projects from the Ghosh group employing the diamidopyridine pincer ligand.[1,2] Advantages offered by our Ni precatalyst (**2-2**) include: 1) ease of ligand (**2-1**) preparation (single step from pyridine dicarboxylic acid and 2 equiv of the disubstituted aniline); 2) stability to air and water; 3) potential thermal stability; and 4) ease of Ni separation (vs. Pd) from resulting organic products. Although anionic nickel(II) halide complexes are unusual precatalysts for aryl halide aminations, addition of $KOBu^t$ serves the function of both halide removal and reduction to Ni(I)[3] which is competent for oxidative addition of the aryl halide substrate. It is understood that the base also deprotonates the metal amine complex to an amido ligand that subsequently undergoes reductive N-C bond elimination with the Ni-aryl.[4] Although more effective nickel catalysts have been reported previously by the Stradiotto group,[5,6] their designer Dalphos ligands are considerably more complicated to make. In order to stand out from other simple yet effective catalyst systems such as CuBr/8-hydroxyquinoline-*N*-oxide,[7] development of a catalyst separation strategy that takes advantage of the negative charge could be a game-winner. Bulky phosphonium-based ionic liquids that are compatible with strong bases may offer one promising possibility.[8] Finally, application of inorganic chemistry characterization techniques such as freeze-quench EPR studies, may allow for characterization of paramagnetic Ni(I) and Ni(III) intermediates.[9]

In **Chapter 3** we investigate the nickel coordination chemistry of an SNS^{Me} pincer ligand containing thiolate, imine and thioether donors. Previous studies of this ligand by other members of the Baker group have focused on Fe[10,11] and Co,[12] and more recently Cu and Zn. The origin of this ligand type can be traced to Bouwman's work on hydrogenase enzyme models,[13] using an S-Bu^t substituent instead of S-Me. Although she did isolate and characterize a bis(thiolate) complex, Ni(κ^2-$SNS^{t\text{-}Bu}$)$_2$, analogous to **3-1**, reaction of her ligand with some Ni salts afforded instead a thiolate-bridged dinuclear complex [Ni(μ-κ^3-SNS)]$_2$ due to 'deprotection' of the thioether group, affording the dianionic, imine-dithiolate SNS ligand. In our work, we obtained a structurally similar dicationic, thiolate-bridged dinuclear complex $\{[Ni(\mu\text{-}\kappa^3\text{-}SNS^{Me})]_2\}^{2+}$ (**3-3**) by protonation of the bis(thiolate) complex, Ni(κ^2-SNS^{Me})$_2$ (**3-1**). In her 1998 paper, Bouwman noted that attempts to cleave their

dinuclear complex with donor ligands were underway but a follow-up paper has not appeared. In our case, ligand addition proceeds smoothly, affording di- or mononuclear cationic products, **6a,b** and **7a,b**, depending on the ligand. Using 2 equiv of the IPr *N*-heterocyclic carbene ligand, revealed an alternate S-C bond cleavage pathway in which the strong NHC nucleophile abstracts a methylium cation, forming the same dianionic dithiolate ligand that appeared in Bouwman's dimer, but now in a mononuclear Ni(κ^3-SNS)(IPr) complex (**8**).

An unexpected and remarkable feature of our dinuclear dication **3-3** is its ligand dynamics in solution. Even dissolving the crystals at -78°C yields no evidence for its diamagnetic structure in solution. Instead, the hemilabile thioether group allows for the formation of the paramagnetic, pseudo-octahedral Ni(κ^3-SNS)$_2$ unit, two of which bind to a central square planar Ni^{2+} center through thiolate bridges in trinuclear complex **3-4** and three to a central octahedral Ni^{2+} center in tetranuclear complex **3-5**. As the SNS ligand:Ni ratio increases from 1 to 1.33 to 1.5 h going from **3-3** to **3-4** to **3-5**, the co-product must be Ni(NTf_2)$_2$ although we were unable to identify a UV-vis signature for the latter. In spite of this unprecedented 'X-ligand' dynamics, addition of ancillary ligands L provided no evidence for formation of [NiL$_4$](NTf_2)$_2$ and reaction with CNXylyl even afforded a thiolate-bridged dimer, seemingly derived from **3-3**. We showed that conversion of **3-3** to **3-4** + Ni(NTf_2)$_2$ proceeded in a variety of solvents, including acetone, THF, acetonitrile and even weakly-coordinating DCM. Although we were able to generate triflate salts of the multinuclear Ni complexes from reaction of Ni(OTf)$_2$ with multiple equiv of **3-1,** in future work, it would be interesting to employ more weakly-coordinating anions by performing the protonation of **3-1** using HBF_4 or HB(Ar^F)$_4$ [Ar^F = 3,5-(CF_3)$_2$-Ph]. Perhaps dissolution of these salts in DCM would then allow for the observation of diamagnetic **3-3** structure in solution.

In comparing the Ni SNS coordination chemistry with that of other first row metals, reaction of Fe(OTf)$_2$ with 2 equiv of the $(SNS)^-$ anion affords a similar trinuclear dication in which two diamagnetic, pseudo-octahedral Fe(κ^3-SNS)$_2$ metalloligands bind to a central tetrahedral Fe^{2+} via thiolate bridges.[10] All attempts to isolate the iron bis(thiolate) complex (*cf.* by reaction of Fe[N($SiMe_3$)$_2$]$_2$ with two equivalents of the MPB proligand) afforded instead the Fe(N_2S_3) complex via imine C-C bond coupling as shown in Scheme 3.1.[11] The lone exception is the carbonyl complex, Fe(κ^3-SNS^{Me})(κ^2-SNS^{Me})CO, formed reversibly by carbonylation of Fe(N_2S_3). With Co, reaction of MPB or the $(SNS)^-$ anion with a number of Co(I) or Co(II) salts and neutral precursors all afford the $[Co(S_2N_2)]^-$ anion.[12] In more recent unpublished work, Baker group

researchers have shown that reaction of $CuCl_2$ with the $(SNS)^-$ anion also involves metal reduction, affording monovalent, thiolate-bridged tetramer, $[Cu(\mu\text{-}SNS^{Me})]_4$. Only zinc affords a stable bis(thiolate) complex, $Zn(\kappa^2\text{-}SNS^{Me})_2$, with the expected distorted tetrahedral structure. Several of these complexes have been shown to be effective bifunctional catalysts for hydroboration of carbonyl compounds such as aldehydes, ketones and amides. Although we showed that dication **3-3** catalyzes the hydroboration of pyridine, sluggish activity, poor selectivity and no discernible ligand effects caused us to discontinue this study. For future studies, bifunctional (de)hydrogenation catalysis should be pursued with our nickel complexes to identify a system that takes advantage of the basic thiolate ligand and hemilabile thioether.

In **Chapter 4** an electrochemical study of **3-1** revealed quantitative isomerization of the Ni bis(thiolate) anion to $[Ni(S_2N_2)]^-$ (**3-2**)$^-$. This is an important observation as thermal conversion of **3-1 (**and its $Ni(SN)_2$ analogs) to **3-2** (and the corresponding $Ni(S_2N_2)$ complexes) proceeds in moderate yield at best (max. 56%). In contrast, chemical reduction of **3-1** using cobaltocene followed by oxidation using ferrocenium tetrafluoroborate afforded **3-2** in 85% yield. The electronic structure of d^8 **3-1** is consistent with an open-shell singlet with the two ligand-based electrons paired (i.e. one α and one β). This is in contrast to 'isoelectronic' d^8 $[Co(S_2N_2)]^-$, which is an $S = 1$ open-shell triplet (i.e. both ligand electrons α).[13] Note, however, that the degree of electron-sharing between the ligand and metal d orbitals is so extensive in these complexes that the concept of oxidation state becomes blurred and thus less useful. Presumably the difference between Ni and Co electronic structure arises from the energy difference between the metal and ligand orbitals. Moreover, the two characteristic short C=C bonds (1.36 Å) in the mercapto-anilide portion of the $(S_2N_2)^{2-}$ ligand in **3-2** and (**3-2**)$^-$ are absent in $[Co(S_2N_2)]^-$ which shows nearly equivalent C-C bonds of ca. 1.40 Å. Our understanding of this class of complexes would likely benefit from a high-level *ab initio* molecular orbital calculation of the four redox states of the S_2N_2 ligand shown in Scheme 4.2.

Spectroelectrochemical experiments demonstrated three stable redox states for **3-2** and DFT studies suggest predominantly metal-based reductions from Ni(II) to paramagnetic Ni(I) to diamagnetic Ni(0). Nonetheless, an inspection of the frontier orbitals for both **3-2** and radical anion (**3-2**)$^-$ shows the intimate participation of the redox-active S_2N_2 ligand (**Figure 6.1**). This was also confirmed by the TD-DFT studies which demonstrated that the most intense electronic

transition in the visible region has mixed metal/ligand character. (Scheme 4.11). In a preliminary reactivity study, we performed the CV experiment of **3-2** in the presence of weak acid phenol

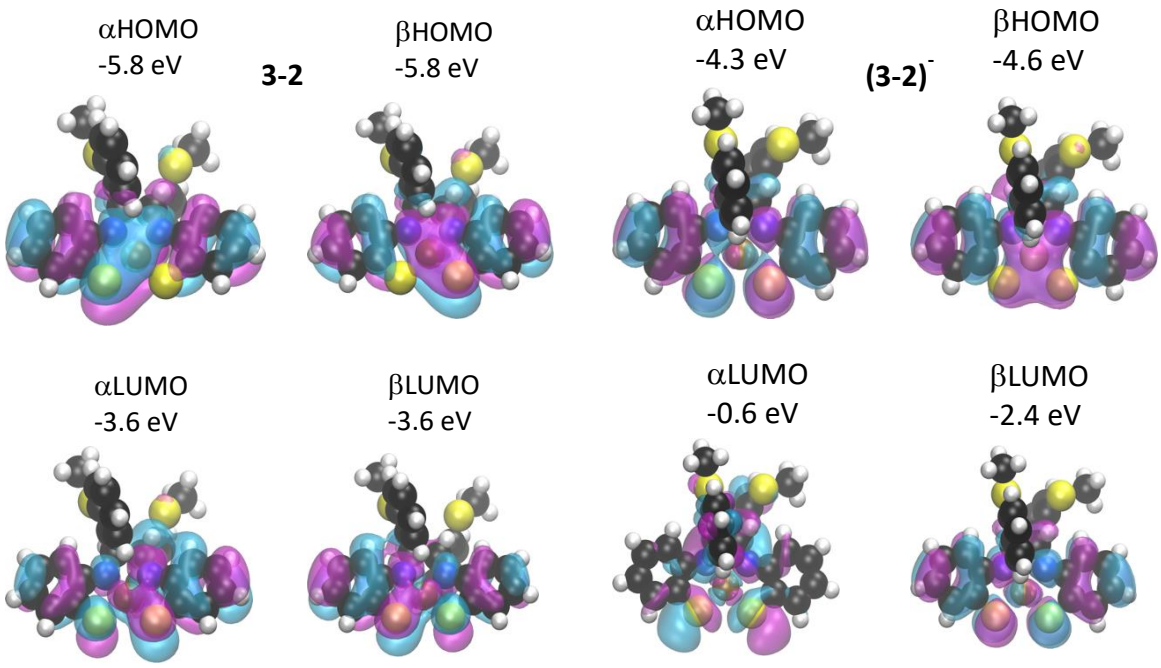

Figure 6.1 DFT frontier orbitals for **3-2** and $(\mathbf{3\text{-}2})^-$.

to assess its ability to generate H_2 by electrocatalysis. Although no reaction was observed with $(\mathbf{3\text{-}2})^-$, the dianion $(\mathbf{3\text{-}2})^{2-}$ clearly reacted with phenol but no catalytic wave was observed and the reaction was shown to be reversible upon reoxidation. Further studies should investigate stronger acids with weakly coordinating anions such as lutidinium-BF_4 or *p*-toluenesulfonic acid (cf. Castillo's study using a thiolate-bridged $[Ni(SNS)]_2$ catalyst in which SNS is an amino dithiolate ligand).[14] Performing the CV experiment with **3-2** under a CO_2 atmosphere again showed no reaction with $(\mathbf{3\text{-}2})^-$ but the second reduction occurred at an increased voltage and was only quasireversible. This promising observation should be followed up in the presence of a weak acid to see if **3-2** shows promising selectivity for CO_2 reduction products. This is an increasingly well studied target as heterogeneous catalysts such as fluorine-modified solid copper have been recently shown to give high yields of C_2 products ethylene and ethanol.[15]

In a second attempt to distinguish the reactivity of the three redox states of $[Ni(S_2N_2)]$ (**3-2**) we turned to strong electron-acceptor fluoroalkenes (FAs) in **Chapter 5**. In this case, dianion $(\mathbf{3\text{-}2})^{2-}$ proved to be too reactive, generating complex reaction mixtures with all FAs tried except

for $CH_2=CF_2$ and $CH_2=CH(CF_3)$ with which no reaction was observed. In contrast, radical anion (**3-2**)$^-$ underwent reasonably selective transformations with TFE, CTFE, PMVE and HFP although the latter required high dilution. Based on previous work by the Beletskaya group in Russia,[16] we propose that all reactions proceed by initial electron transfer from (**3-2**)$^-$ to the FA, followed by either fluoride elimination to give the neutral Ni alkenyl product or hydrogen atom abstraction from solvent which yields anionic fluoroalkyl complexes. The observed F elimination/H abstraction ratio depended on the FA but further quantitative experiments will be required to eliminate possible solvent and concentration effects.

References

(1) Gartia, Y.; Biswas, A.; Stadler, M.; Nasini, U. B.; Ghosh, A. Cross-coupling Reactions of Multiple C-Cl Bonds of Polychlorinated Solvents with Grignard Reagent using a Pincer Nickel Complex. *J. Mol. Catal. A* **2012**, *363–364*, 322–327.

(2) Gartia, Y.; Ramidi, P.; Jones, D. E.; Pulla, S.; Ghosh, A. Nickel Complex-catalyzed Efficient Activation of sp^3 and sp^2 C–H Bonds for Alkylation and Arylation of Oxygen-containing Heterocyclic Molecules. *Catal. Lett.* 2**014**, *144* (3), 507–515.

(3) Barham, J. P.; Coulthard, G.; Emery, K. J.; Doni, E.; Cumine, F.; Nocera, G.; John, M. P.; Berlouis, L. E. A.; McGuire, T.; Tuttle, T. Murphy, J. A. KOtBu: A Privileged Reagent for Electron Transfer Reactions? *J. Am. Chem. Soc.* **2016**, *138* (23),7402–7410.

(4) Zheng, B.; Tang, F.; Luo, J.; Schultz, J. W.; Rath, N. P.; Mirica, L. M. Organometallic nickel(III) Complexes Relevant to Cross-coupling and Carbon–heteroatom Bond Formation Reactions. *J. Am. Chem. Soc.* **2014**, *136* (17), 6499–6504.

(5) Lavoie, C.M.; MacQueen, P. M.; Rotta-Loria, N. L.; Sawatzky, R. S.; Borzenko, A.; Chisholm, A. J.; Hargreaves, B. K. V. McDonald, R. Ferguson, M. J.; Stradiotto, M. Challenging Nickel-catalysed Amine Arylations Enabled by Tailored Ancillary Ligand Design. *Nat. Commun.* **2016,** *7*, 11073.

(6) Tassone, J. P.; England, E. V.; MacQueen, P. M.; Ferguson, M. J.; Stradiotto, M. PhPAd-Dal-Phos: Ligand-enabled, Nickel-catalyzed Cross-coupling of (Hetero)aryl Electrophiles with Bulky Primary Alkylamines. *Angew. Chem. Int. Ed.* **2019**, *58* (8), 2485–2489.

(7) Yang, K.; Qiu, Y.; Li, Z.; Wang, Z.; Jiang, S. Ligands for Copper-catalyzed C−N Bond-forming Reactions with 1 mol% CuBr as Catalyst. *J. Org. Chem.* **2011,** *76* (9), 3151–3159.

(8) Ramnial, T.; Taylor, S. A.; Bender, M. L.; Gorodetsky, B.; Lee, P. T. K.; Dickie, D. A.; McCollum, B. M.; Pye, C. C.; Walsby, C. J.; Clyburne, J. A. C. Carbon-Centered Strong Bases in Phosphonium Ionic Liquids. *J. Org. Chem.* **2008**, *73* (3), 801-812.

(9) Nami, F.; Gast, P.; Groenen, E. J. J. Rapid Freeze-quench EPR Spectroscopy: Improved Collection of Frozen Particles. *Appl. Magn. Reson.* **2016**, *47*, 643-653.

(10) Das, U. K.; Daifuku, S. L.; Gorelsky, S. I.; Korobkov, I.; Neidig, M. L.; LeRoy J. L.; Murugesu, M.; Baker, R. T. Mononuclear, Dinuclear and Trinuclear Iron Complexes Featuring a new Monoanionic SNS Thiolate Ligand. *Inorg. Chem.* **2016**, *55*, 987-997.

(11) Das, U. K.; Higman, C. S.; Korobkov, I.; Gabidullin, B. M.; Hein, J. E.; Baker, R. T. Efficient and Selective Iron Complex-Catalyzed Hydroboration of Aldehydes *ACS Catal.* **2018**, *8*, 1076-1081

(12) Fitchett, B. Oxidation State Roulette: Synthesis and Reactivity of Cobalt Complexes Containing SNS ligands. uOttawa MSc thesis, 2018.

(13) Sproules, S.; Kapre, R. R.; Roy, N.; Weyhermüller, T.; Wieghardt, K. The Molecular and Electronic Structures of Monomeric Cobalt Complexes Containing Redox Non-innocent *o*-Aminobenzenethiolate Ligands. *Inorg. Chim. Acta* **2010**, *363*, 2702-2714.

(14) Mondragón, A.; Flores-Alamo, M.; Martínez-Alanis, P. R.; Aullón, G.; Ugalde-Saldívar, V. M.; Castillo, I. Electrocatalytic Proton Reduction by Dimeric Nickel Complex of a Sterically Demanding Pincer-type NS_2 Aminobis(thiophenolate) Ligand. *Inorg. Chem.* **2015**, *54* (2), 619-627.

(15) Ma, W.; Xie, S.; Liu, T.; Fan, Q.; Ye, J.; Sun, F.; Jiang, Z.; Zhang, Q.; Cheng, J.; Wang, Y. Electrocatalytic Reduction of CO_2 to Ethylene and Ethanol Through Hydrogen-assisted C-C Coupling over Fluorine-modified Copper. *Nature Catal.* **2020**, *3*, 478-487.

(16) Sazonov, P. K.; Oprunenko, Y. F.; Beletskaya, I. P. Predicting the Direction of Nucleophilic Attack in Vinyl Halides: Halogenophilic versus Carbophilic Reactivity of Metal Carbonyl Anions. *J. Phys. Org. Chem.* **2013**, *26* (2), 151–161.

Appendices

Chapter 2

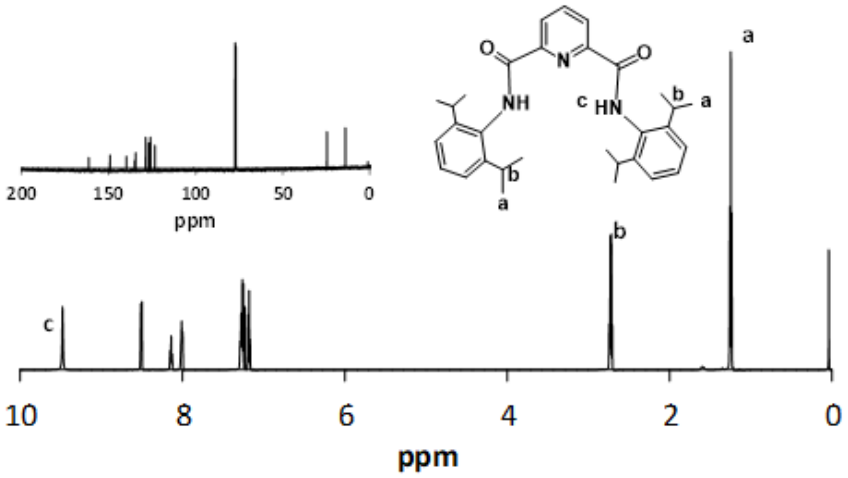

Figure A2.1 ^{1}H NMR spectrum (300 MHz, $CDCl_3$) of ligand **(1)**.[203]

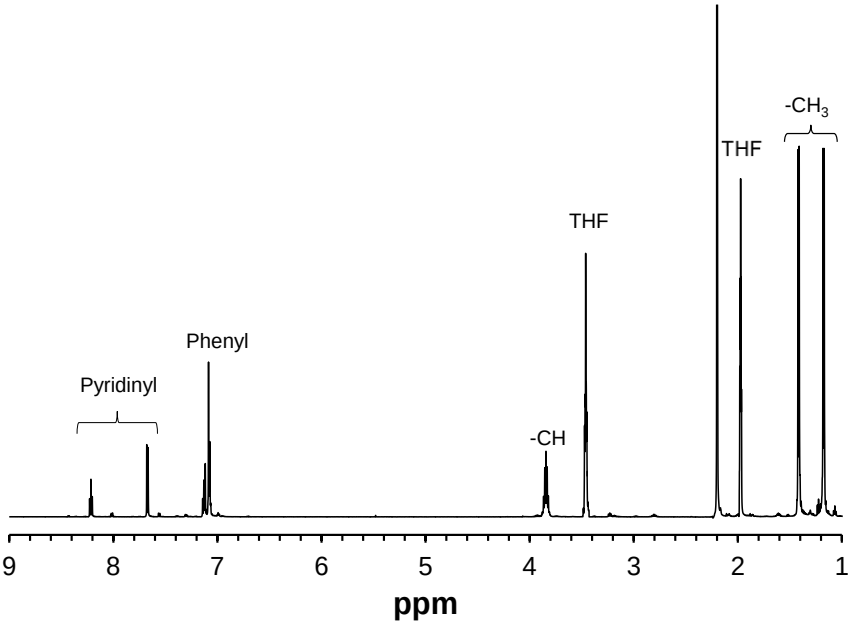

Figure A2.2 ^{1}H NMR spectrum (300 MHz, $CDCl_3$) of nickel complex **(2)**[203]

Ref 203: Gartia, Y.; Biswas, A.; Stadler, M.; Nasini, U. B.; Ghosh, A. Cross-coupling Reactions of Multiple C-Cl Bonds of Polychlorinated Solvents with Grignard Reagent using a Pincer Nickel Complex. *J. Mol. Catal. A Chem.* **2012,** *363–364*, 322–327.

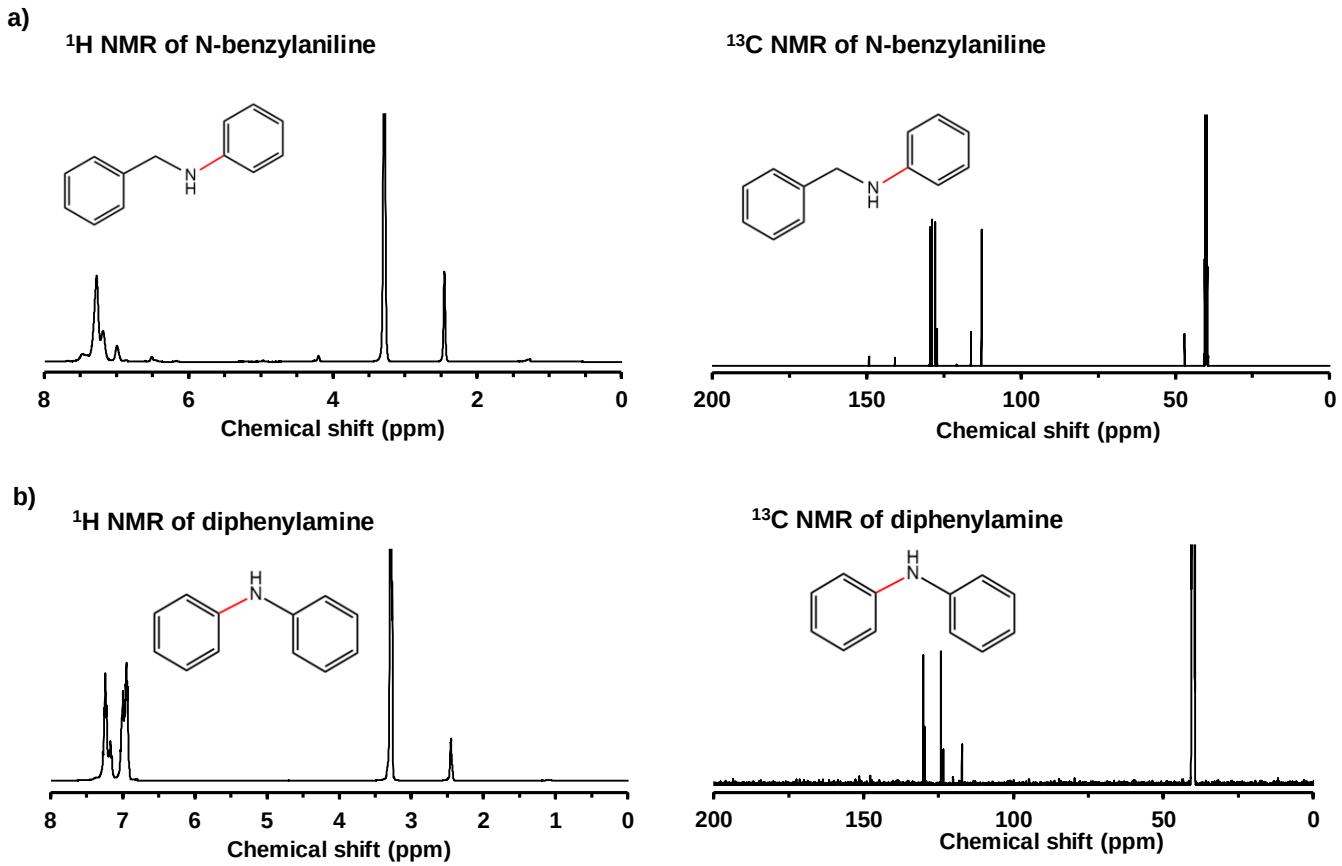

Figure A2.3 ^{1}H and $^{13}C\{^{1}H\}$ NMR spectra (300 MHz, $CDCl_3$) of two isolated products a) *N*-benzylaniline and b) diphenylamine.

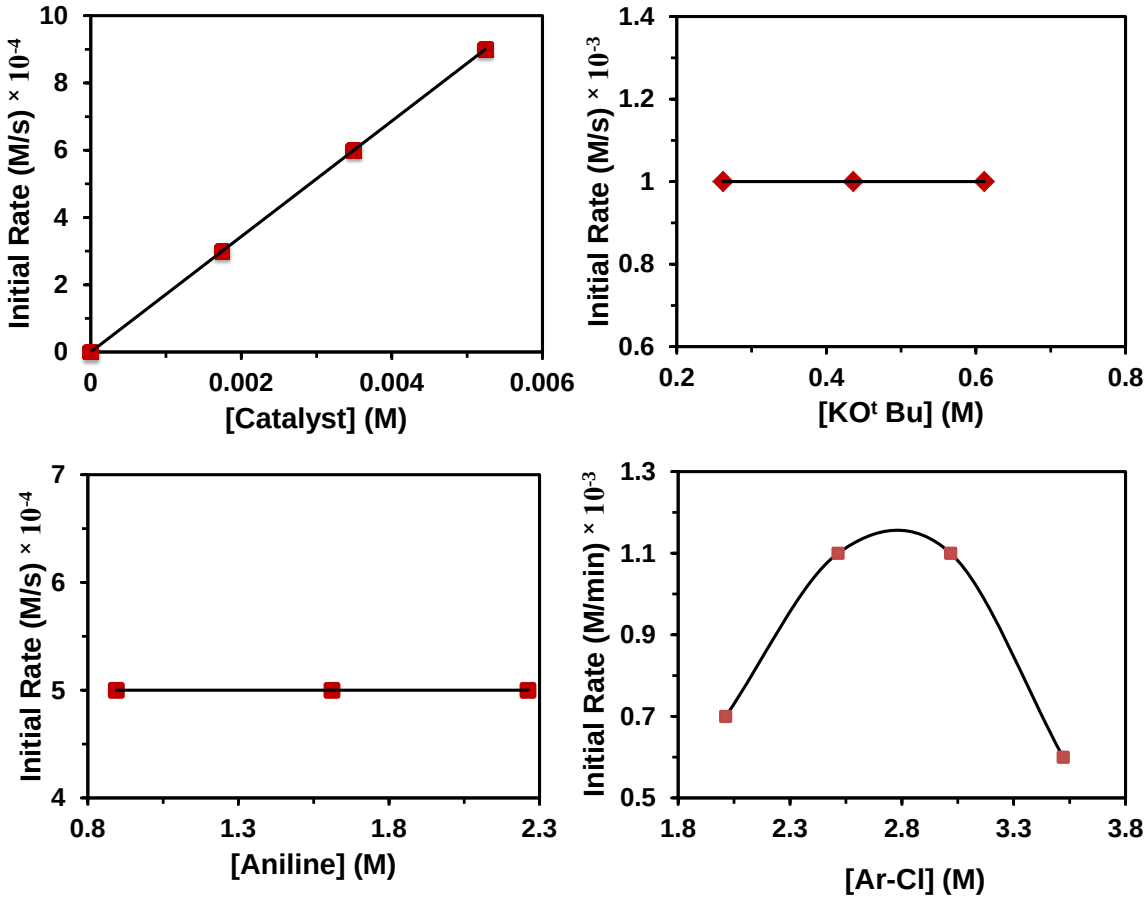

Figure A2.4 Plots of initial rates vs concentration of catalyst, base, aniline, and chlorobenzene for the amination of chlorobenzene with aniline catalyzed by **2** (0.2 mol %) in the presence of KO^{t}Bu at 110 ^{o}C

Remaining data for chapter 2 of this thesis can be found in the supporting information of the following published article:
Y. M. Albkuri, A. B. RanguMagar, A. Brandt, H. A. Wayland, B. P. Chhetri, C. M. Parnell, P. Szwedo, A. Parameswaran-Thankam, A. Ghosh, *Catal. Lett.* **2020,** *150*, 1669–1678.

Appendices
Chapter 3:

	3-1	**3-2**	**3-3**	**3-4**
empirical formula	$C_{28}H_{24}N_2NiS_4$	$C_{28}H_{24}N_2NiS_4$	$C_{32}H_{24}F_{12}N_4Ni_2O_8S_8$	$C_{60}H_{48}F_{12}N_6Ni_3O_8S_{12}$
formula weight ($g \cdot mol^{-1}$)	575.44	575.42	1194.45	1769.89
crystal system	Monoclinic	Monoclinic	Triclinic	Monoclinic
space group	$P\ 2_1/c$	$P\ 2_1/c$	$P\ \bar{1}$	$C\ 2/c$
a (A)	12.2589(7)	13.3113(17)	14.4433(12)	34.3326(17)
b (A)	15.9225(9)	7.7206(9)	16.7533(15)	16.8791(9)
c (A)	14.3728(8)	24.852(3)	19.6255(18)	14.7378(8)
α (deg)	90	90	75.575(2)	90
β (deg)	113.110(1)	100.313(5)	85.075(2)	110.813(2)
γ (deg)	90	90	70.780(2)	90
V (A^3)	2580.3(3)	2512.8(5)	4342.7(7)	7983.3(7)
Z	4	4	4	4
T (K)	200(2)	203(2)	201(2)	200(2)
ρ_{calcd} ($g \cdot cm^{-3}$)	1.481	1.521	1.827	1.473
μ (mm^{-1})	1.097	1.126	1.357	1.093
$2\theta_{max}$ (deg)	55.044	50.052	46.514	52.938
total/unique reflections	35483/5923	23401/4436	11816/11816	45314/8209
Reflections [$I_o \geq 2\sigma(I_o)$]	4283	2761	5393	4833
R_1, wR_2 [$I_o \geq 2\sigma(I_o)$]	0.0379, 0.0847	0.0480, 0.0885	0.1135, 0.2385	0.0451, 0.1042
goodness of fit	1.013	0.995	1.014	1.087
CCDC number	2038642	2038648	2038650	2038645

Table A3.1 X-ray diffraction data collection and structure refinement details for complexes **3-1** through **3-4**

	3-5	**3-6a**	**3-6b**	**3-7a**	**3-8**
empirical formula	$C_{88}H_{79}Cl_3F_9N_{7.5}Na_{0.5}Ni_4O_6S_{15}$	$C_{50}H_{42}F_{12}N_6Ni_2O_8S_8$	$C_{39}H_{40}Cl_6F_{12}N_4O_8P_2S_8$	$C_{19}H_{21}F_6N_2NiO_4PS_4$	$C_{40}H_{45}N_3NiS_2$
formula weight ($g \cdot mol^{-1}$)	2342.17	1456.79	1569.29	673.30	690.62
crystal system	Hexagonal	Triclinic	Monoclinic	Triclinic	Orthorhombic
space group	$P\,6_3\,2\,2$	$P\,\bar{1}$	$P\,2_1/n$	$P\,\bar{1}$	$F\,d\,d\,d$
a (A)	17.9139(6)	10.0747(7)	18.013(3)	10.0605(6)	16.7276(14)
b (A)	17.9139(6)	11.9675(8)	14.766(2)	11.0281(7)	20.602(2)
c (A)	41.2248(15)	12.8285(8)	22.977(4)	13.0236(8)	41.462(4)
α (deg)	90	99.035(1)	90	74.331(2)	90
β (deg)	90	91.730(1)	90.366	75.761(2)	90
γ (deg)	120	108.050(1)	90	76.441(2)	90
V (A^3)	11457.0(9)	1447.22(17)	6111.3(17)	1326.47(14)	14289(2)
Z	4	1	4	2	16
T (K)	213(2)	200(2)	200(2)	296(2)	203(2)
ρ_{calcd} ($g \cdot cm^{-3}$)	1.358	1.672	1.706	1.686	1.284
μ (mm^{-1})	1.055	1.036	1.290	1.179	0.692
$2\theta_{max}$ (deg)	52.962	55.064	46.708	56.694	50.146
total/unique reflections	33015/7930	30449/6655	46759/8869	22462/6626	20753/3174
Reflections [$I_o \geq 2\sigma(I_o)$]	4186	5361	5204	3475	2251
R_1, wR_2 [$I_o \geq 2\sigma(I_o)$]	0.0632, 0.1391	0.0387, 0.0929	0.0795, 0.2192	0.0501, 0.1080	0.0613, 0.1266
goodness of fit	0.963	1.037	1.030	1.052	1.161
CCDC number	2038644	2038649	2038643	2038647	2038646

Table A3.2 X-ray diffraction data collection and structure refinement details for complexes **3-5, 3-6a,b, 7a and 8**

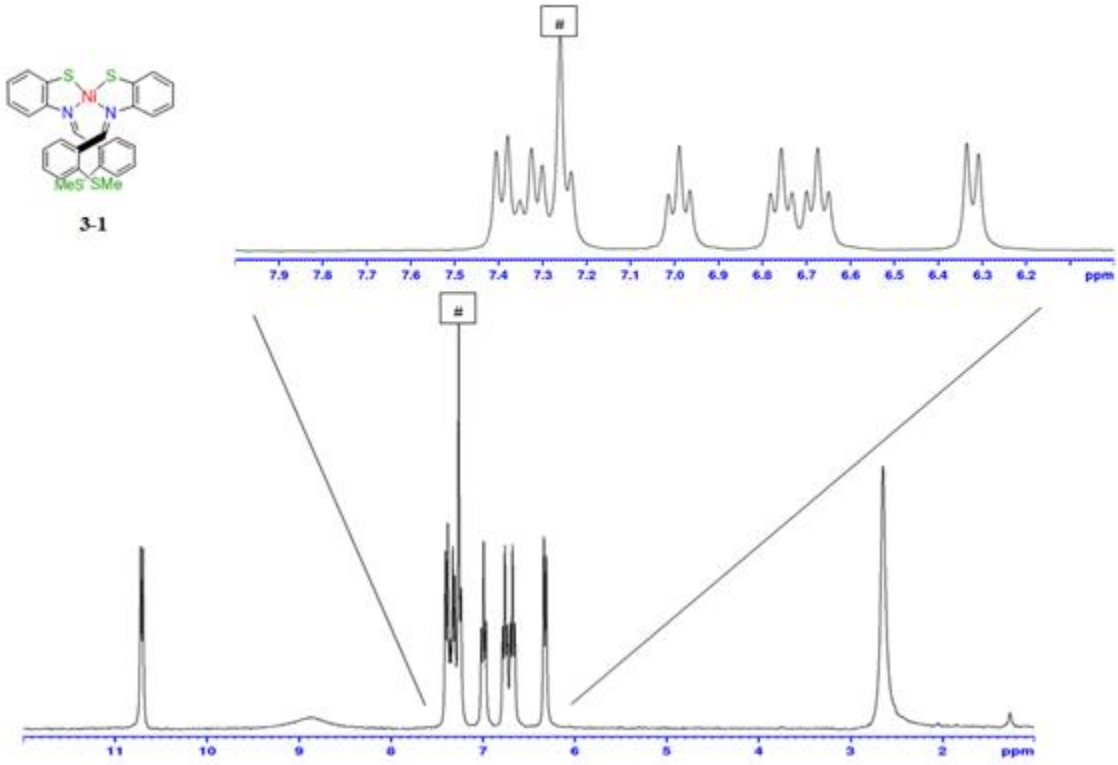

Figure A3.1 ^{1}H NMR spectrum (300 MHz, C_6D_6) of **3-1**.

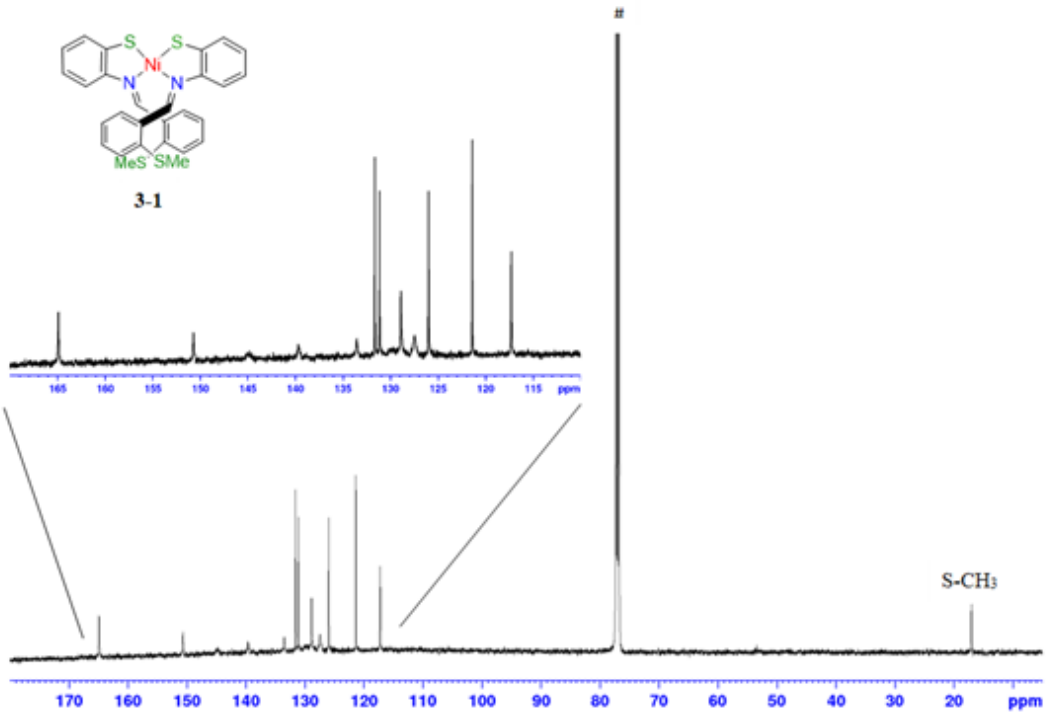

Figure A3.2 $^{13}C\{^{1}H\}$ NMR spectrum (75.5 MHz, C_6D_6) of **3-1**.

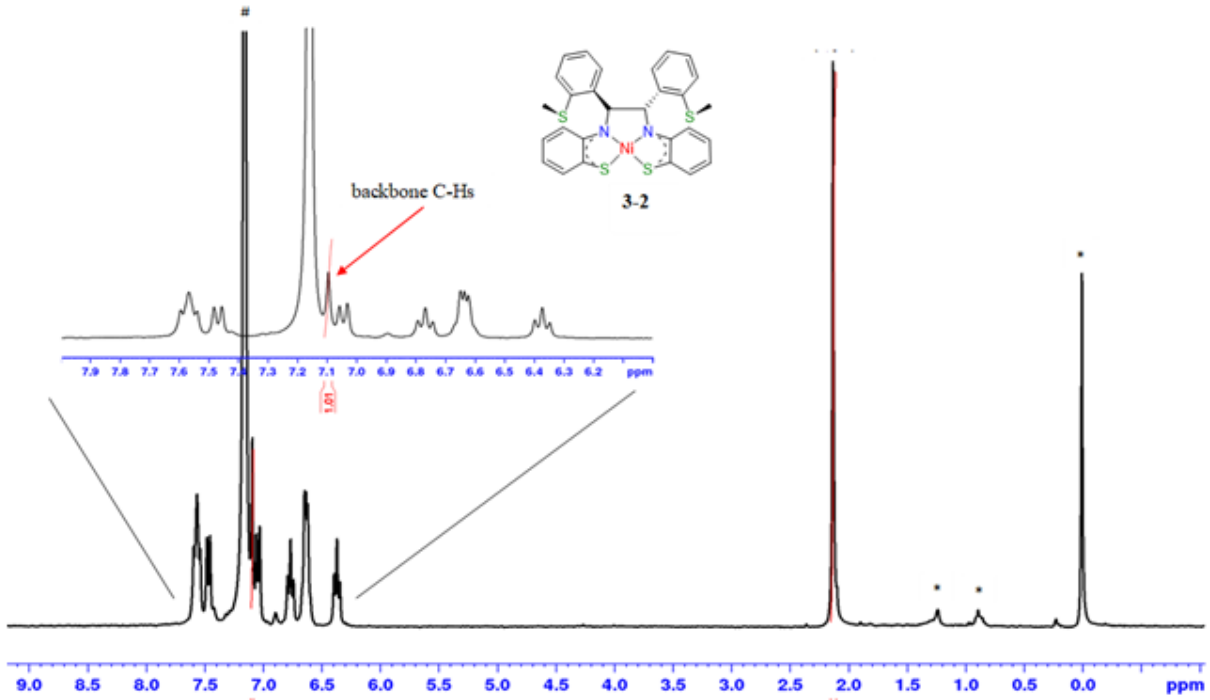

Figure A3.3 ^{1}H NMR spectrum (300 MHz, C_6D_6) of **3-2**.

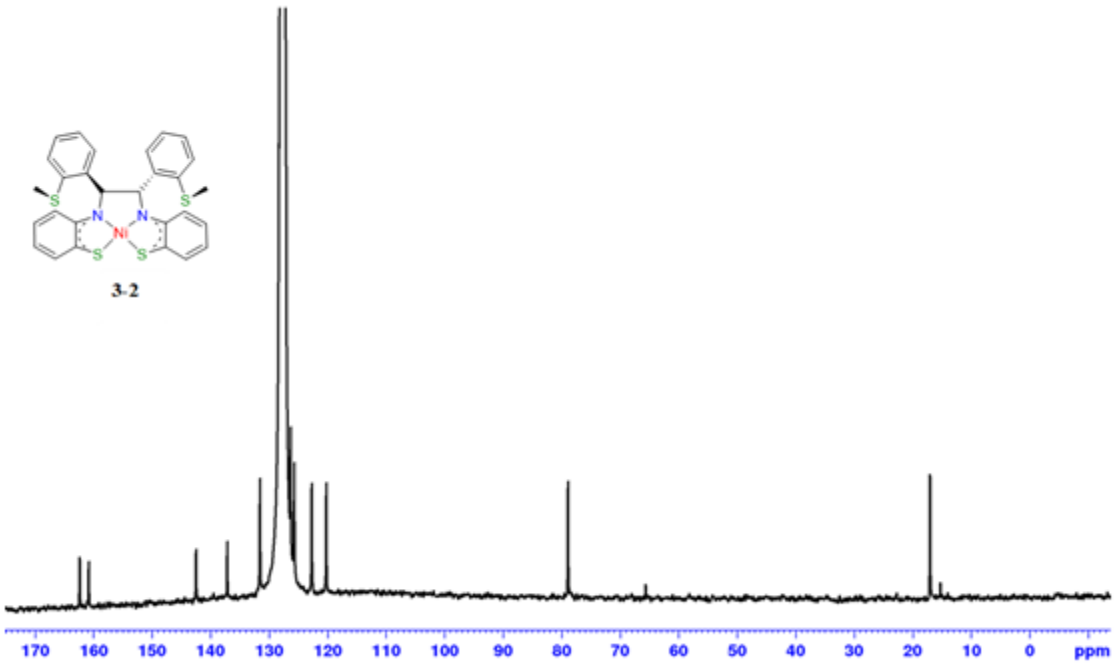

Figure A3.4 $^{13}C\{^{1}H\}$ NMR spectrum (75.5 MHz, C_6D_6) of **3-2**.

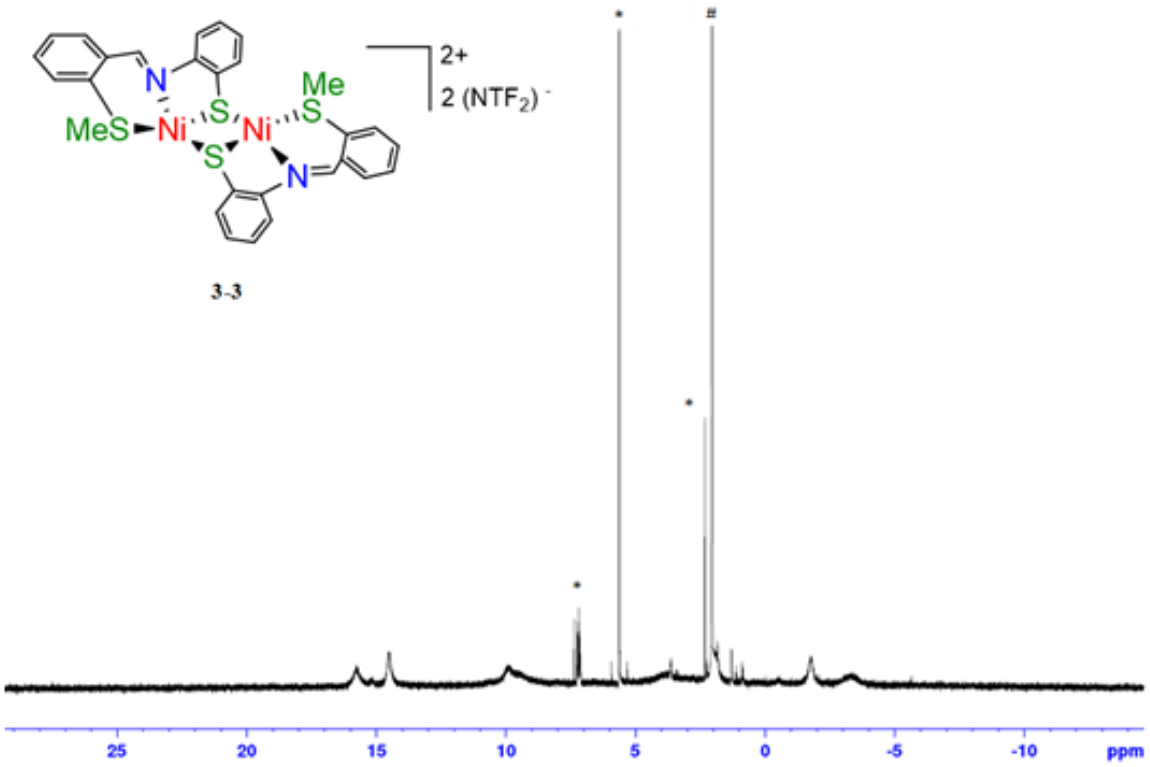

Figure A3.5 ^{1}H NMR spectrum (300 MHz) obtained by dissolution of **3-3** in acetone-d_6.

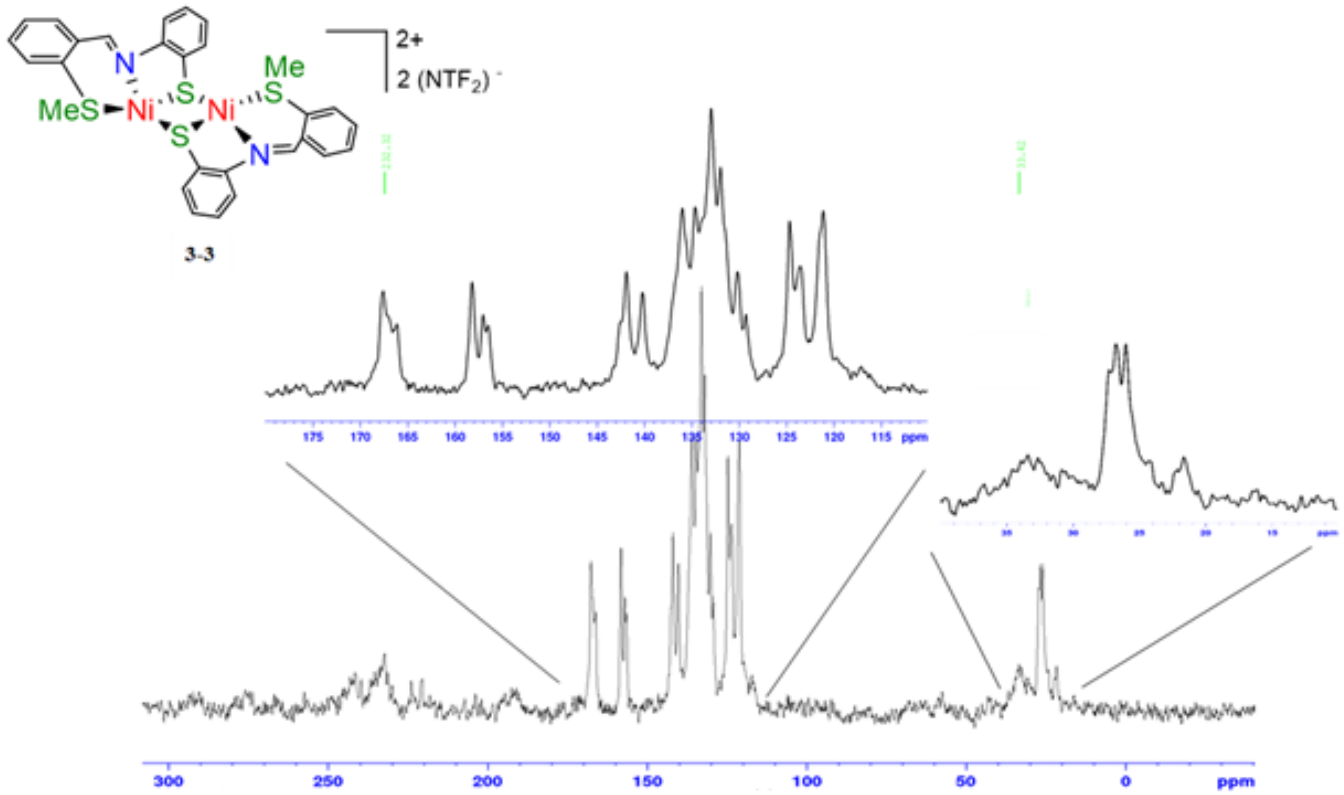

Figure A3.6 ^{13}C{^{1}H} MAS NMR spectrum (50 MHz, solid) of **3-3**.

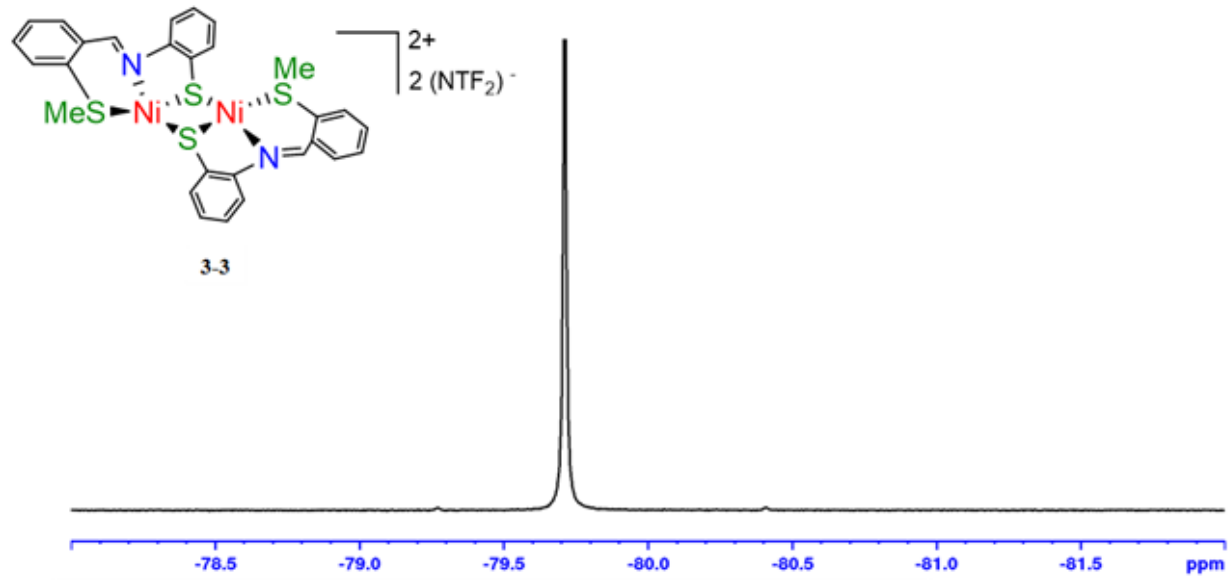

Figure A3.7 ^{19}F NMR spectrum (282 MHz) obtained by dissolution of **3-3** in acetone-d_6.

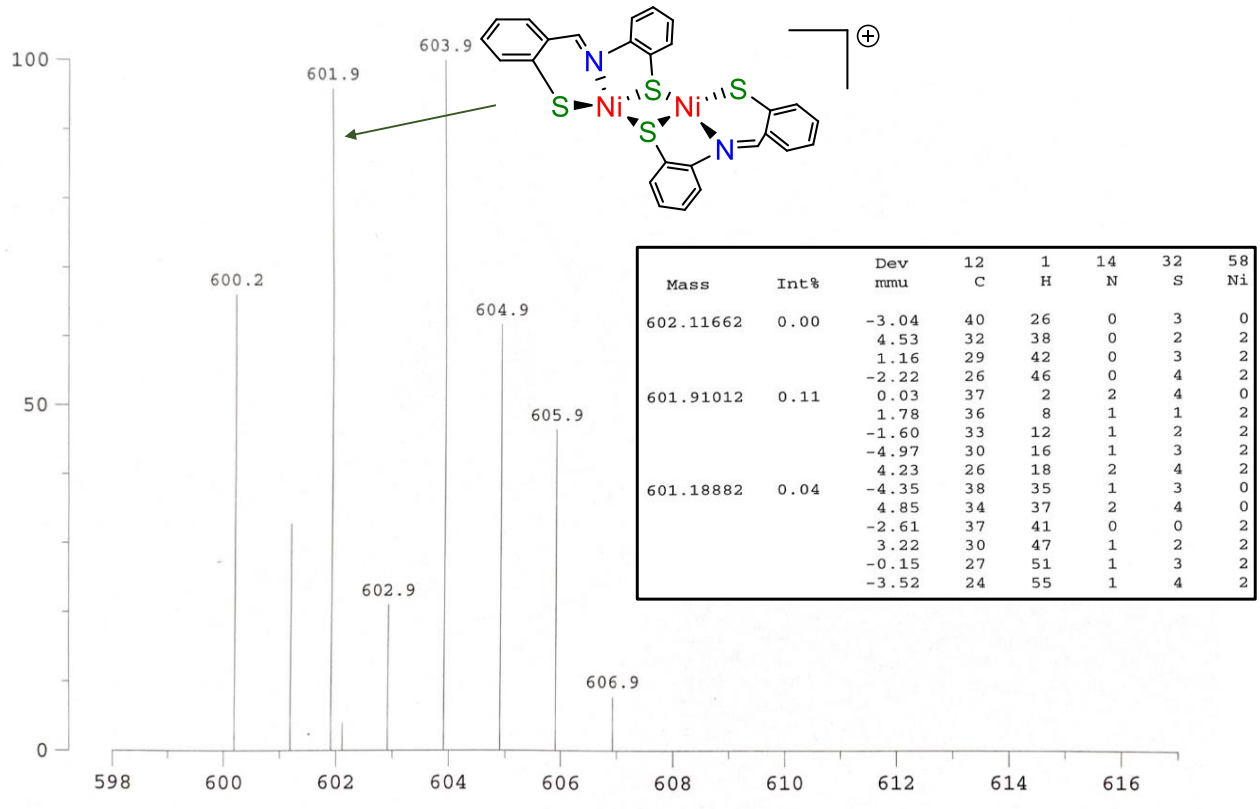

Mass	Int%	Dev mmu	12 C	1 H	14 N	32 S	58 Ni
602.11662	0.00	-3.04	40	26	0	3	0
		4.53	32	38	0	2	2
		1.16	29	42	0	3	2
		-2.22	26	46	0	4	2
601.91012	0.11	0.03	37	2	2	4	0
		1.78	36	8	1	1	2
		-1.60	33	12	1	2	2
		-4.97	30	16	1	3	2
		4.23	26	18	2	4	2
601.18882	0.04	-4.35	38	35	1	3	0
		4.85	34	37	2	4	0
		-2.61	37	41	0	0	2
		3.22	30	47	1	2	2
		-0.15	27	51	1	3	2
		-3.52	24	55	1	4	2

Figure A3.8 EI-MS [M^+-2Me] of **3-3**.

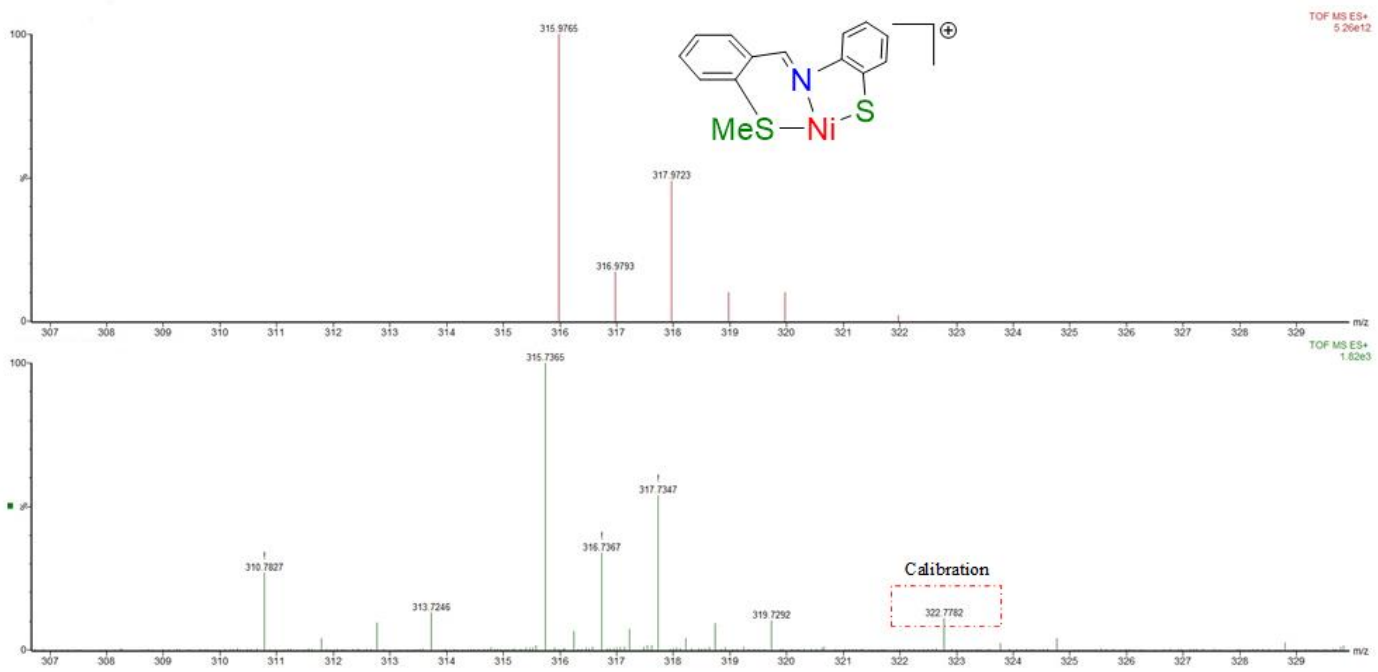

Figure A3.9 Positive-ion ESI-MS of **3-3** showing $[Ni(SNS)]^+$ fragment.

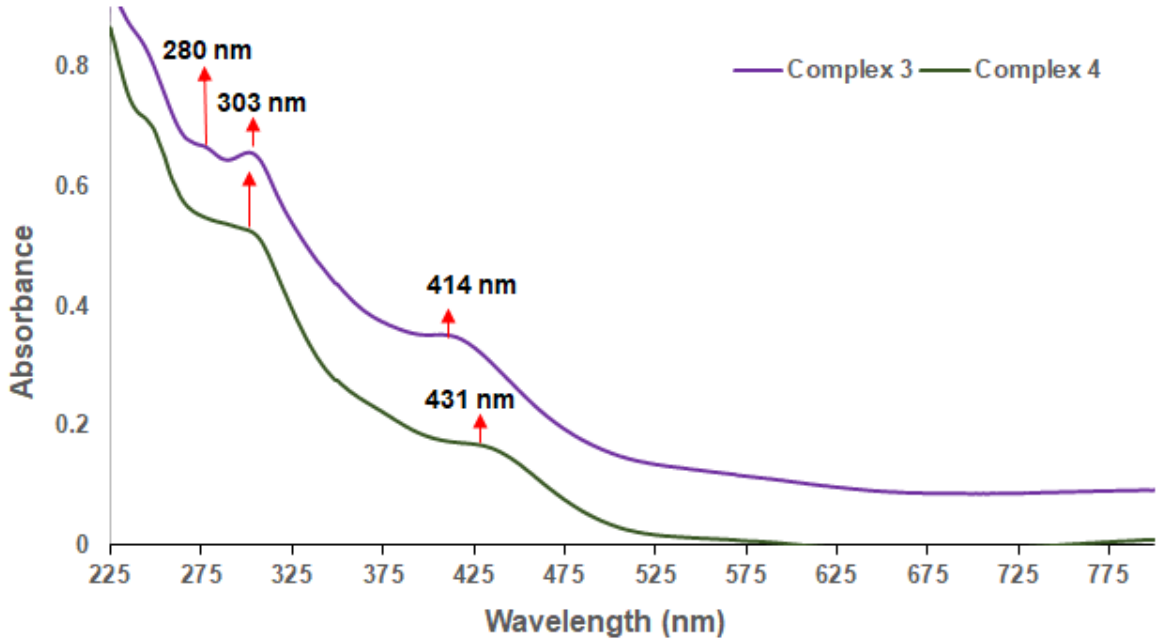

Figure A3.10 UV-vis spectra of **3-4'** and solution obtained by dissolution of **3-3** in DCM.

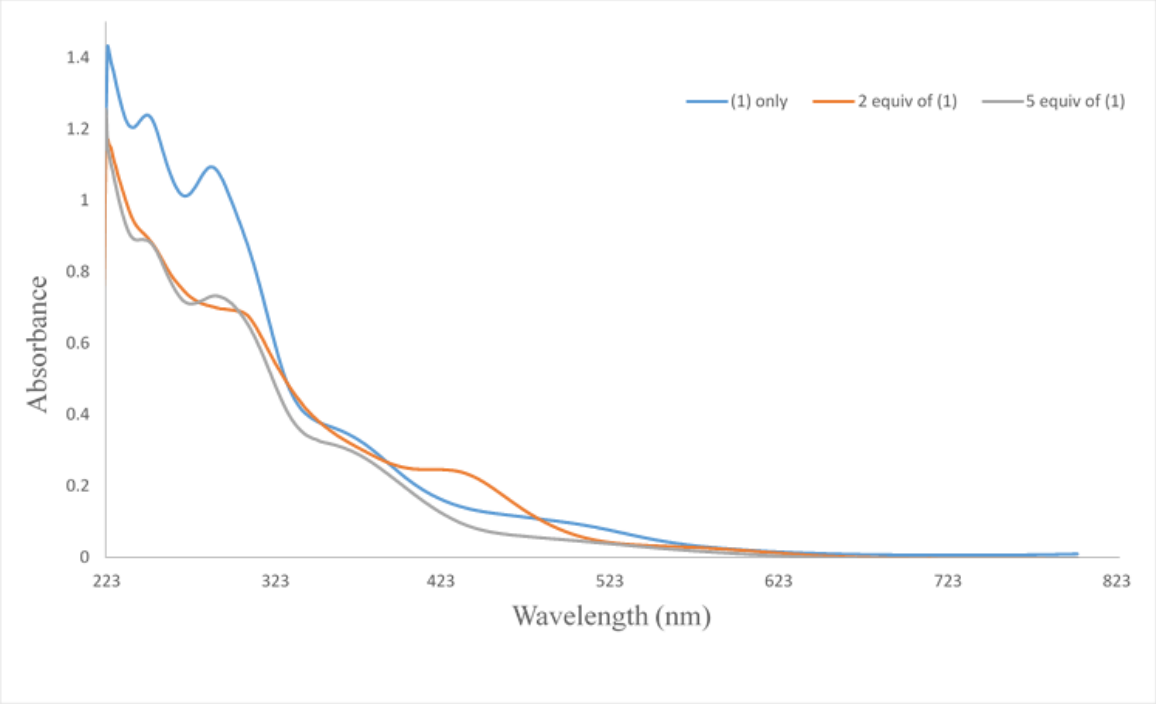

Figure A3.11 UV-vis spectra of complex **3-1** (blue), $Ni(OTf)_2$ + 2 equiv. of **3-1** (red) and $Ni(OTf)_2$ + 5 equiv. of **3-1** (gray).

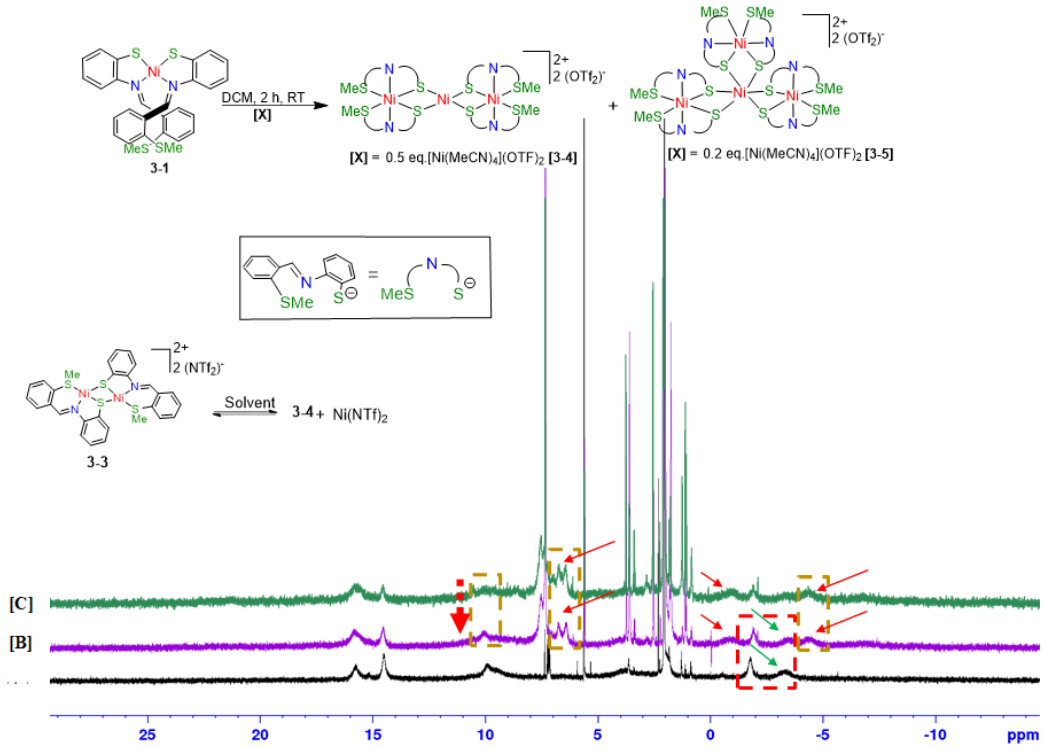

Figure A3.12 ^{1}H NMR spectra (300 MHz, acetone-d_6) of complex **3-3** dissolved in acetone-d_6 (A) and products derived from reactions of **3-1** with 0.5 equiv of Ni triflate (B) and with 0.2 equiv of Ni triflate (C).

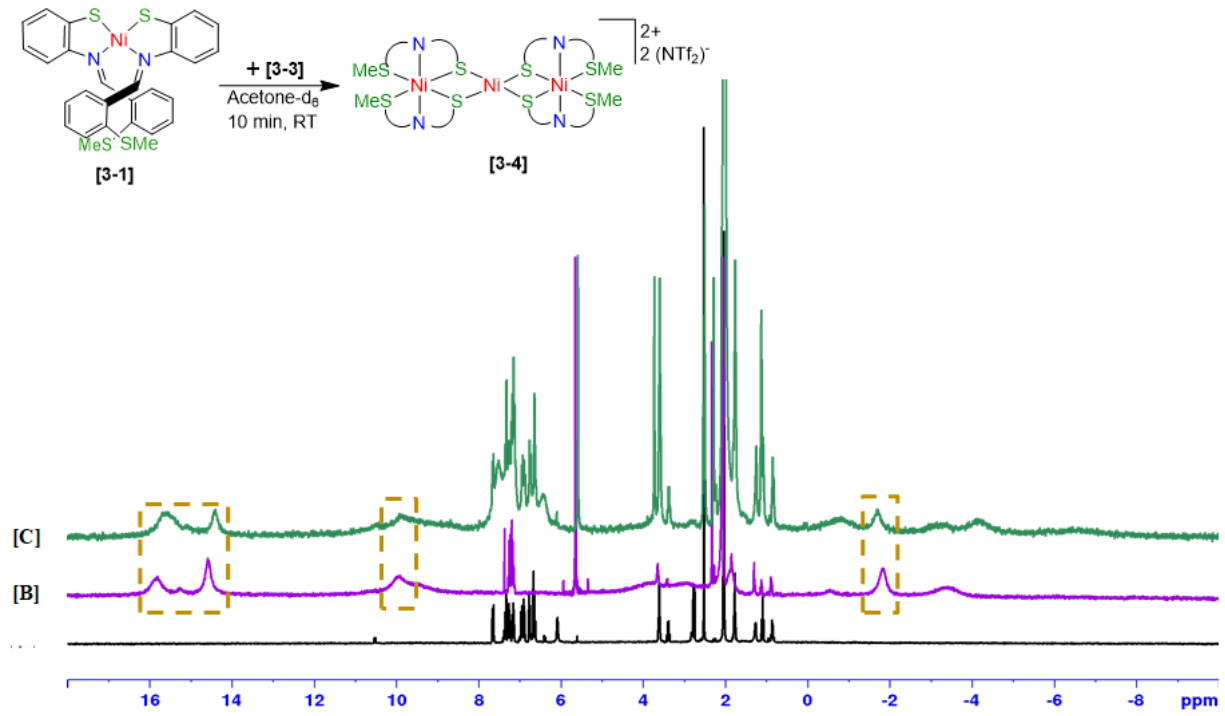

Figure A3.13 ^{1}H NMR spectra (300 MHz, acetone-d_6) comparison of **3-1** (A), **3-3** dissolved in acetone-d_6 (B) and reaction of **3-1** with **3-3** (C), showing formation of **3-4**.

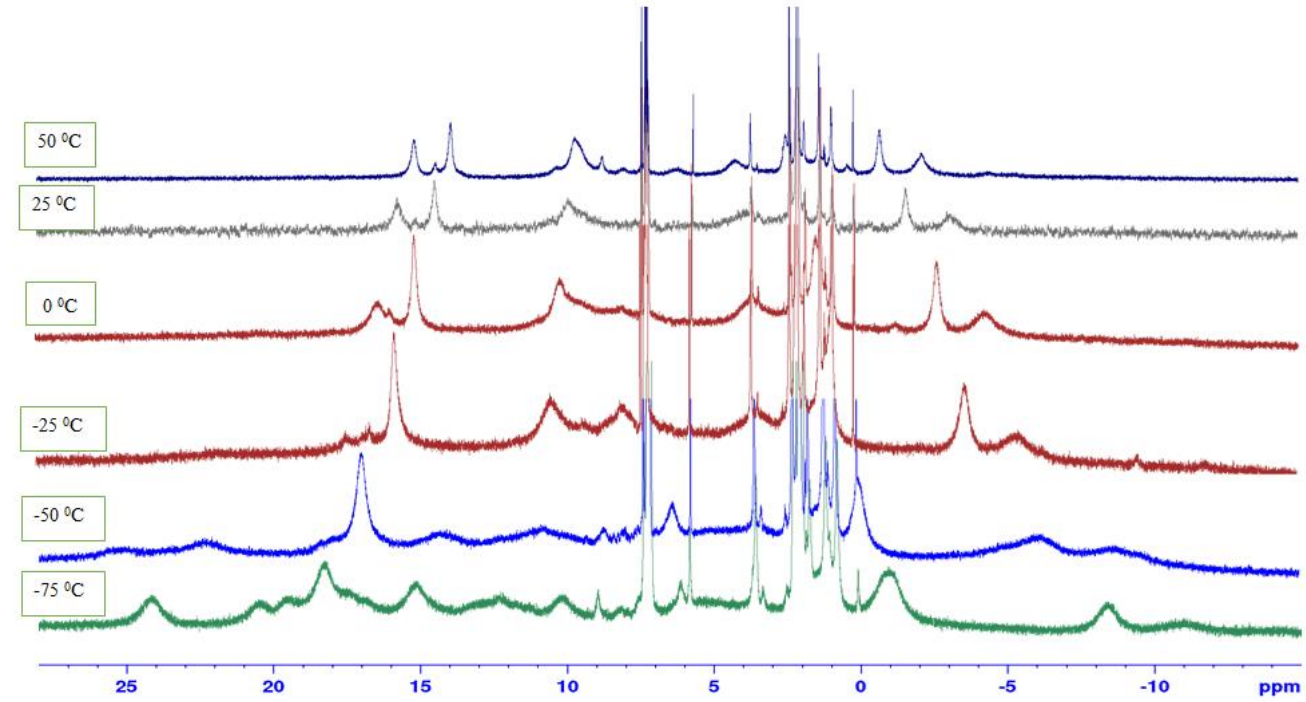

Figure A3.14 ^{1}H NMR spectra (300 MHz, acetone-d_6) derived from melting a heterogeneous mixture of solid **3-3** and frozen acetone-d_6 at -75°C in the NMR probe, followed by eventual warming to 50°C.

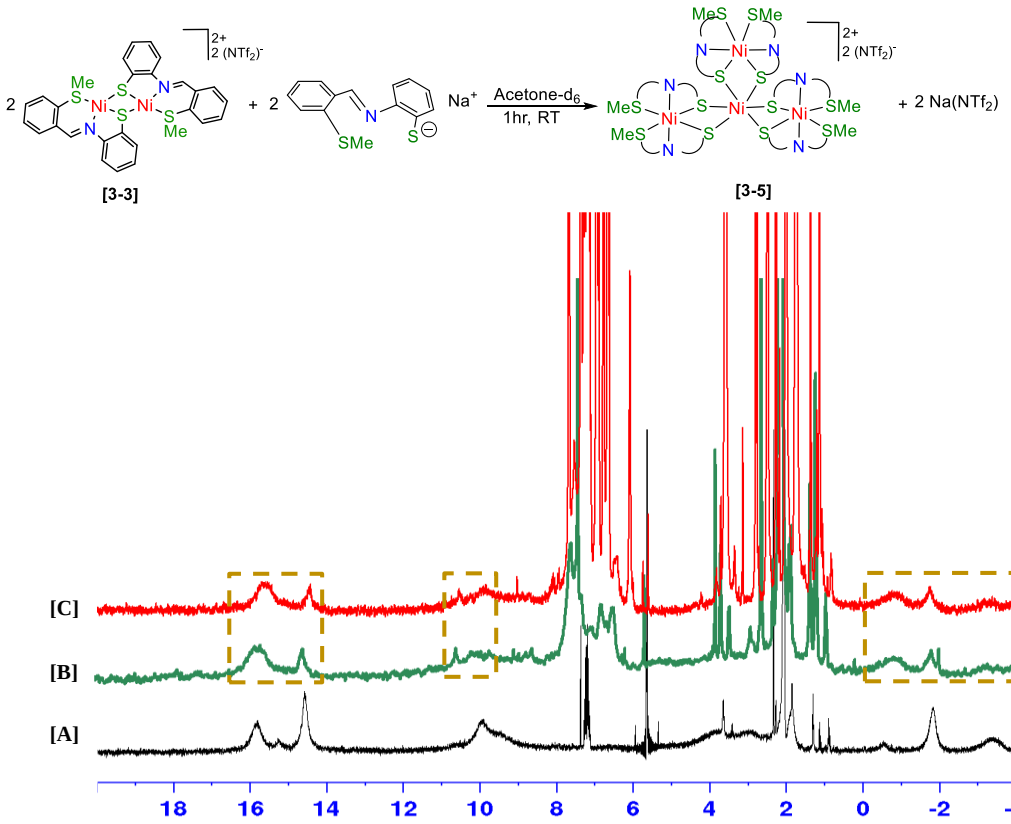

Figure A3.15 ^{1}H NMR spectra (300 MHz, acetone-d_6) comparing **3-3** dissolved in acetone-d_6 (A), reaction of **3-1** with 5 equiv of $Ni(OTf)_2$ to generate **3-5** (B) and reaction of **3-3** with deprotonated thiolate ligand to generate **3-5** (C).

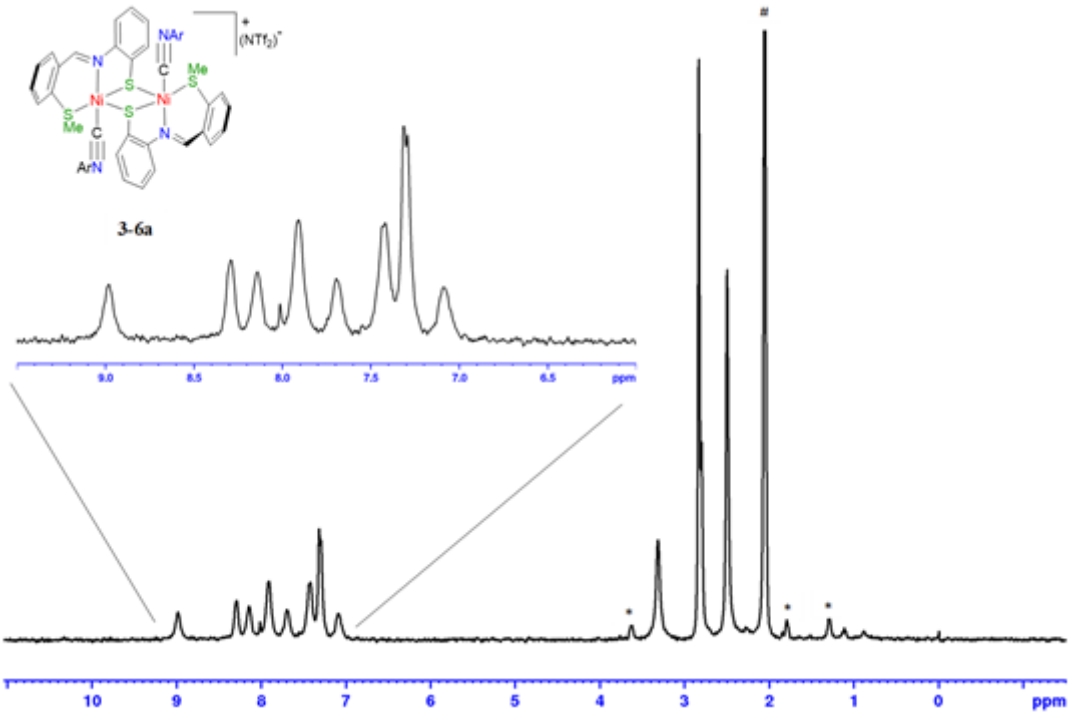

Figure A3.16 ^{1}H NMR spectrum (300 MHz, acetone-d_6) of **3-6a**.

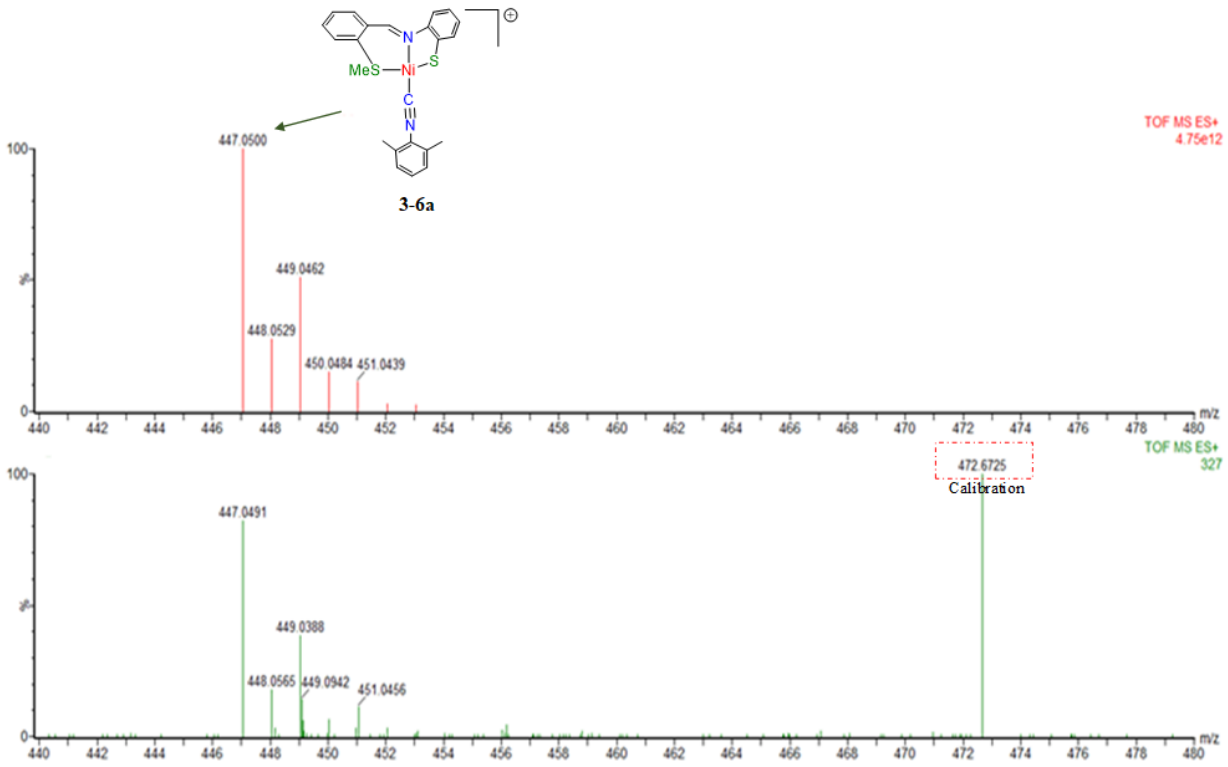

Figure A3.17 Positive-ion ESI-MS of 3-**6a**.

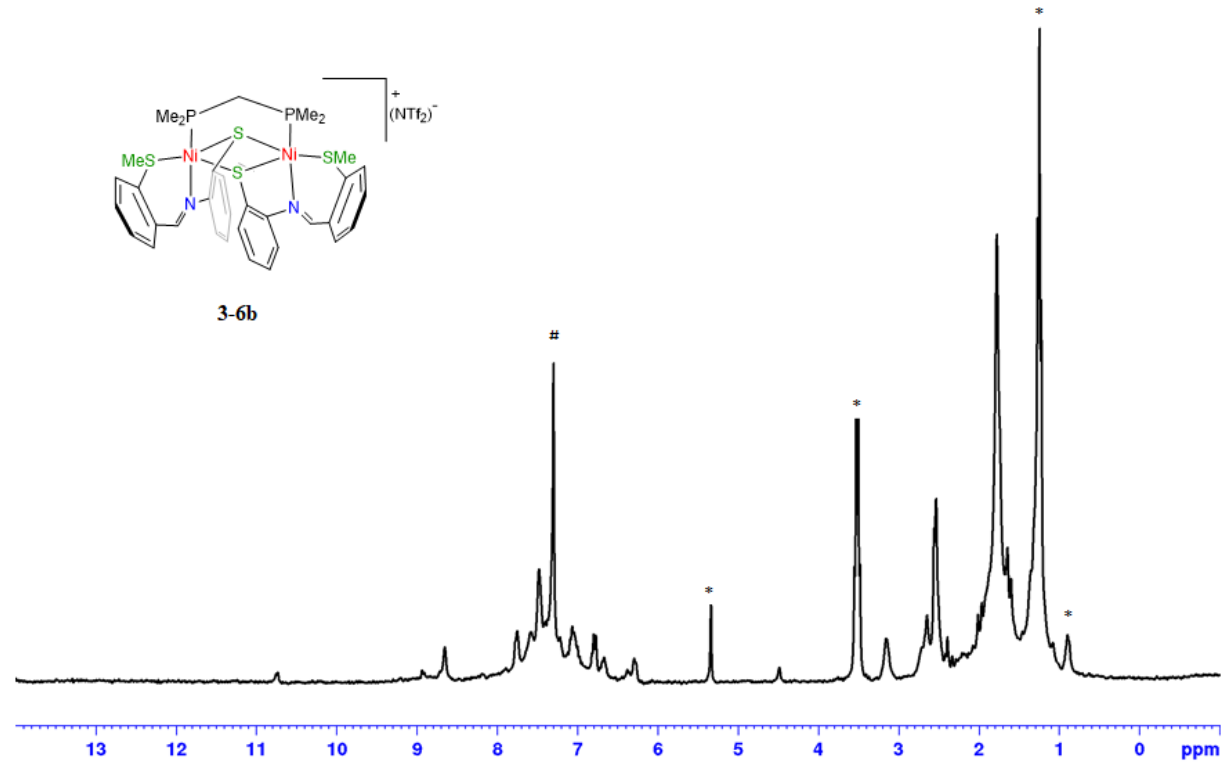

Figure A3.18 ^{1}H NMR spectrum (300 MHz, $CDCl_3$) of **3-6b**.

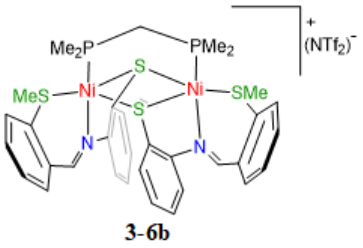

3-6b

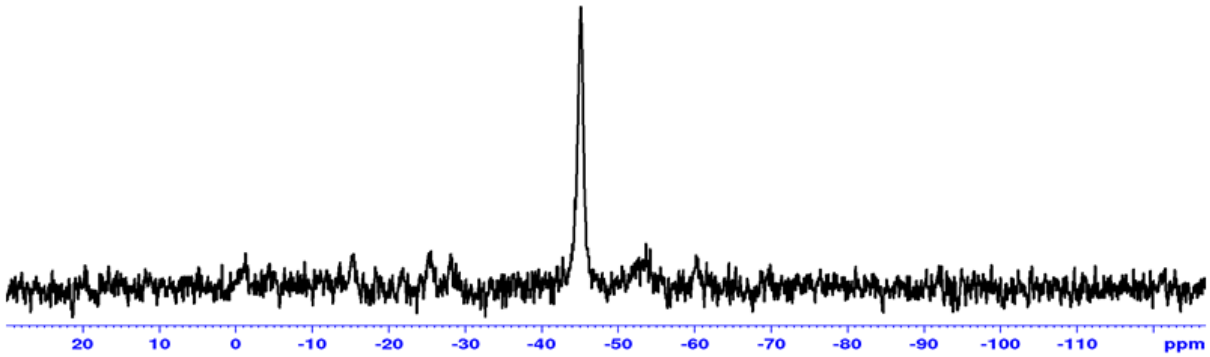

Figure A3.19 ^{31}P NMR spectrum (121 MHz, $CDCl_3$) of **3-6b**.

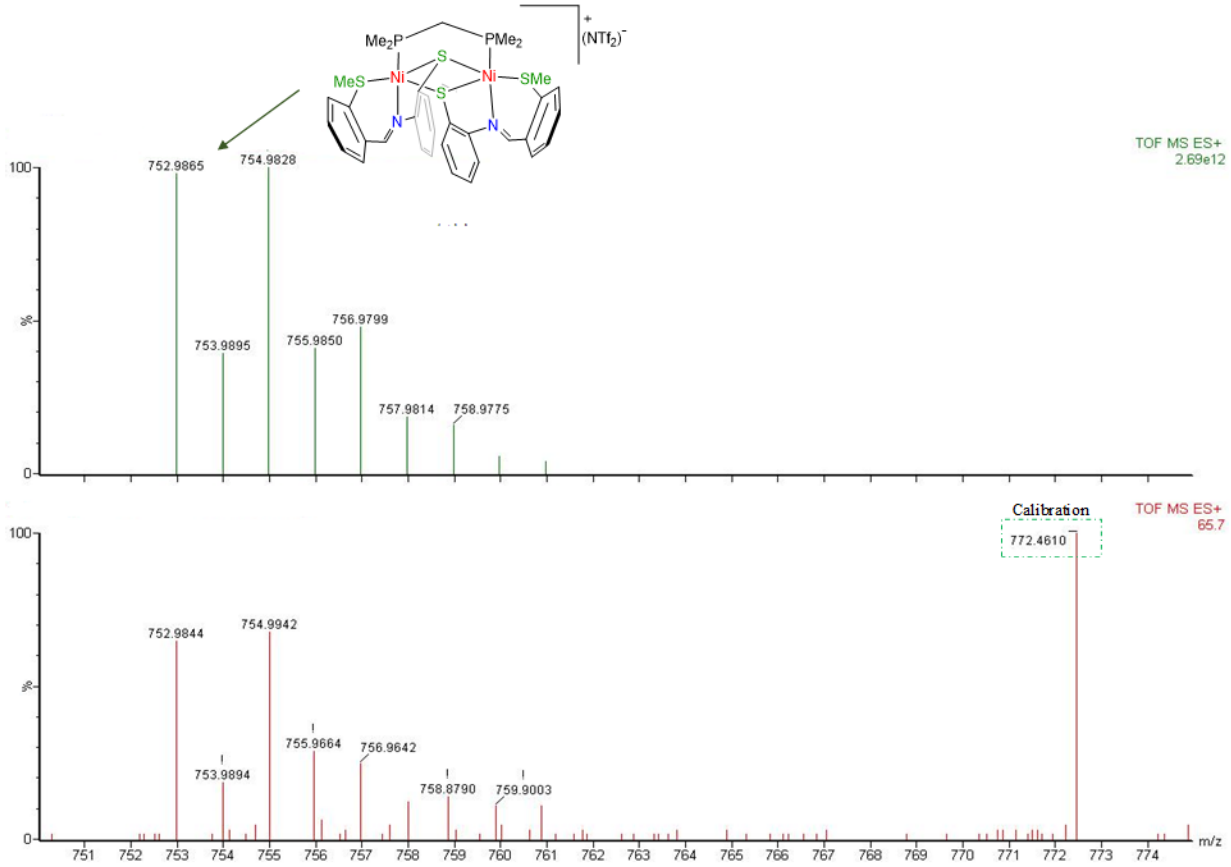

Figure A3.20 Positive-ion ESI-MS [M^+-Me] of **3-6b**.

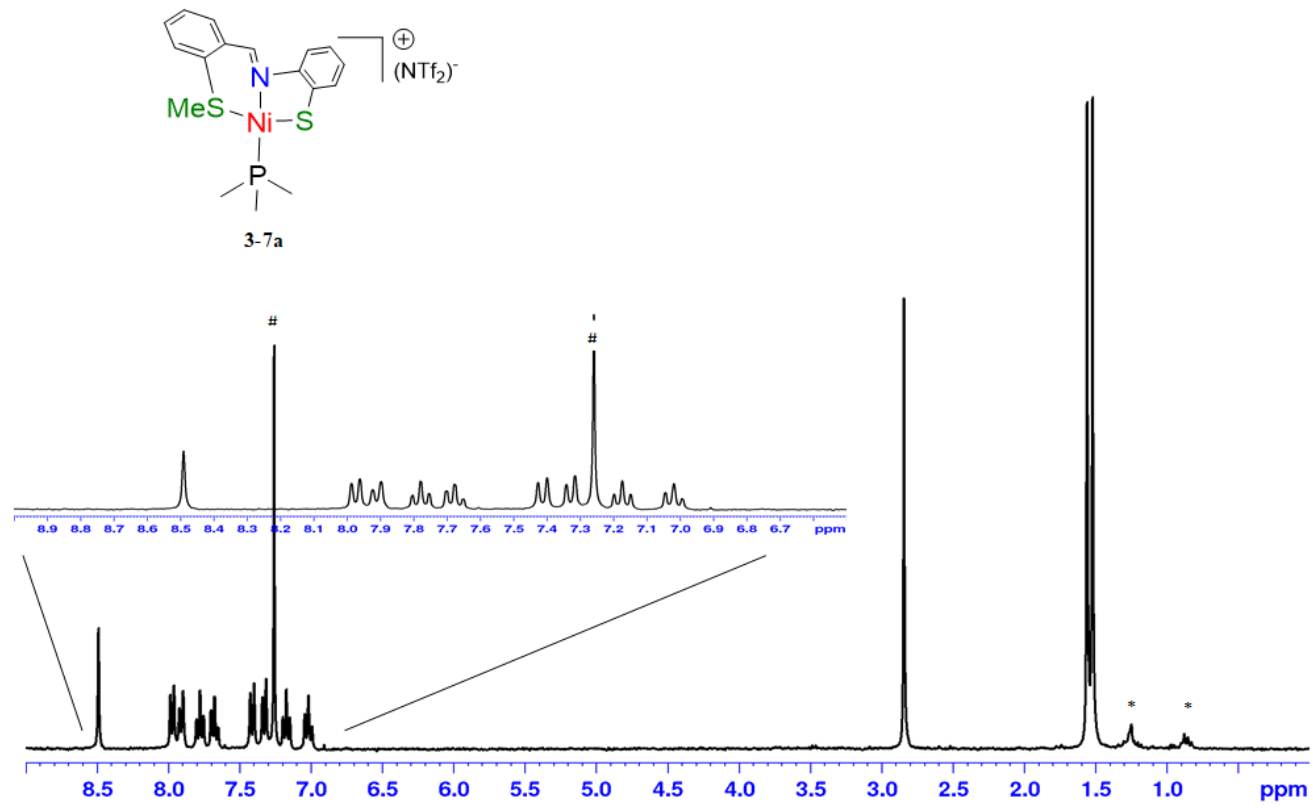

Figure A3.21 ^{1}H NMR spectrum (300 MHz, $CDCl_3$) of **3-7a**.

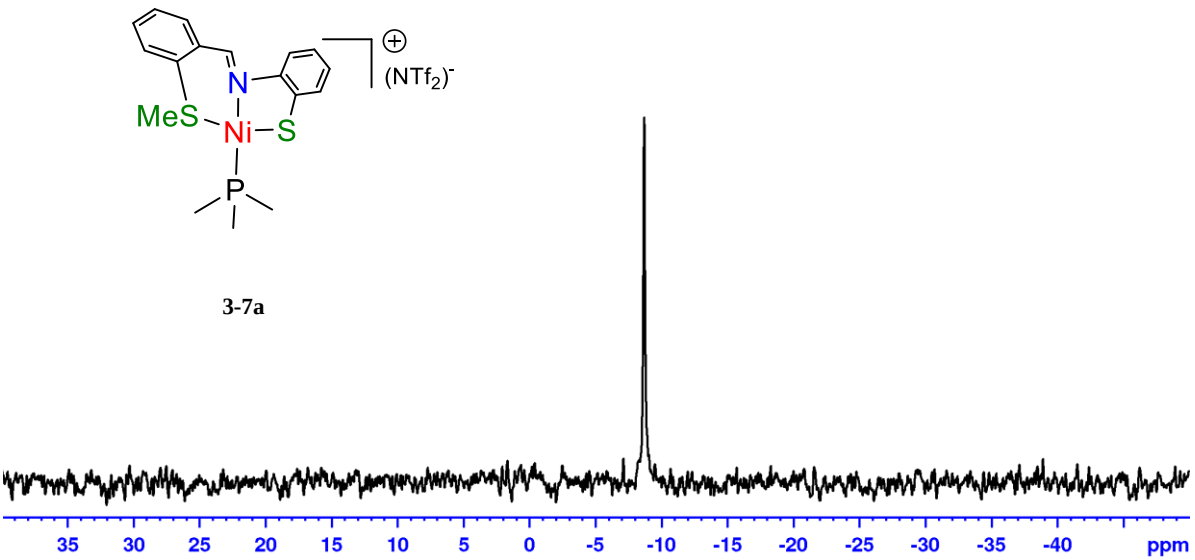

Figure A3.22 ^{31}P NMR spectrum (121 MHz, $CDCl_3$) of **3-7a**

.

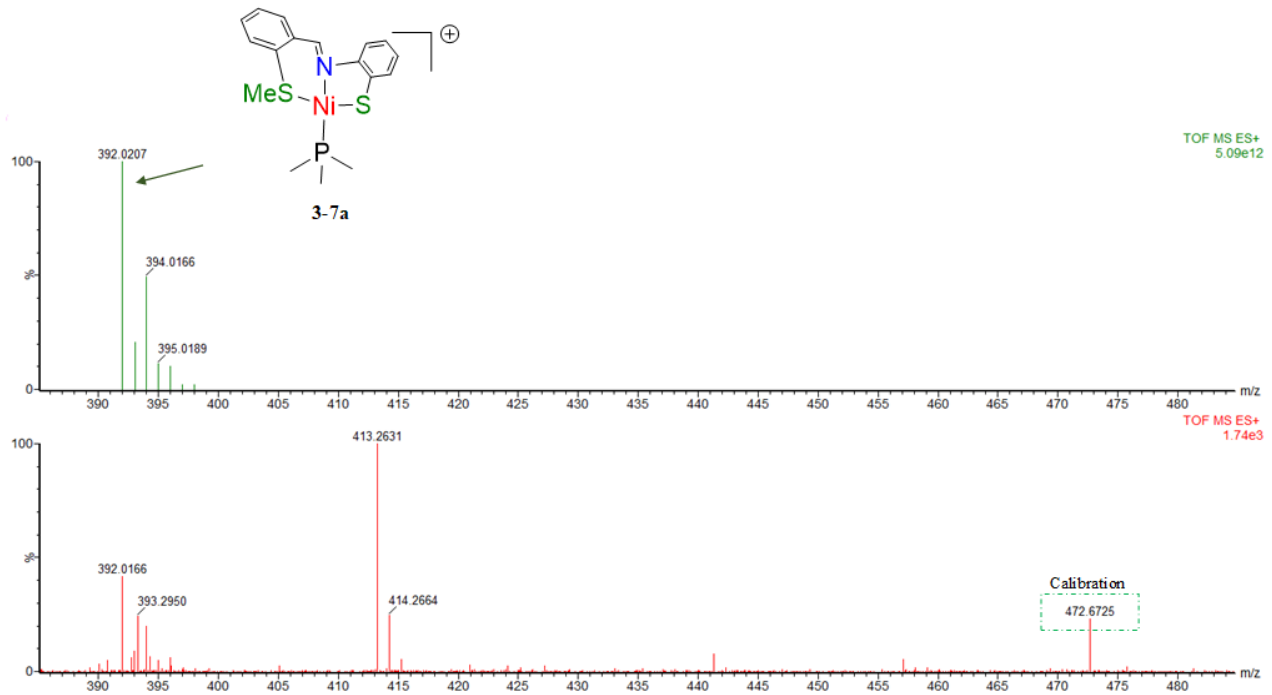

Figure A3.23 Positive-ion ESI-MS of **3-7a**.

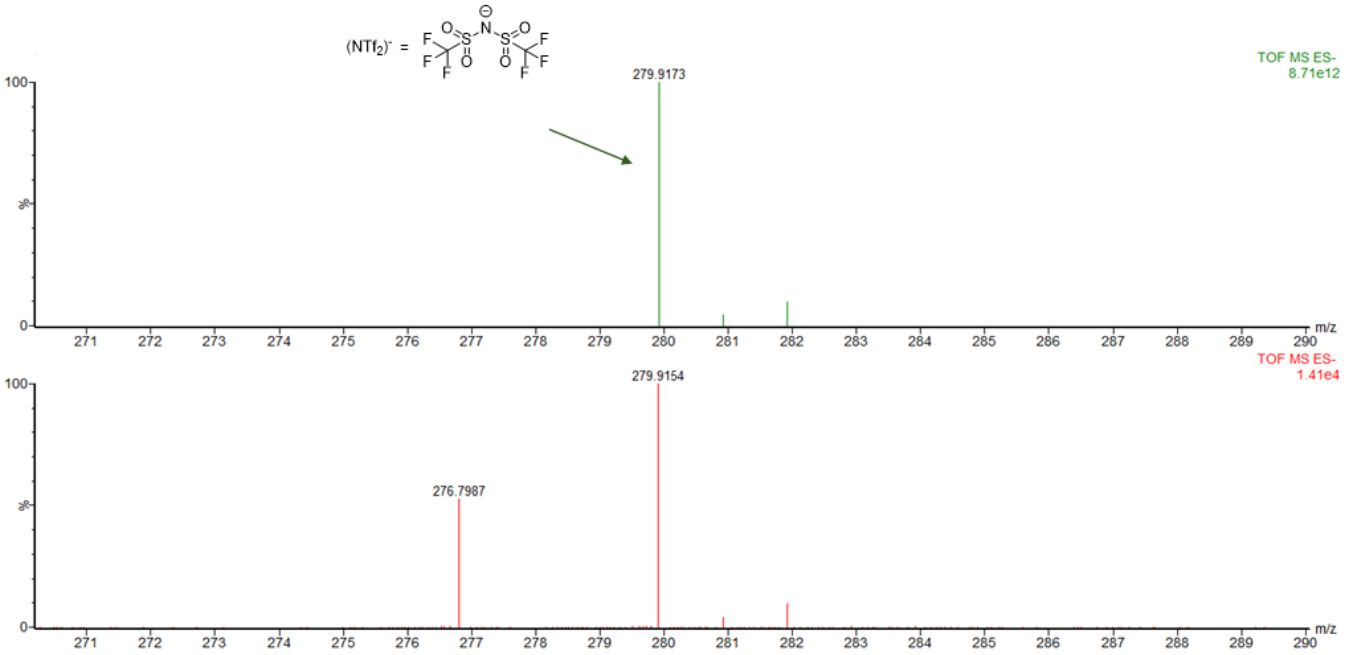

Figure A3.24 Negative-ion ESI-MS of **3-7a**.

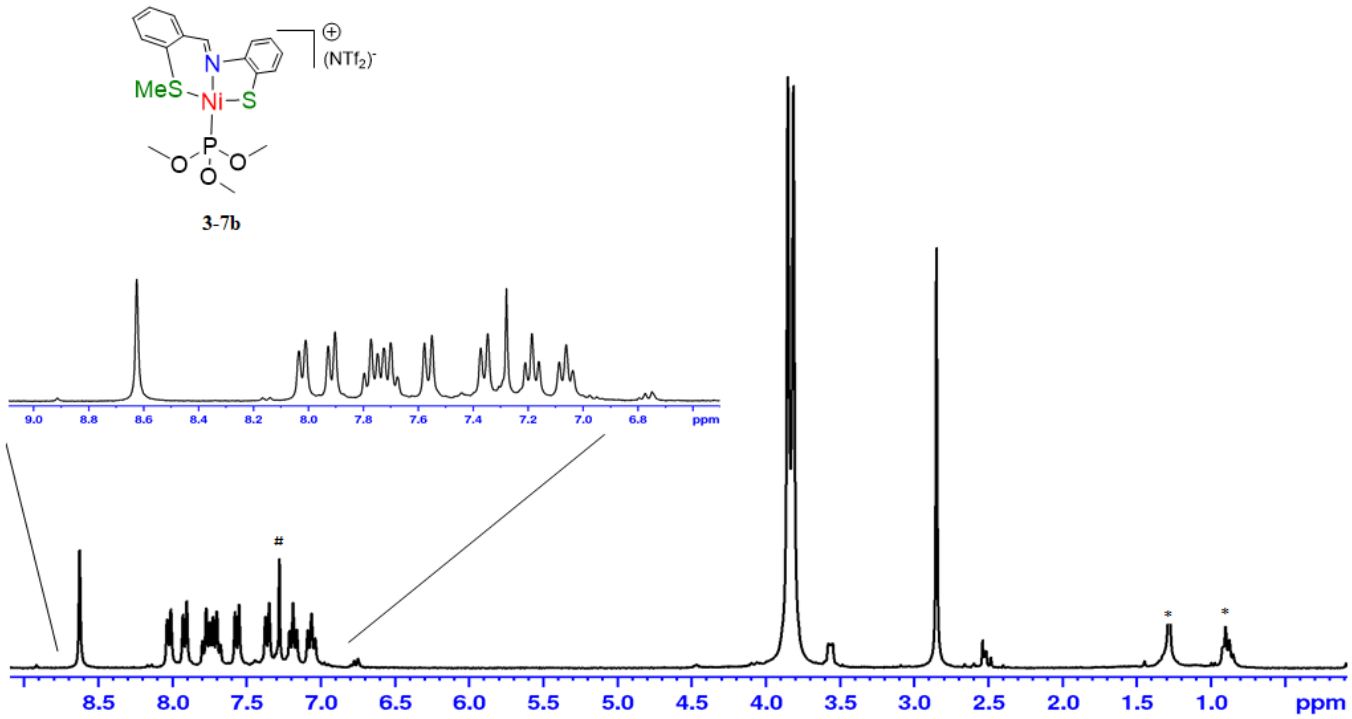

Figure A3.25 ^{1}H NMR spectrum (300 MHz, $CDCl_3$) of **3-7b**.

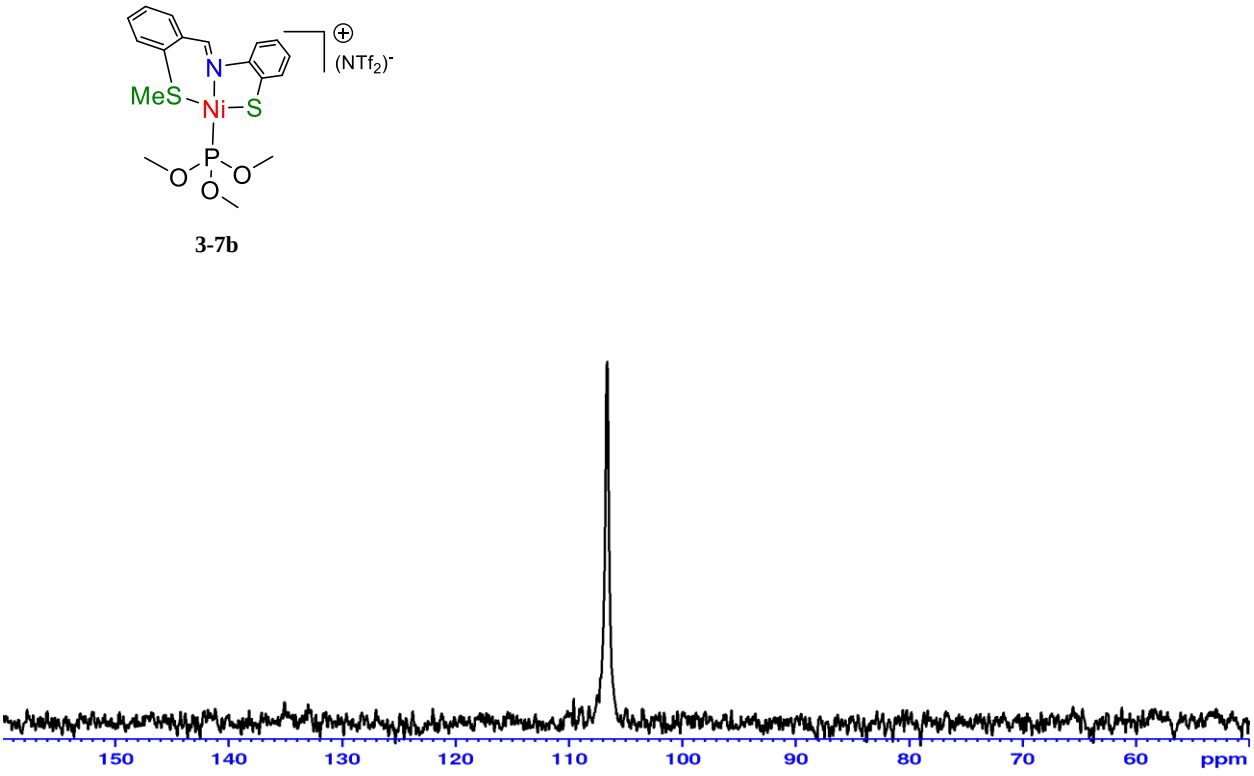

Figure A3.26 ^{31}P NMR spectrum (121 MHz, $CDCl_3$) of **3-7b**.

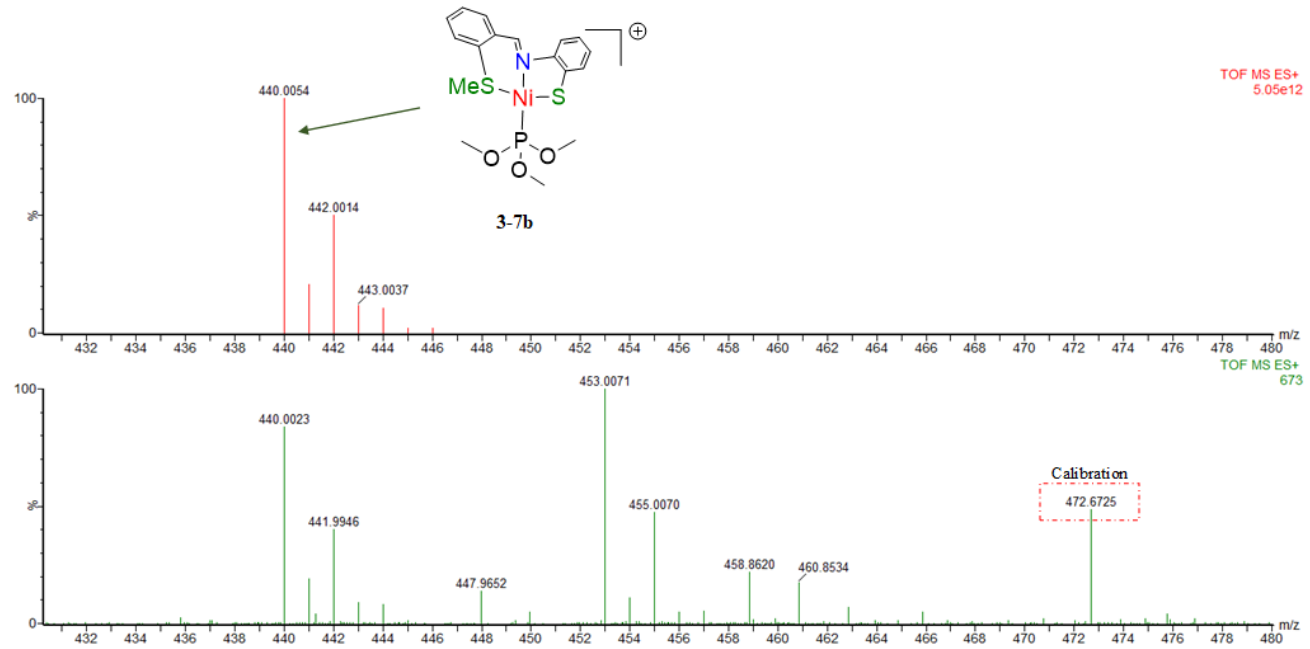

Figure A3.27 Positive-ion ESI-MS of **3-7b.**

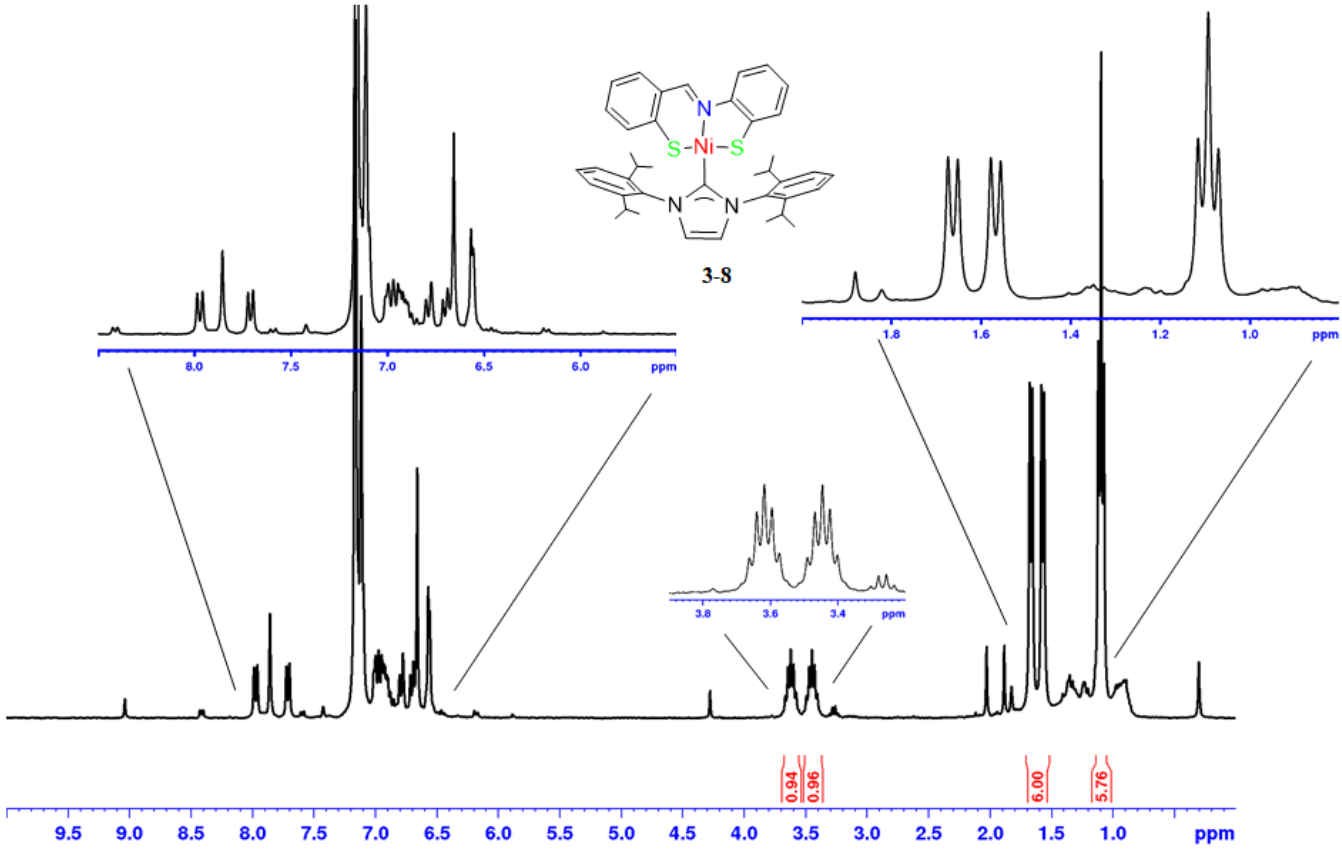

Figure A3.28 ^{1}H NMR spectrum (300 MHz, $CDCl_3$) of **3-8.**

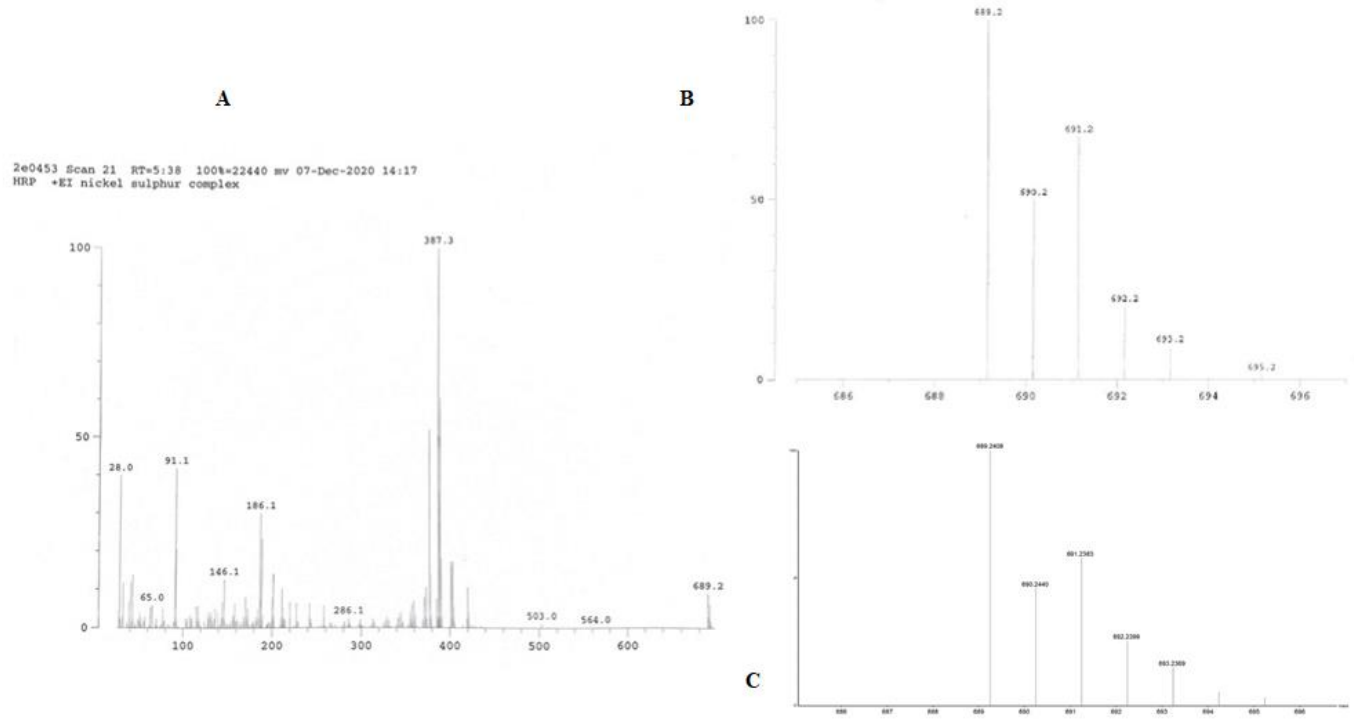

Figure A3.29 EI-MS of **3.8** (A) and experimental (B) and calculated (C) isotope pattern for M^+ ion.

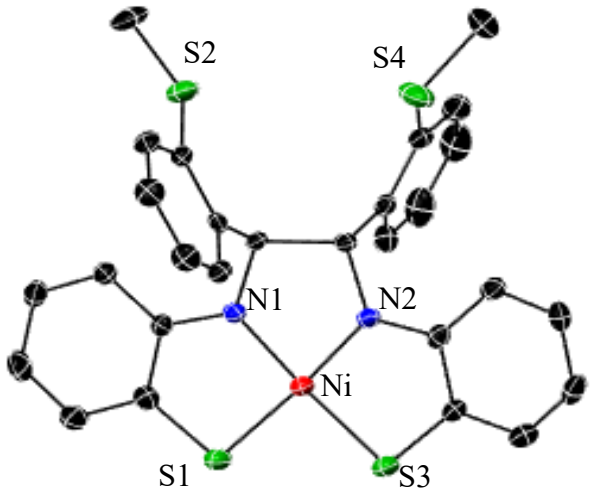

Figure A3.30. Molecular Structure of **3-2:** H atoms are omitted for clarity. Selected bond lengths (Å) and angles (°): Ni−S(1) 2.131 (1), Ni−S(4) 2.1312(9), Ni-N(1) 1.815(2), Ni-N(2) 1.811(2), S(1)-Ni-S(4) 95.10(4), S(1)-Ni-N(1) 89.14(8), S(1)-Ni-N(2) 175.55(8), S(4)-Ni-N(1) 174.37(8), S(4)-Ni-N(2) 89.22(8), N(1)-Ni-N(2) 86.6(1).

Appendices

Chapter 4:

	(**4-2**)[Na(THF)$_6$]
Empirical formula	$C_{59}H_{82}N_2NaNiO_7S_4$
formula weight (g·mol^{-1})	1141.20
crystal system	monoclinic
space group	$P\ 2_1/n$
a (A)	10.7663(6)
b (A)	39.623(2)
c (A)	13.9800(7)
α (deg)	90
β (deg)	94.725(2)
γ (deg)	90
V (A^3)	5943.5(5)
Z	4
T (K)	200(2)
ρ_{calcd} (g·cm^{-3})	1.275
μ (mm^{-1})	0.526
$2\theta_{max}$ (deg)	50.808
total/unique reflections	60042/10903
Reflections [$I_o \geq 2\sigma(I_o)$]	6690
R_1, wR_2 [$I_o \geq 2\sigma(I_o)$]	0.0740, 0.1663
goodness of fit	1.033

Table A4.1 X-ray diffraction data collection and structure refinement details for **(4-2)**$^-$.

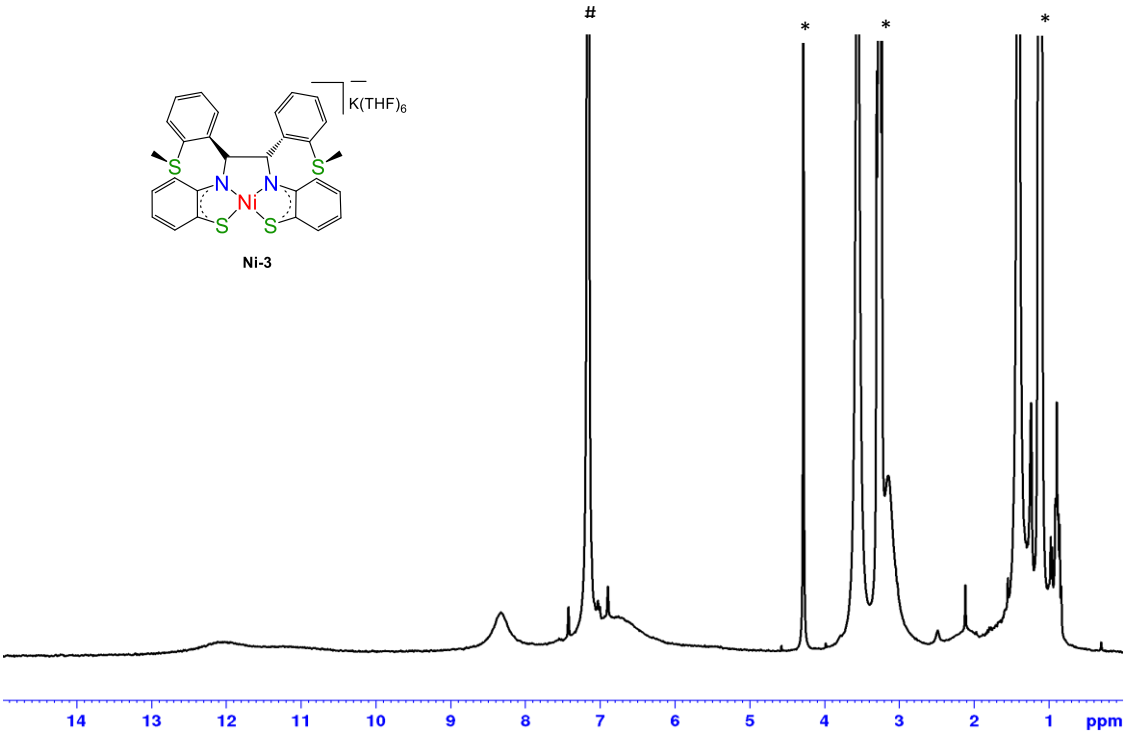

Figure A4.1 ^{1}H NMR spectrum (300 MHz, C_6D_6) of **Ni-3**

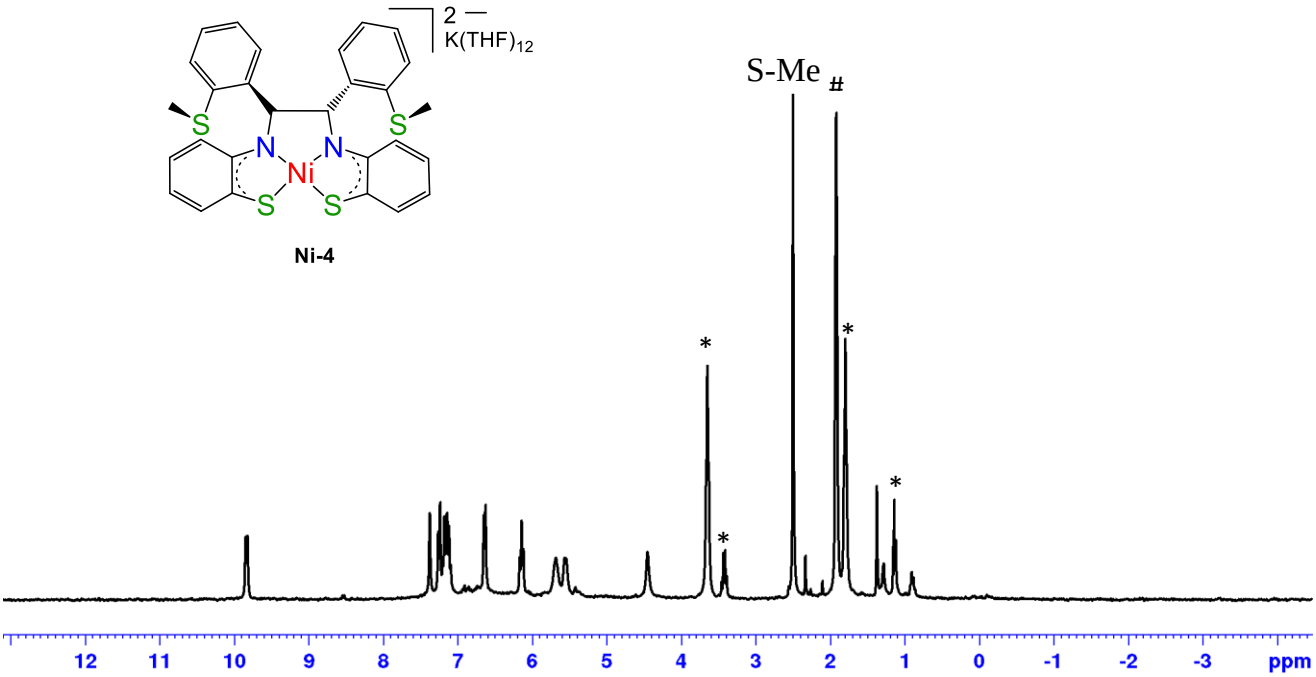

Figure A4.2 ^{1}H NMR spectrum (300 MHz, CD_3CN) of **Ni-4**. # Solvent residual peak, *THF and DEE

Appendices, Chapter 5:

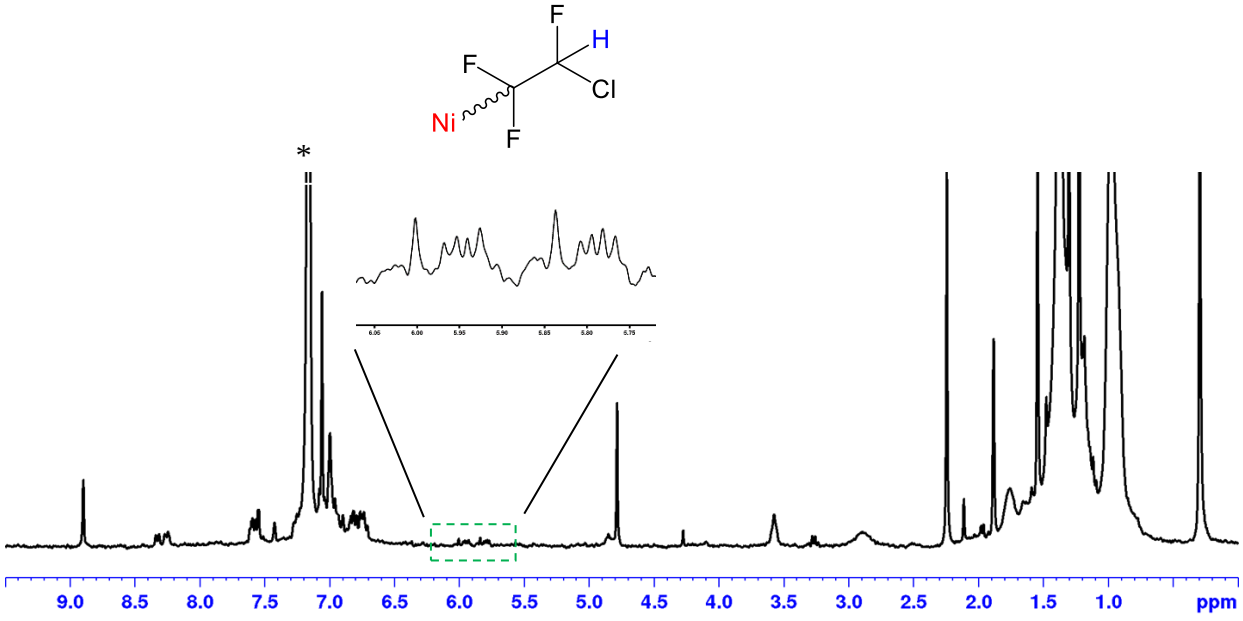

Figure A5.1 ^{1}H NMR (300 MHz, C_6D_6) spectrum of **Ni-7** and **Ni-8**. Insert shows -CFClH ddd. * Solvent residual peak.

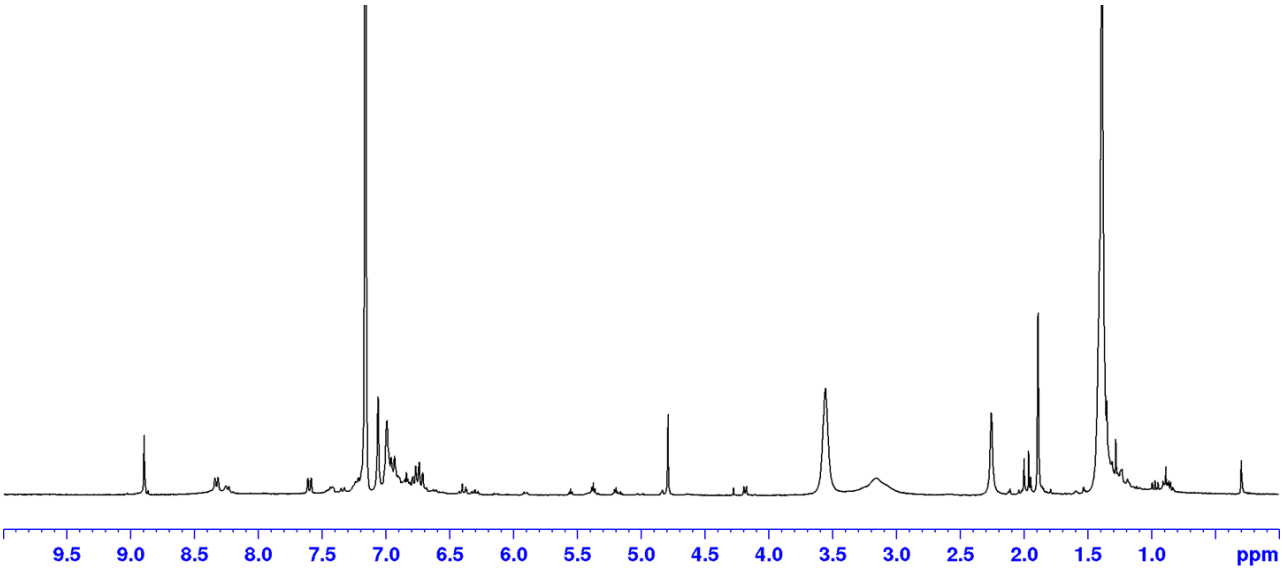

Figure A5.2 ^{1}H NMR (300 MHz, C_6D_6) spectrum of **Ni-11** and **Ni-12**. * Solvent residual peak

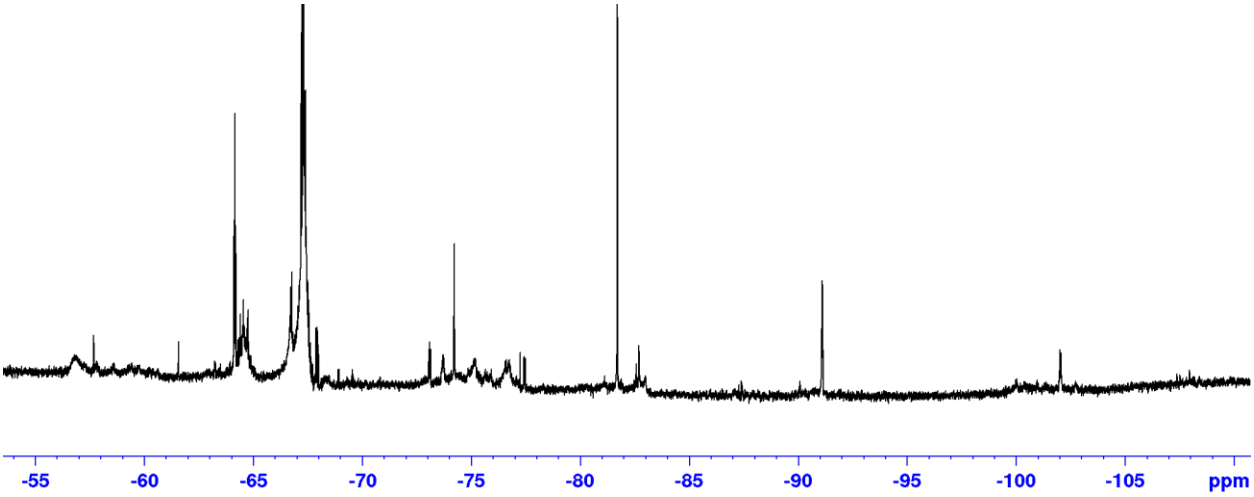

Figure A5.3 ^{19}F NMR (282 MHz, C_6D_6) spectrum of **Ni-4** with TFE.

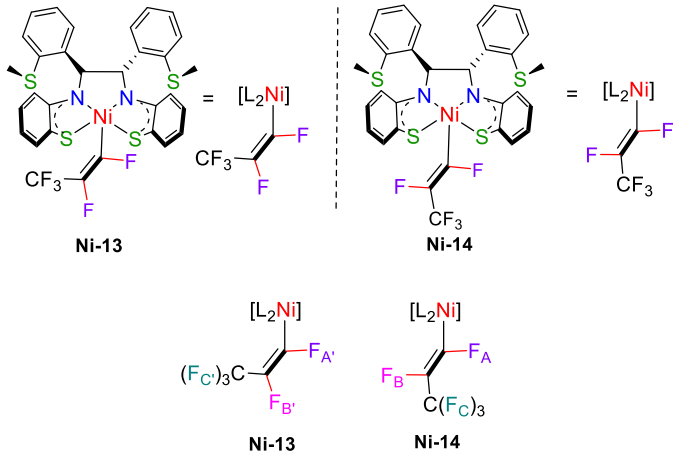

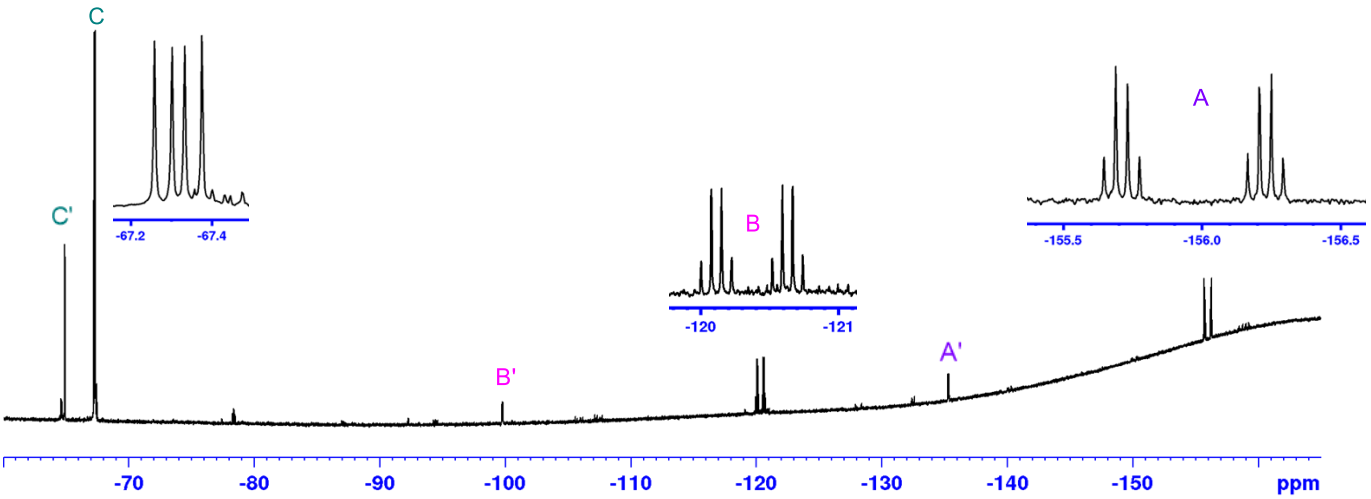

Figure A5.4 ^{19}F NMR (282 MHz, C_6D_6) spectrum of **Ni-13** and **Ni-14** with all fluorine peaks labeled.

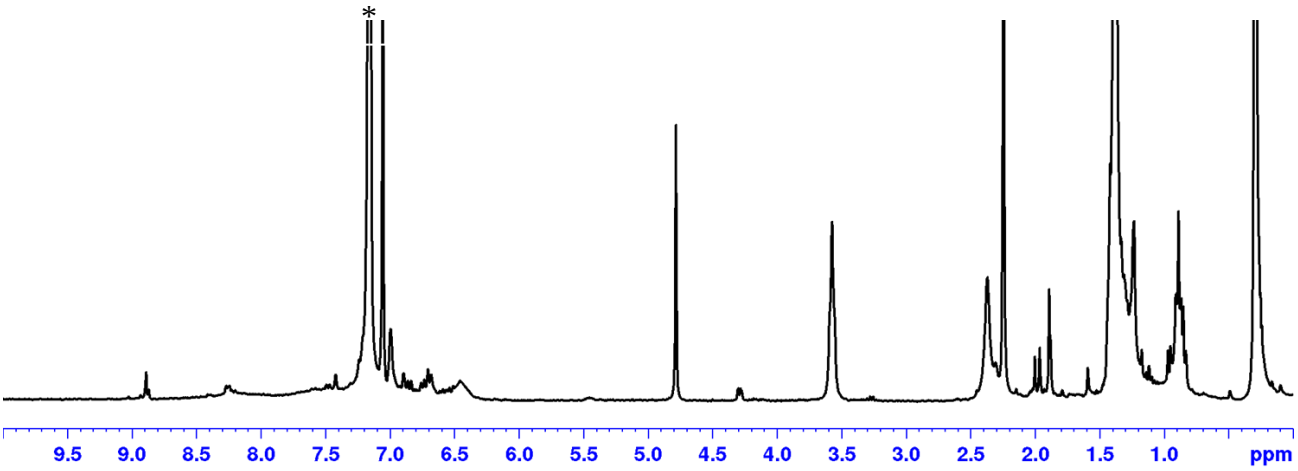

Figure A5.5 ^{1}H NMR (300 MHz, C_6D_6) spectrum of **Ni-13** and **Ni-14.** * Solvent residual peak

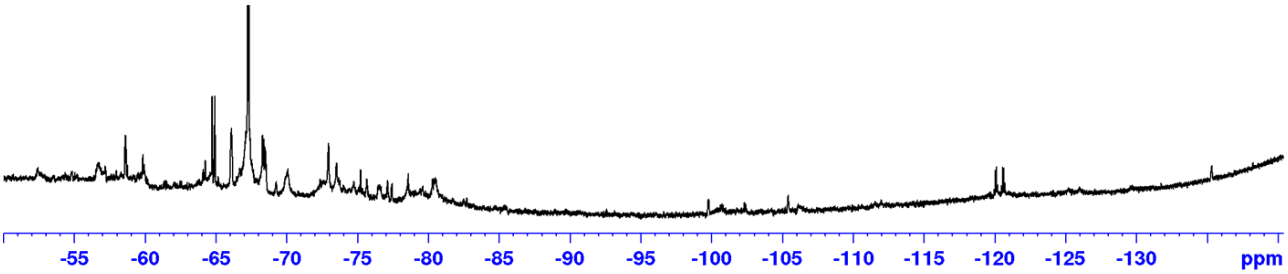

Figure A5.6 ^{19}F NMR (300 MHz, C_6D_6) spectrum of **Ni-3** with HFP

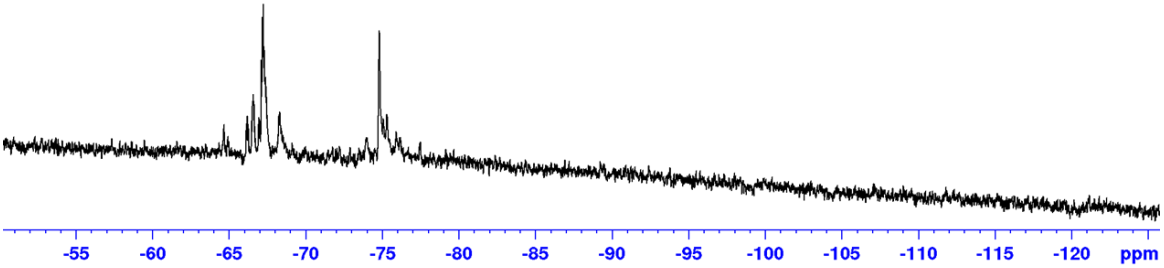

Figure A5.7 ^{19}F NMR (300 MHz, C_6D_6) spectrum of **Ni-4** with HFP.

Figures and Schemes permission:

Schemes: 1.1-1.32, 4.1, 4.2 and 5.1

Figures: 1.1-1.18

Some figures and/or schemes cited from one paper which had only one permission.

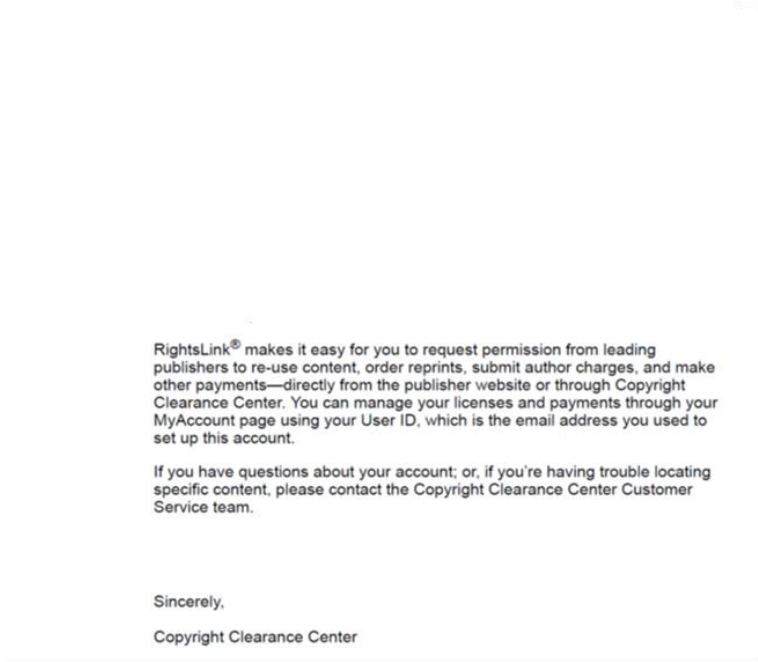

RightsLink® makes it easy for you to request permission from leading publishers to re-use content, order reprints, submit author charges, and make other payments—directly from the publisher website or through Copyright Clearance Center. You can manage your licenses and payments through your MyAccount page using your User ID, which is the email address you used to set up this account.

If you have questions about your account; or, if you're having trouble locating specific content, please contact the Copyright Clearance Center Customer Service team.

Sincerely,

Copyright Clearance Center

Aryl Fluoride Activation through Palladium–Magnesium Bimetallic Cooperation: A Mechanistic and Computational Study

Author: Chen Wu, Samuel P. McCollom, Zhipeng Zheng, et al
Publication: ACS Catalysis
Publisher: American Chemical Society
Date: Jul 1, 2020

JOHN WILEY AND SONS LICENSE
TERMS AND CONDITIONS

May 20, 2021

This Agreement between University of Ottawa -- Yahya Albkuri ("You") and John Wiley and Sons ("John Wiley and Sons") consists of your license details and the terms and conditions provided by John Wiley and Sons and Copyright Clearance Center.

License Number	5058400606157
License date	Apr 29, 2021
Licensed Content Publisher	John Wiley and Sons
Licensed Content Publication	European Journal of Inorganic Chemistry
Licensed Content Title	Coordination of a Hemilabile N,N,S Donor Ligand in the Redox System [CuL2] /2 , L = 2-Pyridyl-N-(2′-alkylthiophenyl)methyleneimine
Licensed Content Author	Johannes Schnödt, Jorge Manzur, Ana-Maria García, et al
Licensed Content Date	Feb 18, 2011
Licensed Content Volume	2011
Licensed Content Issue	9

Type of Use	reuse in a thesis/dissertation
Portion	figures/tables/illustrations
Number of figures/tables/illustrations	1
Format	electronic
Are you the author of this Elsevier article?	No
Will you be translating?	No
Title	C–N Cross-coupling Reactions of Amines with Aryl Halides Using Amide-Based Pincer Nickel(II) Catalyst
Institution name	University of Arkansas at Little Rock
Expected presentation date	Apr 2021
Portions	Scheme 1
Requestor Location	University of Ottawa 1108-1785 forbisher lane Ottawa, ON K1G 3T7 Canada Attn: University of Ottawa
Publisher Tax ID	GB 494 6272 12
Total	0.00 USD

ELSEVIER LICENSE
TERMS AND CONDITIONS

May 20, 2021

This Agreement between University of Ottawa -- Yahya Albkuri ("You") and Elsevier ("Elsevier") consists of your license details and the terms and conditions provided by Elsevier and Copyright Clearance Center.

License Number	5058400877024
License date	Apr 29, 2021
Licensed Content Publisher	Elsevier
Licensed Content Publication	Polyhedron
Licensed Content Title	Iron carbonyl complexes of N,C,S-pincer ligands with a pendant thioether arm: Synthesis, structures and reactivity
Licensed Content Author	Masakazu Hirotsu,Kiyokazu Santo,Yui Tanaka,Isamu Kinoshita
Licensed Content Date	Mar 15, 2018
Licensed Content Volume	143
Licensed Content Issue	n/a
Licensed Content Pages	8
Start Page	201
End Page	208

Licensed Content Pages	6
Type of use	Dissertation/Thesis
Requestor type	University/Academic
Format	Electronic
Portion	Figure/table
Number of figures/tables	2
Will you be translating?	No
Title	C–N Cross-coupling Reactions of Amines with Aryl Halides Using Amide-Based Pincer Nickel(II) Catalyst
Institution name	University of Arkansas at Little Rock
Expected presentation date	Apr 2021
Portions	Schemes: 3 and 4
Requestor Location	University of Ottawa 1108-1785 forbisher lane Ottawa, ON K1G 3T7 Canada Attn: University of Ottawa
Publisher Tax ID	EU826007151
Total	0.00 USD

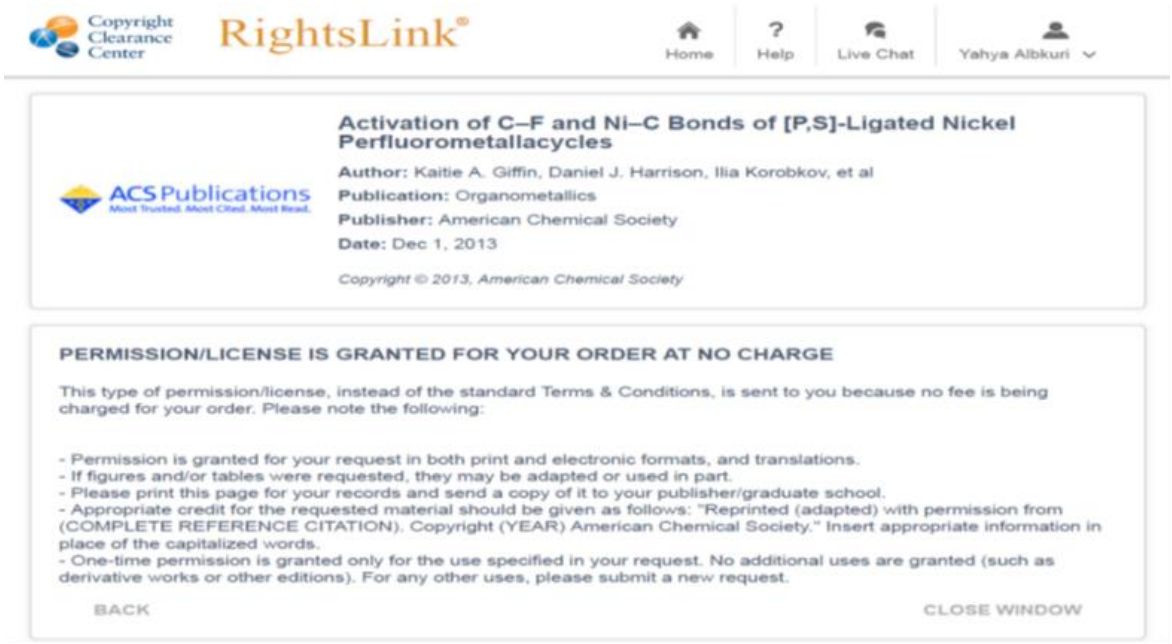

Rightslink® by Copyright Clearance Center

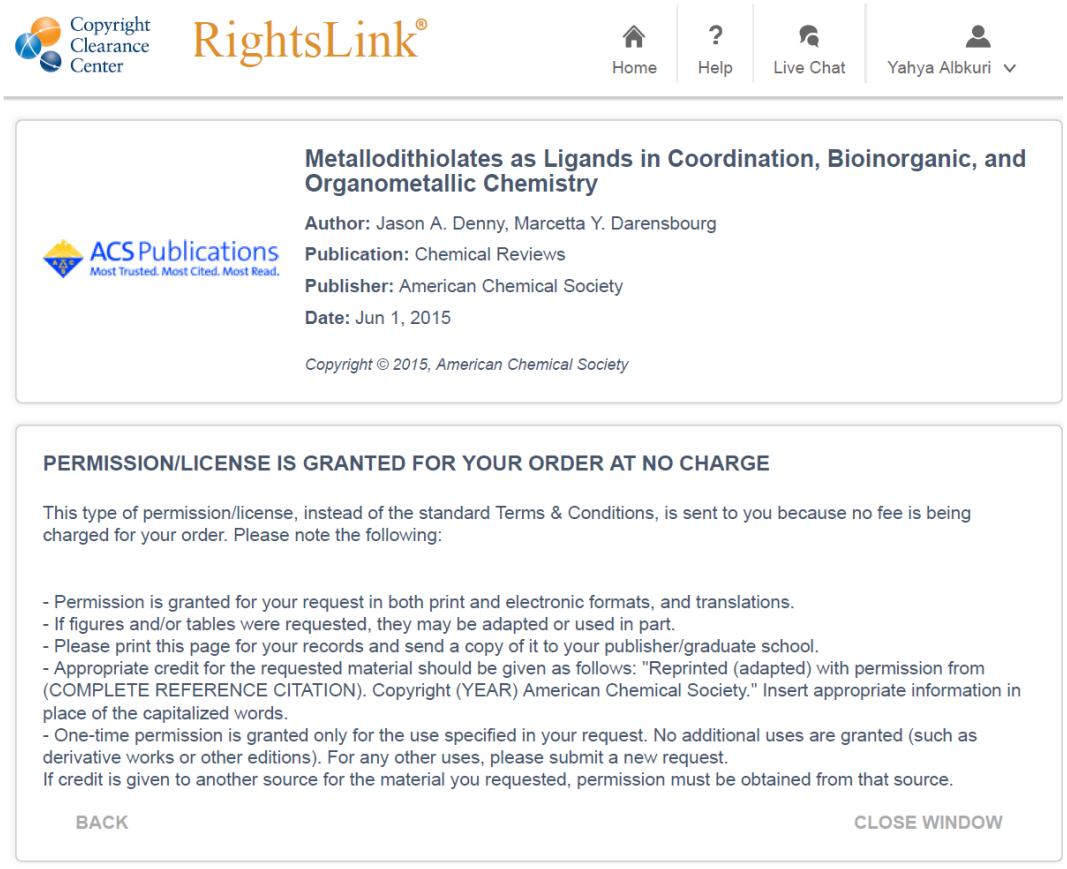

Rightslink® by Copyright Clearance Center

Copyright Clearance Center RightsLink®

Home | Help | Live Chat | Yahya Albkuri

ACS Publications
Most Trusted. Most Cited. Most Read.

Metallodithiolates as Ligands in Coordination, Bioinorganic, and Organometallic Chemistry

Author: Jason A. Denny, Marcetta Y. Darensbourg
Publication: Chemical Reviews
Publisher: American Chemical Society
Date: Jun 1, 2015

Copyright © 2015, American Chemical Society

PERMISSION/LICENSE IS GRANTED FOR YOUR ORDER AT NO CHARGE

This type of permission/license, instead of the standard Terms & Conditions, is sent to you because no fee is being charged for your order. Please note the following:

- Permission is granted for your request in both print and electronic formats, and translations.
- If figures and/or tables were requested, they may be adapted or used in part.
- Please print this page for your records and send a copy of it to your publisher/graduate school.
- Appropriate credit for the requested material should be given as follows: "Reprinted (adapted) with permission from (COMPLETE REFERENCE CITATION). Copyright (YEAR) American Chemical Society." Insert appropriate information in place of the capitalized words.
- One-time permission is granted only for the use specified in your request. No additional uses are granted (such as derivative works or other editions). For any other uses, please submit a new request.

If credit is given to another source for the material you requested, permission must be obtained from that source.

BACK CLOSE WINDOW

This Agreement between University of Ottawa -- Yahya Albkuri ("You") and John Wiley and Sons ("John Wiley and Sons") consists of your license details and the terms and conditions provided by John Wiley and Sons and Copyright Clearance Center.

License Number	5058470796647
License date	Apr 29, 2021
Licensed Content Publisher	John Wiley and Sons
Licensed Content Publication	Chemistry - A European Journal
Licensed Content Title	Carbonylmetallates—A Special Family of Nucleophiles in Aromatic and Vinylic Substitution Reactions
Licensed Content Author	Petr K. Sazonov, Irina P. Beletskaya
Licensed Content Date	Jan 25, 2016
Licensed Content Volume	22
Licensed Content Issue	11
Licensed Content Pages	10

SPRINGER NATURE LICENSE
TERMS AND CONDITIONS

May 20, 2021

This Agreement between University of Ottawa -- Yahya Alhkani ("You") and Springer Nature ("Springer Nature") consists of your license details and the terms and conditions provided by Springer Nature and Copyright Clearance Center.

License Number	5057110681723
License date	Apr 27, 2021
Licensed Content Publisher	Springer Nature
Licensed Content Publication	Catalysis Letters
Licensed Content Title	C–N Cross-coupling Reactions of Amines with Aryl Halides Using Amido-Based Pincer Nickel(II) Catalyst
Licensed Content Author	Yahya M. Alhkani et al
Licensed Content Date	Dec 14, 2019
Type of Use	Thesis/Dissertation
Requestor type	academic/university or research institute
Format	print and electronic
Portion	full article/chapter
Will you be translating?	no

Type of use	Dissertation/Thesis
Requestor type	University/Academic
Format	Print and electronic
Portion	Figure/table
Number of figures/tables	6
Will you be translating?	No
Title	C–N Cross-coupling Reactions of Amines with Aryl Halides Using Amide-Based Pincer Nickel(II) Catalyst
Institution name	University of Arkansas at Little Rock
Expected presentation date	Apr 2021
Portions	6
Requestor Location	University of Ottawa 1108-1785 forbisher lane Ottawa, ON K1G 3T7 Canada Attn: University of Ottawa
Publisher Tax ID	EU826007151
Total	0.00 USD

Terms and Conditions

Circulation/distribution	1000 - 1999
Author of this Springer Nature content	yes
Title	C–N Cross-coupling Reactions of Amines with Aryl Halides Usin Amide-Based Pincer Nickel(II) Catalyst
Institution name	University of Arkansas at Little Rock
Expected presentation date	Apr 2021
Requestor Location	University of Ottawa 1108-1785 forbisher lane Ottawa, ON K1G 3T7 Canada Attn: University of Ottawa
Total	0.00 USD

Type of use	Dissertation/Thesis
Requestor type	University/Academic
Format	Print and electronic
Portion	Figure/table
Number of figures/tables	2
Will you be translating?	No
Title	C–N Cross-coupling Reactions of Amines with Aryl Halides Using Amide-Based Pincer Nickel(II) Catalyst
Institution name	University of Arkansas at Little Rock
Expected presentation date	Apr 2021
Portions	Scheme 1 and 2
Requestor Location	University of Ottawa 1108-1785 forbisher lane Ottawa, ON K1G 3T7 Canada Attn: University of Ottawa
Publisher Tax ID	EU826007151
Total	0.00 USD

SPRINGER NATURE LICENSE
TERMS AND CONDITIONS

May 20, 2021

This Agreement between University of Ottawa -- Yahya Albkuri ("You") and Springer Nature ("Springer Nature") consists of your license details and the terms and conditions provided by Springer Nature and Copyright Clearance Center.

The publisher has provided special terms related to this request that can be found at the end of the Publisher's Terms and Conditions.

License Number	5061601243762
License date	May 03, 2021
Licensed Content Publisher	Springer Nature
Licensed Content Publication	Nature
Licensed Content Title	Recent advances in homogeneous nickel catalysis
Licensed Content Author	Sarah Z. Tasker et al
Licensed Content Date	May 14, 2014
Type of Use	Thesis/Dissertation
Requestor type	academic/university or research institute
Format	electronic
Portion	figures/tables/illustrations

JOHN WILEY AND SONS LICENSE
TERMS AND CONDITIONS

May 20, 2021

This Agreement between University of Ottawa -- Yahya Albkuri ("You") and John Wiley and Sons ("John Wiley and Sons") consists of your license details and the terms and conditions provided by John Wiley and Sons and Copyright Clearance Center.

License Number	5058461470638
License date	Apr 29, 2021
Licensed Content Publisher	John Wiley and Sons
Licensed Content Publication	Journal of Physical Organic Chemistry
Licensed Content Title	Predicting the direction of nucleophilic attack in vinyl halides: halogenophilic versus carbophilic reactivity of metal carbonyl anions
Licensed Content Author	Petr K. Sazonov, Yuri F. Oprunenko, Irina P. Beletskaya
Licensed Content Date	Jul 26, 2012
Licensed Content Volume	26
Licensed Content Issue	2
Licensed Content Pages	11

Number of figures/tables/illustrations	6
High-res required	no
Will you be translating?	no
Circulation/distribution	500 - 999
Author of this Springer Nature content	no
Title	C–N Cross-coupling Reactions of Amines with Aryl Halides Using Amide-Based Pincer Nickel(II) Catalyst
Institution name	University of Arkansas at Little Rock
Expected presentation date	Apr 2021
Portions	Figure 1, 2, 4, 5 and 6
Requestor Location	University of Ottawa 1108-1785 forbisher lane Ottawa, ON K1G 3T7 Canada Attn: University of Ottawa
Billing Type	Invoice
Billing Address	University of Ottawa 1108-1785 forbisher lane Ottawa, ON K1G 3T7 Canada Attn: University of Ottawa
Total	0.00 USD

SPRINGER NATURE LICENSE
TERMS AND CONDITIONS

May 20, 2021

This Agreement between University of Ottawa -- Yahya Albkuri ("You") and Springer Nature ("Springer Nature") consists of your license details and the terms and conditions provided by Springer Nature and Copyright Clearance Center.

The publisher has provided special terms related to this request that can be found at the end of the Publisher's Terms and Conditions.

License Number	5061601243762
License date	May 03, 2021
Licensed Content Publisher	Springer Nature
Licensed Content Publication	Nature
Licensed Content Title	Recent advances in homogeneous nickel catalysis
Licensed Content Author	Sarah Z. Tasker et al
Licensed Content Date	May 14, 2014
Type of Use	Thesis/Dissertation
Requestor type	academic/university or research institute
Format	electronic
Portion	figures/tables/illustrations

ELSEVIER LICENSE
TERMS AND CONDITIONS

May 20, 2021

This Agreement between University of Ottawa -- Yahya Albkuri ("You") and Elsevier ("Elsevier") consists of your license details and the terms and conditions provided by Elsevier and Copyright Clearance Center.

License Number	5058471370286
License date	Apr 29, 2021
Licensed Content Publisher	Elsevier
Licensed Content Publication	Inorganica Chimica Acta
Licensed Content Title	The molecular and electronic structures of monomeric cobalt complexes containing redox noninnocent o-aminobenzenethiolat ligands
Licensed Content Author	Stephen Sproules,Ruta R. Kapre,Nabarun Roy,Thomas Weyhermüller,Karl Wieghardt
Licensed Content Date	Oct 15, 2010
Licensed Content Volume	363
Licensed Content Issue	12
Licensed Content Pages	13
Start Page	2702

Number of figures/tables/illustrations	6
High-res required	no
Will you be translating?	no
Circulation/distribution	500 - 999
Author of this Springer Nature content	no
Title	C–N Cross-coupling Reactions of Amines with Aryl Halides Using Amide-Based Pincer Nickel(II) Catalyst
Institution name	University of Arkansas at Little Rock
Expected presentation date	Apr 2021
Portions	Figure 1, 2, 4, 5 and 6
Requestor Location	University of Ottawa 1108-1785 forbisher lane Ottawa, ON K1G 3T7 Canada Attn: University of Ottawa
Billing Type	Invoice
Billing Address	University of Ottawa 1108-1785 forbisher lane Ottawa, ON K1G 3T7 Canada Attn: University of Ottawa
Total	0.00 USD

SPRINGER NATURE

Recent advances in homogeneous nickel catalysis

Author: Sarah Z. Tasker et al
Publication: Nature
Publisher: Springer Nature
Date: May 14, 2014

Order Completed

Thank you for your order.

This Agreement between Yahya Albkuri ("You") and Springer Nature ("Springer Nature") consists of your order details and the terms and conditions provided by Springer Nature and Copyright Clearance Center.

License number	Reference confirmation email for license number
License date	May, 03 2021

Licensed Content

Licensed Content Publisher	Springer Nature
Licensed Content Publication	Nature
Licensed Content Title	Recent advances in homogeneous nickel catalysis
Licensed Content Author	Sarah Z. Tasker et al
Licensed Content Date	May 14, 2014

Order Details

Type of Use	Thesis/Dissertation
Requestor type	academic/university or research institute
Format	electronic
Portion	figures/tables/illustrations
Number of figures/tables/illustrations	6
High-res required	no
Will you be translating?	no
Circulation/distribution	500 - 999
Author of this Springer Nature content	no

About Your Work

Title	C–N Cross-coupling Reactions of Amines with Aryl Halides Using Amide-Based Pincer Nickel(II) Catalyst
Institution name	University of Arkansas at Little Rock
Expected presentation date	Apr 2021

Additional Data

Portions	Figure 1, 2, 4, 5 and 6

End Page	2714
Type of Use	reuse in a thesis/dissertation
Portion	figures/tables/illustrations
Number of figures/tables/illustrations	2
Format	both print and electronic
Are you the author of this Elsevier article?	No
Will you be translating?	No
Title	C–N Cross-coupling Reactions of Amines with Aryl Halides Using Amide-Based Pincer Nickel(II) Catalyst
Institution name	University of Arkansas at Little Rock
Expected presentation date	Apr 2021
Portions	2
Requestor Location	University of Ottawa 1108-1785 forbisher lane Ottawa, ON K1G 3T7 Canada Attn: University of Ottawa
Publisher Tax ID	GB 494 6272 12
Total	0.00 USD
Terms and Conditions	

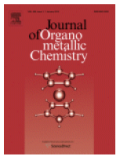

Reactions of fluoro-olefins, chloro-olefins and related molecules with carbonatobis(triphenylarsine)platinum(II) in ethanol

Author: M.J. Hacker,G.W. Littlecott,R.D.W. Kemmitt
Publication: Journal of Organometallic Chemistry
Publisher: Elsevier
Date: 1 January 1973

Order Completed

Thank you for your order.

This Agreement between University of Ottawa -- Yahya Albkuri ("You") and Elsevier ("Elsevier") consists of your license details and the terms and conditions provided by Elsevier and Copyright Clearance Center.

Your confirmation email will contain your order number for future reference.

License Number	5101640197631
License date	Jul 03, 2021

Printable Details

Licensed Content

Licensed Content Publisher	Elsevier
Licensed Content Publication	Journal of Organometallic Chemistry
Licensed Content Title	Reactions of fluoro-olefins, chloro-olefins and related molecules with carbonatobis(triphenylarsine)platinum(II) in ethanol
Licensed Content Author	M.J. Hacker,G.W. Littlecott,R.D.W. Kemmitt
Licensed Content Date	Jan 1, 1973
Licensed Content Volume	47
Licensed Content Issue	1
Licensed Content Pages	5

Order Details

Type of Use	reuse in a thesis/dissertation
Portion	figures/tables/illustrations
Number of figures/tables/illustrations	1
Format	electronic
Are you the author of this Elsevier article?	No
Will you be translating?	No

About Your Work

Title	C–N Cross-coupling Reactions of Amines with Aryl Halides Using Amide-Based Pincer Nickel(II) Catalyst
Institution name	University of Arkansas at Little Rock
Expected presentation date	Jul 2021

Additional Data

Order reference number	1
Portions	1

CHEMISTRY OF THE METAL CARBONYLS. VII. PERFLUOROALKYL IRON COMPOUNDS1

Author: T. A. Manuel, S. L. Stafford, F. G. A. Stone

Publication: Journal of the American Chemical Society

Publisher: American Chemical Society

Date: Jan 1, 1961

Bimetallic lanthanide complexes with lanthanide-transition metal bonds. Molecular structure of (C4H8O)(C5H5)2LuRu(CO)2(C5H5). The use of 139La NMR spectroscopy

ACS Publications
Most Trusted. Most Cited. Most Read.

Author: I. P. Beletskaya, A. Z. Voskoboynikov, E. B. Chuklanova, et al
Publication: Journal of the American Chemical Society
Publisher: American Chemical Society
Date: Apr 1, 1993

Mechanism of Ni-Catalyzed Reductive 1,2-Dicarbofunctionalization of Alkenes

Author: Qiao Lin, Tianning Diao

Publication: Journal of the American Chemical Society

Publisher: American Chemical Society

Date: Nov 1, 2019

Mechanism and Selectivity in Nickel-Catalyzed Cross-Electrophile Coupling of Aryl Halides with Alkyl Halides

Author: Soumik Biswas, Daniel J. Weix

Publication: Journal of the American Chemical Society

Publisher: American Chemical Society

Date: Oct 1, 2013

Reactions of fluoro-olefins, chloro-olefins and related molecules with carbonatobis(triphenylarsine)platinum(II) in ethanol

Author: M.J. Hacker,G.W. Littlecott,R.D.W. Kemmitt

Publication: Journal of Organometallic Chemistry

Publisher: Elsevier

Date: 1 January 1973

Order Completed

Thank you for your order.

This Agreement between University of Ottawa -- Yahya Albkuri ("You") and Elsevier ("Elsevier") consists of your license details and the terms and conditions provided by Elsevier and Copyright Clearance Center.

Your confirmation email will contain your order number for future reference.

License Number	5101640197631
License date	Jul 03, 2021

Printable Details

Licensed Content

Licensed Content Publisher	Elsevier
Licensed Content Publication	Journal of Organometallic Chemistry
Licensed Content Title	Reactions of fluoro-olefins, chloro-olefins and related molecules with carbonatobis(triphenylarsine)platinum(II) in ethanol
Licensed Content Author	M.J. Hacker,G.W. Littlecott,R.D.W. Kemmitt
Licensed Content Date	Jan 1, 1973
Licensed Content Volume	47
Licensed Content Issue	1
Licensed Content Pages	5

Order Details

Type of Use	reuse in a thesis/dissertation
Portion	figures/tables/illustrations
Number of figures/tables/illustrations	1
Format	electronic
Are you the author of this Elsevier article?	No
Will you be translating?	No

About Your Work

Title	C–N Cross-coupling Reactions of Amines with Aryl Halides Using Amide-Based Pincer Nickel(II) Catalyst
Institution name	University of Arkansas at Little Rock
Expected presentation date	Jul 2021

Additional Data

Order reference number	1
Portions	1

Bimetallic lanthanide complexes with lanthanide-transition metal bonds. Molecular structure of (C4H8O)(C5H5)2LuRu(CO)2(C5H5). The use of 139La NMR spectroscopy

Author: I. P. Beletskaya, A. Z. Voskoboynikov, E. B. Chuklanova, et al
Publication: Journal of the American Chemical Society
Publisher: American Chemical Society
Date: Apr 1, 1993

CHEMISTRY OF THE METAL CARBONYLS. VII. PERFLUOROALKYL IRON COMPOUNDS1

Author: T. A. Manuel, S. L. Stafford, F. G. A. Stone
Publication: Journal of the American Chemical Society
Publisher: American Chemical Society
Date: Jan 1, 1961